The American Mineralogist

Journal of the Mineralogical Society of America

VOL. 44 NOVEMBER–DECEMBER, 1959 Nos. 11 and 12

Contents

(Continued on Cover 2)

Published bi-monthly by the Society

Mineralogical Society of America

ASSOCIATED WITH THE GEOLOGICAL SOCIETY OF AMERICA

The enlarged issues of this journal for 1959 are made possible by a grant from the Penrose Fund of the Geological Society of America.

The American Mineralogist—Journal of the Mineralogical Society of America

The journal, containing articles on mineralogy, crystallography, and allied sciences, is issued every two months. Contributions are invited.

The general conduct of the journal is in the hands of the editor, Lewis S. Ramsdell, Department of Mineralogy, University of Michigan, to whom all manuscripts should be submitted. To assist the editor, the Council of the Society has appointed the following Board of Associate Editors:

Authors are requested to submit two copies of each manuscript, typewritten on standard size paper, 8½×11 inches. Photographs submitted for cuts should be glossy prints.

Authors are entitled to 50 free reprints, without covers, of each article published.

Sent to all members and fellows of the Mineralogical Society of America. Membership dues $4.00 annually, fellowship dues $5.00 annually, which includes receipt of the American Mineralogist and GeoTimes, which is published by the American Geological Institute. Subscriptions for libraries, colleges, institutions, companies and similar organizations $6.00 annually.

Entered as second class matter at the post office at Menasha, Wis., under Act of March 3, 1879. Acceptance for mailing at the special rate of postage provided for in section 1103, Act of Oct. 3, 1917, paragraph 4 section 429 P. L. & R. authorized March 13, 1922.

Notice of change of address, orders, and remittances should be sent to Marjorie Hooker, c/o U. S. Geological Survey, Washington 25, D. C.

Printed by the George Banta Company, Inc., Menasha, Wisconsin
Printed in the United States of America

Leitz®

SATISFIES THE MOST EXACTING REQUIREMENTS

RESEARCH POLARIZING MICROSCOPE

DIALUX-POL

The new *LEITZ* DIALUX-pol is the most advanced, universal polarizing research microscope ever manufactured. It was designed for the geologist, minerologist, petrographer, paleontologist, and the industrial research microscopist.

The DIALUX-pol maintains the principle of interchangeability, famous with all *LEITZ* precision instruments, so that it is readily used for transmitted light as well as for reflected-polarized light. With the simple addition of a connecting bar, it provides synchronous rotation of polarizer and analyzer.

In addition to a built-in light source and condenser system, the DIALUX-pol features many other operational advantages: unique single-knob control of both coarse and fine adjustment by alteration of the stage height (and not the tube), thus focusing with maximum operational ease.

Within seconds, the DIALUX-pol, through *LEITZ* accessories, converts for photography (through combined monocular-binocular tube and Leica camera), for ore microscopy (through vertical illuminator), or will accommodate the *LEITZ* Universal Stage, Sodium Vapor Lamp, and other facilities.

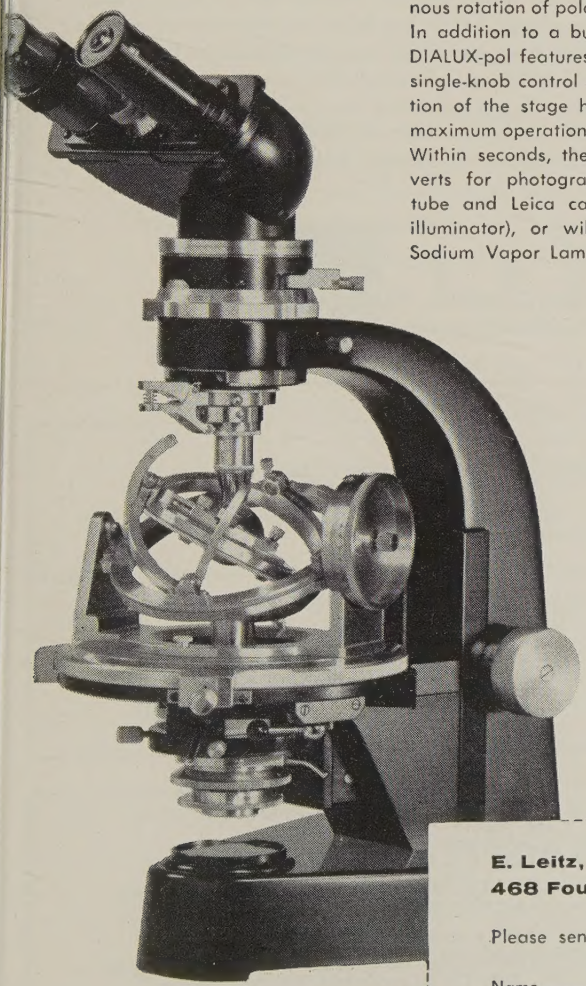

- monocular or binocular vision
- combination tube FS for photography
- synchronous polarizer-analyzer rotation upon request
- dual coarse and fine focusing
- built-in light source; 6-volt, 2.5-amp, variable intensity
- vertical illumination for ore microscopy
- polarizing filters or calcite prisms
- adaptable to all universal stage methods

Send for the DIALUX-pol information bulletin—then see and examine this fine instrument for yourself.

E. Leitz, Inc., Department AM-4
468 Fourth Ave., New York 16, N. Y.

Please send me the *LEITZ* DIALUX-pol brochure.

Name_____

Street_____

City_____ Zone_____ State_____

25150

E. LEITZ, INC., 468 FOURTH AVENUE, NEW YORK 16, N. Y.
Distributors of the world-famous products of
Ernst Leitz G. m. b. H., Wetzlar, Germany—Ernst Leitz Canada Ltd.
LEICA CAMERAS • LENSES • MICROSCOPES • BINOCULARS

THE AMERICAN MINERALOGIST

JOURNAL OF THE MINERALOGICAL SOCIETY OF AMERICA

Vol. 44 NOVEMBER–DECEMBER, 1959 Nos. 11 and 12

YAVAPAIITE, AN ANHYDROUS POTASSIUM, FERRIC SULPHATE FROM JEROME, ARIZONA

C. OSBORNE HUTTON, *Stanford University, California.*

ABSTRACT

Yavapaiite, a new mineral from Jerome, Arizona, has the composition $KFe^{3+}(SO_4)_2$ with two formula units in the unit cell. The mineral, associated with sulphur, voltaite, and other unidentified sulphates, forms pale pink, brittle, adamantine crystals, elongate parallel to [010], with perfect {100}, {001}, and distinct {110} cleavages, and strong conchoidal fracture. The forms $c\{001\}$, $d\{101\}$, $f\{201\}$, $a\{100\}$, and $m\{110\}$ appear to be most frequently developed. H = 2½ − 3, S.G. = 2.88 (meas.), 2.92 (calc.); $\alpha = 1.593$, $\beta = 1.684$. $\gamma = 1.698$, $\gamma - \alpha = 0.105$; $2V_{Na} = 30.5°$ (−), $\rho >$ v strong; $b = Z$, $c \wedge X = 6°$, $a = Y$, or nearly so. $a_0 = 8.12$ Å, ±0.01 Å, $b_0 = 5.14$ Å, $c_0 = 7.82$ Å, $\beta = 94°$ 24′; $a_0 : b_0 : c_0 = 1.5797 : 1 : 1.5214$. Measured cell weight $= 936.41 \times 10^{-24}$ gms. Monoclinic, with space group $C2$, $C2/m$, or Cm. Decomposed in boiling water, but readily soluble in HCl to give stable solutions.

The mineral is named for the Indian tribe that inhabits that part of Arizona in which the inactive mining center of Jerome is situated.

OCCURRENCE

The most complete study of sulphates formed under fumarolic conditions at the United Verde Copper Mine at Jerome, Arizona,* was made by Lausen (1928), and without exception, all of the sulphates reported in that work are hydrous minerals. Furthermore, most of them appear to have crystallized as the result of the extensive fire that first started in the mine in the fall of 1894, although Lausen (1928, p. 205) points out that many of the sulphates may have crystallized "when water was first used to put out the fires. Conditions, however, must have varied from time to time, as the various sulphates are not mutually intergrown, but rather occur as crystals of one composition resting on those of another."

The mineral described herein was collected by Mr. Scott J. Williams of Scottsdale, Arizona, in 1941. Of very limited occurrence, it formed a cement in rubble that was exposed in the open pit operations of the United

* For a more comprehensive account of the geology and ore deposits of Jerome in particular, and the region in general, reference may be made to Lindgren, W. (1926), Ore deposits of the Jerome and Bradshaw Mountains Quadrangles, Arizona: *U.S.G.S. Bull.* **782,** pp. 1–192.

Verde Extension Mining Co. Operations at the pit ceased very soon after 1941, and all traces of the occurrence are now unhappily lost.

The only specimen that was available for study consisted of an irregularly shaped fragment, 20×25 mm. with saccharoidal texture. Yavapaiite, which makes up 90–95 per cent of the specimen, forms rather equidimensional grains that average about 0.2 mm. in diameter, although here and there, in vugs, short, stumpy crystals with some terminal faces occasionally preserved, may reach 0.6 mm. in length. The mineral in question has formed upon very coarsely crystalline voltaite, and at the same time it is dusted over with very minor quantities of sulphur, jarosite, and at least two other sulphates which have not been satisfactorily diagnosed at this time; alunite may be present but its occurrence here has not been definitely proved.

The mineral has been given the name yavapaiite—Y Ā′ V Ā P A I I T[1] or yä′ vä pai ite[2]—after the Indian tribe that inhabited that area of Arizona in which Jerome is situated.

Physical Properties and Crystallography

Crystals of yavapaiite exhibit perfect transparency, vitreous luster that is almost adamantine in some instances, and very pale pink color with a slight purple hue (close to Ridgway's shell pink—11″f, Plate 28). The streak is white but the color of the finely powdered mineral is very pale yellow; the mineral, however, is perfectly colorless in transmitted light, even for fragments 2–3 mm. in thickness. Hardness is $2\frac{1}{2}$–3, and the measured specific gravity, determined by centrifuging in bromoform-diiodomethane-acetone mixtures is 2.88 at 22° C., whereas the calculated value is 2.92. The former value was obtained only after the sample had been finely crushed, dried in air at 110° C. for two hours, and then placed in vacuo; if this procedure is not followed, a value of 2.81 ± 0.02 was obtained for all specimens so measured. The mineral is exceedingly brittle, and those fracture surfaces not determined by cleavage are usually subconchoidal to uneven.

The crystals of yavapaiite do not exceed 0.6 mm. in length, and are usually very much less than this. In some instances, they are singly terminated, but no examples were isolated that would permit accurate and, therefore, worthwhile goniometric treatment. The crystals are short and stumpy in form with the longer dimension parallel to [010]. For one incomplete crystal (Fig. 1) that permitted identification of the faces, {001} is dominant, with {101}, {100}, {201}, and unit prism {110} less

[1] English usage, following the Royal Geographical Society (R.G.S. II) system.
[2] American usage.

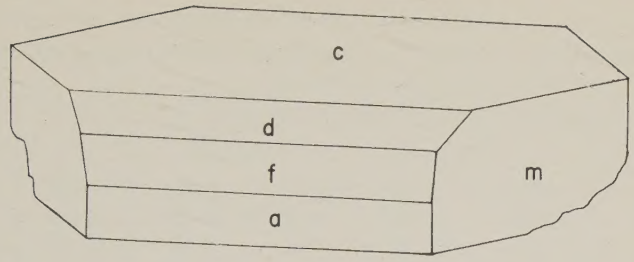

FIG. 1. Incomplete crystal of yavapaiite from Jerome, Arizona, showing development of $c\{001\}$, $d\{101\}$, $f\{201\}$, $a\{100\}$, and $m\{110\}$.

well developed; other faces are poorly represented as the result of fracture or deep growth pits.

Perfect {001}, {100}, and distinct {110} cleavages occur, and the dominance of the two former directions leads to the development of slender prismatic fragments with roughly rectangular cross-sections when crystals are crushed.

A very poor choice of crystals was available, but one doubly terminated fragment (Fig. 1) was selected for measurement with a stage goniometer. The interfacial angles thus determined are set out in Table 1, together with the corresponding angles calculated from data determined by the x-ray study. Most faces exhibit some curvature, and as a result they yielded reflections over a range of as much as 30′ in some instances; these data, which should be considered to be within $\pm 30'$ of the correct values, lead to a linear axial ratio $a:b:c = 1.59:1:1.52$, and an interaxial angle of 94° 30′.

The calculated elements and standard angles for yavapaiite are listed in Table 2, and these data have been derived from cell dimensions determined by the x-ray work.

The optical and other physical properties of yavapaiite are given in Table 3, where they may be compared with similar data for the monohydrate, krausite, and the quadrihydrate, goldichite.

TABLE 1. MEASURED AND CALCULATED INTERFACIAL ANGLES FOR YAVAPAIITE

Faces	Measured	Calculated
100∧110	57°45′	57°35′
001∧101	41°30′	41°48′
001∧201	59°30′	59°08′
201∧100	26°00′	26°28′
001∧011	56°30′	56°36′

TABLE 2. ANGLE TABLE FOR YAVAPAIITE

$a:b:c=1.5797:1:1.5214$; $\beta=94°24'$; $p_0:q_0:r_0=0.9631:1.5169:1$; $r_2:p_2:q_2=0.6592:0.6349:1$; $\mu=85°36'$; $p_0'=0.9658$, $q_0'=1.5214$, $x_0'=0.0769$.

	ϕ	p	ϕ_2	$p_2=B$	C	A
c 001	90°00′	4°24′	85°36′	90°00′	0°00′	85°36′
a 100	90 00	90 00	0 00	90 00	85 36	0 00
m 110	32 25	90 00	0 00	32 25	87 38½	57 35
w 011	2 53½	56 43	85 36	33 23	56 37	87 35
d 101	90 00	46 12	43 48	90 00	41 48	43 48
f 201	90 00	63 32	26 28	90 00	59 08	26 28

When mounted in refractive index media, and due to development of perfect {001} and {100} cleavages, the crushed powder provides a large number of fragments with approximately maximum birefringence, and about an equal number that yield nearly centered, negative, acute bisectrix figures (Fig. 2); the latter orientation, however, is the more obvious one owing to striking anomalous interference tints displayed therein.

X-RAY WORK

Rotation and Weissenberg photographs about the *a*, *b*, and *c* axes were taken with a 57.29 mm. diameter camera; nickel-filtered copper radiation (CuK$\alpha=1.5418$ Å) was employed, and although some degree of fluorescence resulted thereby, it did not prevent satisfactory study and measurement of films.

Appropriate measurement of zero layer Weissenberg films, calibrated with quartz, gave unit cell dimensions as follows:

$$a_0=8.12 \text{ Å}, \pm 0.01 \text{ Å}, b_0=5.14; c_0=7.82; \beta=94° 24'.$$

These data lead to a linear axial ratio of 1.5797:1:1.5214, compared with the figures derived from crystal measurement, *viz.* a:b:c=1.59 :1:1.52.

Indexing of Weissenberg films and a study of the systematic extinctions therein indicates that the space group is $C2$, $C2/m$, or Cm. Unfortunately this ambiguity could not be resolved further at this time.

The *x*-ray diffraction powder pattern is set out in Table 4, column 1, and the lines therein have been indexed on the basis of the unit cell constants determined for yavapaiite by single crystal work, and the reflections recognized on Weissenberg films. Indexing is not complete in the sense that each reflection observed on single crystal Weissenberg photographs has had a corresponding *d*-value calculated for it, since, at angles greater than about 79° 2θ, most of the lines are weak and many are quite

TABLE 3. COMPARISON OF YAVAPAIITE WITH THE MONOHYDRATE AND QUADRIHYDRATE

	Yavapaiite $K\,Fe^{3+}(SO_4)_2$ (This study)	Krausite $K\,Fe^{3+}(SO_4)_2 \cdot H_2O$ (Foshag, 1931)	Goldichite $K\,Fe^{3+}(SO_4)_2 \cdot 4H_2O$ (Rosenzweig and Gross, 1955)
α	1.593±0.002	1.588	1.582
β	1.684	1.650	1.602
γ	1.698	1.722	1.629
$\gamma - \alpha$	0.105	0.134	0.047
2V 5500 Å	29.5°	large	82° (calc.)
2V 5890 Å.	30.5°		
2V 7200 Å.	33.0°		
Optic sign	(−)	(+)	(+)
Dispersion	horizontal with $p>v$, strong	—	$p<v$, strong[1]
b	Z	Z	X
Extinction	$c \wedge X = 6°$ a=Y, or nearly so.	$c \wedge X^2 = 35°$	$c \wedge Z = 11°$
Color	colorless in section; otherwise very pale pink.	colorless in section; pale yellow and weakly pleochroic in thick grains.	colorless in section; greenish-yellow and lavender in artificial light.
Cleavage	{001}, {100} perfect; {110} distinct.	{001} perfect, {100} good.	{100} excellent.
Symmetry	monoclinic	monoclinic	monoclinic
Space group	*C*2, *C*2/*m*, or *Cm*	—	$P\,2_1/c$

[1] Determined by the present writer upon material from the type locality—Dexter No. 7 Mine, Calf Mesa, San Rafael Swell, Utah.

[2] Palache, Berman and Frondel (1951, p. 463) incorrectly state that the angle $Y \wedge c = -35°$.

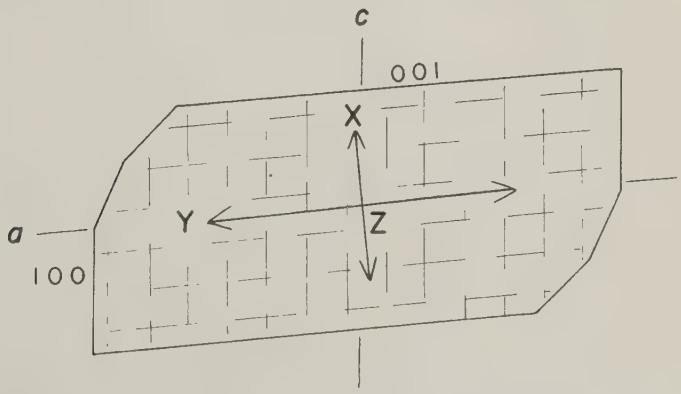

FIG. 2. Optical orientation of yavapaiite.

diffuse; under these circumstances indexing is uncertain. It should be realized, however, that many reflections, additional to those observed in the powder patterns, have been recognized on single crystal films; for in-

TABLE 4. POWDER PATTERNS OF YAVAPAIITE, AND ARTIFICIAL K $Fe^{3+}(SO_4)_2$.

Camera diameter: 114.59 mm. Radiation: CuKα=1.5418 Å.

	1		2	3			1		2	3	
hkl	*d* meas.	*d* calc.	*d* meas.	*d* meas.	I	*hkl*	*d* meas.	*d* calc.	*d* meas.	*d* meas.	I
001	7.85	7.79	7.88	7.82	90	204	1.706	1.706	1.707	1.710	5
110	4.35	4.35	4.35	4.33	5	313	—	1.703	—	—	—
200	4.05	4.05	4.06	4.05	40	$\bar{2}23$	1.700	1.700	1.700	1.701	1
002	3.90	3.90	—	—	2	130	1.6775	1.676	1.6775	1.6775	1
$\bar{1}11$	3.87	3.86	3.88	3.86	80	$\bar{4}03$	—	1.654	—	—	—
111	3.73	3.73	3.74	3.73	75	$\bar{1}31$	1.647	1.644	—	1.647	5
$\bar{2}01$	—	3.71	—	—	—	131	1.636	1.634	—	—	<1
201	3.49	3.49	3.49	3.49	60	223	—	1.633	—	—	—
$\bar{1}12$	2.97	2.96	2.98	2.97	100	420	—	1.590	—	—	—
$\bar{2}02$	2.92	2.92	2.92	—	<1	$\bar{4}21$	1.570	1.580	—	—	8
112	2.842	2.843	2.846	2.842	75	$\bar{3}14$	1.560	1.564	—	—	1
202	2.705	2.708	2.703	2.702	2	005	—	1.560	—	—	—
003	2.603	2.600	2.602	2.606	5	024	1.553	1.554	1.552	1.553	15B
020	2.572	2.570	2.577	2.570	35	$\bar{1}32$	—	1.549	—	—	—
021	2.441	2.441	—	2.441	<1	510	—	1.545	—	—	—
310	2.394	2.391	2.396	2.394	80	403	—	1.544	—	—	—
$\bar{3}11$	2.330	2.330	2.330	—	<1	$\bar{2}05$	1.534	1.540	1.534	—	1
$\bar{1}13$	2.283	2.270	2.285	2.282	20	421,$\bar{5}11$	—	1.537	—	—	—
$\bar{2}03$	2.260	2.266	—	—	<1	132	—	1.531	—	—	—
311	—	2.241	—	—	—	511	1.515	1.519	1.514	1.510	20
113	2.200	2.191	2.192	2.191	<1	$\bar{4}22$		1.505			
220	—	2.170	—	—	—		1.493		1.492	1.490	15B
022	2.151	2.147	2.152	2.152	25	$\bar{1}15$		1.487			
203	—	2.115	—	—	—	$\bar{2}24$	—	1.481	—	—	—
$\bar{2}21$	2.116	2.113	2.116	—	30	$\bar{5}12$	—	1.473	—	—	—
$\bar{3}12$	—	2.102	—	—	—	314	1.466	1.463	1.466	1.466	10
221	2.065	2.068	2.069	—	<1	$\bar{4}04$	—	1.461	—	—	—
400	2.027	2.024	2.027	2.027	5	115		1.449			
$\bar{4}01$	1.996	1.996	—	—	<1		1.447		1.448	1.446	30B
312	—	1.972	—	—	—	330		1.447			
004	1.951	1.950	1.952	1.953	<1B	422	—	1.443	—	—	—
$\bar{2}22$	1.933	1.930	1.934	1.934	20	$\bar{3}31$		1.433			
401	—	1.925	—	—	—		1.425		1.426	1.425	<1
222	1.867	1.865	1.865	1.867	25	224		1.422			
$\bar{4}02$	—	1.856	—	—	—	205	—	1.420	—	-	—
023	—	1.828	—	—	—	$\bar{1}33$	—	1.419	—	—	
$\bar{3}13$	1.824	1.822	1.824	1.824	35B	331	—	1.412	—	—	—
$\bar{2}04$	—	1.812	—	—	—	512	1.402	1.402	1.403	1.402	10
$\bar{1}14$	—	1.806	—	—	—	133	—	1.399	-	-	—
114	1.757	1.752	1.759	1.759	10	$\bar{4}23$	—	1.395	—	—	-
402	1.742	1.743	1.742	1.741	25	$\bar{3}32$	—	1.375	—	—	—

(*Continued on facing page*)

1. Yavapaiite, Jerome, Arizona.

2. Powder pattern yielded by R. C. Corey's material (author's own diffraction pattern).

3. Artificial K $Fe^{3+}(SO_4)_2$; compound prepared by the Dow Chemical Company, Midland, Michigan, and x-ray work by the present writer.

I=Intensities determined visually and referring specifically to yavapaiite in column 1.

B=Broad and usually diffuse line.

TABLE 4 (*Continued*)

1	2	3		1	2	3	
d meas.	*d* meas.	*d* meas.	I	*d* meas.	*d* meas.	*d* meas.	I
1.350	—	1.350	1	1.098	1.098	1.098	1
1.322	1.323	1.322	5	1.042	1.041	1.042	10B
1.306	1.307	1.306	1	.993	.993	.993	1B
1.286	1.288	1.286	15	.961	.961	.961	1
1.268	1.268	1.266	45	.947	.948	.947	1B
1.215	1.214	1.214	10	.920	.919	.920	1
1.198	1.198	—	15	.911	.911	.910	<1
1.171	1.171	1.170	10	.884	.884	.884	1
1.158	1.158	1.158	10	.811	.810	.810	<1B
1.145	1.144	1.145	1	.796	.796	.796	<1B
1.111	—	1.111	1	.781	.781	.781	<1

stance, between 0.884 and 0.811, 41 reflections have been observed whose *d*-spacings were calculated, but are not reported here.

In the first instance, the nature of this mineral was suspected on account of the similarity of its powder pattern with that recorded on ASTM card No. 3-0617 for artificial K $Fe^{3+}(SO_4)_2$ supplied to the Dow Chemical Company by R. C. Corey of the Combustion Engineering Corporation. Through the generosity of Dr. H. W. Rinn of the Dow Chemical Company of Midland, Michigan, the present author obtained a sample of Corey's material; furthermore, a second sample of K $Fe^{3+}(SO_4)_2$ was generously made available, and this had been prepared by Dow Company officers by vacuum crystallization of a solution containing K_2SO_4 and $Fe^{3+}{}_2(SO_4)_3$ in 1:1 mol ratio and subsequent heat-treatment of the crystallized product at 400° C. The *x*-ray powder patterns yielded by these two artificially prepared samples (Table 4, columns 2 and 3) are closely similar to that obtained with Jerome, Arizona material of natural origin.

At angles greater than about 65° 2θ, many of the reflections in the powder photographs become rather broad and diffuse, especially so at angles greater than 79° 2θ, so that precise measurement thereof is not always possible; nor is there any distinct resolution of α_1, and α_2 lines. This difficulty was not resolved by careful heating of the mineral, because the patterns yielded by yavapaiite heated in air to 280° C. and 400° C. for periods of 17 and 8 hours respectively, were in no sense distinct from the pattern recorded for the unheated material.

CHEMICAL PROPERTIES

When finely powdered yavapaiite is added to hot water, the mineral decomposes immediately with concomitant precipitation of ferric hydroxide, and production of a weakly acid solution. In cold water, on the

other hand, solution is extremely slow and precipitation of the hydroxide is not evident for several days. The mineral is readily soluble in warm 2N HCl to give a pale yellow solution that appears to be quite stable. When yavapaiite is heated in air to about 500° C. the mineral turns pale brown, and slightly stronger heating results in a deep red-brown powder. In a closed tube, the mineral decrepitates slightly, and a strongly acidic water is evolved.

Table 5. Analysis and Empirical Unit Cell Contents of Yavapaiite

	1	2	3		4	5		6
SiO_2+insol.	0.26							
Al_2O_3	0.11	0.11	.0014					
TiO_2	nil							
Fe_2O_3	27.69	27.82	1.9944	2.01	27.89	1.9980	2.0	27.82
FeO	0.07	0.07	.0051					
CaO	tr.							
MgO	0.08	0.08	.0108					
K_2O	15.39	15.46	1.8788	1.99	15.50	1.8836	2.0	16.40
Na_2O	0.62	0.62	.1145		0.62	.1144		
SO_3	55.58	55.84	3.9928	3.99	55.99	4.0012	4.0	55.78
H_2O at 105°C.	tr.							
H_2O-	0.14							
	99.94							

Cell contents: $(K, Na)_{1.99}(Al, Fe^{3+}, Fe^{2+}, Mg)_{2.01}[SO_4]_{3.99}$ or $(K, Na)_2Fe^{3+}{}_2[SO_4]_4$

1. Analysis of yavapaiite (analyst: C. Osborne Hutton).
2. Analysis of yavapaiite with SiO_2 removed; total recalculated to 100.
3. Cations on the basis of 16 oxygen atoms per unit cell.
4. Analysis of yavapaiite with SiO_2, Al_2O_3, FeO, MgO removed; total recalculated to 100.
5. Cations for analysis in column 4 on the basis of 16 oxygen atoms to the unit cell.
6. Theoretical composition of $K\ Fe^{3+}(SO_4)_2$ in weights per cent.

A complete chemical analysis was made of a sample composed of crystal fragments that had been concentrated by hand-picking, and any particles that appeared to be contaminated with sulphur, voltaite, jarosite, or any other extraneous material were rejected. Accordingly, it is believed that the analysis (Table 5) is representative of very nearly pure yavapaiite. Small amounts of SiO_2, Al_2O_3, FeO, and MgO were found to be present, and SiO_2, at least, is possibly an impurity; this oxide has been set aside from the analysis reported in column 2, whereas the other three oxides have been omitted in column 4. In both cases (columns 2 and 4, Table 5) the empirical unit cell contents have been

calculated on the basis of 16 oxygen atoms. The total quantities of ions other than Fe^{3+}, K, Na, and S are very small, and the results of calculations set out in column 3 do not differ significantly from those listed in column 5. It is not clear, therefore, whether the small amounts of Al, Fe^{2+}, and Mg represent contamination of the sample of yavapaiite by minute amounts of other compounds, or not, but the results of a spectrographic analysis (Table 6) of very carefully selected water-clear crystal fragments of this mineral tends to support the conclusion that small amounts of Al and Mg are present in the pure mineral; and the same may be true for SiO_2 as well.

Table 6. Spectrographic Analysis of Yavapaiite

Major Elements:		
Fe > 10 per cent.		
K > 5 per cent.		
Minor Elements:		
Na < 0.3 per cent.	Mn = 0.005–0.01	
Si = 0.1 –0.2	Mo = 0.005–0.01	
Ca = 0.1 –0.15	Cu = 0.001–0.005	(part of this could come from electric motors in operation nearby).
Al = 0.05–0.1		
Mg = 0.01–0.05	Ag = 0.001 ±	
B = 0.01	Ba = 0.001 ±	
Ti = 0.01–0.03	Rb seems to be present, but lines are obscured by CN lines.	
Elements Undetected:		
Li, Sr, V, Cr, Co, Ni, Au, Zn, Cd, Hg, Sn, Pb, Bi, Sb, As, Te, P, Be, Ga, Ge, Th, U, Zr, In, W, Cs, rare earths, and platinum.		

Attempts were made to prepare yavapaiite by careful dehydration of krausite, goldichite, and potassium iron alums, but these experiments failed in every case; none of the products obtained yielded *x*-ray diffraction patterns that were in any way comparable to that typical of yavapaiite.

Acknowledgments

I wish to acknowledge gratefully the kindness of Dr. H. W. Rinn, Spectroscopy Laboratory, The Dow Chemical Company, Midland, Michigan, for his gift of two samples of artificial K $Fe^{3+}(SO_4)_2$, and for his helpfulness in allowing me to record data secured from my study of these samples. It is a pleasure to acknowledge Dr. John Stone's assistance in connection with the spectrographic analysis of yavapaiite, Dr. Michael Fleischer's courtesy in offering an opinion as to the suitability of the name given to the mineral, Mr. Scott J. Williams' donation of ma-

terial that formed the basis of this study, and finally Dr. F. G. Tickell's assistance in the laboratory in many ways.

Literature Cited

Larsen, C. (1928), Hydrous sulphates formed under fumerolic conditions at the United Verde Mine: *Am. Mineral.*, **13,** 203–229.

Foshag, W. F. (1931), Krausite, a new sulphate from California: *Am. Mineral.*, **16,** 352–360.

Palache, C., Berman, H., and Frondel, C. (1951), Dana's System of Mineralogy, 7th ed., vol. 2, John Wiley and Sons, Inc., New York.

Rosenzweig, A., and Gross, E. B. (1955), Goldichite, a new hydrous potassium ferric sulfate from the San Rafael Swell, Utah: *Am. Mineral.*, **40,** 469–480.

Manuscript received January 30, 1959.

THE AMERICAN MINERALOGIST, VOL. 44, NOVEMBER–DECEMBER, 1959

SILICATE GARNET—YTTRIUM-IRON GARNET SOLID SOLUTIONS

S. Geller and C. E. Miller, *Bell Telephone Laboratories, Incorporated, Murray Hill, New Jersey.*

Abstract

In the system $Ca_3Al_2(SiO_4)_3$—$Y_3Fe_2(FeO_4)_3$, a series of solid solutions exists over the range 10–100% $Y_3Fe_2(FeO_4)_3$. Similar to the system spessartite—yttrium-aluminum garnet, this system does not follow a linear composition vs. lattice constant law. Under the conditions of the experiments, a complete series of solid solutions does not exist in the system $Mn_3Al_2(SiO_4)_3$—$Y_3Fe_2(FeO_4)_3$ although there is some solution at the ends. The system $Ca_3Al_2(SiO_4)_3$—$Gd_3Fe_2(FeO_4)_3$ is similar to that of the $Ca_3Al_2(SiO_4)_3$ $Y_3Fe_2(FeO_4)_3$ system but under similar experimental conditions does not appear to have as wide a range.

Introduction

In a continuing program designed to learn more about the crystal chemistry of and interactions among magnetic ions in the garnets (1–4), we have studied in some detail the systems $Ca_3Al_2(SiO_4)_3$ $Y_3Fe_2(FeO_4)_3$ and $Mn_3Al_2(SiO_4)_3$—$Y_3Fe_2(FeO_4)_3$. We have also examined solid solutions in the system $Ca_3Al_2(SiO_4)_3$—$Gd_3Fe_2(FeO_4)_3$.

Grossularite—Yttrium-Iron Garnet System

In the preparation of specimens, the appropriate amounts of oxides were thoroughly mixed. The mixture of reactants was compressed into a pellet. Firing was carried out at 1350–1400° C. Samples containing more than 50 mole % of the silicate reactants melted to form glasses; on annealing these glasses at about 1150° C. for two hours, single garnet phases were obtained. Samples with 50 mole % or less of silicate reactants did not melt; these were usually fired for about 2 hrs, cooled, reground, compacted and refired. The procedure was repeated (2–3 times) until the powder photograph indicated a single phase.

In the $Ca_3Al_2(SiO_4)_3$ -$Y_3Fe_2(FeO_4)_3$ system, solid solutions containing between 0 and 90 mole % $Ca_3Al_2(SiO_4)_3$ were obtained. The lattice constants of the solid solutions (Table 1 and Fig. 1) do not follow a linear law. The behavior is similar to that of the spessartite- -yttrium-aluminum garnet system; (5) that is, the values of a_0 lie above the line joining the lattice constants of the end-members.

Grossularite itself has been studied in great detail (6) and synthesized by Yoder (7) and by Coes (8). Apparently, it has not been found possible to synthesize grossularite at atmospheric pressure or thus far from the dry components, although Yoder (6) has shown that it should be possible for it to form in this way.

TABLE 1. LATTICE CONSTANTS, $Ca_3Al_2(SiO_4)_3-Y_3Fe_2(FeO_4)_3$ SYSTEM

Mole % $Y_3Fe_2(FeO_4)_3$	Lattice constant, Å
0	11.851 (Ref. 7)
10	12.005
30	12.11
50	12.225
80	12.35
90	12.365
100	12.376

Attempts were made to crystallize the garnet phase out of 99, 98 and 95 mole % silicate (reactants) melts under the conditions described above; these were unsuccessful. Nevertheless, it is interesting that the presence of only 10 mole % of the yttrium-iron garnet constituents leads to the nucleation of the garnet phase.

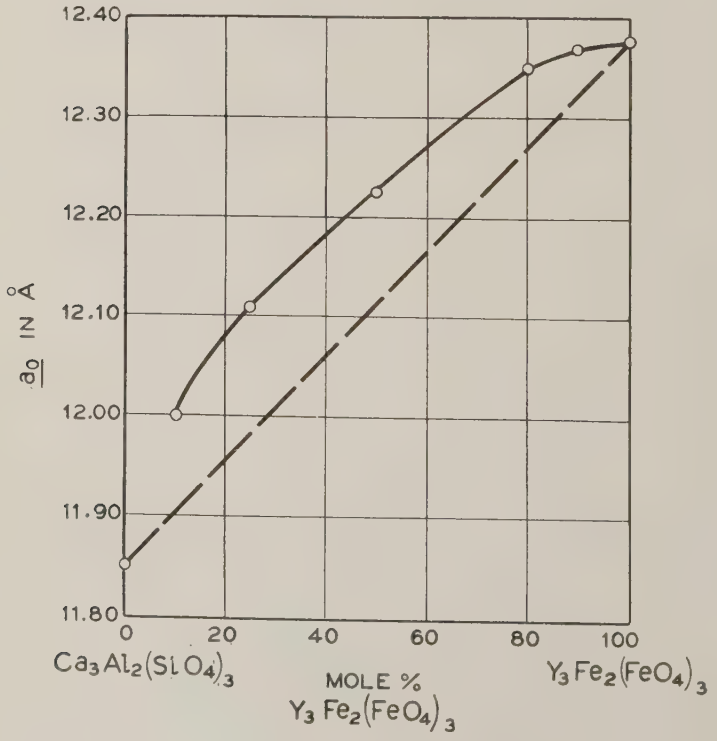

FIG. 1. Grossularite—yttrium-iron garnet system.

Spessartite—Yttrium-Iron Garnet System

The experiments in this system indicate that the two garnets, spessartite and yttrium-iron garnet, are not completely miscible.* There is indication that perhaps somewhat more than 20 mole % $Mn_3Al_2(SiO_4)_3$ will dissolve in $Y_3Fe_2(FeO_4)_3$. Samples containing 50 mole % (reactants) of each gave two or more phases. In all cases garnet phases appeared. Also present was a spinel-type phase, probably $Mn_xSi_yFe_{3-x-y}O_4$.

The samples containing 5, 10 and 90 mole % *yttrium-iron garnet* did not contain extraneous phases. However, a solution range was indicated in the photograph of the 10 mole % specimen. The sample containing 80 mole % $Y_3Fe_2(FeO_4)_3$ was mostly a garnet phase but the powder photograph indicated the presence of an extraneous phase. Thus the lattice constant, 12.229 ± 0.003 Å, of the garnet phase is probably not representative of the 80 mole % solution.

Table 2. Lattice Constants, $Mn_3Al_2(SiO_4)_3-Y_3Fe_2(FeO_4)_3$ System

Mole % $Y_3Fe_2(FeO_4)_3$	Lattice constant, Å
0	11.621 ± 0.004
5	11.68 ± 0.01
10	11.73 ± 0.01
90	12.34 ± 0.01
100	12.376 ± 0.004

The 20 mole % yttrium-iron garnet specimen contained a wide solid-solution range of garnet phases with lattice constant range of approximately 11.71–11.90 Å, indicating that the high end represents an approximately 20 mole % yttrium-iron garnet solid solution. The 50 mole % specimens gave various results; the largest lattice constant observed for a garnet phase in these was 12.02 Å, probably indicating a 30–40 mole % yttrium-iron garnet solid solution.

The lattice constants (Table 2) of the pure garnet phases are plotted in Fig. 2. In this system also, a linear composition vs. lattice constant law is not followed.

Grossularite—Gadolinium-Iron Garnet System

Because the sizes of the Y^{3+} and Gd^{3+} ions do not differ very much, it should be possible to form a series of solid solutions in the $Ca_3Al_2(SiO_4)_3-Gd_3Fe_2(FeO_4)_3$ system, at least as extensive as that of the $Ca_3Al_2(SiO_4)_3-Y_3Fe_2(FeO_4)_3$ system. We have actually studied only

* That is, under the *conditions* of the experiments.

the ends of the system. A very good specimen of the solid solution containing 80 mole % $Gd_3Fe_2(FeO_4)_3$ has been made yielding a lattice constant of 12.402 ± 0.003 Å. As expected, this result gives a point on the

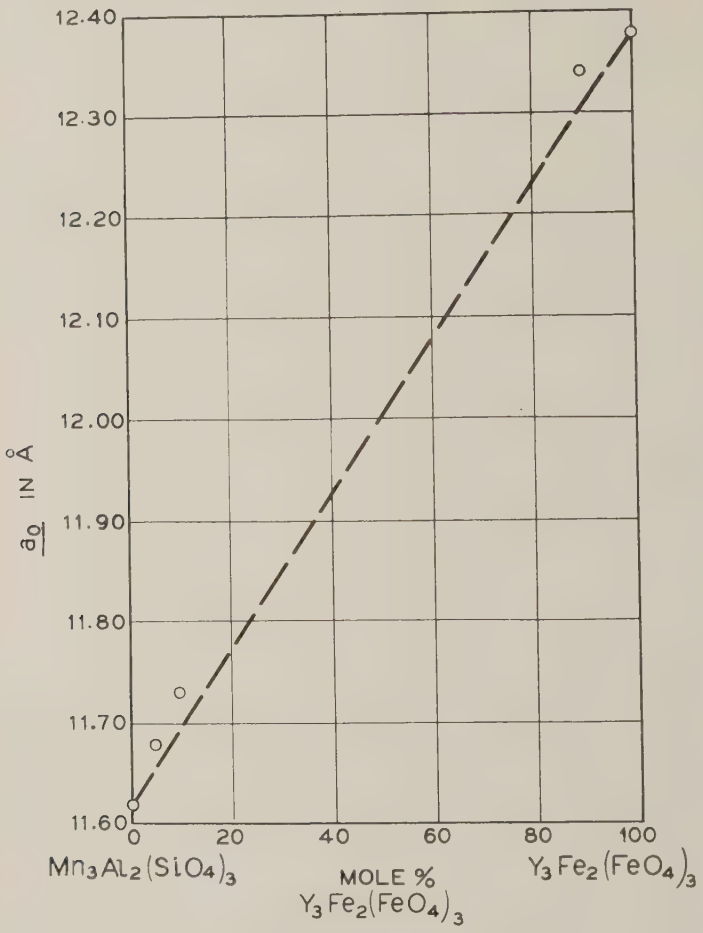

FIG. 2. Spessartite—yttrium-iron garnet system.

lattice constant vs. composition diagram (Fig. 3) lying significantly above the straight line joining the end-member lattice constants.

Attempts to prepare solid solutions containing 10 and 20 mole % $Gd_3Fe_2(FeO_4)_3$ in the same way as in the preparation of like solutions with $Y_3Fe_2(FeO_4)_3$ did not yield garnets. Thus, under these conditions, the series of solid solutions in the $Ca_3Al_2(SiO_4)_3$ —$Gd_3Fe_2(FeO_4)_3$ system does not extend as far as in the $Ca_3Al_2(SiO_4)_3$ —$Y_3Fe_2(FeO_4)_3$ system.

Additional Comments

The deviation of solid solutions of mixed valency garnets from a linear lattice constant law may be a consequence of ion distribution and of the disorder which is caused by the differences in ionic size and electrostatic

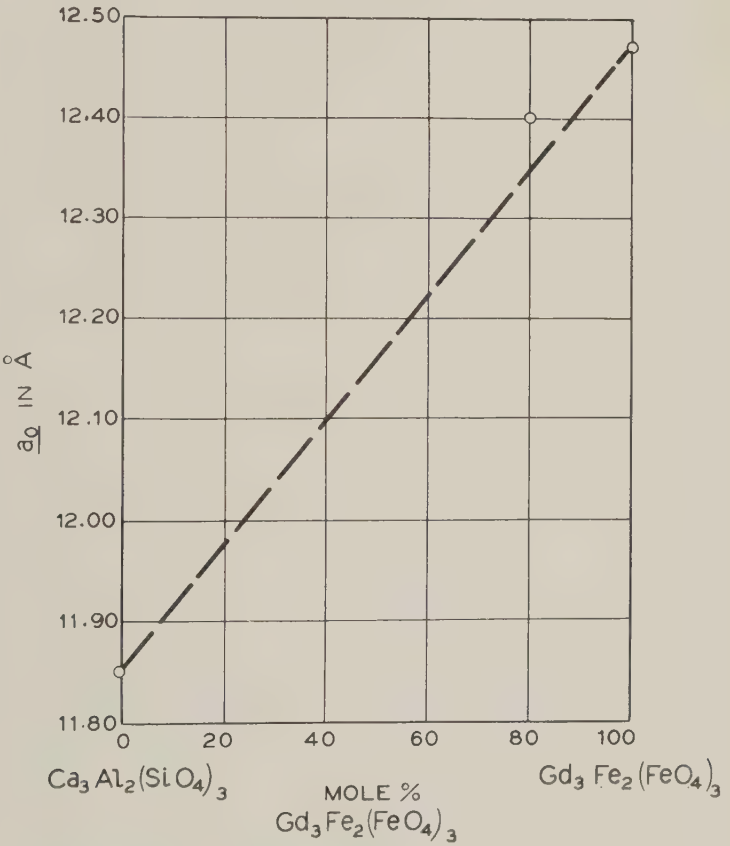

Fig. 3. Grossularite—gadolinium-iron garnet system (in part).

effects arising from valency differences. A report is in preparation on the ionic distribution in some of these solid solutions as determined by means of magnetic susceptibility vs. temperature measurements (9).

References

1. Geller, S. and Gilleo, M. A., *Jour. Phys. Chem. Solids* **3**, 30 (1957).
2. Gilleo, M. A. and Geller, S., *Phys. Rev.* **110**, 73 (1958).
3. Abrahams, S. C. and Geller, S., *Acta Cryst.* **11**, 437 (1958).

4. Gilleo, M. A. and Geller, S., A.I.E.E. Conference on Magnetism and Magnetic Materials, Phila., Pa., Nov., 1958, Paper #131. See also *Jour. Phys. Chem. Solids*, **10,** 187 (1959).
5. Yoder, H. S. and Keith, M. L., *Am. Mineral* **36,** 519 (1951).
6. Yoder, H. S., *Jour. of Geology*, **58,** 221 (1950).
7. Skinner, B. J., *Am. Mineral* **41,** 428 (1956).
8. Coes, L., *Jour. Amer. Ceram. Soc.* **38,** 298 (1955).
9. Bozorth, R. M. and Geller, S., *Jour. Phys. Chem. Solids* (In press).

Manuscript received January 28, 1959.

THE AMERICAN MINERALOGIST, VOL. 44, NOVEMBER–DECEMBER, 1959

THERMOLUMINESCENCE OF ROCKS AND MINERALS

PART I. AN APPARATUS FOR QUANTITATIVE MEASUREMENT

DONALD R. LEWIS, THOMAS N. WHITAKER,* AND CARL W. CHAPMAN,
Shell Development Company, Exploration and Production Research Division, Houston, Texas (Publication No. 190)

ABSTRACT

Equipment which permits quantitative recording of the thermoluminescence emitted by samples with a high degree of reproducibility and sensitivity has been developed. The equipment operates over the temperature range from 25° C. to 600° C. at rates from 10° C. per minute to 100° C. per minute. The apparatus has high light-detection sensitivity and broad spectral response. The construction combines reliability and flexibility with simplicity of operation. Not more than 50 milligrams of sample is ordinarily required.

An analysis of the instrumental and physical factors which determine the precision of making glow curves is made to evaluate the requirements for each section of the apparatus.

INTRODUCTION

Measurements of thermoluminescence have been made for several purposes, such as fundamental physical studies (Halperin, Braner, and Alexander, 1957), radiation dosimetry (Daniels, Boyd, and Saunders, 1953), studies of meteorites (Houtermans, Jäger, Schön, and Stauffer, 1957), applications to stratigraphy (Parks, 1953; Saunders, 1953; Bergstrom, 1956; Pitrat, 1956), age estimation in sediments (Zeller, Wray, and Daniels, 1957), and the identification or determination of certain minerals (Lewis, 1956). The demands of each application require equipment designed to meet the specific needs of the problems for which the thermoluminescence data are to be used. The equipment described in this paper has been designed to measure and record the thermoluminescence of rocks and minerals with sufficient accuracy and repeatability that records may be quantitatively compared over long periods of time. Operation of this equipment has been made as simple and convenient as possible, consistent with the other requirements of the measurements. The equipment is the culmination of several years' experience in measuring the thermoluminescence of natural samples.

The present equipment measures the thermoluminescence of a powdered sample of not more than 50 mg. over the temperature range from 25° C. (room temperature) to 600° C. The rate of temperature rise of the sample is constant over the operating temperature range and may be varied from 10° C. to 100° C. per minute in steps of 10° C. per minute.

The interrelation of the various sections of the equipment is shown in the block diagram (Fig. 1). The constancy of rate of temperature in-

* Present address: University of Houston, Houston, Texas.

crease is accurately maintained by continuous comparison in the program controller of the voltage produced by a thermocouple in the sample heater with a prescribed voltage which corresponds to an exactly constant rate. Any deviation of sample temperature from what has been prescribed at a given instant will modify the amount of heater power which is supplied by the magnetic amplifier.

This method of controlling the heating rate of a sample has been found generally useful and has been adapted to other applications, such as programing temperatures of samples in x-ray diffraction studies (Rowland, Weiss, and Lewis, 1959).

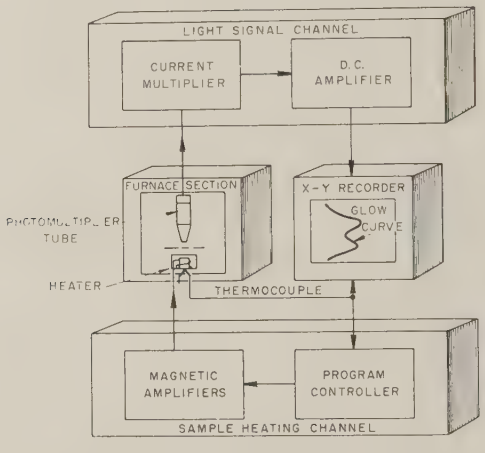

FIG. 1. Block diagram of thermoluminescence equipment showing functional interrelation of various sections.

The glow of the thermoluminescence is detected by a photomultiplier tube operated so that the output current is accurately proportional to the light intensity. Since the intensity of thermoluminescence varies greatly from sample to sample, this detector must operate from the lowest possible levels of light intensity up to the highest levels at which the current output is still proportional to intensity. The limit of low-level operation is determined by the dark current, which is principally produced by thermally liberated electrons in the photomultiplier tube. This dark current is reduced substantially by keeping the tube at $-80°$ C., the temperature of dry ice. By operating in this manner, a range of light intensities of a million to one can be covered quantitatively. The photomultiplier type selected has the broadest spectral response available, since the color of the thermoluminescence varies considerably from one type of mineral to another.

The current from the photomultiplier tube is amplified to a convenient level for recording on a strip-chart recorder. This equipment uses an X-Y recorder indicating light intensity as a function of temperature.

Discussion of Physical Principles of Thermoluminescence

Nature of Thermoluminescence (Garlick, 1949)

When an alpha particle, gamma ray, or other high-energy radiation passes through matter, it transfers some of its energy to this matter by

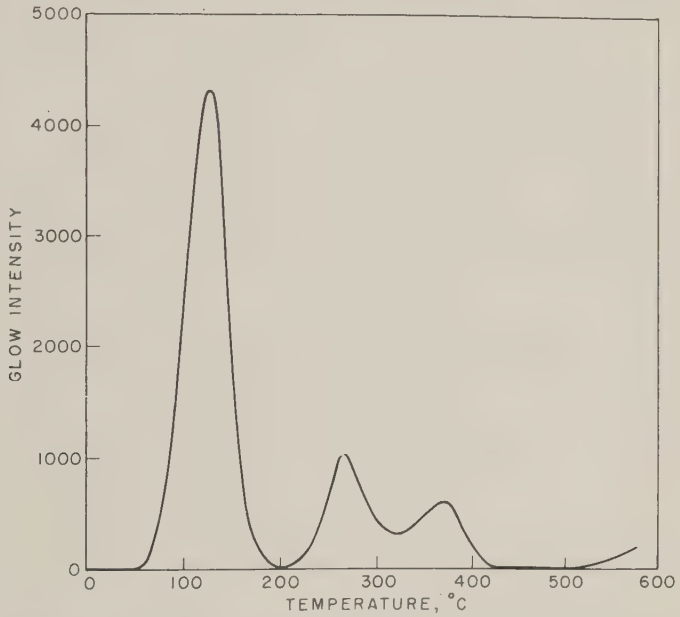

Fig. 2. Typical thermoluminescence glow curve of calcite following gamma irradiation with Cobalt-60. Heating rate 80° C. per minute. Light intensity in arbitrary units.

producing clouds of excited electrons which are dissociated from their original atoms. In metals and semiconductors, these electrons have high mobility in the crystal and dissipate their excess energy as heat. In insulating crystals, however, some of these excited electrons become localized in the crystal at structural defects. If the temperature of the crystal is raised, the probability of escape increases rapidly. As these trapped electrons are released, some of them drop to lower energies by emitting a photon of light. This light emission produced by thermal liberation of stored electrons is called thermoluminescence.

If a sample containing trapped electrons is heated, light is emitted in a series of discrete maxima as the sample temperature rises. Each maxi-

mum in the light intensity corresponds to a certain energy of trapped electrons and is related to the detailed structure of the crystal. A curve of the thermoluminescence light intensity as a function of the sample temperature is called a glow curve. A typical glow curve for calcite following gamma irradiation in the laboratory is shown in Fig. 2. Samples are irradiated in a cylindrical cobalt-60 gamma ray source as previously described (Lewis, 1956; Saunders, Morehead, and Daniels, 1953).

Glow-Curve Equation

The shape of a glow curve can be described mathematically if certain simplifying assumptions are made as follows:

1) The rate of release of trapped electrons is proportional to the number of electrons present.

2) The electrons giving rise to one particular glow-curve peak all have the same energy.

3) When a trapped electron has been released, the probability of its returning to a lower energy is much greater than the probability of its being retrapped.

If any of these assumptions is changed, a different mathematical expression will be necessary to describe the glow curve. However, these assumptions are physically reasonable in many systems and lead to the following equation for each glow-curve peak:

$$I(T) = Cn_0 s \exp\left[-\int_0^T (s/\beta)e^{-E/kT}dT\right] e^{-E/kT} \qquad (1)$$

where

I = thermoluminescence light intensity
T = absolute temperature, degrees Kelvin
C = geometrical constant
n_0 = initial number of trapped electrons
s = frequency factor in seconds^{-1}
β = the heating rate, $\beta = dT/dt$, degrees per second
E = trap energy of electrons, electron volts
k = Boltzman's constant, 8.62×10^{-5} ev/degree

In order to be able to solve this equation, it is necessary to know how the heating rate, β, depends on temperature. The simplest condition is that of constant heating rate, or $\beta = dT/dt =$ constant. Since the intensity depends exponentially on the heating rate, small changes in heating rate will distort the glow curve. For the present equipment a departure of 2° C. from the prescribed ideal linear program is the maximum allowable deviation.

The range of heating rates was selected such that for the size of sample particle regularly used for these studies (40 mesh or finer) and for the chemical compositions normally encountered (mainly ionic solids) there

should not be a temperature spread of more than 2° C. from the top to the bottom of the sample. The maximum rate of 100° C. per minute is within this range and establishes the power requirements of the magnetic amplifier which supplies current to the sample heater.

The temperature range of interest can include the lowest temperatures at which experimental work could be done up to that at which the incandescence of the sample masks any luminescence. Since this equipment is largely directed toward the natural thermoluminescence of samples which have been at geologic formation temperatures for long times, room temperature is a convenient lower limit. The temperature at which the incandescence of the heater dominates the glow of the system depends on the sensitivity at which the detector is operated. This always occurs before 600° C. which fixes the upper limit of operation.

The intensity of the emitted thermoluminescence depends on the following factors, as described by equation (1):

1) The number, n_0, of electrons trapped in the sample initially. This will in turn depend on the number and kind of crystalline defects in the sample, the amount of high-energy radiation which has been absorbed, and the temperature at which the sample has been maintained.

2) The heating rate. In general, the higher the heating rate the higher the peak height. The area of the peak, however, is constant at various heating rates. The limitation on the heating rate is usually determined by the problem of making the temperature within each crystal of the sample follow sufficiently close to the temperature of the heater. For measurements where the primary consideration is to obtain a maximum signal-to-noise ratio, very high heating rates such as 50 degrees per second have been used.

3) The geometrical constant, C. This number includes not only the solid angle of light collection and losses due to multiple internal reflections in small particles, but also the internal absorption due to the color of the sample.

Experimental Considerations

The indicated intensity of thermoluminescence, in addition to these factors, depends on the spectral response of the detector photomultiplier for the particular color of the glow. The glow from minerals of various types covers at least the entire range of the visible spectrum, so that the photomultiplier should be selected whose spectral response most closely matches the spectrum of the samples being studied. For example, thermoluminescence from calcites and dolomites lies in the orange-red region of the spectrum. Measurements on these samples should, therefore, use a photomultiplier with a high sensitivity to red colors.

The intensity of the glow of minerals when heated varies enormously

from the lowest levels of detectability to brilliant glows a million times more intense. As an average for qualitative comparison, a surface brightness of about 10 microlamberts is a typical value for many minerals.

Sources of Error

Sampling

With any natural materials, variations in composition and structure will be reflected as variations in thermoluminescence. This requires that samples be thoroughly blended and quartered if ground materials are used. This is probably the largest single source of variation in the quantitative study of thermoluminescence.

Weighing

In the range of sample weights used in this apparatus, the amount of thermoluminescence produced is directly proportional to the weight of the sample. For quantitative work, all samples are accurately weighed on a torsion-type microbalance which can be read directly to 0.2 mg. At the usual sample weight of 50 mg., this introduces an uncertainty of $\pm 0.4\%$.

Geometrical

This source of variation arises from the fact that light-collection efficiency depends on the mechanical distribution of the sample in the heater. To reduce this source of uncertainty, particle size and sample weights have been selected to insure a sample thickness of one particle layer. As long as the strict proportionality between sample weight and amount of thermoluminescence is maintained, the contribution of geometrical errors is insignificant.

Instrumental

The contributions of the individual portions of the electronics to the variations in measured thermoluminescence are estimated as each section of the equipment is discussed. In general, however, the stability of the electronics is as good as required to make the contribution of the electronics small compared to other sources of error.

Heating-Rate

General Considerations

The heating-rate section must increase the sample temperature along a prescribed path at the rates and with the repeatability required by the use which is to be made of the experimental data. The factors which must be considered for a constant rate of temperature rise are (1) range of

heating rates, (2) reproducibility of average heating rate, (3) allowable variations in instantaneous heating rate, and (4) constancy of temperature rise over operating temperature range.

A brief examination of the fundamental physical principles involved will aid in understanding the requirements for these various factors.

The glow curve is described analytically by equation (1). From this equation it can be demonstrated that the temperature at which a peak of the glow curve appears depends strongly upon the heating rate. As an example, for typical dolomite and calcite samples, a change of 2 degrees per minute in the average heating rate results in a shift of about 5 degrees in the location of these peaks. From equation (1) it can also be shown that variations in the instantaneous heating rate cause pronounced fluctuations in the intensity of the emitted thermoluminescence.

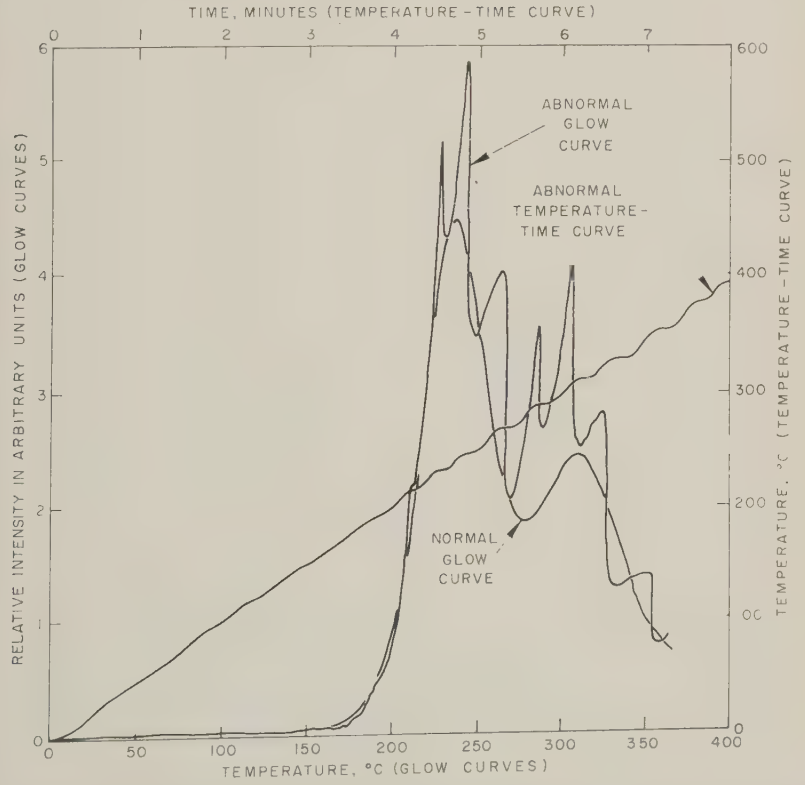

FIG. 3. Distortion of glow curve produced by small fluctuations deliberately introduced in the heating rate. Normal glow curve of same sample with constant heating rate shown for comparison.

As the heating rate, β, increases, traps are emptied at a greater rate and the intensity, I, of the glow increases. The subsequent drop in instantaneous heating rate reduces the rate at which traps are emptied and results in a low intensity. This effect is more pronounced at low heating rate (see Fig. 3).

As the heating rate increases, the thermal gradient in the sample also increases. To limit this temperature differential within the sample to less than 2° C., the heating rate is limited to 100° C. per minute. In this equipment, ten heating rates are provided ranging from 10° C. to 100° C. per minute. The operating temperature range is from 25° C. to approximately 600° C.

For fulfilling these requirements, the general approach to the design of equipment is to use a high-gain electrical-thermal feedback system. High sensitivity and power gain are provided by a vacuum-tube amplifier driving a two-stage magnetic amplifier. The basic plan of the heating channel is shown in Fig. 4.

Temperature-Sensing Element

For optimum usefulness in this system, the temperature-sensing element should have the following output characteristics:

1) Produced as an electromotive force.
2) High sensitivity to temperature.
3) Electromotive force linear with temperature over operating range.
4) Rapid thermal response.

The chromel-alumel thermocouple very nearly satisfies all these requirements. It has an average sensitivity of 41.5 microvolts per degree centigrade over the entire operating range; the sensitivity never departs from this value by more than 2 per cent. Excellent thermal response is obtained by imbedding the separate thermocouple leads on opposite sides of a silver block on which the sample is heated and across which there is a negligible temperature gradient.

Program Controller

The function of the program controller unit is to develop a voltage which increases linearly with time and corresponds in magnitude to the thermocouple voltage desired at each instant. This voltage is compared continuously to the actual thermocouple voltage, and this difference or error signal is used to control the instantaneous power to the heating coils.

The thermocouple voltage is also used as the input to the Y axis chart drive of the recorder to produce a deflection proportional to the sample temperature.

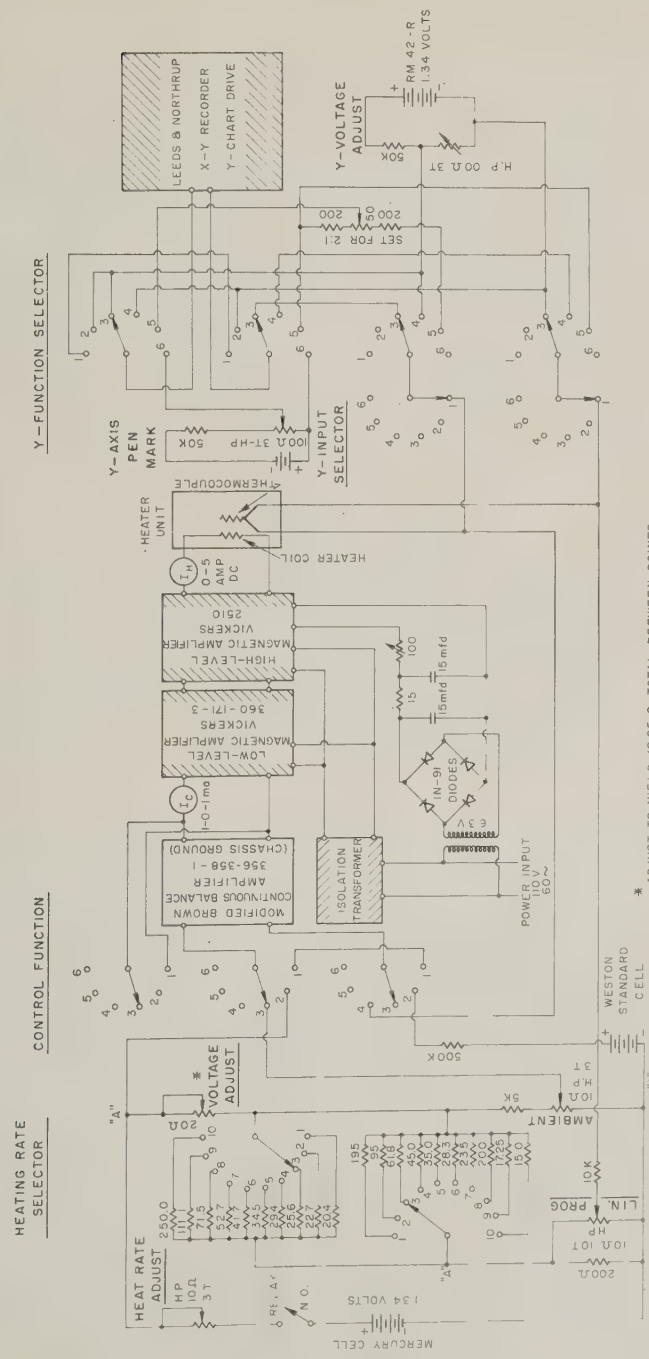

FIG. 4. Schematic electrical circuit of the heating rate section of the thermoluminescence equipment.

The linear increase of voltage is obtained by using a small synchronous motor to drive a precision potentiometer, the output voltage of which is proportional to time. The various heating rates are selected by switching different resistors in series with the heating rate potentiometer to change the voltage across its terminals. This produces a proportional change in the rate at which the control voltage raises. All of the components of this section are selected for long-term stability.

The precision with which a particular heating rate is programed depends upon both the precision with which the potentiometer voltage can be established and any fluctuations in the speed of the synchronous motor. A standard reference cell is provided to permit precise measurement of the voltage supplied to the potentiometer. When operated from normal commercial electric power sources, the synchronous motor will not ordinarily introduce an uncertainty of more than 0.05 per cent in the heating rate.

Error-Sensing Amplifier

The difference voltage or error signal which results when the thermocouple output differs from the program controller voltage is supplied to a high-gain, chopper-stabilized amplifier.* The output circuit of this amplifier has been modified to provide a direct current suitable for control of the magnetic amplifier. The amplifier produces about 100 microamperes per microvolt input which corresponds to about 4 microamperes for 0.001° C. equivalent error signal.

Magnetic Amplifiers

The error-sensing amplifier drives the low-level magnetic amplifier which, in turn, supplies control current for the high-level magnetic amplifier. The low-level unit has a current gain of about 750. The overall gain of the two magnetic amplifiers together is such that a temperature error of 0.001° C. results in a change of approximately 15 watts power to the heater coils. The rated maximum output is 280 watts into a 12-ohm heater coil. The system saturates so that the maximum power output obtained in use is about 350 watts.

Heater

There are four basic requirements to be met by the heater used in this thermoluminescence equipment:

1) Even heating of sample.
2) Constant brightness of heater cup surface.

* Minneapolis-Honeywell Brown Electronik® Amplifier Type 3563581 modified as shown in Reference Drawing 21-G-95, MH Instruction 6002.

3) Small differences in temperature within the heater.

4) Electrical characteristics of the heater which match available power sources.

In the design of the heater, several types of construction were considered. At one extreme is the massive heater with a long thermal time constant. By supplying sufficient power to this block, the temperature can be raised linearly and minor variations will be smoothed by the thermal inertia. However, power demands are great for such a system. At the other extreme is the heater with the smallest possible thermal time

FIG. 5. Cutaway drawing showing construction details of plug-in heater units. Sample is placed in the well in the center of the heater.

constant. In this case, the temperature responds quickly and consequently makes severe demands on the control system. The heater used lies between these two extremes. This results in a system which responds quickly but also has enough thermal inertia to provide reasonable filtering action. The closer matching of the thermal and electrical time constants renders the amplifier system less sensitive to the choice of the operating point.

Radiation losses have been reduced by a ceramic heat-reflecting shield placed coaxially around the heater block. Without this, power demands become excessive as radiation becomes the significant mode of heat transfer. This radiant shield does not affect the linearity at low temperatures since heat losses here are due mainly to conduction and convection.

Some of the details of construction are shown in Fig. 5. The silver fur-

nace is shown in cutaway section. The two chromel-alumel thermocouple leads are silver-soldered into small holes at the bottom of the furnace. The heater coil is a 13-ohm helix of 26 B&S gage nichrome wire wound on the inside of the radiant shield. The heater box is made of transite. Electrical connections are through silver-plated banana plugs to facilitate removal and substitution of heaters. A close-fitting metal ring is placed around the top of the heater block during operation. This prevents light from the glowing heater coil from reaching the photomultiplier if small cracks develop in the transite top because of continued use.

Performance

The over-all performance of the sample-heating section can be checked by recording the output of the heater thermocouple as a function of time. The graph obtained should be a linearly rising line from which the program linearity heating rate, and reproducibility can readily be determined. Typical operating behavior of this equipment is illustrated in Tables 1 and 2.

The Light-Signal

General Considerations

The function of the light-signal section is to detect and record the intensity of the light emitted by the heated sample. From repeated glow curves of the same sample, it has been found that better than 5% pre-

Table 1. Long Term Stability of Average Heating Rate

Date of Experiment	Heater Number	Observed Heat Rate (°C./min.)	Average Heat Rate (°C./min.)	Maximum Deviation from Linearity (°C.)
9- 6-57	110	76.1	77.5	±1.8
9- 6-57	110	76.9		±1.5
9- 9-57	114	79.9		±1.2
10- 6-57	114	77.0		±1.8
2-26-58	114	76.7	78.0	±1.2
2-27-58	113	78.8		±1.5
2-27-58	113	78.8		±2.1
2-28-58	110	77.8		±1.8
10-23-58	111	78.4	78.1	±1.7
10-23-58	110	77.6		±1.8
10-23-58	113	78.6		±1.0
10-23-58	113	77.9		±1.0

Table 2. Linearity of Various Heating Rates

(The Experimental Values Reported Here Are Typical)

Nominal Heat Rate (degree/min.)	Actual Heat Rate (°C./min.)	Maximum Deviation from Linearity (°C.)
10	9.8	±0.1
20	19.7	±1.0
50	49.3	±1.0
80	78.5	±1.0
100	96.0	±1.0

cision can be maintained in the recorded light intensities by proper operator technique. This sets the limit of the precision of the measurements. Any error in measurement introduced by the light electronics is to be less than 1%. Some possible sources of variation are

1) Photomultiplier tube gain changes.
2) Photomultiplier tube fatigue.
3) Variations in phototube dark current.
4) Changes in the resistance values in the signal path.
5) Instability in the dc amplifier or the X-Y recorder.

Since it is known that the wavelengths of the thermoluminescence of minerals extends at least from the near-ultraviolet through the near-infrared, it is important to have a detecting element with the broadest possible spectral response. The intensity of the light emitted covers a very wide range and depends upon the characteristics of the sample and on the heating rate.

Block Diagram

The heart of the light-signal channel is the photomultiplier tube which converts the low-level light intensities into electrical current. Thus current is amplified and recorded on the X axis of a strip-chart recorder. Since the dc amplifier is operated at constant gain, a current multiplier is provided to allow the operator to utilize the full width of the strip chart. The Y-deflection is provided by motion of the paper, which is driven by the heater thermocouple voltage. The resulting curve is a plot of light intensity vs. temperature. The temperature scale is independent of the heating rate, which simplifies the intercomparison of the various glow curves. A block diagram of this channel is shown in Fig. 6.

Photomultiplier Application

The very high light sensitivity of photomultiplier tubes has made these measurements possible. These tubes have excellent signal-to-noise

ratio and current multiplication ratios of a million. Since sufficient gain is available in several tube types, the deciding factor in the selection of the 6217 photomultiplier tube was its spectral response. The 6217 tube has an S-10 spectral response which covers the range from about 3000 to 8000 angstroms. This response is essentially flat (90 per cent of maximum) over the wide spectral range from about 3700 Å (violet) to 5700 Å (yellow), and has good response (above 20 per cent of maximum) from 3100 Å (ultraviolet) to 6700 Å (red).

For those samples whose thermoluminescence spectra are the same at all temperatures, such as limestones and dolomites, the measurements are proportional to the light intensity during the entire glow curve. For samples such as fluorites which may have marked changes in color of emitted light with changing temperature, rough spectra may be obtained by using either narrow band filters or sharp cut-off filters placed between

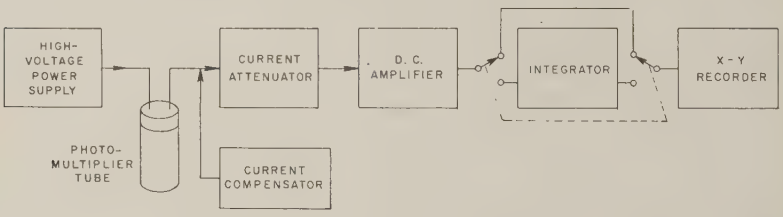

FIG. 6. Block diagram of the light-measuring section of the thermoluminescence equipment showing the interrelation of major operational units.

the sample and the photomultiplier (Fig. 7). An ingenious arrangement of filters to obtain a constant photomultiplier response independent of wavelength of the light has recently been described by Luchner (1957).

In the application of a photomultiplier tube to the detection of low-level light signals, the ultimate limitation is thermionic emission. This arises from the fact that surfaces which are good photo emitters are also good thermionic emitters. This dark current can be greatly reduced by cooling the photocathode (Boeschoten, Milatz, and Smit, 1954; Engstrom, 1947) by chilling the phototube to approximately −80° C. with a solution of dry ice and acetone. In order to reduce the temperature gradient between the hot heater and the cold photocathode and to increase the light-collection efficiency, a Lucite light pipe is used (Harris and Bell, 1956). The light-collection geometry and the cooling system are shown in Fig. 7. The outside of the light pipe is mirrored with aluminum and then painted flat black to prevent extraneous light from reaching the photomultiplier. This also prevents changes in the light-transmitting efficiency of the light pipe should water condense on the cooled

lucite during periods of high relative humidity. This coating reduced the light pipe efficiency approximately 15 per cent from its maximum, but since the addition of the light pipe more than doubled the light-collection efficiency this loss was considered negligible.

Photomultiplier Gain Variations

The current amplification in a photomultiplier tube depends to a large extent upon the voltage per stage. Even slight changes in the applied voltage will result in large changes in output. For example, a 1% change in the supply voltage results in a 7% change in output current. In this equipment the high-voltage power supply is electronically regulated in addition to being operated from a regulated ac voltage source. This

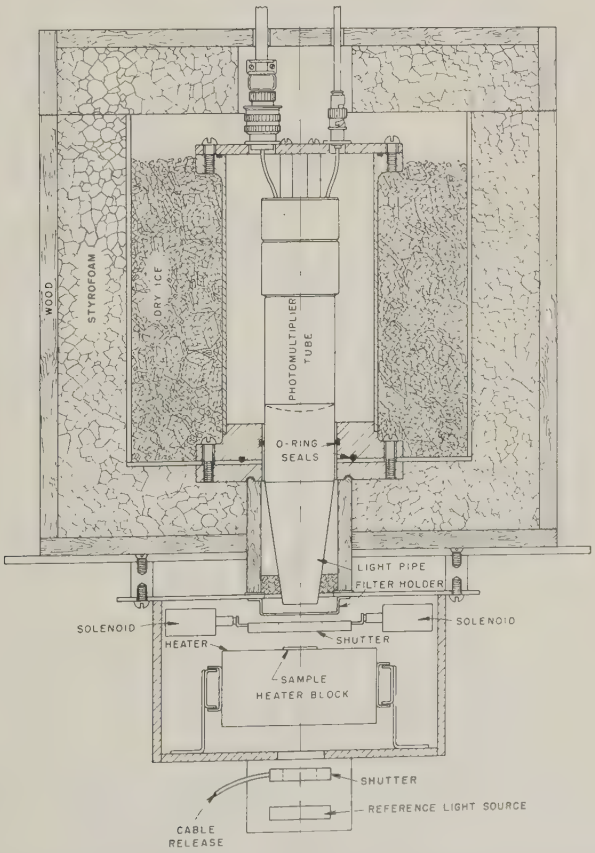

FIG. 7. Cross section of the furnace section. The photomultiplier tube is insulated thermally from the heater and coupled optically by means of a lucite light pipe.

combination supplies high voltage which varies less than 0.01% for 100% load variation and ac supply voltage change from 105 to 125 volts.

To minimize fatigue effects in the photomultiplier tube, an electrically actuated shutter keeps the photomultiplier tube in darkness except when a sample is inserted. The shutter is open only when the sample is fully inserted. The shutter is operated by solenoids as shown in Fig. 8. The shutter is a three-leaf type and has a $1\frac{3}{4}$-inch opening. Since the original plastic leaves warped at the high heater temperatures, they were replaced with metal leaves. These leaves were etched from sheet brass so that the edges would be smooth and flat. To reduce the impact on the

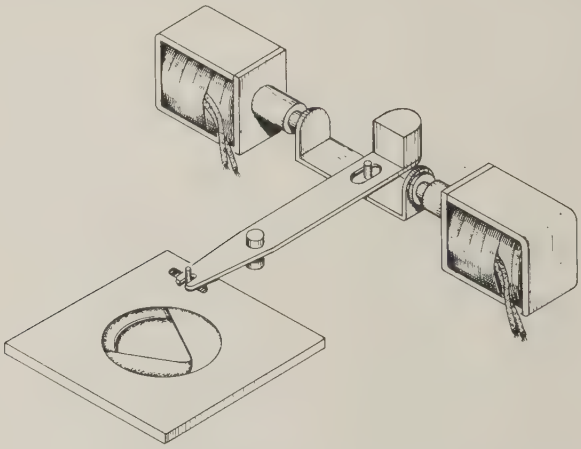

FIG. 8. Detail of shutter-operating mechanism. The solenoids are actuated alternately to open and close the shutter.

shutter pin, a resistor is included in the solenoid circuit. Two lamps on the front panel indicate whether the shutter is open or closed. A push-button switch is also mounted on the front panel to allow the shutter to be closed when the furnace drawer is closed.

The amplification of the photomultiplier tube does not remain constant, but varies with time. The gain usually decreases with use and may be expected to vary by as much as a factor of two (Engstrom, 1947).

Standardization

To compensate for changes in photomultiplier gain and other component variations in the system, the gain of the light channel is standardized by using a reference light source. With the reference light source exposed to the photomultiplier, the high voltage is adjusted to produce a prescribed recorder deflection at a specified sensitivity setting. The ref-

erence light source is a phosphor disc which is activated by a small amount of radioactive strontium-90. The brightness of the standard falls off only with the decay of the radioactive material which has a half-life of 25 years. The light source has an initial brightness of approximately 5 microlamberts, which is of the same order as the glow emitted by many samples.* To prevent excitation of the light-source phosphor by room light, it is kept in a light-tight housing, which is mounted on the furnace (Fig. 7). A shutter in the housing which contains the reference light source opens to allow the photomultiplier tube to view the source.

Using a single reference light intensity requires operating over a very wide range of photomultiplier current. An alternative method of adjusting the photomultiplier voltage to the brightness of the sample requires a series of calibrated light intensities for the various operating ranges of photomultiplier voltage. This method may be useful for very bright samples, but it has been found operationally to be simpler to reduce the sample size for samples which are too bright for the usual photomultiplier voltage.

Current Multipliers

The current multiplier is an attenuator which allows the operator to select the signal level which will produce the optimum recorder deflection. Since the range of sensitivities required is large, this attenuator is made in two sections. The Fine Current Multiplier section has a decade range in nine logarithmic steps. The Coarse Current Multiplier section has six decade steps from one to one-hundred thousand. All resistors used in the multipliers are wire-wound to a tolerance of $\pm 0.1\%$.

Direct Current Amplifier

This direct current amplifier used is the chopper-stabilized, null-balance type with a maximum gain of 10^7 and a minimum measurable current of 10^{-11} ampere.** The accuracy of the amplifier is $\pm 0.5\%$. The maximum output of the amplifier is 10 millivolts for driving the X-input of the recorder.

Output Circuits

An X-input selector switch is included to increase the flexibility of the equipment. One position gives normal linear operation, another permits recording the time integral of the glow curve, and the other positions are left for future developments. The integrating unit produces a curve of

* Available from United States Radium Corporation, Morristown, N. J.

** Leeds and Northrup Company, Type 9836-A.

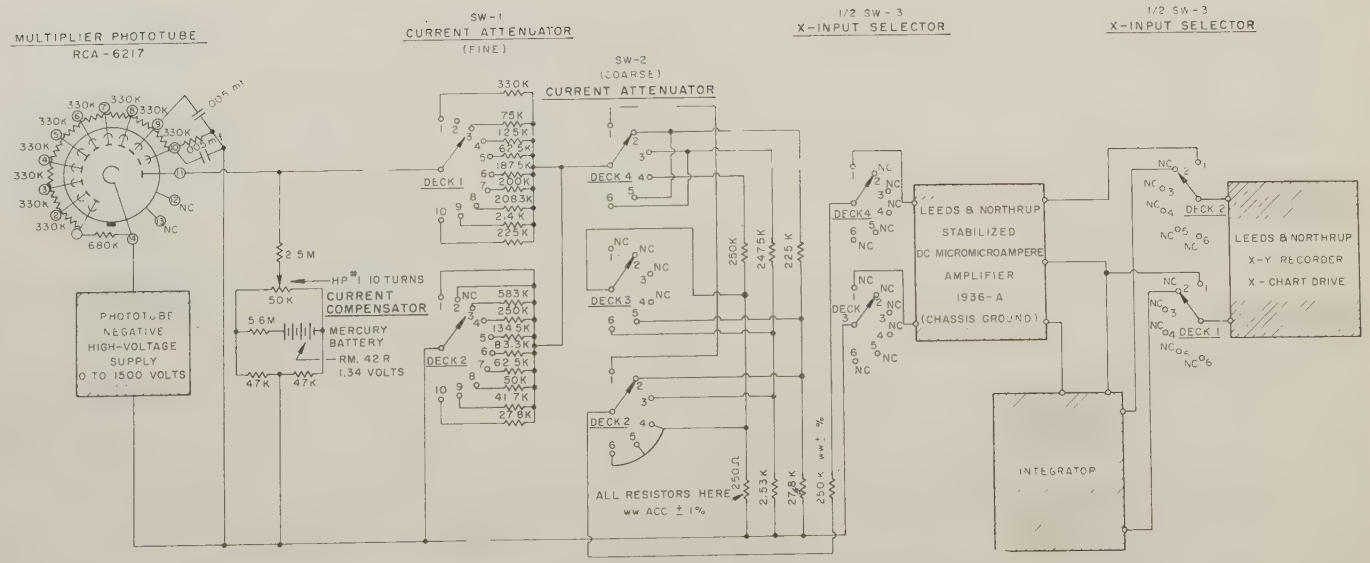

FIG. 9. Schematic diagram for the light-measuring section of the thermoluminescence equipment.

the total light emitted as a function of time.* It is essentially a three-stage operational amplifier integrator. The low drift rate and high inherent stability permit the integration of the electrical signal of glow curves lasting over 6 minutes with less than 1 per cent error.

A complete schematic diagram of the light-signal section is shown in Fig. 9.

Summary and Conclusions

From an analysis of the requirements for each of the measuring sections of the equipment and the sources of error, an apparatus has been developed for convenient and reliable recording of thermoluminescence glow curves of rocks and minerals with high sensitivity and reproducibility. This equipment has been in regular operation for more than a year with a continuous record of trustworthy performance.

References

Bergstrom, Robert E. (1956), Surface correlations of some Pennsylvanian limestones in mid-continent by their thermoluminescence: *Bull. Amer. Assoc. of Petroleum Geol.* **40,** 918–942.

Boeschoten, F., Milatz, J. M. W., and Smit, C. (1954), The application of (RCA 1P28) photomultiplier tubes to the detection of weak light intensities: *Physica,* **20,** 153.

Daniels, Farrington, Boyd, C. A., and Saunders, D. F. (1953), Thermoluminescence as a research tool: *Sci.*, **117,** 343–349.

Engstrom, R. W. (1947), Multiplier photo-tube characteristics: Application to low light levels: *J. Opt. Soc. Amer.*, **37,** No. 6, 420–431.

Garlick, G. F. J. (1949), Luminescent materials: Oxford University Press, London, Chapter II.

Halperin, A., Braner, A. A., and Alexander E. (1957), Thermoluminescence of X-ray colored KCl single crystals: *Phys. Rev.*, **108,** 928–931.

Harris, C. C. and Bell, P. R. (1956), Transmission characteristics of light pipers: *Inst. Radio Engr. Trans. Nuclear Sci.*, **NS-3,** November 1956.

Houtermans, E. G., Jäger, E., Schön, M., and Stauffer, H. (1957), Messungen der Thermolumineszenz als Mittel zur Untersuchung der thermischen und der Strahlungsgeschichte von natürlichen Mineralien und Gesteinen: *Annalen der Physik,* **20,** 283–292.

Lewis, D. R. (1956), The thermoluminescence of dolomite and calcite: *J. Phys. Chem.*, **60,** 698–701.

Luchner, K. (1957), Über die Thermolumineszinz von natürlichen Flusspat, *Zeits. für Physik* **149,** 435–452.

Parks, James M., Jr. (1953), Use of thermoluminescence of limestones in subsurface stratigraphy: *Bull. Amer. Assoc. of Petroleum Geol.*, **37,** 125–142.

Pitrat, C. W. (1956), Thermoluminescence of limestones of Mississippian Madison group in Montana and Utah: *Bull. Amer. Assoc. of Petroleum Geol.*, **40,** 943–952.

Rowland, R. A., Weiss, E. J., and Lewis, D. R. (1959), Apparatus for the oscillating-heating method of X-ray powder diffraction: *J. Amer. Ceramic Soc.*, **42,** 133–138.

* The integrator unit was designed by S. Kaufman of the Exploration and Production Division, Shell Development Company, Houston.

Saunders, Donald F. (1953), Thermoluminescence and surface correlation of limestones: *Bull. Amer. Assoc. of Petroleum Geol.*, **37,** 114–124.

Saunders, D. F., Morehead, F. F., Jr., and Daniels, F. (1953), A convenient source of gamma radiation: *J. Amer. Chem. Soc.*, **75,** 3096.

Zeller, E. J., Wray, J. L., and Daniels F. (1957), Factors in age determination of carbonate sediments by thermoluminescence: *Bull. Amer. Assoc. of Petroleum Geol.*, **41,** 121–129.

Manuscript received February 14, 1959.

THE AMERICAN MINERALOGIST, VOL. 44, NOVEMBER-DECEMBER, 1956

STUDIES OF BORATE MINERALS (VI): INVESTIGATION OF VEATCHITE

JOAN R. CLARK AND MARY E. MROSE, *U. S. Geological Survey, Washington 25, D. C.*; A. PERLOFF AND G. BURLEY, *U. S. National Bureau of Standards, Washington 25, D. C.*

ABSTRACT

Veatchite is a hydrated strontium borate originally described by Switzer (1938). In the present study *x*-ray precession patterns have been correlated with crystal habit and indices of refraction to yield the following data: monoclinic, space group $A2/a-C_{2h}^6$ (or less likely, $Aa-C_s^4$), $a=20.81\pm0.04$, $b=11.74\pm0.03$, $c=6.63_7\pm0.02$ Å, $\beta=92°02'\pm05'$, V=1620 Å^3; dominant forms {100}, {111}, {*h*11} with $h=2$, 3, 4; cleavage perfect parallel to (100) and (011); optical orientation $Z=b$, $X=c$, $Y\wedge a=-2°$. Previous chemical analyses considered together with the present crystallographic data show that the correct formula is $SrO\cdot 3B_2O_3\cdot 2H_2O$, one of two possibilities proposed by Switzer and Brannock (1950). For eight [$SrO\cdot 3B_2O_3\cdot 2H_2O$] per cell, the calculated density is 2.86 g.cm.$^{-3}$; an observed density of 2.78 ± 0.03 g.cm.$^{-3}$ was obtained on the Berman balance for a 2.4 mg. sample of excellent single crystals. *X*-ray powder pattern data are given with calculated interplanar spacings for $d\geq2.300$ Å.

INTRODUCTION

Veatchite from Lang, Los Angeles County, California, was originally described by Switzer (1938) as a hydrous calcium borate. Subsequent chemical analyses (Switzer and Brannock, 1950) showed that veatchite was actually a strontium borate, and two chemical formulas were proposed, either $3(Sr, Ca)O\cdot 8B_2O_3\cdot 5H_2O$ or $SrO\cdot 3B_2O_3\cdot 2H_2O$. The second formula, according to Stewart, Chalmers, and Phillips (1954), agrees well with a chemical analysis of veatchite from the Permian evaporites of Yorkshire, England. On the other hand, the first formula was said by Kramer and Allen (1956) to fit their chemical analysis of material from Los Angeles County, California.

X-ray data taken from rotation and Weissenberg patterns were reported by Switzer (1938). His data are listed in Table 1, column 1; the crystals were identified as monoclinic, and perfect cleavage was found parallel to (010), a secondary cleavage, parallel to (001). Optically veatchite was described as biaxial positive, with indices of refraction (for Na light): $\alpha=1.551$, $\beta=1.553$, $\gamma=1.621$ (all ±0.002), and with $Y=b$, $Z\wedge c=-38°$. Euhedral veatchite crystals were examined by Murdoch (1939), who corrected β to 121°02′ but retained {010} as the dominant form. Indices of refraction found by Murdoch (1939) were "in essential agreement" with those measured by Switzer (1938) and were also confirmed by Stewart *et al.* (1954), who revised the angle $Z\wedge c$ to $-30°$. Specific gravity measurements were reported as follows: 2.69, by suspension in bromoform (Switzer, 1938); 2.58 ± 0.01, by suspension

in Clerici solution (Murdoch, 1939); 2.6, by suspension in bromoform-benzene mixtures (Stewart *et al.*, 1954).

Further examination of veatchite crystals was suggested by C. L. Christ, U. S. Geological Survey, who pointed out that x-ray precession techniques could be used to determine more accurate cell constants and to find the possible space groups. The proposed chemical formulas could then be checked by comparison of observed and calculated densities considered together with the space group requirements. Such an investigation was undertaken first at the U. S. National Bureau of Standards under the direction of Dr. S. Block, and later at the U. S. Geological

TABLE 1. CRYSTALLOGRAPHIC DATA FOR VEATCHITE

Symmetry: monoclinic

	Switzer (1938)	Present Study
a	6.72 kX	20.81 ±0.04 Å
b	41.26	11.74 ±0.03
c	41.20	6.63_7 ±0.02
β	67° (from morphology)†	92°02′±05′
Space Group	not determined	$A2/a-C_{2h}^6$ (or less likely, $Aa-C_s^4$)
Volume		1620 Å^3
Cell Contents	16[(3SrO·8B_2O_3·5H_2O] or 44[(SrO·3B_2O_3·2H_2O]††	8[SrO·3B_2O_3·2H_2O]
Density (calc.)	2.586, 2.590 g.cm.$^{-3}$	2.85_6 g.cm.$^{-3}$
(obs.)	2.69	2.78±0.03

† Murdoch (1939) corrected β to 121°02′.

†† Switzer and Brannock (1950) proposed these formulas and calculated the corresponding densities.

Survey under the direction of C. L. Christ. Density measurements and x-ray single-crystal studies were carried out at both laboratories; other data given here were found during study at the U. S. Geological Survey.

EXPERIMENTAL TECHNIQUES

All crystals of veatchite used in this study originated in drill core no. 5, Four Corners area, Kramer district, San Bernardino County, California, and were supplied to us by Richard C. Erd, U. S. Geological Survey. Single-crystal x-ray studies were made on quartz-calibrated precession cameras with both Mo/Zr and Cu/Ni radiations (λ MoKα=0.7107 Å; λ CuKα=1.5418 Å). Film measurements were corrected for both horizontal and vertical film shrinkage. A 114.59 mm. diameter powder camera was used with Cu/Ni radiation to obtain the powder film

and the measurements from this pattern were corrected for film shrinkage. Indices of refraction were examined only to establish agreement with those previously reported; optical orientation was checked for several crystals by matching to an appropriate index oil a crystallographic direction previously identified from precession x-ray work. Density determinations were carried out at the National Bureau of Standards (NBS) using the bromoform suspension method and at the U. S. Geological Survey (USGS) using the Berman balance with toluene as the immersion liquid, the sample weights ranging from 2 to 15 mg. Because there was insufficient material for a chemical analysis, a semiquantitative spectrographic analysis was made on a sample of about 15 mg.

X-Ray Data and Morphology for Veatchite Crystals

Examination of x-ray precession photographs failed to reveal any distances as large as those of about 40 Å which had been reported by Switzer (1938). Instead the cell constants given in Table 1, column 2, were found. Systematic diffraction extinctions occur for all hkl reflections when $k+l=2n+1$ and for all $h0l$ reflections when $h=2n+1$ (and $l=2n+1$). Possible space groups are therefore non-centrosymmetric $Aa-C_s^4$ and centrosymmetric $A2/a-C_{2h}^6$. Piezoelectric tests of the crystals were made on an apparatus of the Giebe-Scheibe type with negative results. Study of the morphology yields no evidence for assuming departure from centrosymmetry. Although the non-centrosymmetric space group cannot be definitely ruled out, available evidence favors the centrosymmetric $A2/a$.

The Four Corners veatchite crystals used in the present study have the platy habit described by Murdoch (1939) and illustrated in his Figs. 1 and 2. According to the present x-ray data, the monoclinic symmetry axis (taken as b) lies in the plane of the plate, and not normal to it. Therefore, if the convention $c<a$ is followed, the correct indices for the plate form are {100} and the perfect cleavage is parallel to (100) and not to (010) as assumed in all previous work. In the present cell elongation of the plates is in the [011] direction and the secondary cleavage is parallel to (011). The optical orientation now is $Z=b$, $X=c$, $Y\wedge a=-2°$.

Numerous veatchite crystals were measured on an optical goniometer by Murdoch (1939), who indexed observed forms according to the description of the cell by Switzer (1938). It was not found possible to derive a matrix which would transform Murdoch's indices to the indices based on the cell chosen from the present study; it is believed that Murdoch's indexing may be inconsistent. The angular measurements made by Murdoch are shown on the stereogram section of Fig. 1a with

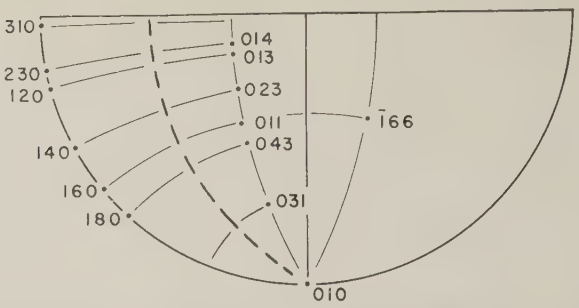

FIG. 1*a*. (above) Stereogram plotted from angular measurements by Murdoch (1939); indices originally assigned by him. Dashed line marks position of correct mirror plane.

his indices; the correct mirror plane and the faces related by the mirror symmetry are marked. Fig. 1*b* shows the same data after appropriate transformation; the faces are now indexed for the present cell. Both sets of indices are compared in Table 2 and the simplification of indices in the present cell is of interest.

X-ray powder data for veatchite have previously been given by Stewart *et al.* (1954) for the Yorkshire material, and by Kramer and Allen (1956) from a diffractometer pattern on material from Los Angeles County, California. Both sets of observed data are given in Table 3, columns 1 and 2. Observed interplanar spacings found on a pattern taken of the Four Corners veatchite are given in Table 3, column 3, and are generally in good agreement with the earlier findings. Interplanar spacings were calculated from the *x*-ray cell constants down to values of 1.5 Å on the USGS Datatron computer with a program developed by D. E. Appleman. Table 3, column 4, lists all calculated spacings for $d \geq 2.300$ Å. Because measurements from the pattern of the present study are

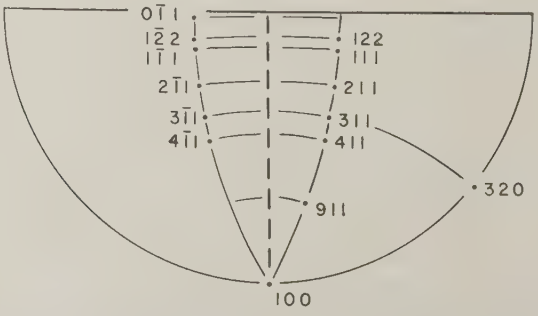

FIG. 1*b*. (below) Stereogram from Murdoch's measurements after transformation; indices are those for the present cell. Dashed line marks the mirror plane.

corrected for film shrinkage, they approach the calculated values more closely than do the earlier measurements.

Chemical Formula and Density of Veatchite

Spectrographic analysis of Four Corners veatchite is in accord with the previous chemical analyses (Switzer and Brannock, 1950; Stewart *et al.*, 1954; Kramer and Allen, 1956), all of which agree well with one another. The correct chemical formula must therefore satisfy these analyses and in addition must meet the crystallographic requirements that follow from the *x*-ray data. First, an integral number Z of formula units in the cell of volume 1620 Å^3 must lead to a calculated density in

Table 2. Observed Forms on Veatchite Crystals

(Original angular measurements by Murdoch, 1939)

Indices {*hkl*} of Observed Forms	
Assigned by Murdoch (1939) (see Fig. 1*a*)	Present Study (see Fig. 1*b*)
010	100†
310	0$\bar{1}$1†
013, 120	111, 1$\bar{1}$1†
023, 140	211, 2$\bar{1}$1
011, 160	311, 3$\bar{1}$1
043, 180	411, 4$\bar{1}$1
014, 230	122, 1$\bar{2}$2
031	911 (?)
$\bar{1}$66	320
not observed	010†

† Forms observed on Four Corners veatchite crystals in present study.

reasonable accord with the observed density. A count can then be made of the total number of each kind of atom present in the cell. Since space groups Aa and $A2/a$ contain only positions of fourfold and eightfold multiplicity, a second crystallographic requirement is that in one cell each kind of atom be present in number as some integral multiple of four. Finally, the postulated total number of atoms per cell must fit into the available 1620 Å^3 volume. Christ (1953) pointed out that in the colemanite series of minerals the calculated volume per oxygen atom ranges from 17.6 Å^3 in colemanite, $CaB_3O_4(OH)_3 \cdot H_2O$, to 20.5 Å in inyoite, $CaB_3O_3(OH)_5 \cdot 4H_2O$. Values toward the lower end of this range are to be expected for the volume per oxygen atom in veatchite because it is a lower hydrate.

The first formula proposed by Switzer and Brannock (1950) is

TABLE 3. X-RAY POWDER DATA FOR VEATCHITE, $SrO \cdot 3B_2O_3 \cdot 2H_2O$

Monoclinic $A2/a$: $a = 20.81 \pm 0.04$, $b = 11.74 \pm 0.03$, $c = 6.63_7 \pm 0.02$ Å; $\beta = 92°02' \pm 05'$

Measured						Calculated†	
Stewart, Chalmers and Phillips (1954)[a]		Kramer and Allen (1956)[b]		Present Study[c]		Present Study	
I	d_{hkl}	I	d_{hkl}	I	d_{hkl}	d_{hkl}	hkl
vs[1]	10.3	10	10.53	100	10.5	10.40	200
		1	8.27[d]	1	8.29[d]		
		1	6.94[e]				
						5.870	020
						5.775	011
m	5.65	1	5.63	6	5.64	5.649	120
						5.609	$\bar{1}11$
						5.521	111
						5.199	400
m	5.13	3	5.22	6	5.12	5.115	$\bar{2}11$
						5.112	220
						4.985	211
w	4.47			2	4.51	4.505	$\bar{3}11$
						4.480	320
		1	4.20	2	4.37	4.372	311
m	3.88[f]	1	3.93	4	3.92	3.924	$\bar{4}11$
		1	3.69	3	3.81	3.892	420
						3.807	411
w	3.48	10	3.47	20	3.47	3.466	600
						3.425	$\bar{5}11$
						3.394	520
				3	3.37	3.370	031
						3.336	$\bar{1}31$
						3.328	511
vs[2]	3.33	2	3.32	35	3.32	3.318	131
						3.316	002
w	3.20			3	3.22	3.223	$\bar{2}31$
						3.192	$\bar{2}02$
						3.190	231
						3.128	202
						3.053	$\bar{3}31$
						3.013	$\bar{6}11$
wb	2.99			3b	3.00	3.010	331
						2.985	620
				2	2.936	2.935	040
						2.933	611
						2.906	140
						2.887	022
m	2.87	3	2.88	9	2.865	2.872	$\bar{1}22$
						2.851	$\bar{4}31$
						2.848	122

† All calculated spacings listed for $d_{hkl} \geq 2.300$ Å.

[a] "Order of intensities: vs[1], vs[2], s[3], m, w, vw, vvw; b indicates broad line. 9 cm. camera cut off at 10.8 kX. Cu-Kα radiation ($\lambda = 1.5374$ kX)." No shrinkage correction; kX units converted to Ångstrom units by present authors.

[b] X-ray diffractometer data, Cu/Ni radiation.

[c] Corrected for film shrinkage; b = broad, d = diffuse. Radiation: Cu/Ni, λCuKα = 1.5418 Å. Lower limit of 2θ measurable: approximately 7° (13 Å).

[d] (200), FeKα radiation.

[e] Not veatchite.

[f] The value of 4.00 kX given in the original listing should have been 3.87 kX (private communication, R. Phillips, 1958).

TABLE 3. (*Continued*)

Measured						Calculated†	
Stewart, Chalmers and Phillips (1954)[a]		Kramer and Allen (1956)[b]		Present Study[c]		Present Study	
I	d_{hkl}	I	d_{hkl}	I	d_{hkl}	d_{hkl}	*hkl*
						2.841	$\bar{4}02$
						2.825	240
		1	2.79	1	2.798	2.806	431
						2.804	$\bar{2}22$
vvw	2.77	1	2.76	1	2.763	2.761	222
						2.753	402
vvw	2.70	1	2.67	1	2.704	2.703	340
						2.695	$\bar{3}22$
						2.675	$\bar{7}11$
						2.651	720
						2.642	$\bar{5}31$
						2.637	322
						2.610	711
s[3]	2.60	10	2.61	25	2.600	2.600	800
						2.596	$\bar{5}31$
				1	2.564	2.558	$\bar{4}22$
vw	2.53			1	2.495	2.556	440
						2.492	422
						2.439	$\bar{6}02$
						2.438	$\bar{6}31$
						2.406	$\bar{5}22$
m	2.39	1	2.40	6	2.398	2.398	540, $\bar{8}11$
						2.395	631
						2.377	820
						2.356	602
						2.344	$\bar{8}11$
						2.339	522
				2	2.245		
m	2.20	1	2.21	3	2.204		
		1	2.17	2	2.171		
w	2.151	1	2.16	2	2.155		
				2	2.115		
m	2.082	9	2.08	6	2.079		
				4	2.045		
m	2.037						
				4	2.029		
vw	1.996						
				3d	1.958		
m	1.936	1	1.924	3	1.925		
				2	1.876		
vw	1.863			2	1.854		
vvw	1.836	1	1.833	2	1.828		
vw	1.801			4	1.784		
wb	1.761	2	1.735	1	1.730		
				1	1.700		
vvw	1.676			1	1.680		
vvw	1.653			3	1.660		
	plus additional lines						
all vw or vvw				all with I≤2			

$3SrO \cdot 8B_2O_3 \cdot 5H_2O$. A minimum of four formula units per cell is needed if the number of Sr atoms is to satisfy the second crystallographic requirement. However, the calculated density for four such formula units is

3.9 g.cm.$^{-3}$, compared to observed values ranging from 2.6 to 2.7 g.cm.$^{-3}$. Furthermore, four of these formula units contain 128 oxygen atoms so that a maximum volume of 13 Å^3 is available to each oxygen atom in the cell. Clearly this chemical formula is unsatisfactory. On the other hand, the second formula proposed by Switzer and Brannock (1950) is $SrO \cdot 3B_2O_3 \cdot 2H_2O$, which, for $Z=8$, gives a calculated density of 2.86 g.cm.$^{-3}$. Each of the 96 oxygen atoms in the cell has available 16.9 Å^3, a value that compares closely to the 17.6 Å^3 per oxygen atom in colemanite (Christ, 1953). The formula, $SrO \cdot 3B_2O_3 \cdot 2H_2O$, therefore satisfies both chemical and crystallographic requirements.

Calculated and observed densities do not agree as well as usually expected, and calculations show that substitution of Ca for some Sr in the formula does not satisfactorily explain the small discrepancy. In the present study an average observed density of 2.66 g.cm.$^{-3}$ was found when normal material was used. However, an average observed value of 2.78 ± 0.03 g.cm.$^{-3}$ was obtained from measurements on the Berman balance for a 2.4 mg. sample of excellent single crystals. Unfortunately larger samples of comparable quality crystals were not available. Veatchite crystals are generally composed of stacked cleavage plates, probably containing entrapped air. When such crystals are immersed in liquid, the cleavage plates have a tendency to flake apart and some even float on the liquid surface, presumably held there by surface tension. These factors account for the low observed values and the variable range of density readings which are obtained when average material is used in the density determinations.

Acknowledgments

This study was suggested by C. L. Christ, U. S. Geological Survey, and directed by him at the Survey and by Dr. S. Block at the U. S. National Bureau of Standards. We are grateful for their critical guidance throughout the study. We are also happy to acknowledge the assistance of several colleagues at the USGS: the crystals of veatchite were supplied by R. C. Erd, some directly and others through W. T. Schaller; calculations of interplanar spacings were carried out by D. E. Appleman; the spectrographic analysis was made by H. J. Rose, Jr.

References

Christ, C. L. (1953), Studies of borate minerals (II): x-ray crystallography of inyoite and meyerhofferite; x-ray and morphological crystallography of $2CaO \cdot 3B_2O_3 \cdot 9H_2O$: *Am. Mineral.* **38,** 912–918.

Kramer, Henry, and Allen, Robert D. (1956), A restudy of bakerite, priceite, and veatchite: *Am. Mineral.* **41,** 689–700.

Murdoch, Joseph (1939), Crystallography of veatchite: *Am. Mineral.* **24,** 130–135.

Stewart, F. H., Chalmers, R. A., and Phillips, R. (1954), Veatchite from the Permian evaporites of Yorkshire: *Mineral. Mag.* **30,** 389–392.

Switzer, George (1938), Veatchite, a new calcium borate from Lang, California: *Am. Mineral.* **23,** 409–411.

Switzer, George, and Brannock, W. W. (1950), Composition of veatchite: *Am. Mineral.* **35,** 90–92.

Manuscript received March 2, 1959.

STUDIES OF BORATE MINERALS (VII): *X*-RAY STUDIES OF AMMONIOBORITE, LARDERELLITE, AND THE POTASSIUM AND AMMONIUM PENTABORATE TETRAHYDRATES*

JOAN R. CLARK AND C. L. CHRIST, *U. S. Geological Survey, Washington 25, D.C.*

ABSTRACT

Synthetic ammonioborite and the ammonium and potassium pentaborate tetrahydrates have been studied by *x*-ray single-crystal techniques. The results for the tetrahydrates are in agreement with those presented by Cook and Jaffe (1957). Ammonioborite is monoclinic $C2/c-C_{2h}^6$ (or less likely, $Cc-C_s^4$), with $a=25.27\pm0.05$, $b=9.65_1\pm0.03$, $c=11.56\pm0.03$ Å; $\beta=94°17.5'\pm05'$. Instead of $(NH_4)_2O\cdot5B_2O_3\cdot5H_2O$ (Schaller, 1933), the ammonioborite formula proposed here is $(NH_4)_2O\cdot5B_2O_3\cdot5\frac{1}{3}H_2O$; this gives the best agreement with present chemical and crystallographic data. Indexed *x*-ray powder data are given for the three substances named above; observed powder data are given for larderellite.

INTRODUCTION

In continuation of a systematic investigation of borate minerals the *x*-ray crystallography of synthetic ammonioborite and of the compounds, ammonium and potassium pentaborate tetrahydrate, have been examined. *X*-ray powder data for these compounds and for larderellite have also been determined.

The chemical formulas of the hydrated ammonium borate minerals, larderellite and ammonioborite, have been considered as uncertain in the mineralogical literature. Palache, Berman, and Frondel (1951) list the formula $(NH_4)_2O\cdot5B_2O_3\cdot5H_2O$ for both minerals, in agreement with the formula originally proposed by d'Achiardi (1930) for larderellite. In his original description of the new mineral ammonioborite, Schaller (1933) assigned the same formula to it and suggested that larderellite and ammonioborite were dimorphous. In the present study single-crystal *x*-ray measurements are combined with the experimentally observed density to derive a chemical formula for ammonioborite which can be compared with the formula obtained by the usual analytical chemical methods. Unfortunately, because larderellite does not occur in crystals large enough for either single-crystal *x*-ray work or density determination, its formula cannot be similarly derived. A preliminary account of this work was given previously (Clark and Christ, 1956).

EXPERIMENTAL TECHNIQUES

The crystals used in this study were obtained from W. T. Schaller, who supplied synthetic preparations of ammonioborite, ammonium pentaborate tetrahydrate (APT), and potassium pentaborate tetra-

* Publication authorized by the Director, U. S. Geological Survey.

hydrate (KPT), as well as samples of natural larderellite and ammonioborite from Larderello, Italy. APT and KPT are well-known salts; a method of synthesis is given by Schaller (1933). Ammonioborite can be prepared in sizes appropriate for single-crystal study by crystallizing APT from water solution at room temperature as directed by Schaller (1933), decanting excess solution and maintaining the resulting system at 95° C. for several weeks (Schaller, private communication). Synthetic ammonioborite was used throughout the present study, the identity of the natural and synthetic materials having been established by comparison of optical and x-ray powder data.

Single-crystal x-ray studies were made with quartz-calibrated precession cameras using both Mo/Zr and Cu/Ni radiations (λ MoKα = 0.7107 Å; λ CuKα = 1.5418 Å). Film measurements were corrected for both horizontal and vertical film shrinkage. A 114.59 mm. diameter power

Table 1. Crystallographic Data for Synthetic Ammonioborite

Symmetry: monoclinic			
a	25.27 ±0.05 Å	Space Group	$C2/c-C_{2h}^6$ (or less likely, $Cc-C_s^4$)
b	9.65_1±0.03	Volume	2811 Å^3
c	11.56 ±0.03	Cell Contents	$12[(NH_4B_5O_8\cdot 2\frac{2}{3}H_2O]$
β	94°17.5′±05′	Density (calc.)	1.758 g.cm.$^{-3}$
		(obs.)	1.765±0.004 (pycnometer)

camera was used with Cu/Ni radiation to obtain the powder films. Measurements on the ammonioborite powder film were corrected for film shrinkage; for all the other powder films, shrinkage corrections were found to be negligible. Interplanar spacings were calculated down to values of 1.5 Å on a Datatron computer, using a program developed by D. E. Appleman. Indices of refraction were examined as necessary to establish agreement with those previously reported; optical orientation was checked on several crystals by matching to an appropriate index oil a crystallographic direction previously identified from precession x-ray work. Density determinations were made both with the Berman balance and with a pycnometer.

X-Ray Study of Ammonioborite

The habit of natural ammonioborite crystals was described by Schaller (1933). The synthetic crystals have a similar habit, *i.e.*, tabular, somewhat elongated, with truncated edges. The cell constants found from single crystal x-ray examination are given in Table 1; ammonio-

borite is monoclinic, possible space groups being $Cc-C_s^4$ or $C2/c-C_{2h}^6$. Piezoelectric tests were made on the crystals with an apparatus of the Giebe-Scheibe type. The negative results, taken together with the holohedral morphology, strongly indicate the presence of a center of symmetry. The most probable space group is therefore $C2/c-C_{2h}^6$.

Description of the morphology of the synthetic crystals in terms of the x-ray cell is as follows: tabular on {100}, elongated parallel to [001], with forms {010}, {310}, and {311} commonly observed. Occasionally crystals are found with {010} dominant. Such crystals can be distinguished by optical examination, the optical orientation being $Y=b$, $Z\wedge c=7°$. Clark and Christ (1956) reported that optical examination showed ammonioborite to be triclinic; further optical studies prove the crystals are in fact monoclinic. Schaller (1933) describes inclined extinction as found on the "large face" and states that the obtuse bisectrix X emerges from this face. However, when inclined extinction is observed, the crystals are lying on {010} with the optic normal $Y(=b)$ emerging.

X-ray powder data for ammonioborite are given in Table 2, which lists both observed and calculated interplanar spacings, the latter for $d\geq 2.600$ Å. All observed lines are satisfactorily accounted for by the chosen cell.

The observed density of ammonioborite is 1.765 ± 0.004 g.cm.$^{-3}$. For the experimentally determined cell volume of 2811 Å^3 (Table 1), a total of 6.1 formula units of $(NH_4)_2O\cdot 5B_2O_3\cdot 5H_2O$ are found. This number is not as close to an integer as would be expected from the accuracy of the data. If 6 formula units are assumed together with the experimentally determined cell volume, a density of 1.737 g.cm.$^{-3}$ is calculated. The variation between calculated and observed densities is about 1.5%; these results indicate a re-examination of the assumed chemical formula is in order. Calculations based on the assumption that variation in water ratio alone is required give the following data:

Oxide formula	*Reduced formula*	*Calculated density*
$(NH_4)_2O\cdot 5B_2O_3\cdot 5H_2O$	$NH_4B_5O_8\cdot 2\frac{1}{2}H_2O$	1.737 g.cm.$^{-3}$
$(NH_4)_2O\cdot 5B_2O_3\cdot 5\frac{1}{3}H_2O$	$NH_4B_5O_8\cdot 2\frac{2}{3}H_2O$	1.758
$(NH_4)_2O\cdot 5B_2O_3\cdot 5\frac{1}{2}H_2O$	$NH_4B_5O_8\cdot 2\frac{3}{4}H_2O$	1.769

These results indicate that the last two formulas give better agreement between observed and calculated densities.

Chemical analyses made by Schaller (private communication) subsequent to his 1933 paper, but as yet unpublished, are in excellent as well as best agreement with the second oxide formula, $1:5:5\frac{1}{3}$. The monoclinic symmetry is such that positions of no less than fourfold multiplicity are indicated. For $6[(NH_4)_2O\cdot 5B_2O_3\cdot 5\frac{1}{3}H_2O]$ per cell the total number of each type of atom is some integral multiple of four,

TABLE 2. *X*-RAY POWDER DATA FOR SYNTHETIC AMMONIOBORITE, $NH_4B_5O_8 \cdot 2\frac{2}{3}H_2O$

Monoclinic $C2/c$: $a = 25.27 \pm 0.05$, $b = 9.65_1 \pm 0.03$, $c = 11.56 \pm 0.03$ Å; $\beta = 94°17.5' \pm 05'$

Measured*		Calculated†		Measured*		Calculated	
I	d_{hkl}	d_{hkl}	hkl	I	d_{hkl}	d_{hkl}	hkl
15	12.5	12.60	200			2.963	$\bar{2}23$
40	8.98	9.01	110			2.947	$\bar{6}03$
		7.19	$\bar{1}11$			2.926	$\bar{3}31$
<3	7.05	7.01	111			2.888	331
15	6.33	6.34	310			2.886	223
		6.30	400	60	2.876	2.882	004
		5.764	002			2.856	$\bar{2}04$
60	5.70	5.690	$\bar{3}11$			2.855	$\bar{8}02$
30	5.44	5.425	311			2.845	$\bar{6}22$
		5.396	$\bar{2}02$			2.826	712
3	5.10	5.099	202	10	2.822	2.822	513
		4.916	$\bar{1}12$			2.803	$\bar{1}32$
20	4.82	4.826	020			2.781	132
		4.798	112			2.777	$\bar{4}23$
		4.506	220			2.767	$\bar{1}14$
		4.467	510	10	2.763	2.765	204
		4.451	021			2.724	114
		4.420	$\bar{4}02$			2.713	622
15	4.37	4.389	$\bar{3}12$			2.712	530
		4.262	$\bar{5}11$			2.698	$\bar{4}04$
		4.236	$\bar{2}21$			2.694	$\bar{3}32$
	4.20	4.200	600			2.689	910
20b	to	4.160	221			2.681	$\bar{3}14$, 802
	4.15	4.149	312			2.664	$\bar{5}31$
		4.103	402			2.661	$\bar{9}11$
		4.076	511		2.671	2.653	423
		3.831	420	5 to 10, b	to	2.638	820
8	3.69	3.700	022		2.629	2.635	332
		3.686	$\bar{4}21$			2.628	$\bar{7}13$
		3.650	$\bar{5}12$			2.616	531
		3.597	$\bar{2}22$			2.607	$\bar{8}21$
10	3.58	3.587	421	3	2.578		
		3.569	$\bar{1}13$	3	2.468		
		3.522	$\bar{6}02$	<3	2.392		
4	3.49	3.505	222	3	2.365		
		3.501	113	15	2.324		
		3.423	512	5	2.262		
10	3.37	3.373	710	5	2.189		
		3.371	$\bar{3}13$	5	2.176		
		3.300	$\bar{7}11$	5	2.122		
		3.280	602	8	2.076		
3	3.26	3.259	$\bar{4}22$	5	2.032		
		3.206	313	5	1.989		
		3.191	130	5	1.963		
		3.178	711	10	1.920		
100	3.16	3.168	620	5	1.888		
		3.150	800	4	1.821		
		3.126	422	5	1.794		
100	3.09	3.100	$\bar{6}21$	<3	1.752		
		3.083	$\bar{1}31$	4	1.711		
		3.068	131	<3	1.661		
		3.014	$\bar{5}13$	<3	1.614		
50	3.01	3.012	621	5	1.581		
		3.006	023	plus additional lines			
		3.004	712, 330	all with I≤4			

* Corrected for film shrinkage; b = broad. Radiation: Cu/Ni, λ CuKα = 1.5418 Å. Lower limit of 2θ measurable: approximately 7° (13 Å). Film no. 8938.

† All calculated spacings listed for $d_{hkl} \geq 2.600$ Å.

TABLE 3. X-RAY POWDER DATA FOR LARDERELLITE, $NH_4B_5O_8 \cdot 2\frac{1}{2}H_2O$

Measured* I	d_{hkl}	I	d_{hkl}	I	d_{hkl}
50	9.45	25	2.816	25	1.887
18	5.91	35	2.713	25	1.882
25	5.79	12	2.663	4	1.855
71	5.44	18	2.623	4	1.818
50	5.12	6	2.545	2	1.790
100	4.70	6	2.476	4	1.775
18	4.60	6	2.444	2	1.764
25	4.30	9	2.416	2	1.730
25	3.99	18	2.325	4	1.710
4	3.88	12	2.257	4	1.683
18	3.81	4	2.206	4	1.669
18	3.66	25	2.156	4	1.623
4	3.53	4	2.138	4	1.615
12	3.45	4	2.124	4	1.578
12	3.42	6	2.094	4	1.561
12	3.34	35	2.041	4	1.536
35	3.14	12	2.013	4	1.501
71	2.960	12	1.989	4	1.482
100	2.921	8	1.937	plus additional	
100	2.887	8	1.923	weak lines	

* Correction for film shrinkage negligible. Radiation: Cu/Ni, λ CuKα = 1.5418 Å. Lower limit of 2θ measurable: approximately 7° (13 Å). Film No. 11101.

whereas for $6[(NH_4)_2O \cdot 5B_2O_3 \cdot 5H_2O]$ the total number of oxygen atoms is not an integral multiple of four. Both chemical and crystallographic evidence thus point to $(NH_4)_20 \cdot 5B_2O_3 \cdot 5\frac{1}{3}H_2O$ as the most probable formula for ammonioborite in view of the present data.

X-RAY STUDIES OF LARDERELLITE

Larderellite has not been synthesized and has been found in nature only as a finely divided crystalline powder, with crystals too minute for single-crystal *x*-ray study. The small quantity of available material and the size of the crystals have made determination of the density infeasible.

Monoclinic symmetry has been assigned to larderellite in the past (Palache, Berman and Frondel, 1951), and examination of the powder pattern seems to rule out all except triclinic and monoclinic symmetries. The observed interplanar spacings are shown in Table 3; the number of these spacings with relatively large *d*-values indicates a large cell. Assuming monoclinic symmetry, trial-and-error methods of indexing the

pattern were tried, but without an observed density value as a check, the results were not considered to be conclusive. Larderellite and ammonioborite can be differentiated both by optical examination and from x-ray powder patterns.

X-Ray Studies of APT and KPT

Cook and Jaffe (1957) have reported on the crystallographic, elastic, and piezoelectric properties of these two borates. Our independent crystallographic studies were completed prior to publication of the Cook and Jaffe paper, and our results are in complete agreement with theirs. A comparison of their crystallographic data with ours is given in Table 4. The densities reported by Cook and Jaffe (1957) are not

Table 4. Crystallographic Data for Ammonium Pentaborate Tetrahydrate and Potassium Pentaborate Tetrahydrate

Space group: $Aba2-C_{2v}^{17}$

	$NH_4B_5O_8\cdot 4H_2O$		$KB_5O_8\cdot 4H_2O$	
	Cook and Jaffe (1957)	Present Study	Cook and Jaffe (1957)	Present Study
a	11.324 ± 0.002 Å	11.33 ± 0.02 Å	11.065 ± 0.002 Å	11.07 ± 0.02 Å
b	11.029 ± 0.001	11.01 ± 0.02	11.171 ± 0.001	11.15 ± 0.02
c	9.235 ± 0.004	$9.22_2\pm0.02$	9.054 ± 0.0006	$9.03_8\pm0.02$
Volume	$1153._4$ Å^3†	—	$1119._1$ Å^3†	—
Cell Contents	$4[NH_4B_5O_8\cdot 4H_2O]$		$4[KB_5O_8\cdot 4H_2O]$	
Density (calc.)	1.567 g.cm.$^{-3}$†	—	1.740 g.cm.$^{-3}$†	—
(obs.)	—	$1.56_7\pm0.005$	—	$1.73_6\pm0.005$

† Calculated by present authors from data of Cook and Jaffe (1957).

designated as calculated or observed; however, our observed values are in excellent agreement with the densities calculated from their cell constants.

Apparently no indexed x-ray powder data have been published for either APT or KPT, although observed interplanar spacings for KPT are listed on ASTM cards 3-0107, 3-0108. Table 5 presents both observed and calculated interplanar spacings for the two substances, calculated values being given for $d \geq 1.650$ Å. ASTM data for KPT have not been repeated here, although they are in agreement with those of the present study, because the present observations are in closer accord with the calculated values. In the APT pattern two lines were found having interplanar spacings that do not correspond to any calculated for this material, and all efforts to identify the lines as belonging to another substance failed. Possibly some alteration product is formed during preparation of the sample for the powder pattern.

TABLE 5. *X*-RAY POWDER DATA FOR AMMONIUM PENTABORATE TETRAHYDRATE, $NH_4B_5O_8 \cdot 4H_2O$, AND POTASSIUM PENTABORATE TETRAHYDRATE, $KB_5O_8 \cdot 4H_2O$

Orthorhombic *Aba*2:

$NH_4B_5O_8 \cdot 4H_2O$: $a = 11.324 \pm 0.002$, $b = 11.029 \pm 0.001$, $c = 9.235 \pm 0.004$ Å
$KB_5O_8 \cdot 4H_2O$: $a = 11.065 \pm 0.002$, $b = 11.171 \pm 0.001$, $c = 9.054 \pm 0.0006$ Å
(Values of the cell constants from Cook and Jaffe, 1957)

$NH_4B_5O_8 \cdot 4H_2O$				$KB_5O_8 \cdot 4H_2O$			
Measured*		Calculated†		Measured*		Calculated†	
I	d_{hkl}	d_{hkl}	*hkl*	I	d_{hkl}	d_{hkl}	*hkl*
100	6.01	6.004	111	15	5.93	5.936	111
		5.662	200	71	5.60	5.585	020
35	5.54	5.515	020			5.532	200
2	4.97	4.958	120	2	4.99	4.986	120
9	4.63	4.618	002	6	4.52	4.527	002
3	4.46	4.422	211	2	4.34	4.348	211
		3.950	220	5	3.93	3.931	220
		3.578	202	84	3.52	3.517	022
71	3.54	3.540	022			3.503	202
9	3.46††						
85	3.38	3.379	122	100	3.36	3.352	122
18d	3.33	3.331	311	18	3.28	3.288	131
18	3.26	3.270	131			3.266	311
2	3.13	3.115	320	1	3.07	3.078	320
4	3.01	3.002	222	6	2.969	2.968	222
9	2.923	2.925	231	6	2.926	2.924	231
		2.868	113	4	2.818	2.817	113
71	2.837	2.831	400			2.793	040
		2.757	040	50	2.767	2.766	400
2	2.682	2.679	140	1	2.710	2.708	140
4d	2.631	2.629	411	4	2.574	2.578	213
		2.627	213			2.574	411
		2.582	322			2.545	322
12	2.532	2.533	331	12	2.517	2.517	331
		2.518	420			2.493	240
		2.479	240	2d	2.483	2.479	420
2	2.414	2.413	402	9	2.375	2.377	042
3	2.369	2.367	042			2.360	402
		2.332	313	4	2.324	2.324	142
12	2.316	2.317	142	9	2.290	2.294	133
		2.311	133			2.286	313

* Not corrected for film shrinkage; d = diffuse. Radiation: Cu/Ni, λ CuKα = 1.5418 Å. Lower limit of 2θ measurable: approximately 7° (13 Å). Film nos. 11151 and 11262.

† All calculated spacings listed for $d_{hkl} \geq 1.650$ Å.

†† Not indexable as APT, nor as any tested impurity.

TABLE 5 (*Continued*)

$NH_4B_5O_8 \cdot 4H_2O$				$KB_5O_8 \cdot 4H_2O$			
Measured*		Calculated†		Measured*		Calculated†	
I	d_{hkl}	d_{hkl}	hkl	I	d_{hkl}	d_{hkl}	hkl
		2.309	004	4	2.259	2.263	004
		2.226	340			2.226	340
6	2.211	2.211	422	21	2.181	2.184	242
		2.184	242			2.174	422
18	2.181	2.180	431	4	2.158	2.159	233
		2.179	233			2.157	431
		2.157	511	2	2.129	2.129	151
		2.138	204	6	2.115	2.111	511
		2.130	024			2.098	024
9	2.102	2.108	151	2	2.093	2.095	204
		2.095	520	3	2.062	2.061	124
		2.093	124			2.057	502
2	2.050	2.048	413	1	2.021	2.019	251
15	2.005	2.006	251, 342			2.006	413
		2.001	333	4	1.999	1.998	342
		1.993	224	2	1.979	1.979	333
		1.975	440			1.965	440
< 6**	1.934††						
	1·907	1.908	522	3	1.962	1.961	224
		1.888	531	4	1.872	1.873	522
		1.887	600			1.870	351
		1.865	351			1.862	060, 531
	1.859	1.855	324			1.844	600
		1.838	060			1.836	160
d	1.820	1.824	611	2	1.825	1.823	324
		1.816	442	4	1.802	1.803	442
		1.814	160			1.789	433
		1.813	433			1.784	611
		1.800	513			1.772	153
		1.799	115			1.765	260, 115
		1.789	404	3d	1.761	1.762	513
		1.786	620			1.758	044
	1.770	1.771	153			1.752	404
		1.770	044			1.751	620
		1.750	540	2	1.738	1.737	144
	1.748	1.749	144			1.734	540
		1.748	260			1.722	062
		1.747	602	2	1.708	1.708	602, 253
		1.734	215			1.707	451
		1.710	451			1.701	162, 215
		1.709	253	1	1.675	1.676	244

(*Continued on next page*)

** I<6 for this line and succeeding lines.

TABLE 5 (*Continued*)

$NH_4B_5O_8 \cdot 4H_2O$				$KB_5O_8 \cdot 4H_2O$			
Measured*		Calculated†		Measured*		Calculated†	
I	d_{hkl}	d_{hkl}	hkl	I	d_{hkl}	d_{hkl}	hkl
	1.706	1.708	062			1.671	424
		1.702	424			1.662	360
		1.690	244	4d	1.611		
		1.689	162	2	1.558		
		1.665	622	6	1.543		
		1.653	360	plus additional			
		1.652	631	lines, I≤6			
	1.636						
	1.539						
	1.435						
plus additional							
weak lines							

ACKNOWLEDGMENTS

We are indebted to several colleagues of the U. S. Geological Survey: W. T. Schaller supplied the crystals and made available his unpublished chemical analyses, Fred A. Hildebrand took the x-ray powder patterns, M. K. Carron made the pycnometer density determination of ammonioborite, and D. E. Appleman carried out calculations of interplanar spacings and provided helpful discussion.

REFERENCES

D'ACHIARDI, G. (1930), Nuovi dati e ricerche sulla larderellite: *Per. Min. Roma* **1,** 208–213.

CLARK, JOAN R. AND CHRIST, C. L. (1956), Ammonioborite and larderellite (Abs.): *Geol. Soc. America Bull.* **67,** 1680.

COOK, W. R., JR., AND JAFFE, HANS (1957), The crystallographic, elastic, and piezoelectric properties of ammonium pentaborate and potassium pentaborate: *Acta Cryst.* **10,** 705–707.

PALACHE, C., BERMAN, H., AND FRONDEL, C. (1951). The System of Mineralogy, 7th ed. Vol. II, (pp. 365–367). New York, John Wiley and Sons, Inc.

SCHALLER, W. T. (1933), Ammonioborite, a new mineral: *Am. Mineral,* **18,** 480–492.

Manuscript received March 2, 1959.

PETROGRAPHY OF SOME ERRATICS FROM CAPE ROYDS, ROSS ISLAND, ANTARCTICA

DUNCAN STEWART, *Carleton College, Northfield, Minn.*

ABSTRACT

A petrographical study is made of a suite of rocks collected by the British Antarctic Expedition, 1907–9, from Cape Royds, Ross Island, Antarctica. Of the 169 thin sections examined, 163 are of erratics. The igneous specimens constitute approximately 80 per cent of the collection, and may be described as typical East Antarctica rocks.

INTRODUCTION

Cape Royds, located in about latitude 77°33′ S and longitude 166°07′ E, is a promontory on the west side of Mount Erebus, Ross Island, Antarctica.

Results of other studies of Cape Royds erratics have been published. Benson's (1916) contribution relates to the dolerites collected chiefly from the moraines. Jensen (1916) records descriptions of anorthoclase trachyte, phonolitic trachytes, biotite-hornblende trachyte, acid and basic types of kenytes, shonkinitic kenyte porphyry, and porphyritic feldspar-olivine basalt. Smith (1954) refers briefly to the erratics of the Cape Royds district. Thomson (1916) in his microscopical studies of inclusions of the volcanic rocks of the Ross Archipelago mentions the occurrence of certain erratics, including a basic type of alkaline trachyte or orthophyre, sanidinite, and biotite microsanidinite. Walkom (1916), in discussing the petrography of pyroxene granulites, groups these rocks into acid, scapolite-bearing, and basic. Woolnough (1916) describes pegmatites, aplite, sodalite syenites, quartz diorite, granophyric granite porphyry, granophyre, feldspar porphyry, minettes, vogesite, porphyrite, sericitized diabase porphyry, sölvsbergites, sapphire-bearing trachyte, corundum-bearing trachyte, spherulitic trachyte, dense porphyritic basalt, actinolite gneiss, tremolite gneiss, actinolite schists, fine tremolite schist, spotted schist, phyllite, quartz schist, and micaceous sandstone.

CLASSIFICATION OF THE ROCKS

The specimens, represented by 169 thin sections, were collected by Sir Raymond E. Priestley, Geologist, British Antarctic Expedition, 1907–9. Aside from rocks 295A thru 295F and B–A thru B–R, whose numbers were either illegible or missing, the original numbering system is retained. Only six sections, 295, 295A–D and F, all kenytes, are of rocks collected *in situ*.

The collection contains 72 plutonites ranging in composition from

leuco-sodaclase adamellite to gabbro, leucoadamellites, adamellites and granodiorites predominating. There are 13 sections of hypabyssal rocks. Of the 54 extrusives, 29 are of basaltic compositions. Sedimentary rocks are represented by one breccia. Of the 28 rocks classified as metamorphic, 20 are gneisses, and of these 12 are granodioritic. One specimen of vein quartz is represented.

The rocks of this suite are: Pegmatite (211), leuco-sodaclase adamellite (195, 273), leucogranite (204, 242, 256, 300, 309, 324), garnetiferous leucogranite (308), leucogranodiorite (189, 244, 258, 287, 307), porphyritic leucogranodiorite (236), leucotonalite (B-K), leucoadamellite (196, 202, 207, 221, 230, 235, 237, 245, 260, 268, 299, 328), garnetiferous leucoadamellite (213), sodaclase granite (192), quartz granodiorite (251), adamellite (176, 180 210, 223, 226, 227, 241, 246, 275, 304), porphyritic adamellite (272, 326, B-F), granodiorite (198, 208, 222, 229, 250, 257, 259, 269, 270, 293, 302, 305, 327, B-G), porphyritic granodiorite (191, 282), tonalite (173, 228, B-N, B-Q), diorite (281), syenogabbro (190), gabbro (200, 225, 240, 262) and melagabbro (279); graphic granite porphyry (261), leuco-sodaclase adamellite porphyry (298), micrographic granite porphyry (271), granophyric adamellite porphyry (186), granophyric granodiorite porphyry (B-I), granodiorite porphyry (234), diabase (206, 219, 332), kersantite porphyry (303) and camptonite (205, 252); granophyre (9, 11), biotite granophyre (B-L), granophyre porphyry (199), spherulitic granophyre porphyry (314, 323), altered vesicular extrusive (233), rhyolite porphyry (247), trachyte (226, 277), kenyte (212), kenyte, acid variety (238, 295, 295A-F), vitrophyric kenyte (183, 194, 243, B-B, B-O), plagioclase kenyte (286), basalt (174, 188, 217, 220, 239, 278, 329, 331), vesicular basalt porphyry (185, 224), olivine basalt (232, 254, B-P), olivine basalt porphyry (1, 184, 249, 274, B-C, B-J), vesicular olivine basalt porphyry (B-A), enstatite basalt (264), orthopyroxene basalt (283), vesicular analcime basalt (218), analcime basalt porphyry (182, 201, 263), basalt tuff (289) and amygdaloid (265); breccia (B-H); biotite-actinolite gneiss (187), leucogranodiorite gneiss (193, 316, 321, B-D), granodiorite gneiss (171, 172, 203, 214, 216, 248, 253, 280, 292, 294, 296, B-M), tonalite gneiss (215, 297) and diorite gneiss (197); biotite-quartz schist (179) and calcareous biotite-quartz schist (231, 284); quartzite (12, 175, 317, B-E); ferruginous slate (B-R); vein quartz (177).

The improved Wentworth recording micrometer was used in the quantitative determination of the constituents of 66 sections of igneous rocks (Table 1). An aggregate distance of 56,600 units was measured in traversing each section 16 times. These rocks have been named and classified in accordance with the system of Johannsen.

Characteristics of the Rocks

Zoned plagioclases are not frequently observed in rocks of East Antarctica, whereas they are commonly noted in acid and intermediate intrusives of West Antarctica. In the Cape Royds suite eight acid and intermediate igneous rocks exhibit distinct zoning of the plagioclases. Indistinct zoning of the plagioclases is observed in over 30% of all erratics examined. Over 50% of the erratics contain microperthite, which characterizes "Atlantic-type" rocks. Myrmekitic intergrowths are

TABLE 1. MINERALOGICAL COMPOSITION OF SOME ERRATICS FROM CAPE ROYDS, ROSS ISLAND, ANTARCTICA

Minerals	Specimens												
	251	307	210	195	223	308	244	192	202	230	304	272	207
Quartz	46.89	44.11	39.32	37.88	36.74	36.73	35.73	34.73	33.21	32.73	32.68	32.48	32.30
K-feldspar	12.04	9.56	26.56	25.27	23.67	43.14	15.13	37.39	30.89	37.90	35.46	24.75	38.41
Albite	—	—	—	34.06	—	—	—	21.44	—	—	—	—	—
Oligoclase	29.68	43.17	25.71	—	33.65	17.00	44.93	—	33.66	27.30	25.33	34.72	27.25
Labradorite	—	—	—	—	—	—	—	—	—	—	—	—	—
Hornblende	3.32	—	—	—	—	—	—	0.32	—	—	0.46	—	—
Chlorite	8.07	3.16	8.09	1.75	5.63	0.97	3.97	5.86	2.06	1.89	6.07	8.05	1.91
Biotite	—	—	—	—	—	—	—	—	—	—	—	—	—
Augite	—	—	—	1.05	p	p	p	p	—	—	p	—	—
Muscovite	p	p	—	p	p	p	p	p	p	p	p	p	p
Apatite	p	p	p	p	p	p	p	p	p	p	p	p	p
Zircon	p	p	p	p	p	—	—	—	—	—	—	—	—
Fluorite	—	—	—	—	—	2.17	—	—	—	—	—	—	—
Garnet	—	—	—	—	—	p	p	p	p	p	p	p	p
Sphene	p	p	p	—	—	—	p	p	—	p	—	p	p
Pistacite	p	p	—	—	—	—	—	—	—	—	—	—	—
Zoisite	—	—	—	—	—	—	—	—	p	p	p	p	p
Allanite	p	—	—	—	p	—	p	p	—	—	—	—	—
Schorlite	—	—	—	—	p	—	—	p	—	—	p	—	—
Pyrite	p	p	p	—	—	—	—	—	—	—	p	p	p
Magnetite	p	p	p	p	p	p	p	p	0.18	0.17	p	p	p
Hematite	p	p	p	p	p	p	p	p	—	—	p	—	—
Leucoxene	—	—	p	p	—	—	—	—	p	p	—	p	—
Calcite	—	—	p	—	—	p	—	—	—	—	—	p	p
Kaolin	p	p	p	p	p	p	p	p	p	p	p	p	p
Sericite	p	p	p	—	p	p	p	p	p	p	p	p	p
Accessories	p	p	0.32	p	0.32	p	0.25	0.26	p	p	p	p	0.14
	100.00	100.00	100.00	100.01	100.01	100.01	100.01	100.00	100.00	99.99	100.00	100.00	100.01

p = present

251. Quartz granodiorite
307. Leucogranite
210. Adamellite
195. Leuco-sodaclase adamellite
223. Adamellite
308. Garnetiferous leucogranite
244. Leucogranodiorite
192. Sodaclase granite
202. Leucoadamellite
230. Leucoadamellite
304. Leucoadamellite
272. Porphyritic adamellite
207. Leucoadamellite

TABLE 1 (*Continued*)

Minerals	Specimens												
	287	293	B–K	237	242	324	245	221	180	236	298	226	189
Quartz	31.97	31.91	31.88	31.88	31.83	31.44	31.41	31.40	31.28	30.80	30.76	30.36	30.14
K-feldspar	21.62	13.20	1.81	38.32	33.33	41.30	31.83	36.72	31.69	18.16	31.04	30.57	9.96
Albite	—	—	—	—	—	—	—	—	—	—	—	—	—
Oligoclase	45.49	43.57	61.76	22.45	31.61	26.72	34.32	31.09	30.09	46.01	34.13	33.79	54.86
Labrodorite	—	—	—	—	—	—	—	—	—	—	—	—	—
Hornblende	—	4.00	—	—	—	—	—	—	—	p	—	—	—
Chlorite	0.65	6.66	4.54	1.15	2.51	0.63	2.22	0.78	6.58	5.03	4.06	5.28	4.88
Biotite													
Augite	—	—	—	—	—	—	—	—	—	—	—	—	—
Muscovite	p	p	—	5.92	—	p	—	p	p	—	p	—	—
Apatite	p	p	p	p	p	p	p	p	p	p	p	p	p
Zircon	p	p	p	p	p	p	p	p	p	p	p	p	p
Fluorite	—	—	—	—	—	—	—	—	—	—	—	—	—
Garnet	—	—	—	—	—	—	—	—	—	—	—	—	—
Sphene	p	p	p	p	p	p	p	p	p	p	p	p	p
Pistacite	—	p	—	p	p	—	p	p	p	p	p	—	p
Zoisite	—	—	—	—	—	—	—	—	—	—	—	—	—
Allanite	—	p	—	—	p	—	p	—	p	—	p	p	—
Schorlite	—	—	—	—	—	—	—	—	—	—	—	—	—
Pyrite	—	—	—	—	—	—	—	p	—	p	—	—	—
Magnetite	p	p	p	0.27	0.61	p	p	p	0.15	p	p	p	p
Hematite	p	p	—			p	p	p		p	p	p	p
Leucoxene	—	—	—	—	—	—	—	—	p	p	p	p	—
Calcite	—	p	—	—	—	p	—	—	p	—	—	p	—
Kaolin	p	p	p	p	p	p	p	p	p	p	p	p	p
Sericite	p	p	p	p	p	p	p	p	p	p	p	p	p
Accessories	0.26	0.65	p	p	0.13	p	0.21	p	0.21	p	p	p	0.16
	99.99	99.99	99.99	99.99	100.02	99.99	99.99	99.99	100.00	100.00	99.99	100.00	100.00

p=present

287. Leucogranodiorite
293. Granodiorite
B–K. Leucotonalite
237. Leucoadamellite
242. Leucogranite
324. Leucogranite
245. Leucoadamellite
221. Leucoadamellite
180. Adamellite
236. Porphyritic leucogranodiorite
298. Leuco-sodaclase adamellite porphyry
226. Adamellite
189. Leucogranodiorite

TABLE 1 (*Continued*)

Minerals	Specimens												
	208	269	260	196	328	222	213	235	270	228	176	259	229
Quartz	29.86	29.53	29.40	29.01	29.01	28.61	28.57	28.31	28.27	28.25	27.64	27.51	27.13
K feldspar	17.58	14.05	26.38	35.42	34.64	15.81	29.69	26.16	26.66	1.92	31.41	11.61	22.55
Albite	—	—	—	—	—	—	—	—	—	—	—	—	—
Oligoclase	44.81	50.62	39.70	32.13	33.85	48.21	40.83	41.60	39.67	59.54	34.48	54.70	43.98
Labradorite	—	—	—	—	—	—	—	—	—	—	—	—	—
Hornblende	0.66	—	—	—	—	—	—	—	—	—	—	—	—
Chlorite	7.00	5.55	4.53	2.98	2.49	7.37	0.30	3.92	5.40	9.24	6.37	6.18	6.17
Biotite											p	—	—
Augite	—	—	—	—	—	—	—	—	—	—	—	—	—
Muscovite	—	—	—	—	—	—	—	—	—	—	—	—	—
Apatite	p	p	p	p	p	p	p	p	p	p	p	p	p
Zircon	p	p	p	p	p	p	p	p	p	p	p	p	p
Fluorite	—	—	—	—	—	—	—	—	—	—	—	—	—
Garnet	—	—	—	—	—	—	p	—	—	—	—	—	—
Sphene	p	p	p	p	p	—	p	p	—	—	p	p	p
Pistacite	p	p	—	p	—	—	—	—	—	p	—	—	p
Zoisite	—	—	—	—	—	—	—	—	—	—	—	—	—
Allanite	p	—	p	p	p	—	—	p	p	p	p	—	p
Schorlite	—	p	—	—	p	—	—	—	—	—	—	—	—
Pyrite	—	—	—	—	—	—	—	—	—	0.27	—	—	—
Magnetite	p	p	p	0.32	p	p	p	p	p		p	p	p
Hematite	p	p	p		p	p	p	p	p		p	p	p
Leucoxene	—	p	p	—	p	p	p	p	—	—	—	p	—
Calcite	p	—	—	—	—	p	p	—	—	—	—	—	p
Kaolin	p	p	p	p	p	p	p	p	p	—	p	p	p
Sericite	p	p	p	p	p	p	p	p	p	p	p	p	p
Accessories	0.11	0.25	p	0.14	p	p	0.60	p	p	0.77	0.12	p	0.16
	100.02	100.00	100.01	100.00	99.99	100.00	99.99	99.99	100.00	99.99	100.02	100.00	99.99

p = present

208. Granodiorite
269. Granodiorite
260. Leucoadamellite
196. Leucoadamellite
328. Leucoadamellite
222. Granodiorite
213. Garnetiferous leucoadamellite
235. Leucoadamellite
270. Granodiorite
228. Tonalite
176. Adamellite
259. Granodiorite
229. Granodiorite

TABLE 1 (*Continued*)

Minerals	Specimens												
	299	327	256	258	B–G	273	B–F	326	186	275	282	227	268
Quartz	26.81	26.78	26.77	26.76	26.49	26.23	26.07	25.19	23.73	23.73	23.72	22.46	22.00
K-feldspar	40.81	20.91	27.22	22.07	34.52	37.75	31.13	35.03	29.88	28.50	9.92	42.07	47.10
Albite	—	—	—	—	—	—	—	—	—	—	—	—	—
Oligoclase	27.46	46.50	43.68	49.50	33.43	32.17	36.16	34.52	39.10	37.88	52.16	29.20	29.07
Labradorite	—	—	—	—	—	—	—	—	—	—	—	—	—
Hornblende	p	—	—	—	—	3.85	1.76	p	7.18	9.50	4.39	—	1.83
Chlorite	4.44	5.81	2.34	1.65	5.56			4.69			9.25	6.27	
Biotite	—	—	—	—	—	—	—	—	—	—	—	—	—
Augite	—	—	—	—	—	—	—	—	—	—	—	—	—
Muscovite	p	p	p	p	—	p	—	p	—	—	—	p	p
Apatite	p	p	p	p	p	p	p	p	p	p	p	p	p
Zircon	p	p	p	p	p	p	p	p	p	p	p	p	p
Fluorite	—	—	—	—	—	—	—	p	—	—	—	—	—
Garnet	—	—	—	—	—	—	—	—	—	—	—	—	—
Sphene	p	p	p	p	p	p	p	p	p	p	p	p	p
Pistacite	p	—	—	—	—	—	—	p	—	p	p	p	—
Zoisite	—	—	—	—	—	—	—	p	—	—	—	—	—
Allanite	p	—	p	—	p	p	p	p	p	p	p	p	p
Schorlite	—	—	—	—	—	—	—	—	—	—	—	p	—
Pyrite	—	—	—	—	—	—	p	—	p	—	—	—	—
Magnetite	p	p	p	p	p	p	p	p	p	p	p	p	p
Hematite	p	—	p	p	—	p	p	p	p	p	p	p	p
Leucoxene	—	—	—	p	p	—	p	—	—	—	—	p	p
Calcite	—	—	—	p	p	—	p	—	—	—	p	—	p
Kaolin	p	p	p	p	p	p	p	p	p	p	p	p	p
Sericite	p	p	p	p	p	p	p	p	p	p	p	p	p
Accessories	0.48	p	p	p	p	p	0.78	0.57	0.11	0.40	0.56	p	p
	100.00	100.00	100.01	99.98	100.00	100.00	100.00	100.00	100.00	100.01	100.00	100.00	100.00

p = present

299. Leucoadamellite
327. Granodiorite
256. Leucogranodiorite
258. Leucogranodiorite
B–G. Adamellite
273. Leuco-sodaclase adamellite
B–F. Porphyritic adamellite
326. Porphyritic adamellite
186. Granophyric adamellite porphyry
275. Adamellite
282. Porphyritic granodiorite
227. Adamellite
268. Leucoadamellite

TABLE 1 (*Continued*)

Minerals	Specimens													
	309	198	191	246	300	302	250	241	B–N	305	257	279	173	190
Quartz	21.67	21.41	20.18	18.97	18.46	16.65	13.31	14.82	12.83	11.23	7.55	6.68	3.32	1.42
K-feldspar	56.02	21.44	23.53	35.63	60.78	25.59	24.65	29.85	p	9.81	5.97	5.37	p	4.12
Albite	—	—	—	—	—	—	—	—	—	—	—	—	—	—
Oligoclase	19.32	51.54	47.51	37.59	16.91	46.10	42.02	45.63	51.85	46.25	68.70	35.32	55.29	—
Labradorite	—	—	—	—	—	—	—	—	—	—	—	—	—	61.77
Hornblende	—	—	0.87	2.20	—	3.38	5.98	1.11	13.59	14.71	9.04	39.27	22.11	
Chlorite	2.99	5.36	7.79	5.62	3.45	8.28	13.71	8.32	19.76	16.67	7.61	12.35	18.16	5.83
Biotite														
Augite	—	—	—		—	—	—	—	1.33	1.33	—	p	p	26.22
Muscovite	—	p	—	p	—	p	p	p	p		—	—	p	—
Apatite	p	p	p	p	p	p	p	p	p	p	p	p	p	p
Zircon	p	p	p	p	p	p	p	p	—	p	p	p	p	p
Fluorite	—	—		—	—	—	—	—	—		—		—	—
Garnet	—	—	—	—	—	—		—	—	—	—	—	—	—
Sphene	p	p	p	p	p	p	p	p	p	p	1.14	p	p	—
Pistacite	—		p	p	p	p	p	p	p	p		—	p	—
Zoisite			—				—	—			—	—	—	
Allanite	p	p	p	—	—	p	p	p	p	p	p		—	—
Schorlite			—	—	—	p	—	—	—		—		—	—
Pyrite			—	—	—		—	p	—	p	—	—	—	
Magnetite	p	p	p	p	p	p	p	p	p	p	p	p	p	0.65
Hematite	p	—	p	p	p	p	p	p	—	p	p	p	—	
Leucoxene	—		—			p	—	—	—	—	—		—	
Calcite			—			—	—	p	p	—	p	—	p	
Kaolin	p	p	p	p	p	p	p	p	p	p	p	p	p	p
Sericite	p	p	p	p	p	p	p	p	p	p	p	p	p	p
Accessories	p	0.24	0.14	p	p	p	0.33	0.26	0.63	p	p	1.02	1.10	p
	100.00	99.99	100.02	100.01	100.00	100.00	100.00	99.99	99.99	100.00	100.01	100.01	99.98	100.01

p = present

309. Leucogranite
198. Granodiorite
191. Porphyritic granodiorite
246. Adamellite
300. Leucogranite
302. Granodiorite
250. Granodiorite
241. Adamellite
B N. Tonalite
305. Tonalite
257. Granodiorite
279. Melagranodiorite
173. Tonalite
190. Syenogabbro

observed in slightly less than 50% of the Cape Royds specimens. Twinned hornblendes, so commonly noted in West Antarctica rocks, are uncommon in those of East Antarctica.

A review of the literature discloses that allanite is practically confined to rocks of East Antarctica. The only references to this mineral in West Antarctica are recorded by Pelikan (1909, p. 36) in a kersantite collected in Osterrieth Mountains, Anvers Island, Palmer Archipelago, and by Stewart (1945a, p. 147; 1947, p. 230) in intrusives of the Melchior Islands, Palmer Archipelago. Allanite and allanite (?) are observed in 8 of 125 thin sections.

Allanite in Antarctic rocks was first reported by Prior (1902, p. 323) in descriptions of a biotite granite boulder found on the plateau of Cape Adare, Victoria Land, and a boulder of biotite-hornblende granite from "Geikie Land" (Geikie Ridge), collected by the Southern Cross Antarctic Expedition, 1898–1900.

Prior (1907, p. 127), describing the rocks collected by the National Antarctic Expedition, 1901–4, refers to allanite in specimens from Cathedral Rocks, Victoria Land. Mawson (1916, p. 211), in his descriptions of rocks collected from the mainland of Victoria Land by the British Antarctic Expedition, 1907–9, states, "Allanite is by far the commonest of the accessory minerals appearing in nearly all the granites in our collections." On page 217, he refers to allanite in aplitic granite porphyry. Cotton (1916, p. 235–236) mentions allanite (?) in an augite porphyrite from Cape Ross, south of Depot Island, Victoria Land. Smith (1924, p. 183), in referring to hornblendic biotite granites of Granite Harbour and Ferrar Glacier areas, McMurdo Sound, Victoria Land, states, "Allanite (orthite) was found as an accessory in all typical specimens." In this same publication, page 185, he remarks that orthite as thin prisms (0.6 mm.×0.06 mm.) is a rare but constant accessory in aplite and pegmatite dikes of the McMurdo Sound region. He, also, reports allanite in quartz-orthoclase porphyries and mentions the mineral as a constant accessory in orthoclase porphyries. Biotite and hornblendic biotite granites contain allanite in the Terra Nova Bay region, Victoria Land.

Although Wade (1937) and Warner (1945) do not record allanite in their thin sections, Stewart (1945*b*) reports allanite in 9 of 30 slices of quartz-bearing intrusives from Marie Byrd Land, which rocks show affinities with both East and West Antarctica types.

Wade (1945) did not observe allanite in rocks of the Rockefeller Mountains, Edward VII Peninsula, nor did Stewart (1945*b*).

The occurrence of allanite is notable in the specimens collected by the Australasian Antarctic Expedition, 1911-14, from Adélie, George V, and eastern Queen Mary Coasts, as recorded in the writings of Glastonbury (1940*a*, *b*, *c*), Kleeman (1940), Nockolds (1940), Stillwell (1918, 1923), and Summers and Edwards (1940). Allanite is reported in granite, felsite, porphyry, granophyre, metamorphosed dolerite, gneiss, hybrid gneiss, schist, amphibolite and marble. On page 52, in describing the rocks of eastern Queen Mary Coast, Nockolds states, "A feature of this province, if province it can be called, is the universal presence of orthite in all acid rocks."

Although Woolnough (1916) does not mention the occurrence of allanite in Cape Royds erratics, a distinguishing feature of this suite from Cape Royds is the presence of allanite, being observed in 52 sections of acid igneous rocks and three of intermediate composition, as well as in eight gneisses and two schists. Allanite exhibiting neither twinning nor zoning is seen in 10 sections; zoned and twinned in 33 slides; zoned only in 19 thin sections, and twinned only in two slices.

Acknowledgments

Carleton College was the recipient of the suite of rocks from Cape Royds, a gift of The Academy of Natural Sciences of Philadelphia. The author offers his thanks to Professor C. E. Tilley, F. R. S., and to Dr. S. O. Agrell, Mineralogy and Petrology Department, of the University of Cambridge, in whose laboratories the qualitative studies were made. Available for comparative purposes were 1,500 cataloged and 102 uncataloged thin sections of Antarctic rocks, including 236 slices of Cape Royds erratics. The research was made possible through grants from the Penrose Bequest of The Geological Society of America and the Louis W. and Maud Hill Family Foundation.

References

Benson, W. N. (1916), Report on the petrology of the dolerites collected by the British Antarctic Expedition, 1907–1909, *British Antarctic Exped.* 1907–1909, *Rep. Sci. Investigations Geol.*, **2**, pt. 153–160.

Cotton, L. A. (1916), Petrographical notes on some rocks retrieved from the cache at Depot Island, Antarctica, *British Antarctic Exped. 1907–1909, Rep. Sci. Investigations Geol.*, **2**, Appendix pt. 13, 235–237.

Glastonbury, J. O. G. (1940*a*), Acid effusive and hypabyssal rocks (from the moraines), *Austral. Antarctic Exped. 1911–1914, Sci. Rep.*, ser. A, **4**, *Geol.*, pt. 4, 115–134.

——— (1940*b*), Metamorphosed limestones and other calcareous sediments from the moraines, a further collection, *Austral. Antarctic Exped. 1911–1914, Sci. Rep.*, ser. A, **4**, *Geol.*, pt. 8, 295–322.

——— (1940*c*), Some hybrid gneisses from the moraines, Cape Denison, *Austral. Antarctic Exped. 1911–1914, Sci. Rep.*, ser. A, **4**, *Geol.*, pt. 9, 325–333.

Jensen, H. I. (1916), Report on the alkaline rocks of Mount Erebus, Antarctica, *British Antarctic Exped. 1907–1909, Rep. Sci. Investigations Geol.*, **2**, pt. 7, 93–128.

Kleeman, A. W. (1916), Schists and gneisses from the moraines, Cape Denison, Adelie Land, *Austral. Antarctic Exped. 1911–1914, Sci. Rep.*, ser. **A, 4,** *Geol.*, pt. 7, 197–292.

Mawson, Douglas (1916), Petrology of rock collections from the mainland of South Victoria Land, *British Antarctic Exped. 1907–1909, Rep. Sci. Investigations Geol.*, **2**, pt. 13, 201–234.

Nockolds, S. R. (1916), Petrology of rocks from Queen Mary Land, *Austral. Antarctic Exped. 1911–1914, Sci. Rep.*, ser. **A, 4,** *Geol.*, pt. 2, 15–86.

Pelikan, A. (1909), Géologie, Petrographische Untersuchung der Gesteinsproben, Expédition Antarctique Belge, Résultats du Voyage du *S.Y. Belgica* en 1897–1898–1899 sous le commandement de A. de Gerlache de Gomery, *Rap. Sci.*, **1**, 1–49.

Prior, G. T. (1902), Report on rock specimens collected by the Southern Cross Antarctic Expedition, *Rep. Southern Cross Collections* (*British Museum*), 321–332.

——— (1907), Report on the rock specimens collected during the *Discovery* Antarctic Expedition 1901–1904, *National Antarctic Exped. 1901–1904, Nat. Hist.*, **1**, *Geol.*, 101–140.

Smith, W. Campbell (1924), The plutonic and hypabyssal rocks of South Victoria Land, *British Antarctic* (*Terra Nova*) *Exped. 1910, Nat. Hist. Rep. Geol.*, 1 (6), 167–227.

—— (1954), The volcanic rocks of the Ross Archipelago, *British Antarctic* (*Terra Nova*) *Exped. 1910, Nat. Hist. Rep. Geol.*, 2 (1), 1–107.

Stewart, Duncan, Jr. (1945*a*), Preliminary report on some intrusives of the Melchior Islands, Antarctica, *Proc. Amer. Phil. Soc.*, **89** (1), 146–147.

——— (1945*b*), The petrography of some intrusive rocks from Edward VII and Marie Byrd Lands, *Proc. Amer. Phil. Soc.*, **89** (1), 148–151.

——— (1947), Rocks of the Melchior Islands, Antarctica, *Proc. Amer. Phil. Soc.*, **91,** 229–233.

Stillwell, F. L. (1918), The metamorphic rocks of Adelie Land, Sect. 1, *Austral. Antarctic Exped. 1911–1914, Sci. Rep.*, ser. A, *Geog., Physiog., Glaciol., Oceanog., and Geol.*, **3,** pt. 1, 1–230.

——— (1923), Amphibolites and related rocks from the moraines, Cape Denison, Adelie Land, *Austral. Antarctic Exped. 1911–1914, Sci. Rep.*, ser. A, *Geol.*, **3,** pt. 4, 259–280.

Summers, H. S., and A. B. Edwards (1940), Granites of King George Land and Adelie Land, with an appendix by A. W. Kleeman, *Austral. Antarctic Exped. 1911–1914*, ser. A, *Geol.*, **4,** pt. 3, 87–113.

Thomson, J. A. (1916), Report on the inclusions of the volcanic rocks of the Ross Archipelago, *British Antarctic Exped. 1907–1909, Rep. Sci. Investigations Geol.*, **2,** pt. 8, 129–148.

Wade, F. A. (1937), Petrologic and structural relations of the Edsel Ford Range, Marie Byrd Land, to other Antarctic mountains, *Bul. Geol. Soc. Amer.*, **48,** 1387–1396.

——— (1945), The geology of the Rockefeller Mountains, King Edward VII Land, Antarctica, *Proc. Amer. Phil. Soc.*, **89** (1), 67–77.

Walkom, A. B. (1916), Report on the pyroxene granulites collected by the British Antarctic Expedition, 1907–1909, *British Antarctic Exped. 1907–1909, Rep. Sci. Investigations Geol.*, **2,** pt. 10, 161–168.

Warner, L. A. (1945), Structure and petrography of the Southern Edsel Ford Ranges, Antarctica, *Proc. Amer. Phil. Soc.*, **89** (1), 78–122.

Woolnough, W. G. (1916), Petrological notes on some of the erratics collected at Cape Royds, *British Antarctic Exped. 1907–1909, Rep. Sci. Investigations Geol.*, **2,** pt. 11, 169–188.

Manuscript received February 24, 1959.

THE AMERICAN MINERALOGIST, VOL. 44, NOVEMBER-DECEMBER, 1959

THE ALKALI FELDSPARS V. THE NATURE OF ORTHOCLASE AND MICROCLINE PERTHITES AND OBSERVATIONS CONCERNING THE POLYMORPHISM OF POTASSIUM FELDSPAR*

J. V. Smith, *Department of Mineralogy and Petrology, Division of Earth Sciences, The Pennsylvania State University, University Park, Pennsylvania and*

W. S. MacKenzie, *Department of Geology, University of Manchester, Manchester England.*

Abstract

The observations recorded in paper 1 of this series have been extended to cover 37 specimens of orthoclase and microcline perthites. The exsolved sodium phase of the perthitic specimens is usually a low temperature albite or oligoclase, although some specimens falling near the composition $Or_{80}(Ab+An)_{20}$ and with 2V between 50° and 70° contain an anorthoclase instead. The anorthoclase occurs as a pericline twin-type superstructure. Most of the albite-oligoclases are dominantly albite twinned: four specimens show both pericline and albite twinning, while seven specimens with compositions $\sim Or_{70}$ and $2V_\alpha$ between 60° and 80° show mainly albite twin-type superstructure.

The potassium phase is monoclinic in 14 specimens, triclinic in 4 and partly each in 15 specimens. The triclinic components give reflections that vary from sharp to diffuse, with lattice angles α^*, γ^* varying from 90°, 90° to about 90°24′, 92°20′. All the triclinic components are composed of two or more units whose angular relations vary between the extremes of albite and pericline twinning, with the "diagonal" association fairly common.

The optic axial angles fall either in or close to a triangle formed by the three extreme varieties: low albite, Or_0 $2V_\alpha$ 100°; orthoclase, Or_{100} $2V_\alpha$ 35°; and maximum microcline, Or_{100} $2V\alpha$ 80°. There is a moderate, but not good, correlation between the position of the specimens in this triangle and the nature of the potassium-rich component. Specimens which either contain anorthoclase or consist predominantly of the albite twin-type superstructure of low albite-oligoclase fall into two small areas in the 2V versus composition diagram. The preferential occurrence of the superstructure in the more potassium-rich compositions supports the hypothesis that strain favors its existence in orthoclase and microcline perthites. The anorthoclase is thought to occur because the containing specimens have compositions that lie close to a phase boundary, a condition known to favor metastability.

Introduction

In paper 1 of this series (MacKenzie and Smith, 1955), the results of a mineralogical study of some orthoclase perthites were presented. Since then, data on additional orthoclase perthites and on some microcline perthites have been obtained and form the basis of this paper. To conserve space, familiarity with the literature reviews contained in the earlier papers of this series will be assumed. No papers that bear solely

* Contribution No. 58 22, College of Mineral Industries, The Pennsylvania State University.

on the relations between the perthitic components have appeared since these reviews, but a considerable number have appeared that are concerned with the polymorphism of potassium feldspar (Bailey and Taylor (1955), Goldsmith and Laves (1954a,b), Hafner and Laves (1957), Heier (1957), Ferguson, Traill and Taylor (1958)). A detailed review will be given in a later paper of this series which is to be devoted to the polymorphism of potassium feldspar, and it is sufficient for the present purpose to record that Hafner and Laves state that there is a continuous series of structural states between high-sanidine and maximum microcline, that the conversion of a fully disordered to a fully ordered potassium feldspar may occur in innumerable ways by variation of the distribution of Al ions between the four possible sites, and that the distribution of Al in the intermediate states depends on the previous temperature-time relations.

Description of the Specimens

The origin, bulk chemical composition and optic axial angles of the 37 specimens studied by single crystal x-ray methods are recorded in Table 1, together with the lattice angles α^* and γ^* of the triclinic phases, where these have been measured. (All compositions are expressed as weight per cent Or, Ab, An.) Most of the specimens are derived from pegmatites, five are from charnockitic rocks and one each from a quartz monzonite, a porphyroblastic orthoclase gneiss, a granite and from a vein in a low-grade schist. The specimens were originally called orthoclase- or microcline-perthites on the basis of the observed optical symmetry. Fig. 1 shows the relationship between the optic axial angle and bulk chemical composition, where it may be seen that almost all specimens fall in the triangular area formed from the apices low-albite, orthoclase and maximum microcline.

Except for a few which are either very potassium-rich or sodium-rich, the feldspars are perthitic, containing either two or three different phases. These can be most certainly characterized by their α^*, γ^* angles as shown in Fig. 2. The measurements fall into three groups. The first group composed of potassium-rich components, falls on an essentially continuous series (the microcline series), with monoclinic orthoclase at one end. The position of the other end is subject to some uncertainty because one specimen, N, lies off the common trend: neglecting it the other specimens show that the microcline series extends at least as far as α^* 90°24′, γ^* 92°20′—the *maximum microcline* defined by MacKenzie (1954). The triclinic potassium phase of N occurs in an uncommon orientation (Smith and MacKenzie, 1954) which could not be interpreted in terms of the known twin laws, and while the angles may indicate a

TABLE 1. PROPERTIES OF THE SPECIMENS

Specimen Number	Chemical composition				2Vα	Potassium phase		Sodium phase	
	Or	Ab	An	Cs		α^*	γ^*	α^*	γ^*
A	96.1	3.9	0.0	—	34.8°	—	—	—	—
B	91.2	7.9	0.6	0.3	68.4°	—	—	—	—
C	90.8	6.7	2.5	—	43.6°	—	—	—	—
U	85.9	12.7	1.4	—	76.2°	90°05′	90°46′M	—	—
3705	84.9	13.1	2.0	—	83–86°	—	—	—	—
D	84.5	13.8	1.7	—	46.2°	—	—	—	—
V	84.1	14.8	1.1	—	63.9°	—	—	88°29′	89°16′P
E	83.3	14.9	1.8	—	57.6°	90°09′	91°09′M	87°58′	89°05′P
LM3A	82.8	14.3	1.8	1.0	80°	90°19′	91°24′A	—	—
6436	82.5	16.4	1.1	—	69°	—	—	—	—
W	81.6	18.0	0.4	—	81.5°	—	—	86°19′	89°42′A
3708	80.7	17.9	1.4	—	82–84°	—	—	86°45′	89°36′A
X	79.3	19.2	1.5	—	76.0°	—	—	(86.5°	90.0°)P
F	78.8	18.9	2.3	—	52.9°	—	—	—	—
Z	78.2	20.2	1.6	—	70.6°	—	—	88°35′	89°31′P
LM6	77.5	20.9	0.8	0.7	70°	90°21′	91°35′A	86°25′	90°18′A
Y	76.1	22.2	1.7	—	79.4°	—	—	—	—
S347	74.4	24.2	1.4	—	62°	—	—	86°13′	89°19′A
H	72.5	25.8	1.7	—	61.5°	—	—	—	—
4639	71.3	25.8	2.9	—	62–78°	90°27′	92°09′P	—	—
I	69.4	28.9	1.7	—	69.1°	—	—	—	—
J	66.6	32.5	0.9	—	75.0°	—	—	—	—
K	64.4	33.8	1.8	—	61.4°	—	—	—	—
M	57.3	40.3	2.4	—	73.7°	—	—	87°00′	90°32′A
N	53.7	45.6	0.7	—	83.5°	90°50′	92°35′D	86°48′	90°33′A
O	48.5	47.3	4.2	—	82.8°	—	—	86°45′	90°15′A
								86°42′	90°15′P
OF4	46.4	52.5	1.1	—	75°	—	—	86°32′	90°23′A
Q	45.6	50.2	4.2	—	81.7°	—	—	86°52′	90°17′A
R	44.1	51.6	4.3	—	71.3°	—	—	86°44′	90°00′A
								86°45′	89°55′A
								86°48′	89°58′A
OF5	43.3	54.5	2.2	—	90°	—	—	86°29′	90°20′A
								(86.5°	90.5°P)
OF2	43.0	53.7	3.3	—	86°	—	—	86°48′	90°28′A
OF3	41.9	54.5	3.6		80°	—	—	86°38′	90°13′A
OF1	39.0	58.8	2.2	—	90°	90°16′	91°12′A	86°23′	90°25′A
1	31.5	68.3	0.2	—	82.0°	—	—	86°39′	90°34′A
2	19.8	72.7	6.0	1.5	78.5°	—	—	86°13′	89°30′P
								86°29′	89°58′A
S	2.6	96.2	1.2	—	97.8°	—	—	—	—
T	1.4	98.2	0.4	—	102°	—	—	—	—

NOTES. Specimens A–Z were described by Spencer (1930, 1937): Specimens 3705, 6436, 3708 and 4639 by Howie (1955); specimen S347 by Howie (Ph.D. Thesis, Cambridge); specimens LM3A and LM6 by Heald (1950); specimens OF4, 5, 2, 3 and 1 by Oftedahl (1948); specimen 1 by MacKenzie and Smith (1955) and specimen 2 by Tilley (1954). The letters A, D, P, M, after the values for the angles α^* and γ^* denote, respectively, albite twinning, the diagonal association, pericline twinning and measurements made on powder patterns by MacKenzie (1954). Weak pericline twinning of a sodium-rich component was given by specimens X and OF5: the measured values of α^* and γ^* were good enough for identification of the component as low albite-oligoclase but not good enough for plotting on Fig. 2.

genuine structural difference between the potassic phases of N and of the other triclinic potassium feldspars, it is possible that the different nature of the associations have led to a modification of the angles by nothing more than lattice strains.

The angles for the sodium components provide the other two groups. Three fall with the anorthoclase series and twenty-one with the sodic

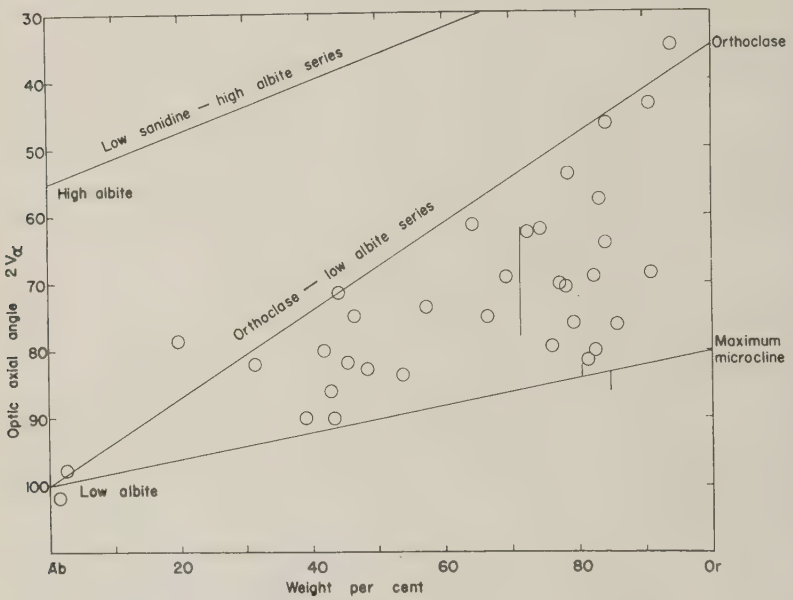

FIG. 1. The relation between the optic axial angle $2V\alpha$ and the bulk chemical composition of the present suite of alkali feldspars. The diagram is a slight modification of the one presented by Tuttle (1952). The short vertical lines indicate a range of variation of optic axial angles.

plagioclases. As described in paper 1, the deviations of angles for the latter group from those of low albites are probably caused by solid solution of potassium and calcium feldspars, though for the latter the duality between structural state and calcium content must be borne in mind.

The triclinic phases consist of two or more components. In addition to the simple albite and pericline twins, pairs of components may occur whose relative orientations lie between those for the albite and pericline twins. In the first described example (Smith and MacKenzie, 1954), the orientation of the components in this *diagonal association* (named from the diagonal directions that relate the pairs of reflections on *b*-axis oscil-

lation photographs) lay half-way between those for albite and pericline twinning (Fig. 3). Further examples have shown orientations that lie in various positions between the two extremes and it seems probable that all variations are possible.

Two further variants in the sodium phases are *albite twin-type superstructure* and *pericline twin-type superstructure* (Laves, 1952; MacKenzie

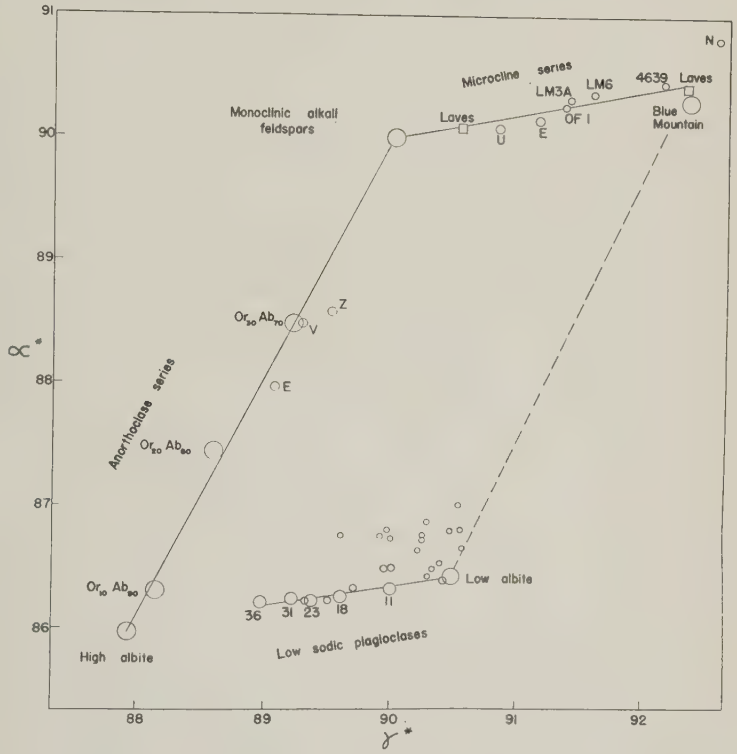

FIG. 2. The relation between the reciprocal lattice angles α^* and γ^* for the sodium and potassium phases. The reference values, shown by large circles, have been obtained for homogeneous feldspars by Donnay and Donnay (1952), MacKenzie (1954) and Smith (1956). The two squares represent the mean of values obtained for adularias and microclines by Laves (1950). The small circles express the data for the present suite of specimens where the lattice angles have been measured. The data are listed in Table 1. Dr. W. L. Brown (private communication) has recently found that large variations in α^* and γ^* can be obtained by heating albite and other feldspars for long periods just under the melting point. This work casts doubt on the determination of composition from α^*, γ^* values, though the authors have found that composition estimated in this way for natural feldspars have generally been very reasonable. Further discussion of this very important point will be given later in this series.

and Smith, 1955). The first type gives reflections which lie along the row lines of *b*-axis oscillation photographs and has been interpreted (Laves, 1952) as the result of a superstructure produced by regular polysynthetic twinning according to the albite law. Many variations between a very regular superstructure and simple albite twinning have been observed. As the albite-twinned sodium phases are invariably albite-oligoclases in

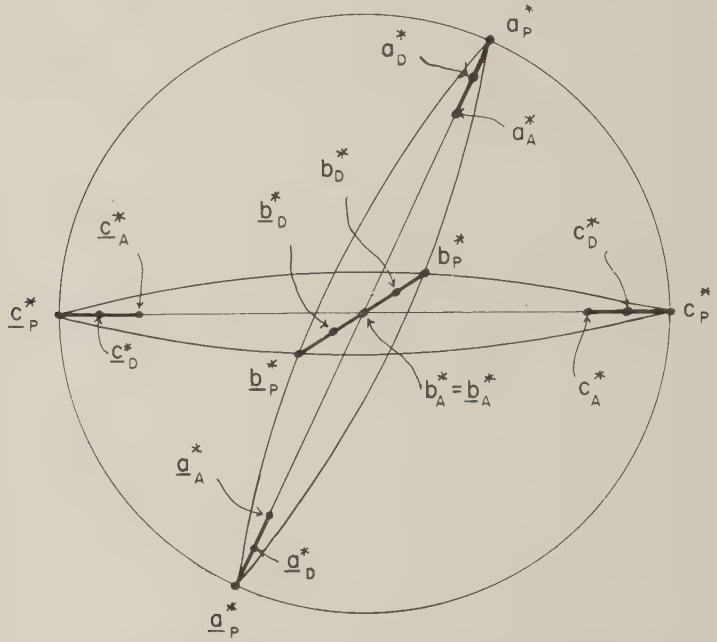

FIG. 3. The relative crystallographic orientation of the two components in a diagonal association. The suffixes A, D and P denote, respectively, albite twinning, diagonal association and pericline twinning. Crystallographic elements from the diagonal association may be anywhere between the extremes for albite and pericline twinning subject to the condition that a^*_D, b^*_D and c^*_D maintain the correct interaxial angles. The deviations of the angles α^* and γ^* from 90° are grossly exaggerated.

this suite of specimens it is natural to suppose that the albite twin-type superstructure is composed of similar material. The pericline twin-type superstructure gives two clusters of reflections lying along the layer lines of *b*-axis oscillation photographs. Values of α^*, γ^* for the centers of the clusters indicate anorthoclase (Fig. 2) and it seems very reasonable to conclude that the superstructure is composed of anorthoclase. (In the following paper, observations on perthites from the Slieve Gullion area in Northern Ireland are used to show that anorthoclase may occur as albite twin-type superstructure. Thus it cannot be assumed that all

albite twin-type superstructure is formed of albite-oligoclase and all the pericline type of anorthoclase, though usually this implication would be valid.)

Figs. 6, 7 and 8 have been prepared to show in a concise way the nature of the exsolved phases. By the use of symbols plotted on graphs of 2V versus bulk composition the nature of the specimens is shown, and what is more important, the relation between the particular displayed property and the optical and compositional variables may be seen.

The Sodium-rich Components

Two specimens are composed solely of a sodium-rich feldspar, three of a potassium feldspar, while the remainder are perthitic, five containing an anorthoclase, twenty-three an albite-oligoclase, two that may contain both, and two containing an unidentified sodium feldspar. The latter specimens were obtained from charnockite rocks and the photographs contain reflections streaked along curves of constant θ, thus precluding a positive identification.

The presence of anorthoclase is remarkable for it would not be expected at first thought to persist in specimens such as these that have been subjected to moderate and low temperatures for long periods of time. A clue to the dilemma is offered by the restricted area occupied by the anorthoclase-containing specimens on the composition $-2V$ diagram (Fig. 4). The fields of one and more than one feldspar may be delineated on the composition $-2V$ diagram. The boundary curve between the two fields may be regarded as a distorted projection of the exsolution dome that occurs in the phase diagram of the system $NaAlSi_3O_8-KAlSi_3O_8$. In fact the whole of Fig. 5 may be imagined as a distorted copy of the solid-phase portion of this system with the optic axial angle being related to the temperature in the phase diagram. (The data for the field boundary has been taken from earlier papers of this series and from other investigations. A full discussion of the phase relations is planned for the concluding paper of this series). It is well known, though not often mentioned in print, that near phase boundaries equilibrium may be established only with difficulty and that unstable forms often develop and persist metastably. Thus it seems reasonable to correlate the presence of the anorthoclase with the proximity of the specimens to the field boundary in Fig. 4. Other specimens in or near the same composition range generally have larger values of 2V thus lying further away from the field boundary. They all contain low-temperature albite-oligoclase in accordance with expectation. Specimen B although it lies in the field of two or more feldspars was found to be homogeneous. It is an adularia, a form of feldspar characteristic of a low-temperature

origin, and may very well have not had sufficient opportunity to exsolve its sodium feldspar. Specimens LM6 and S347 contain low-temperature albite-oligoclase and may also contain a little anorthoclase as well, for weak streaks lie along the layer-lines in *b*-axis oscillation photographs. The direct cause of the persistence of the anorthoclase may well be lattice strain, for it is probably not fortuitous that the anorthoclase occurs in the form of a superstructure and that the α^*, γ^* values correspond to potassium-rich anorthoclase near Or_{30} in composition. For comparison, the α^*, γ^* values of anorthoclase occurring in sanidine perthites indicate compositions more sodium-rich, Or_{18}–Or_{25}. It was suggested in paper 1 of this series that anorthoclase can only invert to low-temperature albite when most of the potassium feldspar has exsolved, and that inversion of anorthoclase in orthoclase perthites was prevented by the presence of a comparatively high content of potassium.

The low sodium-rich feldspar occurs in three different associations:—albite twinning, albite twin-type superstructure and pericline twinning

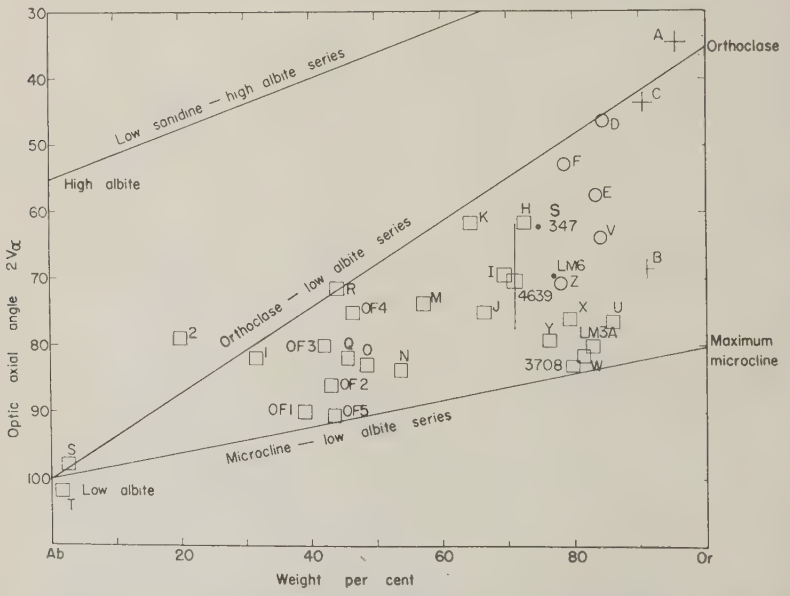

FIG. 4. The nature of the sodium-rich phases. A square indicates that the sodium-rich phase is an albite-oligoclase while a circle indicates anorthoclase. The three specimens represented by plus signs have no sodium phase. Specimens S347 and LM6 (represented by dots) contain two sodium-rich phases, one an albite twinned low-temperature albite-oligoclase and the other a phase which gives weak streaks lying along the layer lines of *b*-axis oscillation photographs. Two specimens, 3705 and 6436, have been omitted from the figure because the reflections were too badly streaked along curves of constant θ for the nature of the sodium-rich phase to be deduced.

(Fig. 6). Pericline twinning is rare, being displayed by only four specimens out of the twenty-five, and even these four also contain albite twinning. It was not possible to determine the type of association for two of the charnockitic specimens. The distinction between albite twinning and albite superstructure is not sharp and it is difficult to evaluate the precise nature of the sodium phase in many specimens. However, an attempt has been made to separate specimens into those in which albite twinning occurs either solely or predominantly and those in which the superstructure is favored. It may be seen from Fig. 6 that the superstructure is more frequent for those specimens with the lower optic axial angles and the greater contents of $KAlSi_3O_8$, though two specimens S347 and LM6 with albite twinning also occur in this region. Laves (1952) has suggested that the superstructure results from the need for the strain to be lessened between the triclinic albite and the monoclinic orthoclase and has shown that the structural misfit is less for the superstructure than for the twinning. Thus it would be expected that the

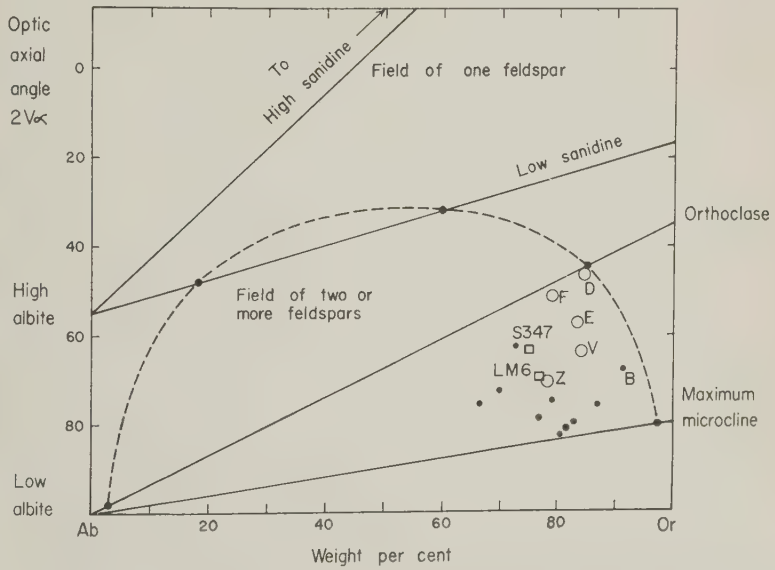

Fig. 5. Correlation of the optical and compositional properties of alkali feldspars with the perthitic or non-perthitic nature of the feldspars. The four straight lines represent the series high albite—high sanidine, high albite—low sanidine, low albite—orthoclase, low albite –maximum microcline. The dotted curve is the approximate boundary between the fields of one feldspar and more than one feldspar. The five circles represent specimens that contain anorthoclase. The squares represent specimens LM6 and S347 which contain low albite-oligoclase and which may also contain anorthoclase (see legend to Fig. 4). The small dots represent specimens that do not contain anorthoclase.

superstructure would be more favored when the proportion of orthoclase increased and this is what is actually found. Nevertheless some of the more potassium-rich specimens such as LM6 contain well-developed albite twinning, and the bulk composition of the sample cannot be the sole factor involved.

Possibly the dimensions of the perthitic units are also of importance for the larger the individual unit the less should be the strain within the unit: consequently the superstructure should decrease as the perthite becomes coarser. In general the perthite should be coarser when the feldspar is in a lower-temperature state, that is when the value of 2V is larger. Therefore for a given bulk composition it would be expected that specimens with larger values of 2V would have less superstructure. Fig. 6 shows slight evidence in favor of this but it is hardly convincing.

In the first paper of this series it was shown that in the orthoclase—low albite series, specimens could be placed into three groups on the basis of the exsolved sodium-rich phase, each group having a characteristic com-

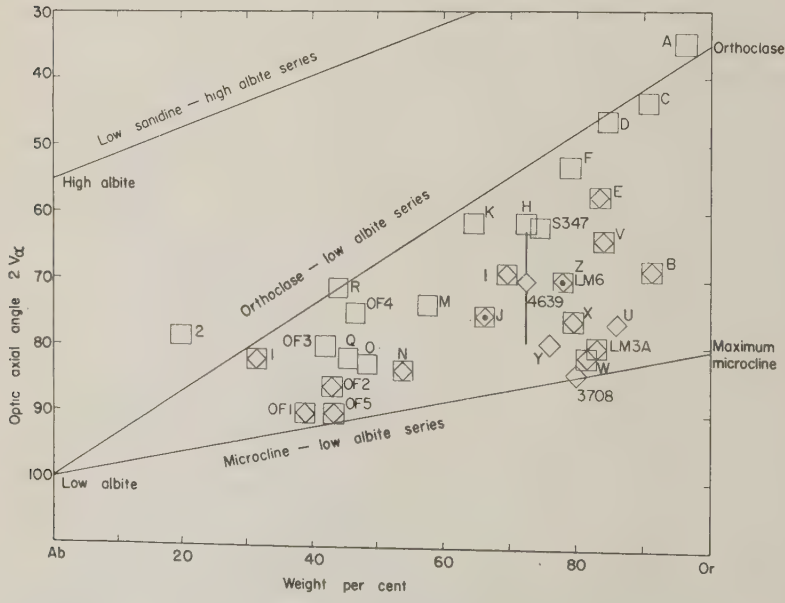

FIG. 6. The occurrence of orthoclase and microcline. The squares indicate a monoclinic potassium phase, the diamonds a triclinic phase and the linked squares and diamonds indicate the presence of both in the same specimen. To avoid confusion the symbols of specimens Z and LM6, both of which contain orthoclase and microcline, are shown as one. The two charnockite specimens 3705 and 6436 are omitted.

position range. The present data shows that this conclusion must be extended and modified. The three groups tend to fall into characteristic areas on the composition—2V diagrams and embrace both orthoclase—and microcline perthites. The group containing anorthoclase with pericline twin-type superstructure is the most potassium-rich and has the lowest values of 2V. The specimens containing a superstructure of albite-oligoclase occupy an adjacent area with slightly greater values of 2V and more sodium-rich compositions. The last group which has mainly an albite twinned, and sometimes pericline twinned, albite-oligoclase covers the largest area including all the sodium-rich specimens and most of the microcline perthites. The areas are not mutually restrictive and some overlap occurs particularly between the last two groups.

The Potassium Phase

The potassium phase may be either monoclinic or triclinic and, in many specimens, both a monoclinic and a triclinic phase occur. Often the triclinic phase yields short diffuse streaks centered on sharp reflections that have monoclinic symmetry, and in some crystals it is not easy to distinguish these streaks from the very weak ones that can be found in heavily exposed photographs of orthoclases (Laves, 1950) and low sanidine. This point will be taken up in detail later on. Fig. 7 shows the distribution of orthoclase and microcline in the specimens; when there was doubt whether a diffuse streak resulted from microcline or not, it was ignored and the feldspar listed as having only a monoclinic potassium component. It will be seen that there is a general sort of correlation between the nature of the potassium phase and the position of the containing specimen on the 2V-composition diagram. Specimens lying near to the straight line joining low albite with orthoclase contain only a monoclinic potassium phase. Intermediate specimens are variable, the majority containing both monoclinic and triclinic components. Those lying close to the low albite—maximum microcline join contain either a single triclinic phase or both a triclinic and a monoclinic phase. In spite of the rough correspondence it is obvious that other factors enter and that the relationships between the optical and structural properties of a perthitic alkali feldspar is not a simple one. The occurrence of a monoclinic component in specimens lying very close to the low albite—maximum microcline join suggests that there may be microcline specimens whose values of 2V lie below the low albite—maximum microcline join in Fig. 1. The specimens of iso-orthoclase described by Barth (1933) and Tsuboi (1936) may be in this category and should be subjected to further investigation.

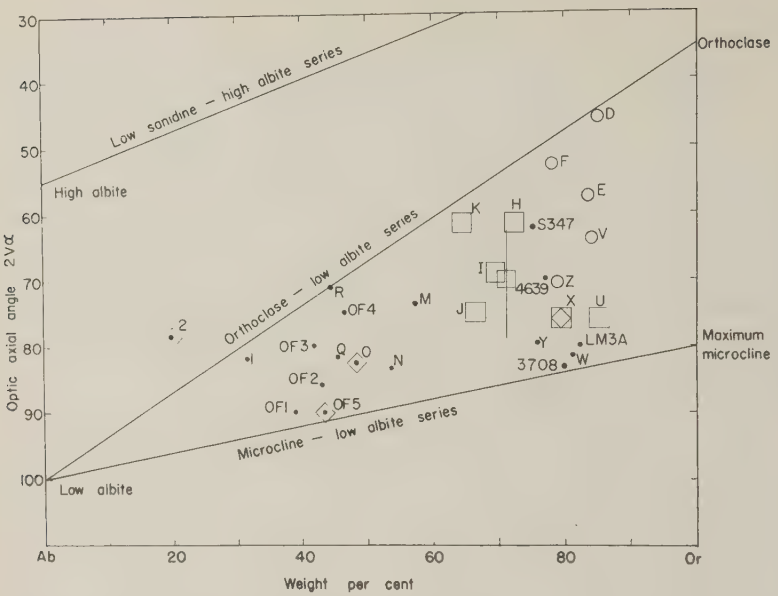

FIG. 7. The nature of the association of the sodium feldspar components. The dots indicate predominant albite twinning, the squares predominant albite twin-type superstructure and the diamonds pericline twinning. The circles show the specimens which contain a pericline type superstructure of anorthoclase. Some specimens contain two types of associations and are indicated by a double symbol. It was not possible to determine with certainty the type of association in the charnockite specimens 3705 and 6436 because of the streaked reflections. Specimens S347 and LM6 which contain an albite-twinned albite-oligoclase also show weak streaks parallel to the layer of b-axis oscillation photographs.

OBSERVATIONS CONCERNING THE POLYMORPHISM OF POTASSIUM FELDSPARS

To form a basis for the discussion of the polymorphism of potassium feldspar in a later paper of this series, pertinent observations are collected in this section. Many observations refer to the present suite of specimens, but others described in earlier and to be described in later papers are also mentioned.

Ideally, a wide range of specimens from a variety of environments should be available for the study of the polymorphism of potassium feldspars, but the range is limited for several reasons. Many specimens from igneous and metamorphic rocks have suffered alteration and it is difficult to measure the optical properties with precision. Other specimens contain large veins or lamellae of exsolved sodium feldspar, again leading to uncertainty in the measurement of the optical properties. Further, the presence of reflections from sodium feldspar seriously in-

terferes with the evaluation of the weak diffuse reflections from the potassium components. Some of the charnockite specimens suffer from a further limitation: x-ray reflections are smeared out along curves of constant θ indicating disorientation, probably the result of the deformation that has left its imprint on the fabric of some of the rocks. Finally, many of the conclusions depend on the estimation of the diffuseness of x-ray reflections, a notoriously difficult operation. Consequently the following conclusions, especially those dealing with diffuse reflections, are not based on as much reliable evidence as would be desired. Some of the variations observed in the x-ray photographs are shown in Figs. 8–12: unfortunately it is extremely difficult to obtain satisfactory illustrations of diffuse reflections.

Many of the observations have been recorded already by Laves (1950,[1] 1952), Goldsmith and Laves (1954a,b), MacKenzie (1954), MacKenzie and Smith (1955), but a complete listing is given so that a logical order may be attained.

1) All the reflections in high sanidine (heated Spencer-A,C,D) and in maximum microcline (Blue Mountain) are sharp and may be indexed on the usual face-centered cell. Strictly speaking, a smaller primitive cell should be used for the triclinic feldspars, but it is customary to retain the larger centered cell.

2) In orthoclase (Spencer-A,C,D) and in low-sanidine (various specimens listed in paper III (MacKenzie and Smith, 1955), both before and after homogenization by heating at 900°C. for a few minutes) two types of reflections occur. The first type are sharp and obey the conditions for the face-centered lattice. The second type occur as weak diffuse streaks, centered on the first type of reflections and extending parallel to the b-axis. They appear to be weaker in low-sanidine than in orthoclase and disappear upon conversion into high-sanidine (Figs. 8 and 9).

3) In intermediate microcline and especially in adularia a variety of structures occur, ranging between the extremes of orthoclase and maximum microcline. The effects may be grouped into two (*a*) those that maintain the C face-centering and (*b*) those that require a primitive symmetry (for the usual size cell, not the smaller one). In the first group the reflections may be either sharp or diffuse, and if of triclinic symmetry are commonly arranged according to the albite and/or pericline law. If both laws occur the albite and pericline units bear to each other the special relation indicative of inversion from monoclinic symmetry. In addition the "diagonal" association may also occur in which two units are formed with orientation $(x\mathrm{A}_1+(1-x)\mathrm{P}_1)$. $(x\mathrm{A}_2+(1-x)\mathrm{P}_2)$

[1] This paper contains some excellent illustrations of diffuse reflections.

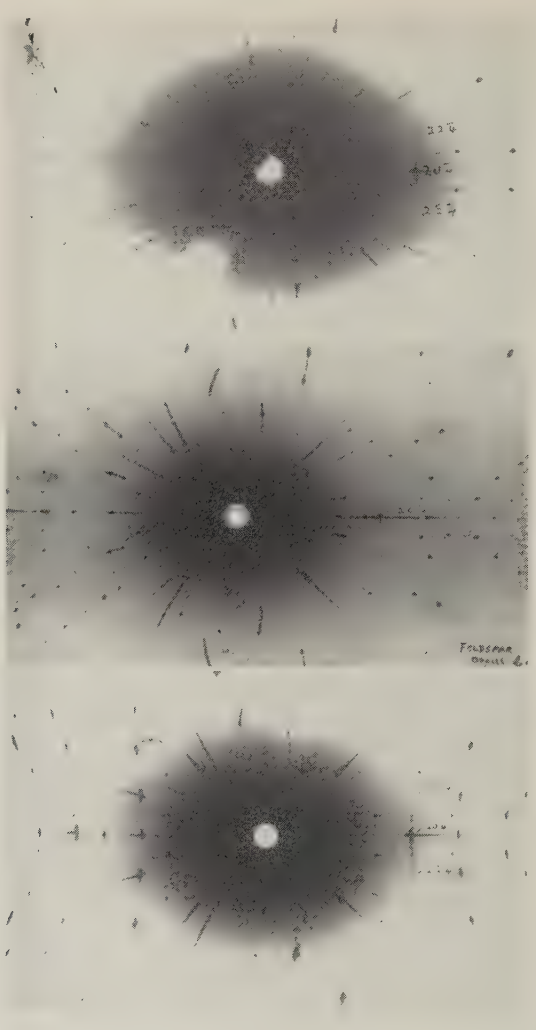

FIG. 8 (above). *b*-axis oscillation photograph of an orthoclase specimen (Spencer C). 5° oscillation used to give greater effective exposure for the $20\bar{4}$, $22\bar{4}$ and $22\bar{4}$ reflections. A very weak streak is centered on the $20\bar{4}$ reflection and weaker ones can just be distinguished for some of the other reflections.

FIG. 9 (middle). *b*-axis oscillation photograph of a low-sanidine taken with the *x*-ray beam in the center of a 15° oscillation (specimen from Pine Creek described in paper 3: homogenized by heating a few minutes at 900° C.). Unfiltered radiation. Only one weak streak is visible, centered on the $20\bar{4}$ reflection.

FIG. 10 (below). *b*-axis oscillation photograph of specimen Spencer B, an adularia, taken with the *x*-ray beam parallel to (001) in the center of a 15° oscillation. The main reflections with $(h+k)$ even each consist of a strong sharp component lying in or near the center of a

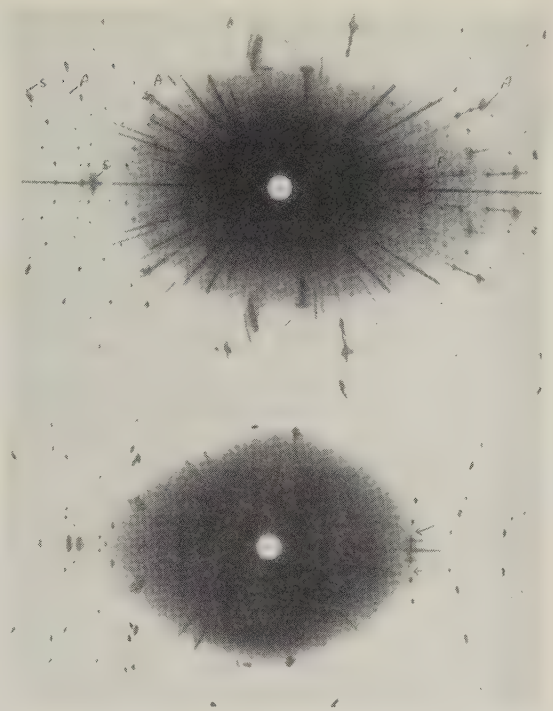

FIG. 11 (above). *b*-axis oscillation photograph of specimen Z, a microcline perthite, taken with the *x*-ray beam parallel to (001) in the center of a 15° oscillation. Unfiltered CuK radiation. The reflections from the potassium phase each have a central sharp reflection lying in a streak (S) that is parallel to the row lines, thus indicating the occurrence of both a monoclinic K-feldspar and an albite-twinned microcline (P) of the potassium phase also occur as in Fig. 8. Weak pericline superstructure of an anorthoclase (A) is also visible.

FIG. 12 (below). *b*-axis oscillation photograph of an orthoclase-microcline-albite-perthite from the Dartmoor pluton, S. W. England. The potassium phase is mainly monoclinic, but some microcline, occurring in a diagonal association close to the orientation for albite twinning, is also present. The sodium phase is mainly albite-twinned but there is some disorientation. This photograph is reproduced chiefly to show that there are no diffuse streaks lying half-way between the reflections $20\bar{4}$, $22\bar{4}$, $22\bar{4}$, the possible positions for the streaks being marked by the arrows.

short streak elongated along the row lines. For (242) an additional streak elongated along the layer lines can just be seen. The streaks indicate microcline of variable intermediate geometry, both albite and pericline twinned in the "M-type" relation (Smith and MacKenzie, 1958) that indicates inversion from an original monoclinic phase. Lying between the reflections $20\bar{4}$, $22\bar{4}$ and $22\bar{4}$ are two weak diffuse streaks elongated along the row lines. These streaks indicate deviation from face-centered symmetry, for the centers of the diffuse streaks lie at the positions where $(h+k)$ would be odd.

where A_1, A_2, P_1, P_2 are the angular positions for albite and pericline twins lying in the aforementioned special association and x is a fraction lying between 0 and 1 (Fig. 3). Untwinned microcline crystals occur but rarely (some crystals of specimen U are untwinned, but most are twinned: Laves and co-workers have discovered several examples). The reflections may be sharp (E, LM3A, OF1, LM6, for example) or diffuse (B, some crystals of U (see above), most crystals of V, W, X, Y, Z, specimens from the Dartmoor granite). If sharp, the deviation from mono-

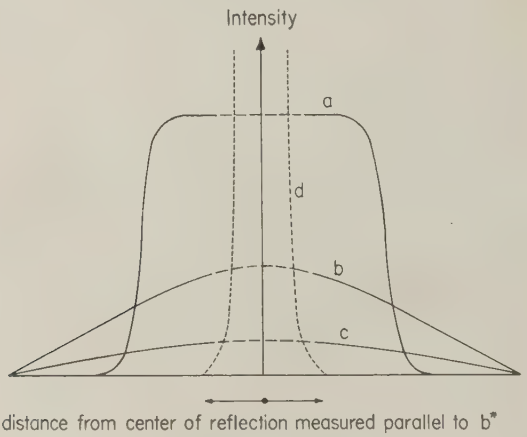

FIG. 13. Intensity variation estimated by eye for reflections from potassium feldspar. Curve *d* shows the distribution for a sharp reflection of monoclinic symmetry: curve *a* gives the variation for the diffuse streak of an adularia such as Spencer B and Spencer Z (see Figures 10 and 11): curve *b* is for an orthoclase such as Spencer C (Figure 8) and curve *c* for a low-sanidine or an orthoclase partly converted into a high-sanidine.

clinic geometry may take all values up to α^* 90°30′, γ^* 92°20′ (the values for maximum microcline). If diffuse, the streaks extend only as far as the separation of the reflections of twinned maximum microcline. Frequently sharp reflections in monoclinic positions occur in addition to the ones with triclinic symmetry. (See Figs. 10, 11 and 12.)

In some crystals, extra diffuse reflections occur that extend parallel to the *b*-axis and are centered on the positions rendered vacant by the *C* face-centering restriction. These diffuse reflections occur most strongly for Spencer B and U (the twinned crystals) and are absent for orthoclase (Spencer A, C and D) and maximum microcline, and are not observed in specimens from the Dartmoor granite (Figs. 8, 9, 10, 11 and 12). Although the data are admittedly subject to some limitations it seems probable that these extra reflections are strongest in intermediate

microclines and that they are more pronounced in adularia than in granitic specimens. To explain these reflections, it seems necessary to assume primitive symmetry as stated by Laves (1952).

Although the diffuse reflections in orthoclase and low sanidine occupy the same positions as the first type of diffuse reflections in intermediate microclines it is thought that they have a different character, and this difference is thought to be important (Fig. 13). The diffuse reflections in orthoclase and low-sanidine are much weaker than those in intermediate microclines and a distinction can be made on this basis for most specimens. Further, it appears that the diffuse reflections in orthoclase and low-sanidine have a more uniform drop of intensity and extend a little further than the diffuse reflections in intermediate microclines (as in Fig. 13). However, visual estimation of diffuseness is very difficult, and until quantitative measurements of the streaks have been made, the above conclusion should be treated with some caution. In view of the conflicting views on the nature of orthoclase, such quantitative measurements would appear to be of considerable importance.

Acknowledgments

We are indebted to the following for the specimens: the late Drs. Edmondson Spencer, and N. L. Bowen, Professors C. E. Tilley and O. F. Tuttle and Drs. M. T. Heald, R. A. Howie and C. Oftedahl.

References

Bailey, S. W., and Taylor, W. H. (1955): The structure of a triclinic potassium feldpar: *Acta Cryst.*, **8**, 621–632.

Barth, T. F. W. (1933): An occurrence of iso-orthoclase in Virginia: *Am. Mineral.*, **18**, 478–9.

Donnay, G. and Donnay, J. D. H. (1952): The symmetry change in the high-temperature alkali-feldspar series: *Am. Jour. Sci., Bowen Volume*, 115–132.

Ferguson, R. B., Traill, R. J. and Taylor, W. H. (1958): The crystal structures of low-temperature and high-temperature albite: *Acta Cryst.*, **11**, 331–348.

Goldsmith, J. R. and Laves, F. (1954a): The microcline-sanidine stability relations: *Geochim. et Cosmochim. Acta*, **5**, 1–19.

——— and ——— (1954b): Potassium feldspars structurally intermediate between microcline and sanidine: *Geochim. et Cosmochim. Acta*, **6**, 100–118.

Hafner, St. and Laves, F. (1957): Ordnung/Unordung und Ultrarotabsorption. II Variation der Lage und Intensität einiger Absorptionen von Feldspaten: Zur Struktur von Orthoklas und Adular. *Zeit. Krist.*, **109**, 204–225.

Heald, M. T. (1950): Structure and petrology of Lovewell Mountain quadrangle, New Hampshire: *Bull. Geol. Soc. America*, **61**, 43–89.

Heier, K. S. (1957): Phase relations of potash feldspar in metamorphism: *Jour. Geol.*, **65**, 468–479.

Howie, R. A. (1955): The geochemistry of the charnockite series of Madras, India: *Trans. Roy. Soc. Edinburgh*, **52**, 725–768.

LAVES, F. (1950): The lattice and twinning of microcline and other potash feldspars: *Jour Geol.*, **58,** 548–571.

— —— (1952): Phase relations of the alkali feldspars: *Jour. Geol.*, **60,** 436–450: 549–574.

MACKENZIE, W. S. (1954): The orthoclase-microcline inversion: *Mineral. Mag.*, **30,** 354–366.

—— AND SMITH, J. V. (1955): The alkali feldspars. I. Orthoclase-microperthites: *Am. Mineral.*, **40,** 707–732.

OFTEDAHL, C. (1948): Studies on the igneous rock complex of the Oslo region. IX. The Feldspars: *Norsk vidensk.-acad. Oslo Skr. I Math.-natur. Kl.*, No. **3,** 63–133.

SMITH, J. V. (1956): The powder patterns and lattice parameters of plagioclase feldspars I. The soda-rich plagioclases: *Mineral. Mag.*, **31,** 47–68.

——— AND MACKENZIE, W. S. (1954): Further complexities in the lamellar structure of the alkali feldspars: *Acta Cryst.*, **7,** 380.

——— AND ——— (1958): The alkali feldspars, IV, The cooling history of high-temperature sodium-rich feldspars: *Am. Mineral.*, **43,** 872–889.

SPENCER, E. (1930): A contribution to the study of moonstone from Ceylon and other areas and of the stability relations of the alkali feldspars: *Mineral. Mag.*, **22,** 291–367.

——— (1937): The potash-soda feldspars. I Thermal stability: *Mineral. Mag.*, **24,** 453–494.

TILLEY, C. E. (1954): Nepheline-alkali feldspar parageneses: *Am. Journ. Sci.*, **252,** 65–75.

TSUBOI, SEITARO (1936): Petrological notes (11)–(18): *Japanese Journ. Geol. Geogr.*, **13,** 333–337.

TUTTLE, O. F. (1925): Optical studies of alkali feldspars: *Am. Jour. Sci., Bowen Volume,* 553–567.

Manuscript received March 12, 1959.

THE AMERICAN MINERALOGIST, VOL. 44, NOVEMBER–DECEMBER, 1959

THE ALKALI FELDSPARS VI. SANIDINE AND ORTHOCLASE PERTHITES FROM THE SLIEVE GULLION AREA, NORTHERN IRELAND*

C. H. Emeleus, *Department of Geology, Durham Colleges in the University of Durham, Durham, England and* J. V. Smith, *Department of Mineralogy and Petrology, Division of Earth Sciences, Pennsylvania State University, University Park, Penna.*

Abstract

Detailed field and mineralogical studies of the associated porphyritic felsite and granophyre ring dykes of Slieve Gullion, N. Ireland, have been made to elucidate the genesis of the rock and of the alkali feldspars. Central, acentric subsidence of country rock within the ring fracture allowed the partially-crystalline magma to rise. Upon crystallization of one-third of the magma the roof shattered to form agglomerate, and the loss of volatiles led to rapid crystallization of the felsite. A subsequent subsidence without roof shattering led to formation of the granophyre.

The majority of the alkali feldspar phenocrysts fall between the sanidine and orthoclase series, consisting of intergrowths of monoclinic K-feldspar, anorthoclase and sodium-rich plagioclase. Two crystals from the granophyre consist of intergrowths of orthoclase, microcline and low-temperature plagioclase. It is thought that the majority of the phenocrysts are true phenocrysts formed slowly at considerable depth. During the cooling period they changed from homogeneous sanidine into their present assemblages through a sequence of unmixing and ordering reactions. It is thought that the local content of volatiles was probably the dominant factor in determining the extent of adjustment to the low-temperature assemblages. The occurrence of microcline is remarkable in hypabyssal rocks. It is thought probable that it results from fragments of Newry granodiorite caught up in the magma, although it might have arisen from plagioclase crystals by ionic exchange.

Introduction

Earlier papers of this series have been mainly concerned with obtaining a comprehensive catalogue of the structural changes to be found in the alkali feldspars, and, for convenience, attention has been focussed on well-crystallized specimens for which analyses were available. No attempt was made to obtain a representative coverage of rock types, the majority of the specimens being derived either from pegmatites or volcanic rocks. The remaining papers will deal mainly with the alkali feldspars from the common igneous rocks and two objectives will be kept in mind: obtaining a more balanced viewpoint on the distribution of the various structural types, and correlating the mineralogy of the alkali feldspars with the petrology of the host rocks.

The study has been confined to igneous[1] rocks and has concentrated

* Contribution No. 58-100, College of Mineral Industries, The Pennsylvania State University.

[1] Possibly the larger bodies might arise from metamorphic or metasomatic reactions.

mainly on the Tertiary rocks of Britain. The relative youth of these rocks has helped to reduce the likelihood of later complicating metamorphic effects, and the detailed mapping of British rocks has helped in the estimation of the conditions of their consolidation. Tuttle and Keith (1954) in a study of the Beinn an Dubhaich granite have provided a useful signpost in demonstrating the coexistence of orthoclase and sanidine perthites. These feldspars have been re-examined by the more refined methods now available and the results will be presented in a later paper. To extend the data for the feldspars transitional between those from volcanic rocks (papers III and IV) and the Beinn an Dubhaich granite, the Slieve Gullion composite ring dyke of porphyritic felsite and porphyritic granophyre was chosen. The ring dykes vary in width from a few feet to over a mile, and a wide variation in conditions was thereby anticipated. To extend the coverage to include larger masses, the Arran and Mourne granites (both about 7 miles in diameter) were chosen and a further extension was obtained by a study of the older and much larger Dartmoor pluton and the Tertiary S. California batholith. Additional information has been obtained by a study of the larvikites from Norway (Muir and Smith, 1956: Smith and Muir, 1958).

The appearance of the feldspar in these rocks is quite different from that of the feldspars studied in the earlier papers. In contrast to the clear euhedral crystals obtained from the pegmatites and volcanic rocks, the specimens from the granites, granophyres and felsites are usually anhedral and turbid. The cleavage is irregular and the optical properties of grains large enough for single crystal work (ca. 0.2 mm.) are difficult to measure. Consequently some refinement of the simple techniques described in paper II has been necessary as will be described separately.

The Petrology of the Slieve Gullion Ring Dyke Rocks

In order that the conditions of crystallization and subsequent history of the feldspars may be assessed, it is necessary to give an outline of the petrology of the ring dykes. The general structure and petrology of the ring complex was described by J. E. Richey and H. H. Thomas (1932) and certain other aspects of the complex by D. L. Reynolds (1941, 1950, 1951, etc.), E. M. Patterson (1953) and E. B. Bailey and W. McCallien (1956). A full account of the western part of the ring dyke complex is in preparation by one of us (C.H.E.). A simple sketch map of the Slieve Gullion dykes is shown in Fig. 1; reference should be made to the excellent maps prepared by Richey and Thomas if further details are required.

The Porphyritic Felsite ring dyke, the older of the two acid intrusions, is a conspicuously porphyritic rock with phenocrysts of feldspar and quartz set in a fine-grained and often flow-banded matrix. In hand

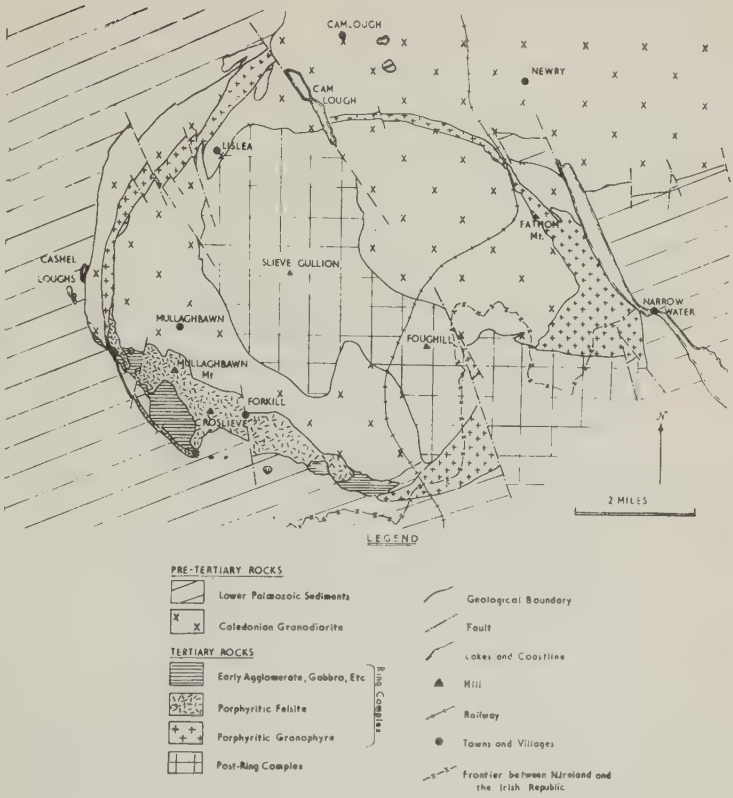

FIG. 1. Geological sketch map of the Slieve Gullion area.

specimens the felsite varies from a dark, semi-vitreous rock near the margins to a light-colored gray or buff rock in the more central parts of the intrusion. Phenocrysts are usually not more than 3 mm. in diameter and include, in addition to alkali feldspar and bipyramidal quartz, plagioclase (An_{25-35}), hedenbergitic clino-pyroxene and fayalite. The groundmass of the marginal felsite consists of innumerable minute octahedra of magnetite in a dark crypto-crystalline base whereas the groundmass of the more central parts is a finely granular aggregate of quartz, alkali feldspar, subordinate amounts of plagioclase, magnetite and green amphibole. The amphibole occurs as poikilitic crystals enclosing grains of quartz and feldspar; frequently it develops as a mantle about clino-pyroxene and fayalite phenocrysts. Occasionally the groundmass consists of spherulitic growths of turbid alkali feldspar and quartz. The phenocrysts tend to be rounded and resorbed in appearance; many sections also contain fragments of original euhedral crystals (Fig. 2*a*).

Flow banding is a persistent feature of the felsite and varies considerably in character. The marginal felsite has a very fine-scale banding frequently associated with elongated drusy cavities rimmed with coarsely crystalline rock (Figs. 2*b* and *c*). Felsite away from the margins has coarser banding which becomes progressively less obvious until, in the central felsite, it is rather uncommon. The flow banding in the central parts consists of layers 5–10 mm. thick of relatively coarsely crystalline rock, often markedly spherulitic.

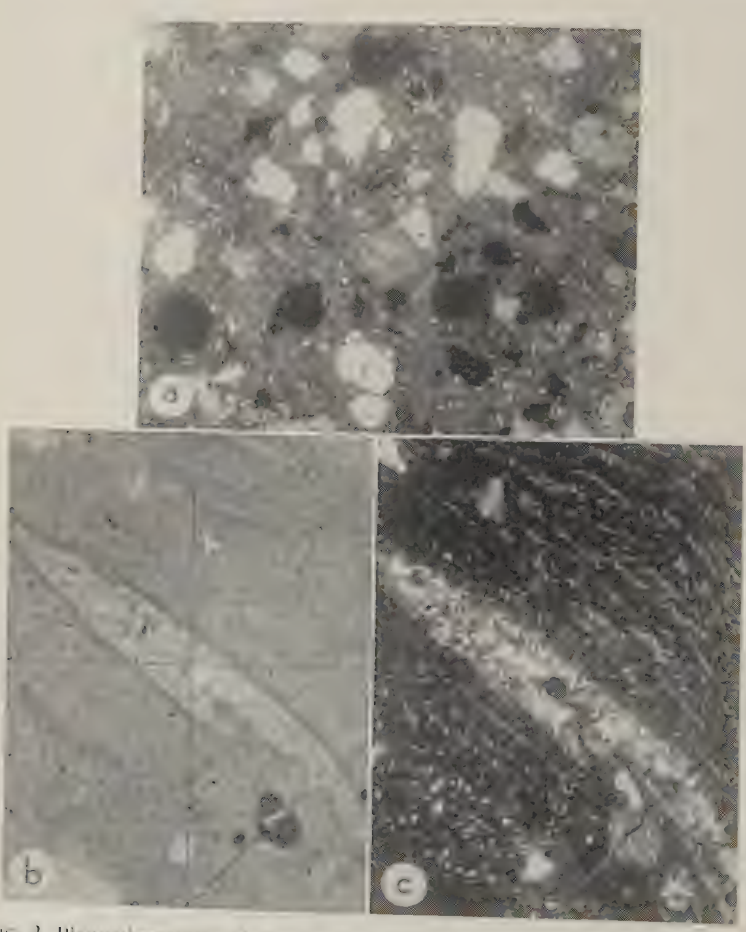

FIG. 2. Photomicrographs of Porphyritic Felsite. (a) shows resorbed and fragmented character of some of the phenocrysts. Specimen number G45, crossed nicols, ×3. (b) shows fluxion structure outlined by trails of magnetite granules. Specimen G4, ordinary light, ×15. (c) shows coarse crystallization about a drusy cavity. Specimen G4, crossed nicols, ×15. By comparing the last two photographs, encroachment of the coarsely crystallized part on the fluxion-banded part of the rock may be seen.

The flow banding and phenocrysts provide direct evidence of late stage recrystallization within the felsite. Originally the flow banding consisted of magnetite granules concentrated into trails and streaks. Where the bands adjoin druses associated with the coarsely crystalline felsite, and especially where the growth has been spherulitic, they may be traced through the relatively large crystals of quartz and feldspar (Compare Figs. 2*a* and 2*b*), or they may be interrupted, with the minute magnetite crystals replaced by larger grains or by amphibole in irregular, poikilitic crystals of small size. Away from the margins the small-scale banding dies out as the minute magnetite octahedra give way to larger grains or are replaced by the poikilitic amphibole. Where magnetite and amphibole occur together, the groundmass in the immediate vicinity of the amphibole is depleted in ore; evidently much of the finely disseminated amphibole developed at the expense of original ore. A similar feature was clearly demonstrated in the Porphyritic Felsite of Dibidil, Isle of Rhum (Hughes, 1956). There is also textural evidence for the replacement of fayalite and clinopyroxene by amphibole for the amphibole occurs as rims about the olivine and clinopyroxene. In the Porphyritic Granophyre replacement in this manner appears to be complete.

The Porphyritic Granophyre is extremely variable in hand-specimen and thin section. The marginal granophyre is fine-grained with phenocrysts of quartz and feldspar set in a dark-colored matrix which is sometimes flow-banded. The grain size of the groundmass increases rapidly away from the margins and in much of the intrusion the rock is, in effect, a porphyritic microgranite. The phenocrysts include quartz (with indications of bipyramidal habit in the marginal granophyre), alkali feldspar, plagioclase (An_{15-30}), hedenbergitic clinopyroxene, fayalite and a green, hastingsitic amphibole. The approximate modal proportions are given in Table 4. Unlike the felsite, the granophyre contains amphibole as the dominant mafic mineral; biotite also occurs while magnetite, apatite, zircon and orthite are present in accessory amounts.

Texturally the groundmass may vary from a granophyric intergrowth of quartz, turbid alkali feldspar and plagioclase to a microgranitic aggregate of these minerals accompanied by green amphibole and sparse flakes of greenish-brown biotite. The olivine and pyroxene phenocrysts are almost invariably rimmed by amphibole, a relationship particularly well developed in the marginal granophyre. Towards the central parts of the intrusion the proportion of amphibole increases with the eventual exclusion of olivine (which is never common) and pyroxene. The marginal granophyre may be felsitic or aplitic in texture. Typically the Porphyritic Granophyre is drusy, the small cavities being lined with quartz, feldspar, dark mica, and, rarely, green epidote.

Table 1. Chemical Analyses of Rocks from the Slieve Gullion Ring Dyke

	(1)	(2)	(3)
SiO_2	71.91	74.66	76.91
Al_2O_3	13.42	12.62	11.79
Fe_2O_3	1.62	1.52	1.00
FeO	1.96	1.24	0.99
MgO	0.27	0.31	trace
CaO	0.84	0.66	0.68
Na_2O	3.65	3.62	3.33
K_2O	5.49	5.02	4.98
H_2O^+	0.21	0.20	0.23
H_2O^-	0.35	0.13	0.12
CO_2	nil	nil	nil
TiO_2	0.07	0.16	0.16
P_2O_5	0.07	0.05	0.02
MnO	0.07	0.04	0.04
	99.93	100.23	100.25

(1) Porphyritic Granophyre. Cashel Plantation, 7 miles WSW of Newry, 4 miles NW of Forkill. (Approx. same as G. 70).

(2) Porphyritic Felsite. Scarp, ½ mile NW of Forkill. (Approx. same as G. 315.) Analyst for (1) and (2): E. M. Patterson (Patterson, 1953).

(3) Porphyritic Felsite. Knoll just south of Mullaghbawn Lough. Analyst: F. Harwood, unpublished analysis done for J. E. Richey. (Approx. same as G. 31.)

In the granophyre, the phenocrysts are larger than in the felsite, particularly the alkali feldspar and plagioclase which may reach as much as 1 cm. across. The number of individual phenocrysts in a given volume is less than in the felsite, although the modal proportions of phenocrysts and groundmass are similar (Table 4). A further difference between the phenocrysts is that in the granophyre they generally occur as aggregates; usually the groups are monomineralic but sometimes they may be composite. It is noticeable that plagioclase and alkali feldspar enter readily into the aggregates, quartz almost never does and participation of mafic minerals is uncommon but by no means unknown. A more detailed description of the aggregates is given later.

Three chemical analyses are available for the ring-dyke rocks (Table 1) Both intrusions are typical of the majority of the British Tertiary granites, granophyres and felsites in their high silica, high FeO/MgO ratio, low absolute amount of magnesia, and in having potash in excess of soda. The felsite is somewhat more siliceous than the granophyre while the latter is appreciably richer in total iron and total alkalis. (Alkali determinations on six specimens from each intrusion show that a

slight relative alkali enrichment characterizes the granophyre.) Amongst the other acid Tertiary rocks, the felsite compares closely with the more acid of the Mourne Mountain granites (Brown, 1956) while the granophyre is closely comparable with the more mafic facies of the Mourne Feldspathic granite, G1 (Richey, 1928; Brown, 1956). This similarity extends to the mineralogy for hastingsitic amphibole is abundant in both, the analysis of the Mourne amphibole revealing an extreme FeO concentration (Brown, 1956).

The Alkali Feldspars

Techniques and Data

Pure specimens of the alkali feldspar phenocrysts were obtained by crushing, magnetic separation and centrifuging the porphyritic felsite, and by hand picking the crushed porphyritic granophyre.

Only the felsite phenocrysts have been analysed so far. The alkalis were determined by the flame photometer using sodium oxalate and potassium nitrate for calibration, and the standard granite G1 and diabase W1 for checks. The results were reproducible to 0.03% of the weight quoted in Table 2, representing a spread of about 0.2 wt. % on the calculated orthoclase and rather less on the albite. Semi-quantitative spectro-

Table 2. Chemical Composition of Alkali Feldspar Phenocrysts and the Host Rock

Specimen Number	Alkali Feldspar				Phenocrysts		Total	Host Rock	
	K_2O	Na_2O	CaO	or.	ab.	an.		K_2O	Na_2O
	Weight per cent								
G.45	7.54	5.60	0.59	44.6	47.4	2.9	94.9	5.07	3.23
G.31	7.06	5.93	0.41	41.7	50.1	2.0	93.8	4.52	3.23
G.105	10.5	4.0	0.63	62.1	33.8	3.1	99.0	6.98	2.67
G.106*	9.51	4.72	0.69	56.2	39.9	3.4	99.5	5.90	3.03
G.107	8.45	5.25	0.66	50.0	44.4	3.3	97.7	5.66	3.35
G.108	8.30	5.25	0.72	49.1	44.4	3.6	97.1	5.48	3.19
G.109	9.30	4.70	0.63	55.0	39.8	3.1	97.9	4.46	3.01
G.111	7.67	5.58	0.93	45.3	47.2	4.6	97.1	4.46	3.01
G.313	7.44	5.81	0.61	44.0	49.1	3.0	96.1	5.96	3.85
G.314	7.95	5.50	0.65	47.0	46.5	3.2	96.7	5.39	4.50
G.315	7.66	5.76	0.38	45.3	48.7	1.9	95.9	4.54	3.23
G.317	7.41	5.60	0.67	43.8	47.4	3.3	94.5	5.23	3.47
G.396	8.70	4.92	0.40	51.4	41.6	2.0	95.0	4.57	3.23
G.398a	8.70	5.20	0.44	51.4	44.0	2.2	97.6	4.79	3.26

* Additional data on alkali feldspar in G.106: SiO_2, 65.22; Al_2O_3, 19.92; Total: 100.06. Analyst for SiO_2, Al_2O_3 and CaO: E. A. Vincent.

graphic determinations, using $SrCO_3$ as an internal standard, were made of CaO, yielding fairly reproducible results with a variation corresponding to ± 0.1 wt.% calculated anorthite.

For several of the alkali feldspars the total of Or+Ab+An (Table 2) calculated from the figures for K_2O, Na_2O and CaO falls short of 100% by as much as 5%. This deficiency is thought to be genuine in view of the reproducibility of the chemical methods. Microscopic examination of mounted grains did not reveal the presence of anything like enough macroscopic impurity, such as quartz, to account for the discrepancy. The feldspars, however, are very turbid and at first sight it was thought that the turbidity arose from an alteration involving the loss of alkalis. Detailed analysis of G106, an exceptionally turbid specimen, tends to

Table 3. Optical Properties of the Alkali Feldspar Phenocrysts

Specimen Number	Distance from Margin*	or. content†	$n_\alpha \pm 0.001$	Optic axial angle, $2V\alpha$		
				average	range	number of crystals
G.31	150 yards	44.5	1.520	58	56–59	6
G.45	300 yds.	47.9	1.522	57	51–63	8
G.105	at contact.	62.8	1.520	50	40–72	23
G.106	1′	56.5	1.520	49	37–72	7
G.107	2′	51.2	1.521	48	38–66	14
G.108	3′	50.6	1.520	48	43–58	9
G.109	14′	56.2	1.520	55	44–66	10
G.111	30–40 yds.	46.6	1.522	49	41–55	10
G.313	45 yds.	46.8	1.524	63	56–68	7
G.314	25–30 yds.	48.6	1.523	64	55–70	9
G.315	ca. 300 yds.	47.3	1.522	59	55–67	7
G.317	70 yds.	46.3	1.522	62	60–63	6
G.396	9″	54.2	1.521	47	38–53	8
G.398a	18″	52.7	1.521	49	44–55	8
G.407	ca. 120 yds.	—	—	53	37–64	6
79085	50 yards	—	—	53	48–57	8
79086	at contact.	—	—	58	49–68	4
79087	2 yds.	—	—	53	48–57	10
79090	15 yds.	—	—	53	45–56	6
79091	60 yds.	—	—	53	39–61	10
79092	1′–2′	—	—	57	48–63	5
79094	350 yds.	—	—	56	45–60	9
79099	220 yds.	—	—	60	54–66	9
79102	80 yds.	—	—	59	44–65	6
79105	?	—	—	54	46–62	7

* Distances over 5 yds. are estimated.

† Wt. per cent or./total feldspar.

discredit this possibility, for gravimetric measurements of CaO, SiO_2 and Al_2O_3 made by Dr. E. A. Vincent along with photometric estimation of the alkalis yielded a calculated content of feldspar close to 100%. The cause of the turbidity is also uncertain for the data for G106 would indicate that loss of alkalis was not the reason and that some other factor, perhaps an iron-bearing impurity, was the culprit. It is worth noting that many past analyses have recorded a deficiency of calculated feldspar that has been ascribed to solid solution with silica. The present data should not be used to support this idea.

The α refractive index (Table 3) was measured on a number of grains using a single-variation (temperature) method. Little spread was observed about the mean value of 1.521 (Na light). Measurement of the optic axial angles was carried out on a five-axis Universal stage employing the extinction method for thin sections and the conoscopic method for separated grains. Measurements were made only when both optic axes were accessible. As the turbid character of the feldspars rendered difficult the determinations on grains, thin sections were much the more satisfactory, particularly as variation within single crystals could be detected and correlated with morphological features. An accuracy of about 2° was obtained in the values listed in Table 3.

From the separated phenocrysts about forty fragments were selected and thirty of these gave good x-ray oscillation photographs (details of techniques given in paper II of this series, Smith and MacKenzie, 1955). Values of α^* and γ^* were determined for the triclinic sodium-rich components and plotted on Fig. 3. There is no point in giving a detailed account of each specimen for the structural states found in these 30 specimens are so varied that only a much larger number would have any statistical significance. It is sufficient to list the type and nature of the different assemblages in the following table:

Monoclinic potassium feldspar	x	x	x	x	x	x
Triclinic potassium feldspar						x
Sodium-rich sanidine	x		x			
Anorthoclase		x		x		
Albite-oligoclase			x	x	x	x
Number of crystals	1	2	3	17	5	2

Some typical photographs are shown in Figs. 8–12 and described in the final section.

The Alkali Feldspars of the Porphyritic Felsite

The composition of the alkali feldspar phenocrysts ranges from Or_{62} to $Or_{44.5}$. At contacts there is a variation in the composition as is especially well shown in the series G105-109 taken at the contact with the earlier

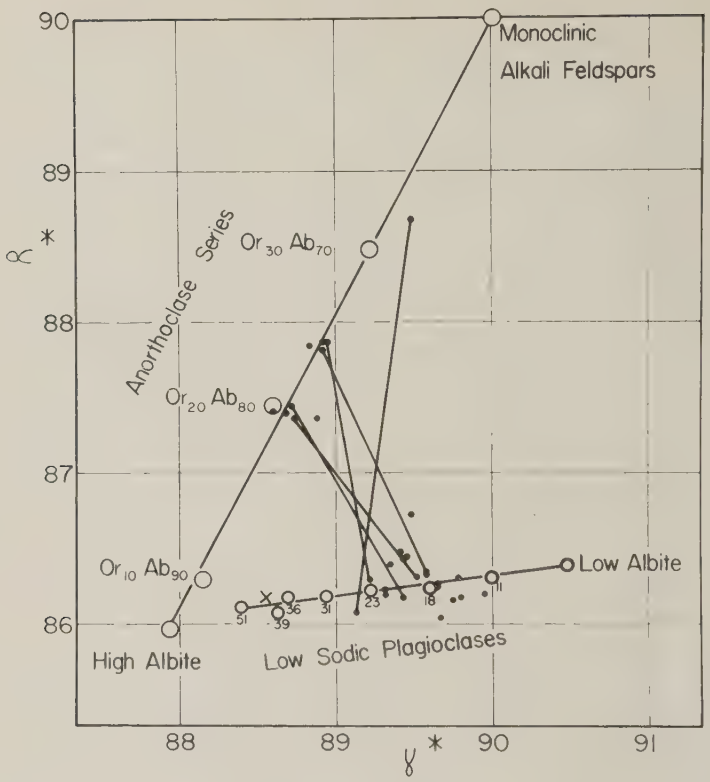

FIG. 3. Values of α^*, γ^* determined from sodium-rich components of the alkali feldspars from the felsite and granophyre. Circles give reference values measured for homogeneous feldspars of known composition (see earlier papers in series for source of these data) Dots show values from the Slieve Gullion alkali feldspars. Tie lines join values obtained for anorthoclase and albite-oligoclase in the same specimen. The duality between anorthite content and structural state should be remembered when the α^*, γ^* values of the plagioclase specimens are considered. The indicated An-content is the maximum value and corresponds to a low structural state. Lower An-contents are possible if the structural state is not fully low. However, even if the An-content is zero, which is most unlikely, the structural state cannot be more than half-way towards the extreme high state. Consequently the designation low-temperature is used for the specimens. An uncertainty in the use of α^*, γ^* angles as indicators of composition and structural state has recently arisen from the demonstration by Schneider (1957) and other workers at Zürich that crystals become monoclinic at room temperature following prolonged heating just under the melting point. However, it is thought that this work does not affect conclusions reached for natural specimens, for deductions made for a large number of specimens, such as the Slieve Gullion ones, have been very reasonable.

The cross (×) shows values of α^*, γ^* determined for an albite-twinned plagioclase crystal. The *x*-ray photograph also revealed the presence of a very weak monoclinic potassium-rich phase.

agglomerate on the south-west side of the Croslieve. The potash content is highest at the contact falling to a minimum after about three feet, and then rising slightly. A similar but smaller drop in potash content was found at the contact west of Mullaghbawn mountain (G396–G401). The variation could be caused by an early potash-rich phase of the Porphyritic Felsite grading imperceptibly into the normal variety away from the margins. The alkali contents of a number of felsite specimens were determined (Table 2). As might be expected there is a sympathetic variation in alkalis between phenocrysts and host rock with the phenocrysts the more potassic.

Table 4. Modal Compositions

	Porphyritic Felsite	Porphyritic Granophyre
Groundmass	68.8	72.7
Phenocrysts		
Quartz	9.1	6.0
Alkali Feldspar	19.7	19.4
Plagioclase	0.5	1.3
Pyroxene, Olivine Amphibole	0.9	0.6
Inclusions	1.0	nil

Note: All modal analyses determined on thin sections using a point counter. Felsite is average of 32 specimens, granophyre average of 9. The granophyre specimens are from the chilled marginal parts. In the center differentiation between true phenocrysts and groundmass is rendered difficult by the general coarse crystallization.

A considerable range of optic axial angles was found from specimen to specimen, crystal to crystal, and in a single crystal. The variation scheme was similar in nearly all the single crystals. In thin section many of the crystals are inhomogeneous; water-clear areas are bordered by turbid feldspar, and spindles and small areas of perthitic plagioclase are common. In perthitic crystals the feldspar immediately adjacent to the plagioclase spindles almost invariably gave the maximum value of $2V_\alpha$ for the crystal. This area commonly was the most turbid although some exceptions occurred. Two examples illustrate the variation:

specimen G108. Perthitic crystal. Major part turbid with 2V 58°. Small clear area 2V 43°.

specimen G109. Crystal not visibly perthitic. Turbid part 2V 55°. Small clear area 2V 44°.

A small number of crystals show zoning with a core of lower optic axial angle, presumably attributable to compositional variation, (c.f. Muir and Smith, 1956). The variation from crystal to crystal in the same hand

specimen appears to be caused by effects similar to those producing the variation within single crystals, for clouded crystals generally give higher values of 2V than clear ones. This was especially noticeable in the marginal specimens. The average values of 2V for marginal and internal specimens are not sufficiently different to have statistical significance although the average of the marginal values is actually lower in accordance with expectation.

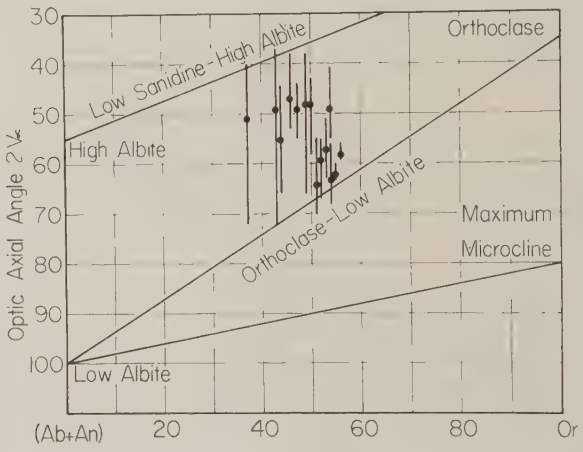

FIG. 4. The relationship between the bulk chemical composition and the optic axial angle, $2V_\alpha$, of the Slieve Gullion alkali feldspars. The length of the line shows the measured variation for each specimen and the dot gives the average. The nomenclature and position of the lines for the various series of feldspars has been slightly modified from Tuttle (1952).

The combination of the chemical, optical and x-ray data shows that the alkali feldspars lie between the low sanidine-anorthoclase and orthoclase-low albite series as defined by Tuttle (1952). The spread of optical properties (Fig. 4) is very similar to that found in the Tertiary granite of Beinn an Dubhaich, Isle of Skye by Tuttle and Keith (1954).

The Porphyritic Granophyre

Study of the granophyre has been less detailed and at present there are no chemical data for the separated alkali feldspars. The optical properties of the feldspar phenocrysts were very similar to those of the felsite. Where the groundmass alkali feldspar was sufficiently coarse grained to permit determination, the optic axial angle was generally larger than in the associated phenocrysts (*e.g.* 79086; phenocrysts $2V_\alpha$ 46°, 47°, 55°; groundmass 55°, 55°, 56°, 62°.) While many of the feldspars

in the granophyre are not strongly perthitic, the development of coarse perthite is much more common than in the feldspars of the felsite.

The aggregated, or glomero-porphyritic habit of the phenocrysts is common, especially among the feldspars. Within an aggregate the individual crystals develop good crystal faces where they adjoin the groundmass but against each other the outlines are irregular and rounded (Fig. 5). The optical break between crystals may be accentuated by a line of quartz blebs. The individual crystals often contain

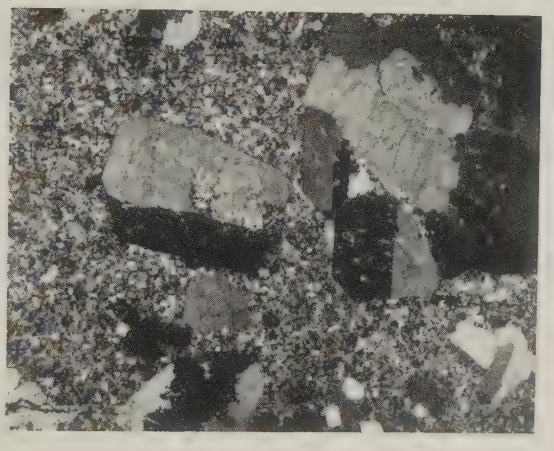

FIG. 5. Photomicrograph of porphyritic granophyre showing the aggregated habit of alkali feldspar phenocrysts. Note the irregular boundaries within the aggregate and the well developed crystal faces towards the granophyric matrix. Specimen G76, crossed nicols, ×3.

inclusions of quartz and groundmass, both with cuspate outline. Rather rare crystals contain such a high proportion of included material that they resemble sieve-textured plagioclases described from acid rocks in the Central Layered Complex of Slieve Gullion (Reynolds, 1950, fig. 7). Part of the apparently included material probably represents groundmass crystallization within a sieved and "corroded" crystal. In a number of the alkali feldspar aggregates, a rim of alkali feldspar or plagioclase, often in optical continuity, separates the aggregated crystals from the groundmass (Fig. 6a,b). A few aggregates of plagioclase of similar properties are also found (Fig. 6b) but in none of these is quartz found in any significant quantity. The quartz that does occur in these aggregates is almost wholly confined to small bleblike or cuspate inclusions within the feldspar or along their mutual boundaries. Only one example (G347) was found of an aggregate of equal quantities of quartz or feldspar and one (G374) of alkali feldspar and fayalite. In one specimen, 79105,

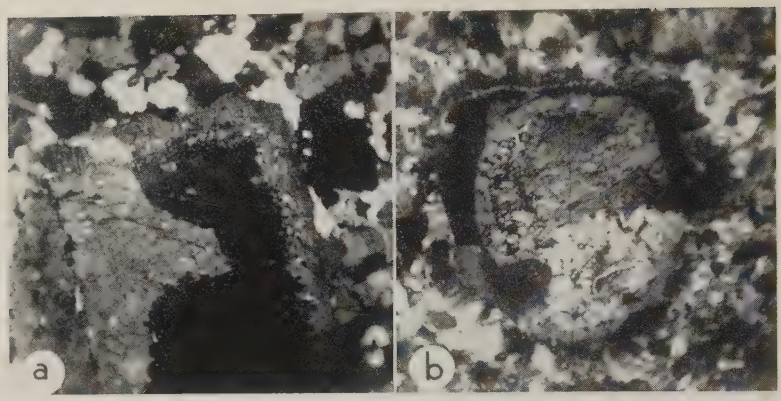

FIG. 6. Photomicrographs of porphyritic granophyre. (a) Aggregated alkali feldspar phenocrysts with a rim of plagioclase between core and groundmass. Specimen G62, crossed nicols, ×8. (b) Aggregated plagioclase phenocrysts with a rim of alkali feldspar between aggregate and groundmass. Specimen G74, crossed nicols, ×8.

aggregates of plagioclase, hornblende, mica and a little alkali feldspar occur, which are almost certainly fragments of Newry Granodiorite.

Discussion

From the respective settings of the two intrusions in the composite ring dyke, it is possible to obtain a probable explanation of the mode of emplacement and the reasons for the marked textural differences between the felsite and granophyre. The close spatial association between the felsite and agglomerate was noted by Nolan in 1877, and a close connection in time was advocated by Richey (1928) who considered that gases responsible for the formation of the agglomerate were derived from the acid magma which then consolidated to give the Porphyritic Felsite. This suggestion is accepted, but with the reservation that the the gases largely escaped before the magma was intruded into the present level. The Porphyritic Granophyre, the later intrusion, is regarded as having consolidated in the presence of its own volatiles. Hughes (1956) has come to a similar conclusion for the felsite and granophyre of South East Rhum, and regards the two as originating from a common magma.

The detailed sequence of events is thought to begin with an initial rise of acid magma into the lower parts of the ring fracture, followed by a period of crystallization. Central, acentric subsidence of the country rock within the ring fracture allowed the partially crystalline magma to advance to higher levels in the south-western part of the complex, the rate of crystallization increasing. After crystallization of about one-third of the magma, the vapor pressure proved too great for the covering rocks

and the roof shattered to form the agglomerate. The rapid escape of volatiles caused the fragmentation of some of the early-formed crystals. Subsequent rise of the acid magma into the higher parts of the ring fracture led to a rapid chilling in the marginal parts without noticeable thermal effects on the country rocks. The high viscosity caused considerable heterogeneity within the felsite with segregations of volatile-rich material trapped within volatile-poor parts producing a drusy structure with the cavities lying in the direction of the flow.

After the emplacement of the felsite a further subsidence occurred, this time acentric to the southeast, allowing acid magma to rise around three-quarters of the circumference. This time the volatiles did not escape, as is attested by the abundance of amphibole and the numerous small drusy cavities, leading to the relatively coarse microgranitic and granophyric textures of the groundmass, and replacement of pyroxene and olivine by amphibole. The alteration of the country rocks was marked, the granodiorite being baked and some of the crush rocks converted into fine-grained biotite-quartz-plagioclase hornfelses.

The formation of the aggregated phenocrysts, which comprise one-third of the rock, is a matter for speculation. If they are true phenocrysts, some mechanism must have caused them to aggregate together, followed by further crystallization both inside and outside the aggregate. Alternatively they could consist of fragments of pre-existing acid rocks of granitic composition. Although fragments of Newry granodiorite can be recognized clearly, and some of the phenocrysts resemble the altered granodiorite crystals in part of Slieve Gullion, the Newry Granodiorite would not seem to be a suitable source for the bulk of the aggregates, because a very large metasomatic transformation of plagioclase (An_{20}) into alkali feldspar would be needed. Furthermore, there is a fundamental difficulty in deriving the aggregates from any holocrystalline granite parent. The aggregates strongly tend to be mono-mineralic instead of having "granitic" texture: also fayalite and hedenbergite are found only occasionally in granodioritic rocks. As the phenocrysts of the aggregates have compositions which would be expected to be in equilibrium with a melt of granitic composition, and because the phenocrysts of the felsite and granophyre are very similar in properties it is regarded as highly probable that the majority are true phenocrysts. The aggregation may have been the result of eddy currents produced around the phenocrysts by movement of the magma, causing the crystals to come together like bubbles on a water surface.

The nature of the alkali feldspar formed the second main interest of the investigation. Initially, it was hoped that it would be possible to show that the thicker the ring-dyke, the more the feldspar would have pro-

gressed to the low-temperature structural state. This would be the obvious result if the state of the feldspar was governed solely by the cooling rate of the rock. However, it soon became clear that this was apparently not more than a small factor for the correlation between the structural properties, as measured by the optic axial angle, and the local thickness of the ring-dyke was rather small, certainly near the border line of having any significance at all.

Examination of Fig. 4 shows that there is a wide variation of properties in each hand specimen, closely comparable to that found by Tuttle and Keith (1954) in the Beinn an Dubhaich granite. The majority of the optic axial angles fall between the sanidine and orthoclase series but a few lie just the other side of the orthoclase series in the area occupied by the microcline series. The single-crystal x-ray study of the phenocrysts shows a wide variation of properties as described earlier, but with the majority of crystals containing albite-oligoclase, anorthoclase and a K-phase. The extreme specimens are three which contain no low-temperature plagioclase, and two which contain microcline in association with monoclinic potassium feldspar (orthoclase) and low-temperature plagioclase. Both of the microcline-bearing rocks are Porphyritic Granophyre (specimen 79105 and 79102). Occurrence of microcline in these hypabyssal rocks is remarkable, for microcline is regarded as the low-temperature form of potassium feldspar by most observers (but see Ferguson, Traill and Taylor, 1958, and later discussion by MacKenzie and Smith, 1959) and has not previously been recorded in hypabyssal rocks. Indeed many recent granites contain only orthoclase as will be shown in later papers of this series.

The reactions which have led to the present assemblages of alkali feldspars are thought to be as follows. Phenocrysts in the true sense grew to a large size while the magma was at considerable depths. Upon movement to higher levels the temperature would begin to fall and crystallization become more rapid. After consolidation of the rock, cooling continued and the feldspar began a structural readjustment to the states stable at the lower temperatures. The extent of this readjustment would depend on three main factors: the cooling rate, the local content of volatiles and the chemical composition. It is thought likely that the most important factor may well have been the local content of volatiles thus explaining the great variability of the structural states in a single hand specimen and the poor correlation between the mean optic axial angle and the cooling rate inferred from the local width of the ring dyke. The rare crystals now occurring as two sanidines would probably have occurred in a drier portion of the rock. Those occurring in the wetter portion would have proceeded further, passing into the stage where the

sodium-rich sanidine was partially inverted into a low-temperature albite-oligoclase. (For a detailed account of the reaction sequence and the probable temperatures see Smith and Muir (1958)). It is thought to be extremely unlikely that the rare microcline-bearing specimens are the product of unmixing and inversion of an original single-phase sanidine. The Newry granodiorite contains microcline as is shown in Fig. 7, and small xenoliths of the granodiorite can be definitely identified in the felsite and granophyre. The microcline-bearing phenocrysts therefore could reasonably be regarded as being xenocrysts and not true

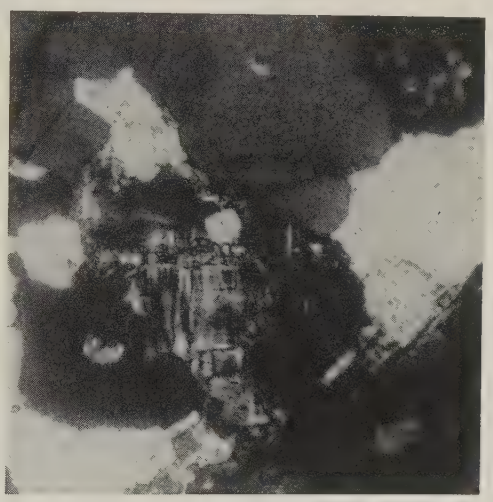

FIG. 7. Photomicrograph of Caledonian Newry Granodiorite showing the familiar cross-hatched twinning of microcline. Specimen G 171, crossed nicols, ×4.

phenocrysts and their reaction scheme would be the following: some of the xenoliths caught up in the intrusion of the magma would be disrupted so that separate crystals were produced. The resistance of microcline to conversion into high-sanidine by heating is strong, for prolonged heating at temperatures of about 1050°C in the dry state and not less than 500°C in the presence of high-pressure water (Goldsmith and Laves, 1954) is needed. Thus it seems reasonable to suppose that the microcline would remain essentially unchanged during the short period required for the intrusion. During the period of cooling it would remain in much the same state, possibly undergoing some further slight unmixing. An alternative mode of formation of the microcline is based on the experimental work on ionic exchange in alkali feldspars. According to Laves (1951), Wyart and Sabatier (1956), Hafner and Laves (1957), microcline

can be produced from low-albite by exchange of the sodium and potassium ions. Laves produced microcline by heating a specimen of albite in contact with a glass of potassium feldspar composition. Wyart and Sabatier used fused potassium chloride as the source of the potassium. Thus it would not be inconceivable that microcline could be produced from plagioclase in rocks by a process of potassium metasomatism. Possibly then, the microcline in the Slieve Gullion rocks has been produced by a metasomatic process from a true phenocryst following an earlier inversion from a sodium-rich sanidine to a low-temperature albite-oligoclase. Alternatively a xenocryst of plagioclase might have undergone ionic exchange. Of the three origins for the microcline, the xenocrystal origin without ionic exchange is thought to be much the more likely. Thus the sanidine and orthoclase-perthites are regarded as the truly characteristic alkali feldspars of these hypabyssal rocks and are considered to represent the type of feldspars to be found in conditions lying between the very rapidly-cooled volcanic and the slowly-cooled granitic rocks.

Details of the *x*-ray Photographs

In order not to break up the main discussion of the paper technical details concerning the *x*-ray data are given here. Figure 8 is a typical photograph showing a monoclinic potassium phase and two sodium phases, dominant anorthoclase occurring as pericline superstructure and weak albite twinned albite-oligoclase. The reflections from the anorthoclase occur in two closely-spaced clusters which may be merged in the reproduction. Figure 9 shows a different type in which one monoclinic potassium phase and three sodium phases occur. One of the sodium phases is pericline twinned anorthoclase. The other two are both albite-twinned, one being anorthoclase and the other albite-oligoclase. That there are two albite-twinned phases is most clearly seen in the group of reflections for the $40\bar{5}$ planes, shown at the right of the enlarged portion. The outer reflections of the five that lie on the row line come from the albite-twinned albite-oligoclase, the central reflection from pericline-twinned anorthoclase, and the other two from albite-twinned anorthoclase. The other reflection of the group comes from the K-phase. On the left-hand side of the main photograph, the reflections for the two albite-twinned components overlap, giving the impression that only one albite-twinned phase occurs. Fig. 10 is a photograph of a perfect example of albite twin-type superstructure. The distinction between this photograph and Fig. 9 is obvious: but when superstructure is poorly developed or when reflections from twins are distorted for some reason or another, it may be appreciated that distinction is not so easy and may be impracticable. In fact, a certain identification was not possible

for one or two specimens from this and other rock areas. Two details are illustrated in the enlargements. In insert one, the wing shape of two of the clusters is well illustrated. In the other the occurrence of satellite reflections about the potassium-phase reflections and the presence of streaks connecting the reflections from the two phases is shown. Figure 11 shows a monoclinic potassium phase together with anorthoclase occur-

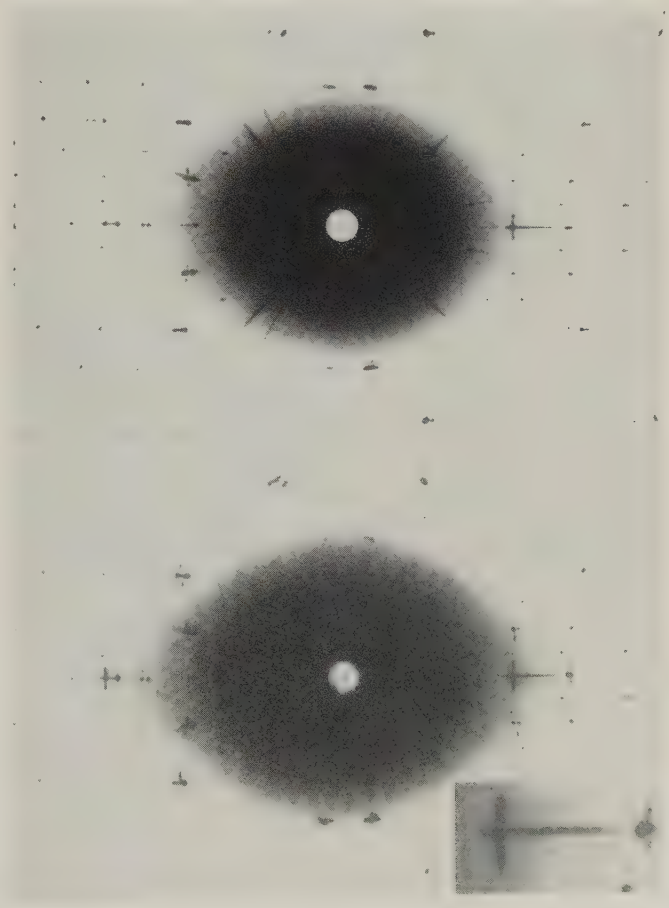

FIG. 8 (above). Oscillation photograph of monoclinic K phase-anorthoclase-albite/oligoclase perthite taken about *b*-axis in standard orientation (Smith and MacKenzie, 1955). See text for detailed explanation.

FIG. 9 (below). Oscillation photograph in standard orientation of a perthite composed of a monoclinic K-phase and two Na-phases showing albite type superstructure. A portion of the photograph that contains the reflection $40\bar{5}$ has been enlarged and shown in the bottom right hand corner. See text for detailed explanation.

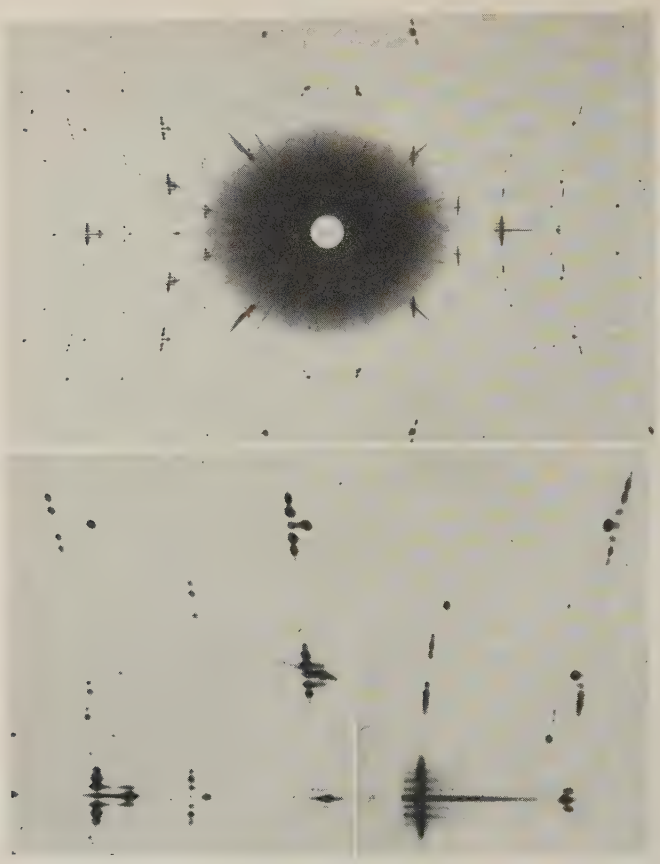

FIG. 10. Oscillation photograph in standard orientation of a perthite composed of a monoclinic K phase and an Na-phase showing perfectly developed albite-twin type superstructure. Two portions of the photograph have been enlarged and shown below the main photograph. See text for detailed explanation.

ring both in albite and pericline orientations. As there are no sharp doublets characteristic of twinning, this type is best classified as both albite and pericline superstructure. If the ends of the streaks are imagined to correspond to reflections from twin-components, the α^*, γ^* angles measured from them correspond to anorthoclase. A streak connects the potassium-phase reflection to the cluster of sodium phase reflections as is most clearly seen for reflection 442. In Fig. 12, the reflections for the potassium phase show a strong sharp center lying in a weak diffuse streak elongated nearly along the row lines. The sodium phase gives reflections composed of two streaks with maxima lying near to the positions for albite and pericline twinning. Measurements of α^*, γ^* for the

sodium phase show that it is an albite-oligoclase from which it may be deduced that most of the potassium phase is orthoclase. The diffuse streaks of the potassium-phase reflections reveal the presence of a little intermediate microcline, which is almost in the orientation for albite twinning. The occurrence of streaking between the albite and pericline twinned components of sodium phases is very common and often the maxima on the streaks do not correspond exactly to those to be expected

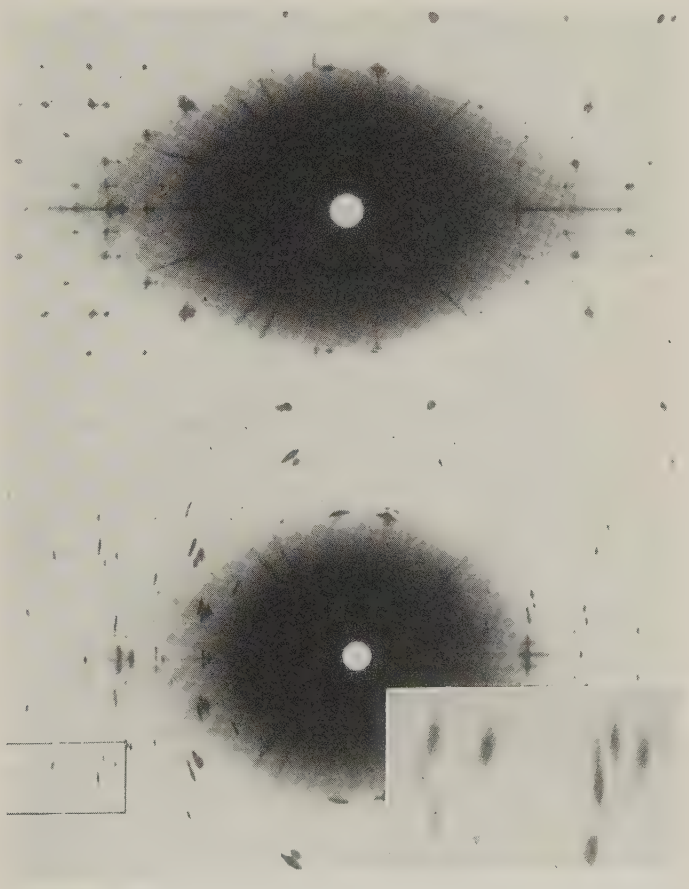

FIG. 11 (above). Oscillation photograph in standard orientation of a perthite composed of a monoclinic K-phase and of anorthoclase showing reflections that lie on both layer lines and row lines. See text for detailed explanation.

FIG. 12 (below). Oscillation photograph in standard orientation of a perthite composed of both a monoclinic and a triclinic K-phase and of a sodium-rich plagioclase both albite and pericline twinned. The inset is an enlargement of the area outlined in the main photograph. See text for detailed explanation of the photograph.

for a strict obeyance of the albite and pericline laws. Intermediate positions of the streaks correspond to the "diagonal association" (see paper V of this series, Smith and MacKenzie, 1959, for a stereographic projection showing the angular relations).

Acknowledgments

Much of this work was carried out in Oxford, where C. H. E. wishes to acknowledge the advice and assistance received from Prof. L. R. Wager, Drs. E. A. Vincent and G. M. Brown, and in Cambridge, where J. V. S. wishes to thank Prof. C. E. Tilley for his continued advice and Dr. S. O. Agrell for suggesting the suitability of the Slieve Gullion Rocks and for accompanying him on a collection trip. The cost of this trip was generously defrayed by the Geophysical Laboratory, Washington D.C. at which J. V. S. and Dr. Wm. Scott MacKenzie, now of Manchester, England, began this program of work on the alkali feldspars. We also wish to thank Dr. J. E. Richey for allowing us to use an unpublished analysis of the felsite. C. H. E. also wishes to acknowledge financial help from the Burdett-Coutts Scholarship fund of Oxford University and from the Ministry of Education, N. Ireland.

References

Bailey, E. B. and McCallien, W. J. (1956) Composite minor intrusions and the Slieve Gullion Complex, Ireland. *Liverpool and Manchester Geological Journal*, **1**, 466–501.

Brown, P. E. (1956) The Mourne Mountain Granites—a further study. *Geol. Mag.*, **93**, 72–84.

Ferguson, R. B., Traill, R. J. and Taylor, W. H. (1958) The crystal structures of low-temperature and high-temperature albite. *Acta. Cryst.*, **11**, 331–348.

Goldsmith, J. R. and Laves, F. (1954) Potassium feldspars structurally intermediate between microcline and sanidine. *Geochimica et Cosmochimica Acta*, **6**, 100–118.

Hafner St. and Laves, F. (1957) Ordnung/Unordnung und Ultratotabsorption II. Variation der Lage und Intensitat einiger Absorptionen von Feldspäten. Zur Struktur von Orthoklas und Adular. *Zeit. für Krist.*, **109**, 204–225.

Hughes, C. J. (1956) Petrographical and structural studies in South-East Rhum, Inverness-shire. D. Phil. Thesis, Oxford University, England.

Laves, F. (1951). Artificial preparation of microcline. *Jour. Geol. Chicago*, **59**, 511–512.

MacKenzie, W. S. and Smith, J. V. (1959) Charge balance and the stability of alkali feldspars. *Acta Cryst.*, **12**, 73.

Muir, I. D. and Smith, J. V. (1956) Crystallization of feldspars in larvikites. *Zeit. Krist.*, **107**, 182–195.

Nolan, J. Explanation of Sheet 70, Ireland. *Mem. Geol. Survey, Ireland.*

Patterson, E. M. (1953) Petrochemical data for some acid intrusive rocks from the Mourne Mountains and Slieve Gullion. *Proc. Royal Irish. Acad.*, **55B**, 171–188.

Reynolds, D. L. (1941) A gabbro-granodiorite contact in the Slieve Gullion area and its bearing on Tertiary petrogenesis. *Quart. Jour. Geol. Soc. London*, **97**, 1–38.

—— - (1950) The transformation of Caledonian granodiorite to Tertiary granophyre on

Slieve Gullion, Co. Armagh, Ireland. *Internat. Geol. Congress, 18th Session, Gt. Britain*, **1948** Part *III*, 20–30.

——— (1951) The geology of Slieve Gullion, Foughill and Carrickarnan: an actualistic interpretation of a Tertiary gabbro-granophyre complex. *Trans. Roy. Soc. Edinburgh*, **62,** 85–143.

Richey, J. E. (1928) The structural relations of the Mourne granites (Northern Ireland). *Quart. Jour. Geol. Soc. London*, **83,** 653–688.

——— and Thomas, H. H. (1932) The Tertiary ring complex of Slieve Gullion, Ireland. *Quart. Jour. Geol. Soc. London*, **88,** 776–847.

Schneider, T. R. (1957) Röntgenographische und optische Untersuchung der Umwandlung Albit-Analbit-Monalbit. *Zeit. Krist.*, **109,** 245–271.

Smith, J. V. and MacKenzie, W. S. (1955) The alkali feldspars II. A simple *X*-ray technique for the study of alkali feldspars. *Am. Mineral.*, **40,** 733–747.

——— and Muir, I. D. (1958) The reaction sequence in larvikite feldspars. *Zeit. Krist.*, **110,** 11–20.

Tuttle, O. F. (1952) Optical studies on alkali feldspars. *Am. Jour. Sci.*, **Bowen Volume,** 553–567.

——— and Keith, M. L. (1954) The granite problem: evidence from quartz and feldspar of a Tertiary granite. *Geol. Mag.*, **91,** 61–72.

Wyart, J. and Sabatier, G. (1956) Transformations mutuelles des feldspaths alkalins reproduction du microcline et de l'albite. *Bull. Soc. Franc. Minér. Crist.*, **79,** 574–581.

Manuscript received March 12, 1959.

NEW WURTZITE POLYTYPES FROM JOPLIN, MISSOURI*

HOWARD T. EVANS, JR. AND EDWIN T. MCKNIGHT,
U. S. Geological Survey, Washington, D. C.

ABSTRACT

Small, hemimorphic hexagonal crystals implanted on botryoidal zinc sulfide from the Zig Zag Mine, Joplin, Missouri, have been studied by crystallographic and x-ray diffraction techniques. They are identified as a new wurtzite polytype, wurtzite-10H. The unit cell data are: space group, $P6_3mc$; $a=3.824$ Å, $c=31.20$ Å; cell contents, 10ZnS. Comparison of diffraction intensity data indicates that the published structure of SiC-10H (stacking sequence 3223) is different from that of wurtzite-10H. Calculation of intensities for various models shows that the stacking sequence for wurtzite-10H is 55. Crystals of wurtzite from Joplin described by A. F. Rogers (1904) were evidently wurtzite-10H. Powder diffraction data revealed the presence of another polytype, wurtzite-8H, with a hexagonal unit cell: space group $P6_3mc$; $a=3.82$ Å, $c=24.96$ Å; cell contents 8ZnS. Wurtzite-6H was also found at the Zig Zag Mine. The wurtzite polytypes evidently form a homologous series (2H, 4H, 6H, 8H, 10H) resulting from growth phenomena based on screw dislocations.

OCCURRENCE

During the course of a study of the Zig Zag Mine in north Joplin, Missouri, by one of us (E.T.McK.), specimens of an unusual stalactite formation of zinc sulfide were collected. Optical examination of the radiating structure of these stalactitic forms in thin section showed that the mass consisted of about 90 per cent isotropic sphalerite and 10 per cent of an anisotropic zinc sulfide phase. On the surface of some of the stalactites small wurtzite-like pyramidal crystals were found implanted on their points, in a manner resembling prickly-pear fruit. This resemblance is most apt for the imperfect, rounded crystals which greatly outnumber those with well-defined crystal faces. As shown in the photograph in Fig. 1, a secondary crystal is occasionally found growing out of the base of the larger crystals. When clean, the crystals are brown to light brown, but their color is often obscured by a black stain covering the surface of the stalactites. None of them ranges over 2 mm. in size. These crystals have been proved by crystallographic and x-ray diffraction study to be a previously unreported polytype of wurtzite.

CRYSTALLOGRAPHY

The crystal habit is characterized by a negative base and a steep positive pyramid. The faces of the best crystals gave poor signals on the goniometer, but good enough to indicate an inclination angle (ρ) of about $77\frac{1}{2}°$. This angle corresponds to the form $l\{50\bar{5}2\}$ as listed in Palache, Berman and Frondel (1944, p. 227). Frondel and Palache (1950) found in

* Publication approved by the Director, U. S. Geological Survey.

their study of the wurtzite polytypes from western Pennsylvania that the pyramidal form reflected the dimensions of the internal structure, but they report none having the form found on the Joplin crystals. It was suspected, therefore, that the Joplin wurtzite might constitute a new polytype, and this possibility was borne out by the x-ray study.

Buerger precession photographs were made of the ($h0.l$) net in the

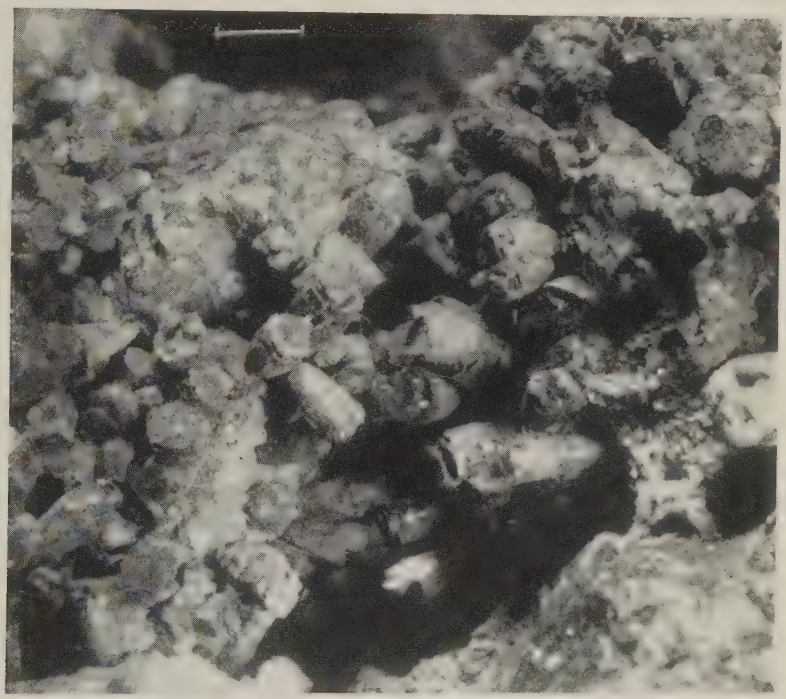

FIG. 1. Wurtzite-10H crystals in vug of botryoidal sphalerite from Zig Zag Mine, Joplin, Missouri. Bar at top indicates one mm. Photograph by J. A. Denson.

hexagonal lattice. The resulting data for the Joplin wurtzite are given in Table 1. No polytype of zinc sulfide of these dimensions has been previously reported in either natural or artificial specimens (Frondel and Palache, 1950; Strock and Brophy, 1955). Also, the Joplin wurtzite, which in the notation of Frondel and Palache will be designated wurtzite-10H, constitutes the first natural occurrence of wurtzite polytypes outside of the western Pennsylvania (eastern Ohio) localities described by Seaman and Hamilton (1950). Table 2 compares the unit cell data for all the natural wurtzite polytypes, and shows that wurtzite-10H fits well in the series.

Among the abundant crystals of wurtzite-10H, crystals are sometimes found which have a somewhat more obtuse pyramid angle. Buerger precession photographs of one of these showed that they are wurtzite-6H, identical with that described by Frondel and Palache. The surfaces of these crystals were so poor that the crystal forms could not be identified, but they are characteristically more blunt in appearance than wurtzite-10H.

TABLE 1. CRYSTALLOGRAPHIC DATA FOR NEW WURTZITE POLYTYPES

Polytype:	8H	10H
Space group:	$P6_3mc$	$P6_3mc$
Cell constants:	$a=3.82\pm.01$ Å $c=24.96\pm.08$ Å $c/a=6.53$ $p_0=7.53$	$a=3.824\pm.004$ Å $c=31.20\pm.03$ Å $c/a=8.159$ $p_0=9.421$
Cell contents:	8ZnS ($Z=8$)	10ZnS ($Z=10$)
Forms:	—	$-c\{0001\}$ $l\{10\bar{1}2\}$ ($\rho=78°01'$)
Structure parameters:	(provisional) $2Zn_1$ in (a), $z=0$ $2Zn_2$ in (b), $z=1/8$ $2Zn_3$ in (b), $z=3/8$ $2Zn_4$ in (b), $z=3/4$ S_1, S_2, S_3, S_4 corresponding to Zn atoms above, with $z_S=z_{Zn}+3/32$	(established) $2Zn_1$ in (a), $z=0$ $2Zn_2$ in (a), $z=3/10$ $2Zn_3$ in (b), $z=1/10$ $2Zn_4$ in (b), $z=2/5$ $2Zn_5$ in (b), $z=7/10$ S_1, S_2, S_3, S_4, S_5 corresponding to Zn atoms above, with $z_S=z_{Zn}+3/40$

The dark-stained, almost black stalactitic specimens appear to be coated with a late, very fine, crystalline deposit, possibly of sphalerite. Gently crushed crystal fragments of one of the wurzite polymorphs show under the microscope a fine banding of isotropic sphalerite parallel to the basal pinacoid. Precession photographs of crystals of wurtzite-6H taken from one of the coated stalactitic specimens show prominent but very diffuse spots corresponding to sphalerite, twinned on (111) and in oriented relation to the wurtzite-6H lattice. Photographs of clean, brown crystals of wurtzite-10H also show weaker sphalerite reflections. Consistent with optical observations, the x-ray patterns thus show the pres-

ence of sphalerite, either as an intergrown or alteration phase, or a surface coating, or both.

It should be noted that comparison of form symbols for the pyramidal forms is based on the dimensions of the unit cell assumed. Thus, $l\{10\bar{1}2\}$ for wurtzite-10H ($c:a=8.159$) is the same form (i.e., has the same ρ angle) as $l\{50\bar{5}2\}$ of wurtzite-2H ($c:a=1.6358$) and $l\{50\bar{5}1\}$ of A. F. Rogers ($c:a=0.8179$) (see below).

Crystal Structure

Frondel and Palache (1950) found that the 4H, 6H, and 15R polytypes of wurtzite all had structures corresponding to previously known silicon carbide polytypes (Strukturbericht, 1931). It was natural, therefore, to compare the wurtzite-10H structure with that of silicon carbide-10H as described by Ramsdell and Kohn (1951). A close comparison of the diffraction intensities of the two crystals showed conclusively that the structures of ZnS-10H and SiC-10H are not the same.

There is a limited number of possibilities for different structures of a 10H polytype based on tetrahedral stacking sequences. The usual method of designating the stacking sequence consists of a series of digits, each digit representing the number of layers in an unbroken cubic sequence run, each run separated by a hexagonal layer shift (Ramsdell, 1947). Such a symbol will have an even number of digits which add up to the number of layers of tetrahedra in the repeat unit. The stacking symbols for the various wurtzite polytypes are given in Table 2. It can be shown that the only hexagonal sequences possible for wurtzite-10H, in either space group $P6_3mc$ or $P3m$, are:

55	212212
82	221122
4114	311113
3223	131131
7111	321211
6121	321112
5131	21111112
4312	11211211

Structure factor calculations show that the only sequence which at all accounts for the observed intensities is 55. In Fig. 2, the squares of the unitary structure factors for typical reflections are indicated. The apparent agreement is sufficient to prove the postulated stacking sequence. The structure may now be defined by the parameters given in Table 1. No attempt has been made to refine the structure of wurtzite-10H.

In the silicon carbide polytypes, the largest cubic run found in any case is 4 and most stacking sequences are combinations of 2 and 3

TABLE 2. UNIT CELL DATA FOR WURTZITE POLYTYPES

Data (except for 8H and 10H) from Frondel and Palache (1950)

Polytype Source	2H artificial	4H Pennsyl- vania	6H Pennsylva- nia, Missouri	8H Missouri	10H Missouri	15R Pennsyl- vania
Space group	$P6_3mc$	$P6_3mc$	$P6_3mc$	$P6_3mc$	$P6_3mc$	$R3m$
a, Å	3.819	3.814	3.821	3.82	3.824	3.830
c, Å	6.246	12.46	18.73	24.96	31.20	46.88
Z	2	4	6	8	10	15
c/Z, Å	3.123	3.116	3.121	3.12	3.120	3.126
Stacking	11	22	33	44	55	323232

(Structure Reports, 1951). For no really good reason, it has in the past been inferred from the known series of polytypes that the length of a cubic run in the ZnS and SiC polytypes is limited to 4 layers. Obviously, this assumption can no longer be held.

POWDER DIFFRACTION DATA

One of the brown crystals was gently crushed, without grinding, for making an x-ray powder diffraction photograph. The pattern strongly

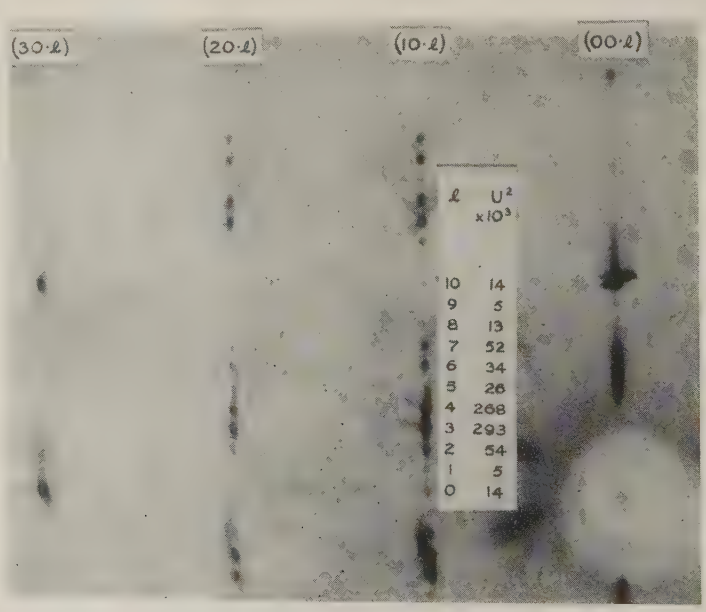

FIG. 2. Buerger precession photograph of ($h0l$) net of wurtzite-10H. Calculated values of the squares of the unitary structure factors (U^2, right column) agree well with photographic intensities.

resembles that of ordinary sphalerite, with the addition of many weak extra lines. The spacings observed are well accounted for by those predicted for wurtzite-10H, except for eight lines. Of these, one at 2.71 Å is associated with sphalerite, and indicates the presence of this mineral. The remaining seven could not be accounted for in terms of any of the postulated polytypes for which d-spacing data are given by Smith (1955) (2H, 4H, 6H, 9H, 15R, 21R).

On the assumption that the extra lines are produced by an unknown wurtzite polytype, an attempt was made to index them in terms of the single-layer hexagonal sub-cell with $a = 3.824$ Å, $c' = 3.120$ Å. The extra lines are all in the region where their indices would have the form $10.l'$, where l' will have fractional values depending on the number of layers in the polytype producing the lines. Then,

$$l' = \frac{\sqrt{1/d^2 - 0.09117}}{0.3205} .$$

For the seven lines the following results were obtained:

d	l'(obs)	l'(calc)	l
3.20	.251	.250	2
3.09	.363	.375	3
2.76	.625	.625	5
2.61	.736	.750	6
2.49	.826	.875	7
1.977	1.266	1.250	10
1.871	1.375	1.375	11

The comparison of the second and third columns leaves little doubt that the additional phase is an 8H polytype. Wurtzite-8H is therefore present with wurtzite-10H, and has a hexagonal unit cell with $c = 24.96$, corresponding to 8 ZnS layers.

Complete data are given in Table 1. Wurtzite-8H is subordinate to wurtzite-10H in quantity, and is probably interlaminated with it. No evidence of the presence of wurtzite-8H could be seen on the single crystal photographs.

In Table 2 the observed powder data are compared with the calculated d-spacings for wurtzite-10H, wurtzite-8H and sphalerite. Below $d = 1.600$ Å, only the sphalerite-like lines are indexed.

Chemical Composition

The composition of the wurtzite-10H from the Zig Zag Mine was determined on two single crystals by I. Adler of the Geological Survey, using a micro-probe, spectrographic method (Alder and Axelrod, 1957). The analysis showed 1.4 ± 0.2 wt. per cent Fe. No other metallic constit-

TABLE 3. INTERPRETATION OF *X*-RAY POWDER DIFFRACTION DATA FOR WURTZITE FROM JOPLIN, MISSOURI

CuKα radiation, camera diameter 114.6 mm.; film by M. E. Mrose

Joplin, observed		Wurtzite-10H		Wurtzite-8H		Sphalerite	
d(obs.)	Int.	*hk.l*	*d*(calc.)	*hk.l*	*d*(calc.)	*hk.l*	*d*(calc)
3.31	1	10.0	3.312	10.0	3.312		
		10.1	3.293				
				10.1	3.283		
3.26	6	10.2	3.240				
3.20	3			10.2	3.201		
3.16	2	10.3	3.156				
3.12	100	00.10	3.120	00.8	3.120	111	3.121
3.09	4			10.3	3.077		
3.05	4	10.4	3.049				
2.93	6	10.5	2.926	10.4	2.926		
2.81	1	10.6	2.794				
2.76	2			10.5	2.760		
2.71	3					200	2.705
2.66	1	10.7	2.659				
2.61	1			10.6	2.591		
2.52	1	10.8	2.525				
2.49	1			10.7	2.427		
		10.9	2.395				
		10.10	2.271	10.8	2.271		
		10.11	2.155				
				10.9	2.127		
2.08	2	10.12	2.045				
1.977	1			10.10	1.994		
1.937	1	10.13	1.944				
1.904	50	11.0	1.912	11.0	1.912	220	1.912
1.871	2			10.11	1.872		
1.841	1	10.14	1.849				
1.756	3	10.15	1.762	10.12	1.762		
1.678	1	10.16	1.681				
		20.0	1.656	20.0	1.656		
		20.1	1.654				
				20.1	1.652		
1.649	1	20.2	1.647				
				20.2	1.641		
		20.3	1.635				
1.626	35	11.10	1.630	11.8	1.630	311	1.631
				20.3	1.624		
		20.4	1.620				
1.598	1	20.5	1.601	20.4	1.601		
1.572	1						
1.558	1						
1.350	1					400	1.352
1.294	1						
1.239	4					331	1.240
1.207	1	11.20	1.209	11.16	1.209	420	1.209
1.168	1						
1.103	6	30.0	1.104	30.0	1.104	422	1.103
1.071	1						
1.039	4	30.10	1.041	30.8	1.041	511	1.040
		00.30	1.040	00.24	1.040		
.955	3	22.0	.958	22.0	.958	440	.956
.914	6	11.30	.914	11.24	.914	531	.914

uents were found within the range of the x-ray spectrograph. A chemical analysis of the massive zinc sulfide associated with wurtzite reported by Rogers (1904) gave 2.73 wt. per cent Fe. Mr. Adler also estimated Fe in a western Pennsylvania crystal at 3.7 wt. per cent, using the same microprobe technique.

Earlier Description of Wurtzite from Joplin

Wurtzite-10H, as described above, is probably the same as the wurtzite from Joplin described by A. F. Rogers (1904, p. 461–2). His crystals came from an abandoned mine in eastern Joplin. Rogers describes the occurrence of his crystals as follows:

"Wurtzite occurs as small hemimorphic crystals, averaging about two mm. in length and one mm. in thickness in cavities in massive zinc sulfide (wurtzite?). One end of the crystal is terminated by the basal plane (pedion), while the other end, which is usually the one attached to the matrix, is terminated by the pyramid $l\{50\bar{5}1\}$ $5P$, · · · .

"The massive zinc sulfide upon which the wurtzite crystals are implanted usually assumes a botryoidal, mammillary or stalactitic form."

He reports an inclination angle for the pyramid form of 78°5′, showing that the form of his crystals is identical with that of ours. Rogers' crystal drawings, reproduced in Fig. 3, serve to illustrate our crystals equally as well as his. There seems little doubt that the crystals that Rogers described were actually wurtzite-10H.

General Observations

The discovery of wurtzite-10H with stacking sequence 55 suggests the existence of a homologous series of polytypes: 2H, 4H, 6H and 10H, with stacking sequences 11, 22, 33 and 55 respectively. The presence of wurtzite-8H revealed by the powder diffraction patterns as described above provides a fifth member of this series. While the structure of wurtzite-8H has not been proved, there is good reason to believe that it

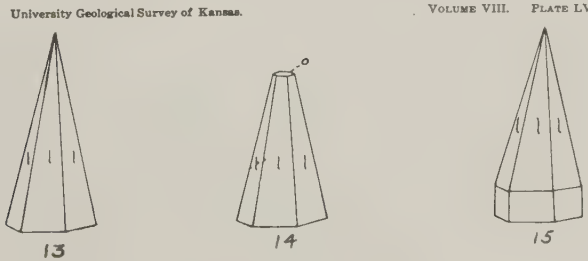

Fig. 3. Figures reproduced from Rogers (1904) which illustrate the crystal habit of wurtzite-10H showing $l\{10\bar{1}2\}$.

has the stacking sequence 44. This structure is the same as that of SiC-8H found by Ramsdell and Kohn (1952). It is understood that the polytypic structures may arise from accidents of spiral growth resulting from screw dislocations (Frank, 1951). This explanation is especially logical for the homologous series suggested here. The known members of the series evidently correspond to screw dislocations involving from 1 to 5 layers.

There are as yet no apparent clues as to what conditions of environment are responsible for the formation of wurtzite polytypes. While Smith (1955) has shown that incipient polytypism is present in all sphalerite and wurtzite crystals, only at Joplin and western Pennsylvania have homogeneous crystals of individual polytypes been found. About the only features in common to the wurtzite genesis at the two localities is that the crystals were apparently formed from mineralizing solutions (low in iron) at low temperatures ($<100°C$). While some polytypes have been found at only one locality, there is no reason to suppose that these and other polytypes should not be found eventually in many places. The presence of the homologous series at both the known localities indicates that the same growth phenomena prevail in both environments.

References

Adler, I. and Axelrod, J. M. (1957), Reflecting curved-crystal x-ray spectrograph—a device for the analysis of small mineral samples: *Econ. Geol.* **52,** 694–701.

Frank, F. C. (1951), The growth of carborundum, dislocations and polytypism: *Phil. Mag.* **42,** 1014–1021.

Frondel, C. and Palache, C. (1950), Three new polymorphs of zinc sulfide: *Am. Mineral.* **35,** 29–42.

Palache, C., Berman, H. and Frondel, C. (1944), Dana's System of Mineralogy, 7th ed.: John Wiley & Sons, Inc., New York, N. Y.

Ramsdell, L. S. (1947), Studies on silicon carbide: *Am. Mineral.* **32,** 64–82.

Ramsdell, L. S. and Kohn, J. A. (1951), Disagreement between crystal symmetry and x-ray diffraction data as shown by a new type of silicon carbide, 10H: *Acta Cryst.* **4,** 111–113.

——— (1952), Developments in silicon carbide research: *Acta Cryst.* **5,** 215–224.

Rogers, A. F. (1904), Minerals of the Galena-Joplin lead and zinc district: *Univ. Geol. Survey Kansas Rep.* **8,** 445–537.

Seaman, D. M. and Hamilton, H. (1950) Occurrence of polymorphous wurtzite in western Pennsylvania and eastern Ohio: *Am. Mineral.* **35,** 43–58.

Smith, F. G. (1955), Structure of zinc sulfide minerals: *Am. Mineral.* **40,** 658–675.

Strock, L. W. and Brophy, V. A. (1955), Synthetic zinc sulfide polytype crystals: *Am. Mineral.* **40,** 94–106.

Structure Reports (1951), Vol. 11, for 1947–1948, A. J. C. Wilson, ed.; Silicon carbide, pp. 226–235; Internat. Union of Crystallography, N. V. A. Oosterhoek's Uitgevers Mij, Utrecht.

Strukturbericht (1931), Vol. 1, for 1913–1928, P. P. Ewald and C. Hermann, eds.; Siliciumcarbid, SiC: pp. 144–146; Zeit. für Kristallographie, Akademische Verlagsgesellschaft M.B.H., Leipzig.

THE AMERICAN MINERALOGIST, VOL. 44, NOVEMBER–DECEMBER, 1959

EFFECT OF HEAT ON AN ORGANO-MONTMORILLONITE COMPLEX

JAMES L. MCATEE, JR. AND CHARLES B. CONCILIO, *Baroid Division, National Lead Company, Houston 1, Texas*

ABSTRACT

An organo-montmorillonite was heated under atmospheres of air, oxygen and nitrogen while following the changes in the basal spacing with a heating-oscillating *x*-ray diffractometer.

It has been shown that up to a temperature of about 180° C. a reversible expansion of the basal spacing takes place. With further heating this is followed by a very rapid collapse to a single organic layer between each two montmorillonite plates. Further heating reduces this to a system comprised of a monolayer of carbon between each two plates and then finally to a decrease in spacing to 9.8 Å, a fully collapsed montmorillonite.

INTRODUCTION

The utilization of an oscillating-heating *x*-ray diffraction technique to study the clay minerals has been reported in several papers by Rowland, Weiss, and co-workers 1,2,3. Using the techniques described by these authors, oscillating-heating *x*-ray diffraction studies were made on an organo-montmorillonite complex formed by means of large organic cations. The decomposition of the organic portion of the organo-montmorillonite has been studied to gain knowledge with respect to the mechanism of interaction between the inorganic montmorillonite plates and the organic cation.

EXPERIMENTAL PROCEDURE AND RESULTS

The organo-montmorillonite used in these experiments was prepared from centrifuged Wyoming bentonite and dimethyldioctadecylammonium chloride. The bentonite was obtained from a deposit in the Mowry formation in the Colony, Wyoming area. Purification of the bentonite was accomplished by means of a Merco C-9 type centrifuge. The resulting bentonite slurry contained montmorillonite particles less than 0.8 micron in the largest dimension.

The organo-montmorillonite was prepared by adding dimethyldioctadecylammonium chloride

$$\left[\begin{array}{c} R \\ | \\ R—N—CH_3 \\ | \\ CH_3 \end{array}\right]^{+} Cl^{-}$$

to an aliquot of clay slurry, filtering, washing and drying. The sample

was then ground and the exact amount of organic retained on the clay was determined by loss on ignition. The sample used in these experiments contained 115 *me* of organic/100 g. dry clay base.

The organo-montmorillonite sample was dispersed in methylethyl ketone and several drops of the dispersion were allowed to dry on a platinum—10% rhodium plate producing an oriented film of the organo-

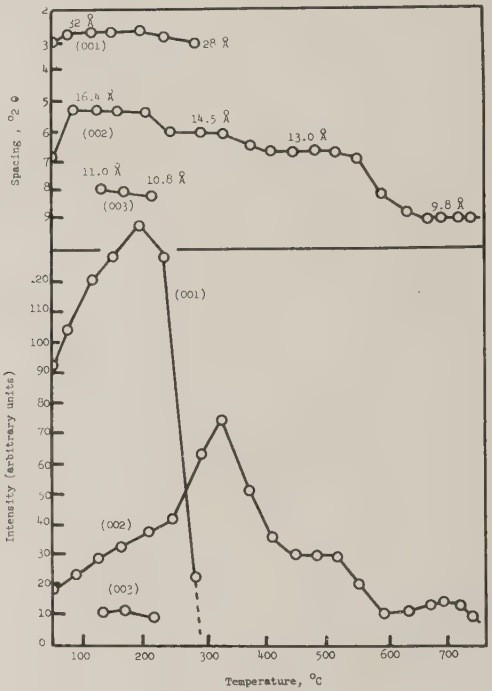

FIG. 1. Organo-bentonite, heated in air.

montmorillonite. The oriented sample was then placed in the furnace holder and a preliminary run made at room temperature to locate the positions of the diffraction maxima. The goniometer was then set to oscillate over the maxima to be scanned. The temperature of the furnace was then raised at a rate of approximately 5° C. per minute while oscillating and recording the diffraction maxima.

The graphs in Figs. 1 and 2 show changes in 2θ and intensity of the diffraction maxima of the organo-montmorillonite with increasing temperature. Figure 1 shows the data while oscillating over a wide enough region to follow the (001), (002) and (003) diffraction peaks and their changes. (The spectrometer trace is shown in Fig. 3.) The curves shown

in Fig. 2 were produced while oscillating over a very narrow range of 2θ and manually changing the limits of oscillation so that the (001) diffraction maximum and its intensity could be accurately followed. The spectrometer trace for this experiment is shown in Fig. 4. The figures show that the (001) maximum drifts from 3.2° 2θ to 2.8° 2θ with increasing intensity up to a temperature of 75° C. It then stabilizes at

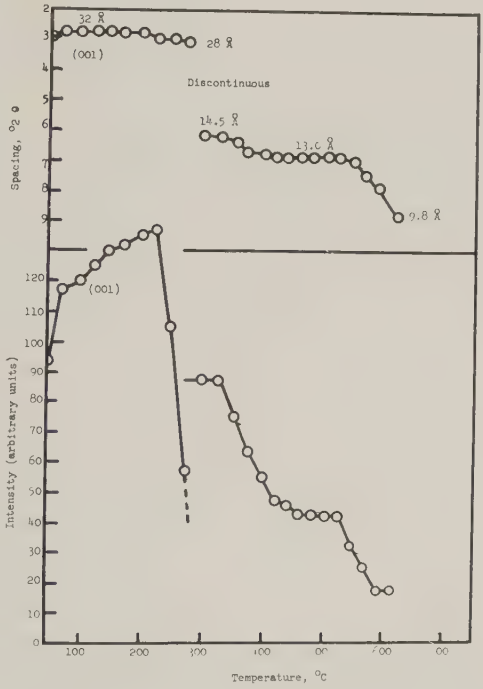

FIG. 2. Organo-bentonite, heated in air, oscillated over (001).

2.8° 2θ with continued increasing intensity up to a temperature of about 220° C. Then follows a very rapid decrease in intensity and a slight change in spacing to 3.2° 2θ up to a temperature of approximately 275° C., after which the diffraction maximum completely disappears.

In Figs. 1 and 3 it is shown that the (002) diffraction maximum persists throughout the entire heating range of the experiment. This maximum at room temperature has a 2θ value of 7°. Heating causes the line to shift to 5.4° 2θ (75° C.) and remain there with a slight increase in intensity to a temperature of about 250° C. whereupon a very rapid increase in intensity takes place followed by a shift to 6.2° 2θ. The increase in intensity and spacing change occur simultaneously with the disappearance of the

(001) diffraction maximum. The intensity of the (002) line increases up to a temperature of 325° C.; it then decreases as the line shifts to 6.8° 2θ. Both the position and intensity of the line then remain constant to a temperature of about 525° C., after which the intensity decreases and the line shifts to 9.0° 2θ and remains constant to the end of the run.

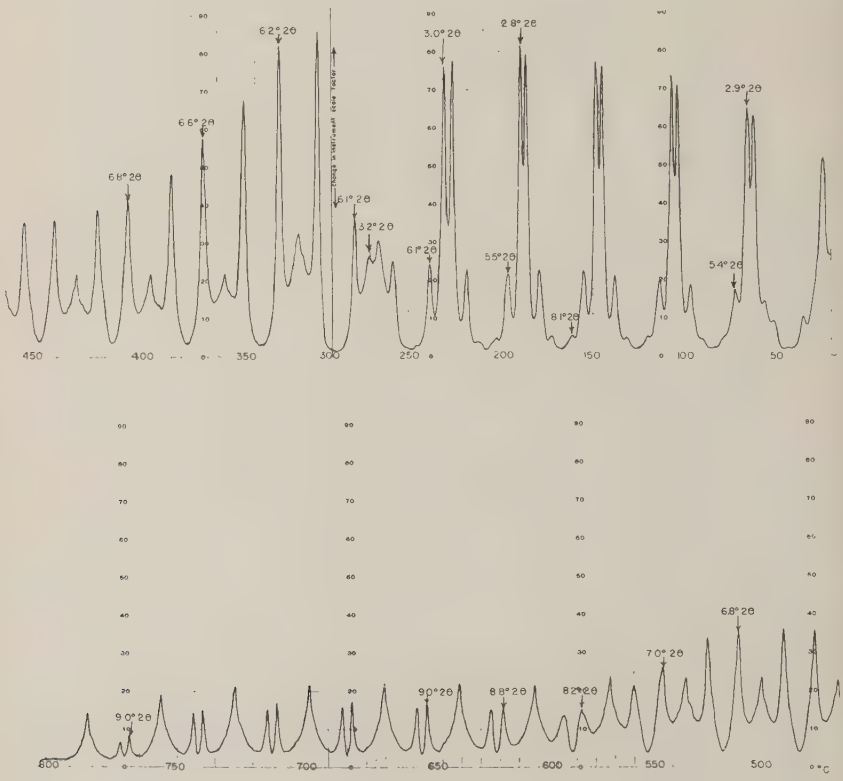

FIG. 3. Oscillating-heating X-ray diffraction diagram of (001), (002) and (003) for organo-bentonite heated in air from room temperature to 750° C.

The (003) line appears for only a short interval, approximately over the range of maximum intensity of the (001) maximum. The oscillation of the spectrometer was not over a wide enough range to determine the higher order spacings at temperatures above 250° C.

The curves shown in Fig. 2 and diffractometer trace in Fig. 4 demonstrate that the (001) diffraction maximum is discontinuous in the region of about 300° C. This demonstrates a rapid and complete change in the spacing between the montmorillonite sheets.

Separate portions of the organo-montmorillonite were heated in the *x*-ray oscillating furnace under oxygen and nitrogen atmospheres. This was accomplished by flowing the gas into the sample area at a rate sufficient to displace the air. The 2θ values and intensities for the several diffraction maxima for the sample heated in nitrogen and oxygen are shown in Figs. 5 and 6, respectively. The temperatures at which changes in the spacings occurred for the sample heated in oxygen are almost identical with those found when the sample was heated in air. The intensity curve

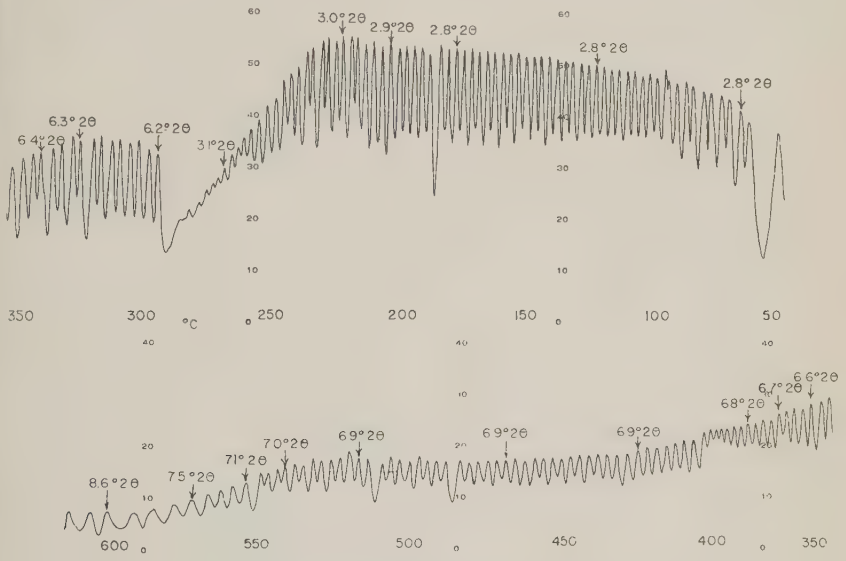

FIG. 4. Oscillating-heating *X*-ray diffraction diagram of (001) for organo-bentonite heated in air from room temperature to 625° C.

of the (001) is also about the same, but the intensity of the (002) has a plateau from about 300° to 525° C. of fairly high intensity.

The 2θ and intensity curves for the sample heated under nitrogen (Fig. 6) are almost identical to the curves obtained when the sample was heated under air. About the only difference is a slight shift in the (002) from 6.8° 2θ to a value of 7.1° 2θ at a temperature of 450° C.

Curves showing the basal expansion and contraction of the organo-montmorillonite upon repeated heating and cooling are shown in Fig. 7. The oriented sample was heated from room temperature to a temperature of 170° C., the electricity turned off and the furnace allowed to cool to about 40° C. This was repeated several times, following the changes in position and intensity of the (001) and (002) diffraction peaks.

One dimensional Fourier synthesis curves for the organo-montmorillonite heated to various temperatures are shown in Figs. 8 and 9. To obtain the diffraction data needed for the Fourier synthesis, the sample was heated to the desired temperature and this temperature maintained while a complete diffractometer trace was obtained. From the position and intensity of the basal lines, the one dimensional Fourier curves were

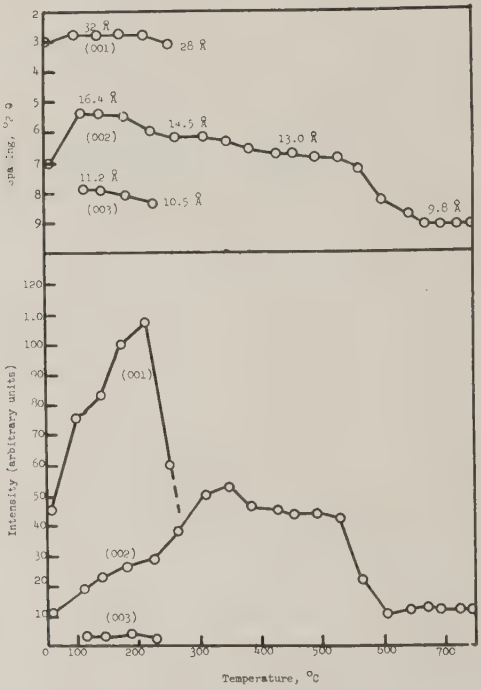

FIG. 5. Organo-bentonite, heated in O_2.

calculated. Fourier curves were obtained for diffractometer traces obtained at room temperature, 170, 280 and 425° C. These temperatures correspond to points of maximum intensity or plateaus found on the oscillating-heating diagram shown in Fig. 1. (The curves shown have not been normalized with respect to each other.)

DISCUSSION

The general features of the oscillating-heating curves show that with slight heating the organo-montmorillonite undergoes a reversible type expansion from about 28 Å to 32 Å. Further heating causes a very sudden collapse of the expanded system from a four organo-layer system to a

one layer system with a basal spacing of 14.5 Å. Additional heat causes the system to collapse slightly to 13.0 Å, then finally the lattice collapses completely to 9.8 Å.

The Fourier synthesis obtained for the organo-montmorillonite at room temperature shows a well established four-layer organo-montmorillonite (Figure 8A). The Fourier synthesis curves are "electron

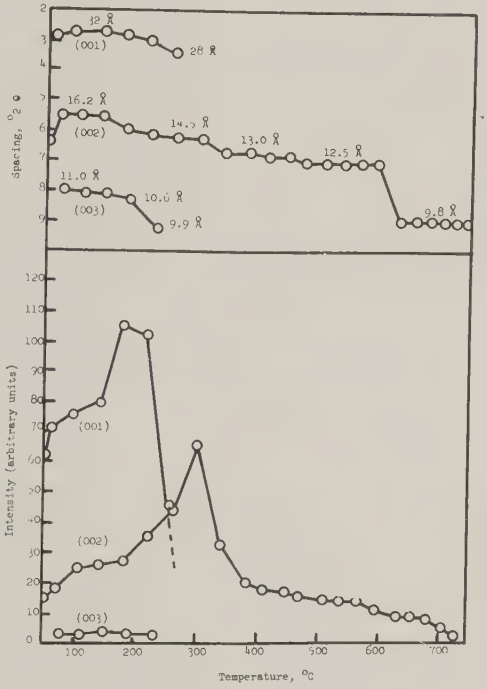

FIG. 6. Organo-bentonite, heated in N_2.

density" maps along the "*c*-axis" of the montmorillonite-organic complex. A maximum indicates a concentration of electrons and the distance between maxima is the distance from the center of a layer of atoms to the center of another layer of atoms. The distance from the center of the montmorillonite surface oxygen layer to the center of the first organic layer is about 3.9 Å, while the distance from the center of the first to the center of the second organic layer is 4.5 Å. These distances correspond very well with established data of Bradley (5) for his study of various organic materials associated with montmorillonite. The slight heating from room temperature to 170° C. causes a basal expansion to 32 Å. The corresponding Fourier synthesis is shown in Fig. 8B. Reference to Fig. 8

makes it apparent that the expansion takes place mainly between the two center organic layers. The negligible expansion of the layers associated with the montmorrillonite platelet surface shows that there is a high amount of energy of association and that the amount of heat added is not sufficient to cause many of the organic chains to become free. The expansion that is obtained (i.e., a change from 4.6 to 8.4 Å for the distance between the two central layers) along with the broadness of the second organic peak shows that some of the chains apparently become thermally active and cause the system to expand. Along with this

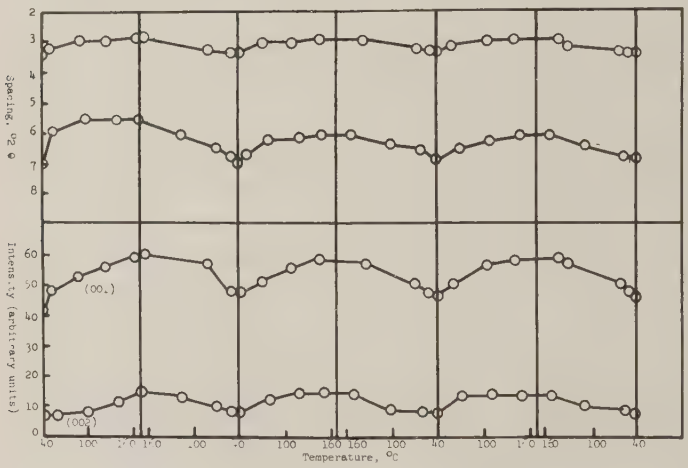

FIG. 7. Organo-bentonite, heated in air, sample repeatedly heated and cooled.

expansion there is a very noticeable increase in the intensity of the (001) diffraction maximum. About 12% of this increase can be accounted for due to the increase in the Lorentz-Polarization factors with a decrease in 2θ. The total increase in the intensity of the (001) maximum is much greater than this as can be seen from Fig. 1. It is believed, therefore, that the system must be changing into a higher degree of order as the temperature is raised. The apparent change from "disorder" to "order" is reversible as shown in Fig. 7, therefore the higher order must be associated with the higher thermal energy of the organic chains at the elevated temperature. It is visualized that upon heating, some of the hydrocarbon chains begin to become thermally active and are able to move around to positions of greatest freedom. The heating, therefore, causes a certain amount of untangling of the hydrocarbon chains which in turn tends to cause a more uniform packing which gives rise to an increase in the intensity of the diffraction peak.

Following the initial expansion and upon heating the sample to a temperature of about 200° C., the hydrocarbon chains very suddenly start decomposing or desorbing so that the organo-montmorillonite loses the equivalent of two complete organic layers. In this region (shown as discontinuous in Fig. 2) there is an inefficiently x-ray scattering mixed layer assemblage collapsing to a single organic layer complex, which becomes apparent in the diffraction diagrams suddenly as its

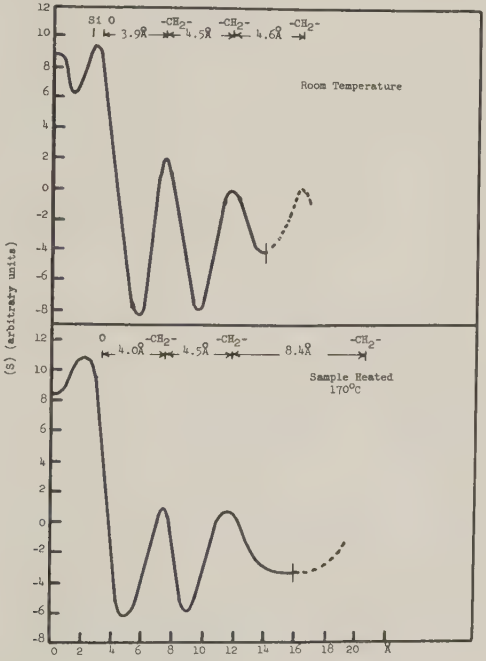

FIG. 8. Organo-bentonite, one dimensional Fourier synthesis.

regularity improves. This type of collapse explains the changes in intensity of the (001) and (002) diffraction peaks shown in the various figures. The thermal decomposition or desorption leaves a residue consisting of a mixture of methylene groups, carbon and short chains on the nitrogen.

In order to determine if this decomposition was strictly due to oxidation of the hydrocarbon chains, samples were x-rayed while heating and oscillating, while the sample area was flooded with oxygen and with nitrogen. Examination of the curves shown in Figs. 5 and 6 shows that an oxygen atmosphere does not cause the changes to take place at a lower temperature, nor does a nitrogen atmosphere allow the sample to be heated to a higher temperature before a collapse of the organo-clay

takes place. This indicates that it is not oxidation of the chains that causes the sudden collapse, but a thermal rupture or pyrolysis of the bonds, or a thermal desorption of the molecule. Differential thermal curves shown by Jordan (4) indicate that above a temperature of 300° C. pyrolysis of the organic matter takes place for the larger organic cations.

The conclusions that can be drawn from the x-ray diffraction patterns and Fourier curves for the samples heated to 200–250° C. are that the

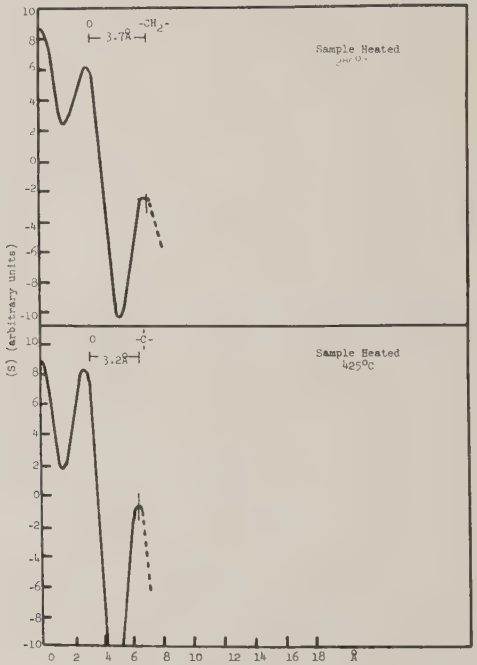

FIG. 9. Organo-bentonite, one dimensional Fourier synthesis.

interaction between the —CH_2— groups and the oxygen on the clay surfaces must be greater than simple Van der Waals forces and is probably an augmented attraction of the nature of a C-H—O bond as suggested by Bradley (5). At a temperature of about 225° C. there is enough heat available and the thermal activity is great enough so that the —CH_2— groups can break away from the surface oxygens and/or the methylene groups dehydrogenate allowing the system to contract to 14.5 Å.

Further heating of the sample, in air, oxygen or nitrogen causes a more complete decomposition of the hydrocarbon, probably leaving a residue of carbon and nitrogen. The presence of the carbon is quite apparent in

that over the temperature range of 400° to about 550° C.; the sample is very black. The basal spacing during this period of heating is 13.0 Å which corresponds to the thickness of the montmorillonite plate, 9.6 Å, with a "graphite" layer of carbon, 3.4 Å. The c_0 distance reported for the hexagonal graphite is 6.707 Å (6), but this distance is for two complete basal layers of hexagonally associated carbon. Dividing 6.707 by 2 gives a value of 3.35 Å which is very close to the 3.4 Å distance found on heating the organo-montmorillonite to 400° C. This indicates, then, that a monolayer of carbon between each two montmorillonite plates is produced at this temperature.

At a temperature of about 500° C. the sample once more contracts, this time to a collapsed montmorillonite spacing of about 9.8 Å. The theoretical spacing for collapsed montmorillonite is 9.6 Å, therefore, with further heating of the organo-montmorillonite a slight reduction in the spacing may result. It is of interest to note that the final collapse of the organo-montmorillonite takes place at about the same temperature when the sample is heated in air, oxygen or nitrogen.

References

(1) Weiss, E. J. and Rowland, R. A. (1956), Oscillating-heating *X*-ray diffractometer studies of clay mineral dehydroxylation: *Am. Mineral.* **41,** 117–127.

(2) Rowland, R. A., Weiss, E. J. and Bradley, W. F. (1956), Dehydration of monoionic montmorillonites: *Proc. Fourth Natl. Clay Conf., Clays and Clay Minerals, Natl. Res. Coun., Pub. No.* **456,** 85–95.

(3) Bradley, W. F., Rowland, R. A., Weiss, E. J. and Weaver, C. E. (1958), Temperature stabilities of montmorillonite- and vermiculite-glycol complexes: *Proc. Fifth Natl. Clay Conf., Clays and Clay Minerals, Natl. Res. Coun., Pub. No.* **566,** 340–355.

(4) Jordan, J. W. (1949), Alteration of the properties of bentonite by reaction with amines: *Miner. Mag.* **28,** 598–605.

(5) Bradley, W. F. (1945), Molecular associations between montmorillonite and some polyfunctional organic liquids: *J. Am. Chem. Soc.* **67,** 975–981.

(6) Wyckoff, R. W. G. (1948), Crystal Structures: Interscience Publishers, Inc., New York, N. Y.

Manuscript received March 23, 1959.

THE AMERICAN MINERALOGIST, VOL. 44, NOVEMBER–DECEMBER, 1959

INORGANIC-ORGANIC CATION EXCHANGE ON MONTMORILLONITE

JAMES L. MCATEE, JR., *Baroid Division, National Lead Company Houston 1, Texas*

ABSTRACT

Replacement of the inorganic cations on montmorillonite by base exchange with organic compounds has been followed by step-wise additions of the organic compound to the clay. It has been shown that a primary amine has enough basic character to react with montmorillonite by the base exchange mechanism. Data are also given showing the replacement of sodium, calcium and magnesium for montmorillonite and hectorite treated with a large quaternary ammonium salt. The sodium on montmorillonite is replaced stoichiometrically while calcium and magnesium require greater than the stoichiometric amount of organic for replacement.

INTRODUCTION

The alteration of montmorillonite from a hydrophilic to an organophilic material by the addition of organic compounds has led to many interesting uses of montmorillonite. The study of montmorillonite-organic reactions has also led to important analytical procedures whereby montmorillonite can be differentiated from other clay minerals, base exhange values determined, surface areas calculated, etc. To understand more fully the reaction between montmorillonite and organic amines and amine salts, a study was initated to follow the displacement of montmorillonite exchangeable cations by these organic substances.

EXPERIMENTAL DETAILS

Centrifuged Wyoming bentonite and centrifuged hectorite were used as the clay minerals in these experiments. The Wyoming bentonite was from the Colony, Wyoming area. Centrifugation was accomplished by means of a commercial Merco C-9 type centrifuge. The maximum particle size in both samples was less than 1.5 microns.

Homoionic Na-bentonite was prepared by passing a 1–2% suspension of the clay through an ion exchange column containing Amberlite IR-120 (Rohm and Haas Company) in the sodium form. The clay slurry and the column were preheated to about 65° C. so as to get complete ion exchange of the clay with a single pass.

The amine, amine salt and quaternary salts were commercial materials produced by Armour Chemical Division and by Onyx Oil & Chemical Company.

Increasing amounts of the amine, amine salt and quaternary salts were added to separate aliquots of the clay slurry. The resulting material was filtered in a high pressure filter cell and the sample washed four to

five times with distilled water. The filtrate and washings were retained and made up to a standard volume and the various cations determined by routine analytical methods.

Blanks were run on the bentonite and hectorite samples as follows: Portions of each clay slurry were filtered in the high pressure filter cell. The filtrate and washings were made up to a standard volume and the total cations determined. These values were considered as excess soluble cations and were subtracted from the values obtained with the organic treated clays.

In order to determine the amount of amine or quaternary salt being retained by the clay after washing, a portion of the filtered and washed residue was dried at 105° C. The dried residue along with a sample of the dried clay base were ignited at 1000° C. in a muffle furnace. From the differences in the loss on ignition of the sample and blank and the molecular weight of the organic compound, the milliequevalents (*me*) of the organic substance retained by the clay were calculated as follows:

$$me \text{ organic}/100 \text{ g. clay} = \frac{(I - C) \times 100{,}000}{(100 - I)W}$$

where

I = Ignition loss of clay-organic complex in per cent.
C = Ignition loss of the clay in per cent.
W = Molecular weight of the amine or quaternary ammonium cation.

Results

Cation replacement curves resulting from the addition of octadecylamine and octadecylamine hydrochloride to centrifuged Wyoming bentonite are shown in Fig. 1. The curves demonstrate the ability of

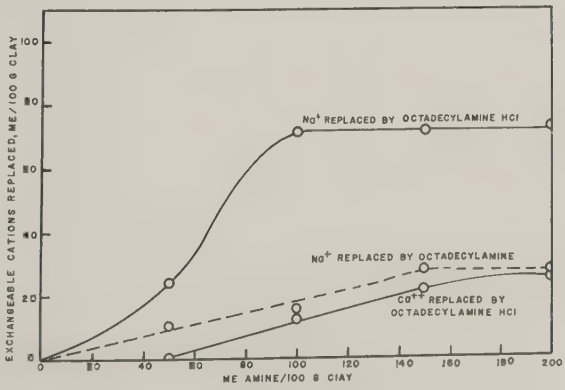

Fig. 1

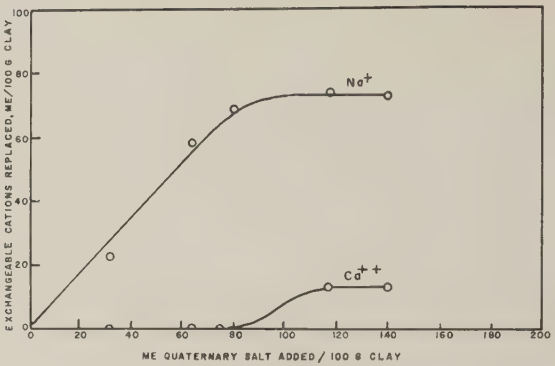

FIG. 2

octadecylamine hydrochloride to replace sodium and calcium exchangeable ions. It will be noted that half or more of the sodium is replaced before any of the calcium ions are removed from the clay.

The third curve shown in Fig. 1 is the replacement of sodium ions by the octadecylamine. This curve shows that octadecylamine has some basic character, indeed enough to replace 27 *me* of the sodium ions upon the addition of 150 *me* of the amine. The addition of 50 *me* amine replaces about 10 *me* of sodium. No calcium was replaced by the amine.

Figure 2 shows curves for the exchangeable sodium and calcium replaced upon the addition of the quaternary salt, dimethyldioctadecylammonium chloride. The replacement of the sodium ion by the quaternary is practically a 1:1 relationship, with all of the sodium being replaced before any calcium is removed.

The addition of the quaternary salt, dimethylbenzyllaurylammonium chloride, to centrifuged Wyoming bentonite causes cation exchange replacement as shown in Fig. 3. Again as with the dimethyldioctadecyl-

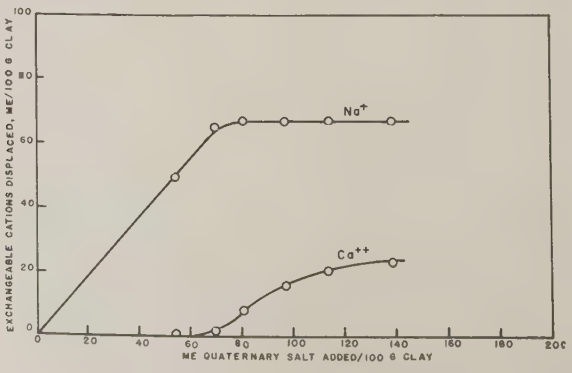

FIG. 3

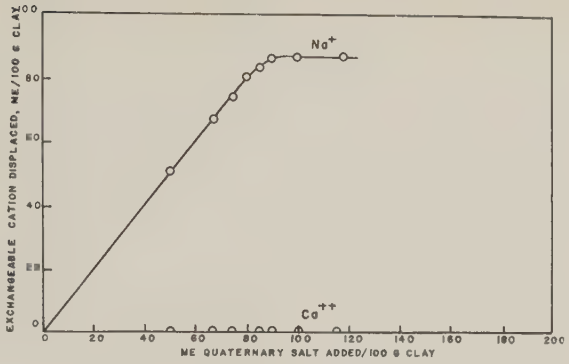

FIG. 4

ammonium quaternary, sodium is replaced stoichiometrically. At the start of calcium replacement there is required about one and a half *me* of quaternary to remove one *me* of the calcium ion. As more and more calcium is removed, it takes greater amounts of the quaternary cation to remove a single *me* of the calcium ion. Between the addition of 97 and 111 *me* of the quaternary cation, only 4 *me* of calcium are removed, indicating, therefore, that it is becoming increasingly more difficult to remove the remaining exchangeable cations.

Homoionic Na-bentonite was reacted with varying amounts of dimethylbenzyllaurylammonium chloride. The resulting cation exchange curves are shown in Fig. 4. It will be noted that almost an exact 1:1 replacement of sodium by the quaternary cation is obtained up to the exchange capacity of the clay (the B.E.C. value was found to be 92 *me*/100 g. dry clay).

The curves shown in Fig. 5 are for the replacement of divalent cations, Ca^{++} and Mg^{++}, from a centrifuged Wyoming clay passed through a

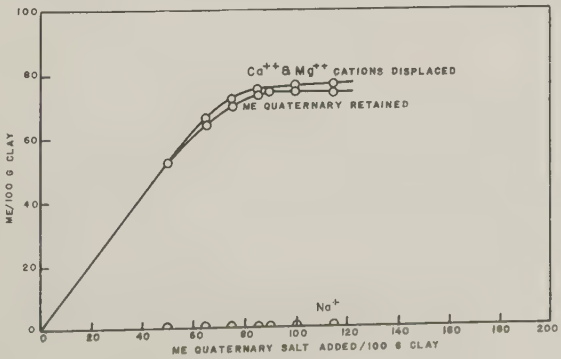

FIG. 5

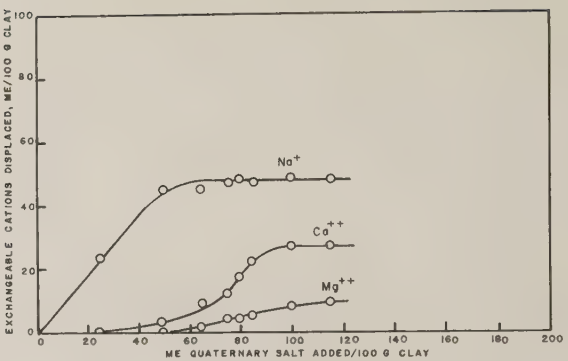

FIG. 6

calcium ion exchange column. The clay blank contained 62 *me* Ca^{++}, 13 *me* Mg^{++} and 1 *me* Na^{+}/100 g. dry sample. Also shown in Fig. 5 is a curve for the *me* of quaternary salt actually retained by the clay after washing and drying compared with the amount added. It is interesting to note that the two curves coincide up to an addition of 115 *me* of quaternary salt.

Hectorite, the trioctahedral magnesium montmorillonite, was reacted with dimethylbenzyllaurylammonium chloride. The resulting cation exchange curves are shown in Fig. 6. It will be observed that most of the sodium is replaced by the quaternary ion, then the calcium and finally the magnesium.

Curves showing the retention of dimethylbenzyllaurylammonium chloride by various samples after washing with distilled water and drying are shown in Fig. 7. It will be noted that the homoionic sodium bentonite and the hectorite retain practically all of the quaternary ion

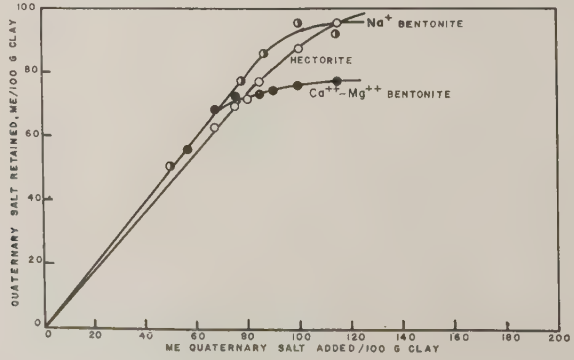

FIG. 7

that was added. The Ca^{++}-Mg^{++} clay, on the other hand, retains only approximately 70 *me.*

Discussion

A comparison of the curves shown in Figs. 1, 2, 3 and 6 show that the sodium exchangeable cation is the first to be replaced by the amine salt or quaternary salts. It is of interest to note that the large quaternary compounds replace sodium much easier than does the octadecylamine hydrochloride. Furthermore, from the rates of calcium removal shown in the various curves, the larger organic cations also remove calcium ions at a greater rate than does the simple primary amine ion. As already shown, the primary amine, octadecylamine has enough basic character (probably due to hydrolysis with water) so that it will replace some of the sodium ion from exchange positions of centrifuged Wyoming bentonite. This is demonstrated by the following equations:

$$RNH_2 + HOH \rightleftarrows (RNH_2H)^+ + OH^-$$

$$\text{Na-Montmorillonite} + (RNH_2H)^+ \rightarrow RNH_2H - \text{Montmorillonite} + Na^+$$

This replacement is not as rapid, nor as complete as with the corresponding amine hydrochloride, but certainly takes place to an extent corresponding to its relative basic character.

A comparison of the replacement of sodium from the homoionic Na-bentonite with the replacement of divalent Ca^{++} and Mg^{++} from the Ca-Mg bentonite is of interest. These curves again show the relative ease with which sodium is replaced by the large organic cation compared to the divalent ions. It is of particular interest to note the much greater retention of the organic cation by the Na-bentonite compared to the Ca-Mg bentonite (Fig. 7). Due to the large groups of flocculated clay in the Ca-Mg system, the quaternary cation probably cannot effectively exchange onto the clay nor even have room to become adsorbed after approximately 75 *me* has been added. On the other hand, the sodium bentonite and hectorite both retain all of the organic cation added up to at least 100 *me*/100 g. clay.

The centrifuged Wyoming bentonite used in these experiments had an ammonium acetate base exchange capacity of 92 *me*/100 g. dry clay. The total exchangeable cations and soluble cations were 113 *me* Na^+, 30 *me* Ca^{++}, and 13 *me* Mg^{++}. After subtracting the values found for the soluble cations, the exchangeable cations were found to be 67 *me* Na^+, 30 *me* Ca^{++} and 13 *me* Mg^{++}. Comparing the B.E.C. values of bentonite with the various curves, it can be seen that upon the addition of 92 *me* of amine or quaternary salt, only the homoionic sodium clay has an almost exact stoichiometric replacement of cations. The difference be-

tween the amount of organic added and cations removed at 92 *me* organic for the octadecylamine salt is 13 *me*, 17 *me* for the dimethyldioctadecyl quaternary and 12 *me* for the dimethylbenzyllauryl quaternary on centrifuged bentonite. The difference for the dimethylbenzyllauryl quaternary on the Na and Ca-Mg bentonites is 5 *me* and 18 *me*, respectively.

The centrifuged hectorite used had a B.E.C. of 93 *me*/100 g. dry clay and 47, 37 and 24 *me* Na^{+}, Ca^{++} and Mg^{++} exchangeable cations, respectively. A total of 90 *me* of cations are replaced upon the addition of 93 *me* of dimethylbenzyllauryl quaternary. This indicates that the cations on hectorite are somewhat easier to replace than those on Wyoming bentonite.

Further examination of Fig. 6 shows that for hectorite the calcium ion starts being removed slightly before all of the sodium ion is replaced. Between the addition of 65 and 90 *me* of the dimethylbenzyllauryl-ammonium chloride, a total of 25 *me* of Ca^{++} and Mg^{++} are removed. This is a 1:1 replacement of divalent ions, which is totally unlike that found with centrifuged Wyoming bentonite.

The differences shown in Figs. 3 and 6 for the replacement of the cations of hectorite and Wyoming bentonite are probably due to the differences in the origin of the cation exchange. The Wyoming bentonite used has roughly 50% of its cation exchange capacity originating in the tetrahedral layer and 50% originating in the octahedral layer (1). On the other hand hectorite has almost all of its cation exchange originating in the octahedral layer resulting from substitution of the magnesium by lithium (2). Grim (3) states: "Since the charges resulting from substitutions in the octahedral sheet would act through a greater distance than the charges resulting from substitutions in the tetrahedral sheet, it would be expected that cations held because of the latter substitutions would be bonded by a stronger force than those held by forces resulting from substitutions in the octahedral sheet." It would be expected, therefore, that the exchangeable hectorite cations would be easier to replace than the exchangeable cations on Wyoming bentonite which is indeed shown by the results of these studies.

References

(1) Osthaus, Bernard B. "Interpretation of Chemical Analysis of Montmorillonites": *Clays and Clay Technology*, Department of Natural Resources, Division of Mines, State of California, Bulletin 169, 1955.

(2) Ross, C. S. and Hendricks, S. B. "Minerals of the Montmorillonite group, their origin and relation to soils and clays": U.S. Geol. Survey Prof. Paper 205-B (1945).

(3) Grim, R. E. *Clay Mineralogy* (1953), McGraw-Hill Book Co., Inc., New York, p. 133.

Manuscript received March 6, 1959.

THE AMERICAN MINERALOGIST, VOL. 44, NOVEMBER-DECEMBER, 1959

AN INTERLAYER COMPLEX OF HALLOYSITE WITH AMMONIUM CHLORIDE

Koji Wada, *Faculty of Agriculture, Kyushu University, Fukuoka, Japan*

Abstract

An NH_4Cl-halloysite complex with a basal spacing of 10 Å was prepared by drying halloysite from an NH_4Cl solution or by dry mixing it with NH_4Cl crystals. In addition to the change in basal spacing, orientation of NH_4Cl between the silicate layers caused variations in the relative intensities and peak shapes of some of the *hk* bands. The oriented NH_4Cl no longer gives *x*-ray reflections as does the normal salt, and shows some distinctive features, such as loss of the transformation at 185° C., and the shift of the thermal decomposition to a temperature 30 to 50° C. higher. The orientation maximum of NH_4Cl is estimated at 325 to 330 m. mols. per 100 gms. of air-dried clay (2 molecules of NH_4Cl per unit cell of halloysite). Two molecules of the interlayer water are replaced by one molecule of NH_4Cl in the first stage of the complex formation.

Introduction

Earlier studies (6, 7) have shown that the basal spacing of hydrated halloysite will expand from 5 to 45% when dried from certain K, NH_4, Rb and Cs salt solutions, but not from Li and Na solutions. Since the reaction is reversible, and specific for certain pairs of cations and anions, a type of intermolecular complex formation has been suggested. The data indicate that an important factor controlling the reaction is the relation of the cation size to the size of the cavity in the oxygen network of the Si-O sheet. It is here proposed that the cation penetrating between the silicate layers is trapped in this cavity. The anions orient themselves around the trapped cation to neutralize its excess positive charge, forming a two-dimensional ionic layer.

If the complex forms through this reaction mechanism, the number of the salt molecules per unit cell should be two, provided the size of the anion allows for the two anions to orient per unit cell. The first purpose of this study is to estimate the number of the salt molecules oriented per unit cell of halloysite, utilizing the fact that the oriented form no longer contributes to *x*-ray diffraction as the normal salt (6). The oriented salt is also expected to differ from the normal salt in respect of thermal transformations. In view of the bond formation and possible steric hindrance, it seems worth while to know what effects appear on the thermal transformations of the interlayer material. The second purpose is to illustrate this on DTA curves. The third is to study the behavior of the interlayer water upon penetration of the salt molecules into the interlayer spaces. It might give a better understanding of the nature of the reaction together with that of the interlayer water. An NH_4Cl-halloysite complex with a 10.5 Å basal spacing (6) is adopted as the subject of this study on account of its simple composition and stability.

Materials and Methods

Experiments were made on hydrated halloysite from Yoake, Oita, Japan (1) (6), and on metahalloysite prepared by heating it at 300° C. Half gram samples of the clay (<150 mesh) were soaked in 1 ml. NH_4Cl solutions containing from 0 to 3.00 m.mols of NH_4Cl, and allowed to dry at 30° C. in an atmosphere with relative humidity of 65% for two weeks. The samples were then weighed and their water content determined.

X-ray diffraction patterns were obtained by means of a Philips diffractometer with Cu-Kα radiation. Flat plates of the samples were mounted according to McCreey's procedure (4). DTA was carried out on a portion of each sample corresponding to 100 mg. of the untreated air-dry clay at the heating rate of 10° C. per minute.

Results and Discussion

Characteristics of the X-ray Pattern of the NH_4Cl-Halloysite Complex

X-ray diffraction patterns of halloysite and NH_4Cl-treated halloysite (400 m.mols. NH_4Cl per 100 gms. air dried clay) are shown in Fig. 1. The (001) and (003) reflections of halloysite shift from 10.1 and 3.36 Å to 10.5 and 3.49 Å, respectively. These reflections of the NH_4Cl-halloy-

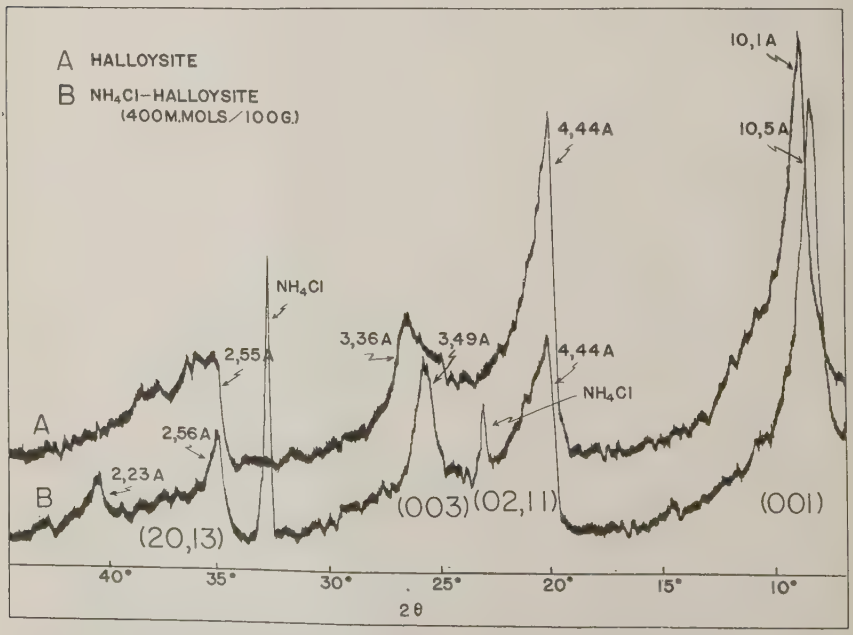

Fig. 1. X-ray diffraction patterns of halloysite and NH_4Cl-treated halloysite.

site complex are estimated to be about 1.3 to 1.5 times as strong as those of halloysite, after making allowance for a dilution effect due to the presence of NH_4Cl not oriented in the treated sample. The basal reflections of the original halloysite spread slightly on the high-angle side probably due to partial dehydration, while the symmetry of these peaks increases remarkably as the result of the complex formation. It might be interpreted in terms of penetration of NH_4Cl into the interlayer spaces partially dehydrated. Otherwise, there would be a shifting of the 10.5 Å (001) reflection towards 7-Å, indicating a random interstratification of 10.5- and 7-Å layers.

While (*hk*) reflections show no essential change in spacings for their low-angle termination upon penetration of NH_4Cl, considerable variations are found in their relative intensities and peak shapes (Fig. 1). The height of the low-angle termination of the (02, 11) band shows remarkable reduction, even taking the dilution effect into consideration. Further, two rather symmetrical peaks appear in the (20, 13) band at 2.56 Å. and 2.22 Å., while the (24, 31, 15) and (33, 06) bands are hardly affected. The reaction causes no alteration in the cell dimension a_0 and b_0 of halloysite, but clearly does produce a definite change in its structure factor, implying that the interlayer NH_4Cl probably assumes a regular configuration. In further studies, it might be possible to deduce the configuration of the salt molecules oriented between the silicate layers from such variations in the (*hk*) bands together with those in the (00*l*) reflections. Similar variations in the *x*-ray pattern were not observed for the NH_4Cl-treated metahalloysite.

Estimation of the Amount of NH_4Cl Oriented on Halloysite

The salt oriented two-dimensionally on halloysite no longer contributes to the *x*-ray diffraction as the salt (6). If diffraction intensities of NH_4Cl are measured on the NH_4Cl-treated samples, it is possible to estimate the amount of NH_4Cl not oriented on halloysite or metahalloysite (free NH_4Cl), and hence find the amount oriented by subtraction. Estimation of the free NH_4Cl was made according to the procedure of Alexander and Klug (4) using quartz as an internal standard. The diffraction intensities were measured from the peak height on automatic recording charts after calibration of the recorder response.

The observed intensity ratio of the 2.72 Å NH_4Cl and the 1.54 Å quartz lines (I_1/I_s) is plotted against the rate of NH_4Cl addition in Fig. 2. The weight fraction of the free NH_4Cl was calculated by multiplying the intensity ratio I_1/I_s by an empirical factor 0.0229 (weight fraction of quartz: 0.25), and then the amount of NH_4Cl oriented (Fig. 3) was calculated from this, taking the water content of the samples (Fig. 6) into consideration.

The 10.5 Å spacing of the NH_4Cl-halloysite complex fully develops with salt addition corresponding to 300 m. mols per 100 g. of air-dried clay. The orientation maximum of NH_4Cl is estimated at 325 m.mols per 100 g. of air-dried clay on the basis of the data in Fig. 3. Taking the unit cell of halloysite as $Al_4Si_4O_{10}(OH)_8 \cdot 4\ H_2O$, this corresponds to 1.93 molecules of NH_4Cl per unit cell of halloysite, suggesting that two molecules of NH_4Cl orient per unit cell either on the internal or on the external surface. The value accords well with that expected from the reaction

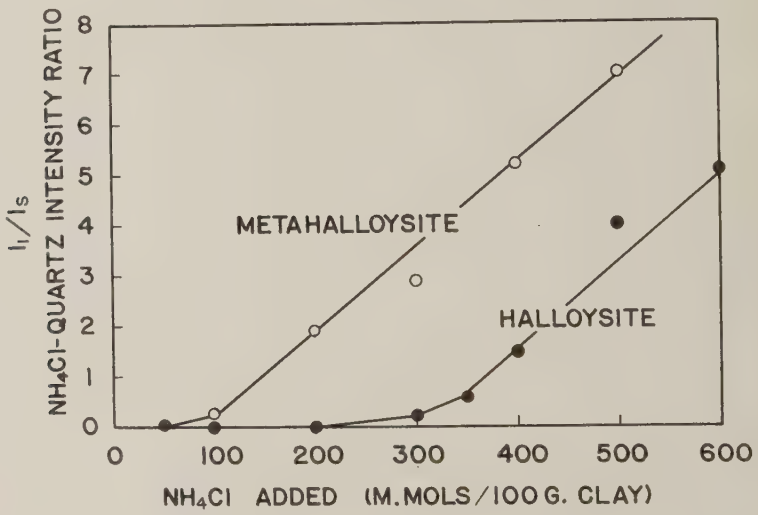

FIG. 2. NH_4Cl-quartz diffraction intensity ratio for NH_4Cl-treated halloysite and metahalloysite.

mechanism proposed at the beginning of this paper, that is, the geometrical fitting of the cation into the cavity of the oxygen hexagon allows the reaction. In view of the geometrical fitting, it seems fair to assume that NH_4^+ probably orients into the cavity and Cl^- lies on the oxygen hexagon forming a monomolecular salt layer, though the relation between the changes in the peak shape (Fig. 1) and the arrangement of the interlayer NH_4^+ and Cl^- is as yet not clear.

It may seem curious that NH_4Cl also orients on the external surface, but, if the same reaction mechanism is assumed, a monolayer of NH_4Cl should be formed on the exposed SiO-sheet. Actually the orientation maximum of NH_4Cl is estimated at 140 m.mols per 100 g. of air-dried clay in the case of metahalloysite (Fig. 3). It may be allocated to the NH_4Cl oriented on the external surface of halloysite, and the difference between halloysite and metahalloysite (185 m.mols), to that oriented between the

silicate layers of halloysite. This assumes that the external surface of halloysite is not affected by heating at 300° C., and the same heat treatment completely precludes the entry of NH_4Cl into the interlayer spaces. The plausibility of the assumption will be discussed later.

Thermal Transformations of NH_4Cl Oriented on Halloysite

DTA curves of halloysite and metahalloysite treated with 100 and 400 m.mols of NH_4Cl are reproduced in Fig. 4 with those of NH_4Cl

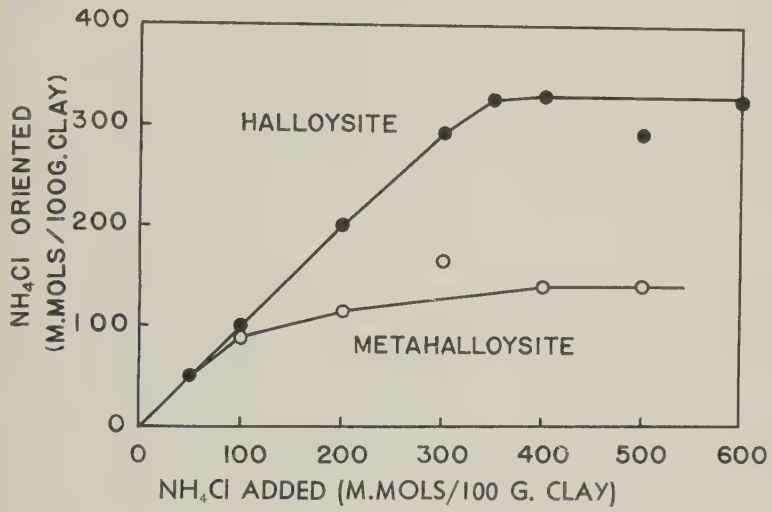

FIG. 3. Estimation of NH_4Cl oriented on halloysite and metahalloysite on the basis of the x-ray data.

diluted with α-alumina for comparison. The effect of orientation appears at first on the endothermic peak due to the transformation of NH_4Cl from α to β at 185° C. Although the appearance of the peak is considerably affected by mere physical grinding of the NH_4Cl crystals, it appears safe to conclude that the α-β transformation can not occur in the oriented NH_4Cl as is expected in view of the orientation-induced-polymorphism.

Although the peak temperature of the thermal decomposition peak of NH_4Cl varies with the amount of NH_4Cl involved in the samples (Fig. 5), it clearly shifts to the higher temperature side in the case of the NH_4Cl-treated halloysite (Fig. 4). When more than 300 m.mols of NH_4Cl is added, another peak, probably due to the presence of the free NH_4Cl, appears on the lower temperature side, and two apexes are clearly found on the shifted peak, although the reason for this is not understood at present.

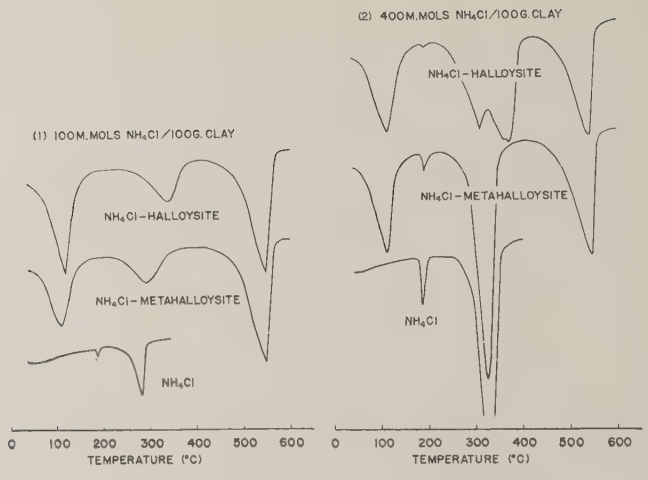

FIG. 4. DTA curves of NH_4Cl-treated halloysite and metahalloysite.

The shift of the peak temperature is characteristic of the interlayer NH_4Cl, whereas the peak shape is affected, even in the case of metahalloysite (Fig. 4), where the peak is broadened and increases in symmetry in comparison with the NH_4Cl alone. This tendency, however, becomes obscured with the increase in the rate of NH_4Cl addition, as is shown in comparison between the treatments with 400 and 100 m.mols of NH_4Cl. In the NH_4Cl-treated halloysite, more asymmetrical peaks are shown, and even if there is a composite effect of the interlayer and external NH_4Cl, the decrease in the degree of symmetry seems still to remain as a characteristic of the interlayer NH_4Cl.

Since treating halloysite with NH_4Cl hardly affects the endothermic peak due to the dehydroxylation of halloysite (Fig. 4), possibilities that NH_4Cl or its thermal decomposition products react with halloysite and bring about alterations of the DTA curve, may be excluded. Also, it is unlikely that the reaction scheme in the thermal decomposition changes due to the orientation. Thus, observed variations of the DTA curve may be treated as variations in the rate of the thermal decomposition vs. temperature behavior, since all empirical factors that may possibly contribute to alterations of the DTA curve are maintained fixed in this case.

In general, the reaction rate for this type of solid decomposition can be described by an equation

$$\frac{dx}{dt} = A(1-x)^n e^{-E/RT}$$

where dx/dt is the reaction rate, A is the frequency factor, x is the frac-

tion reacted, n is the empirical order of the reaction, and E is the activation energy. The shift of the reaction to the higher temperature side on the DTA curve as shown with the interlayer NH_4Cl means the decrease in the reaction rate at a given temperature. It may result either from the decrease in the frequency factor A or from the increase in the activation energy E. The former would be expected from a steric hindrance that is conceivably probable as the site of the reaction is confined to the interlayer spaces, and the latter, from a stabilizing effect, as a new bond is formed between halloysite and NH_4Cl.

Stone (5) explained the shape of an endothermic peak on a DTA curve by that of the distribution curve of the energy of a bond concerned in the reaction. Kissinger (3) demonstrated the effect of varying order of the reaction on the degree of symmetry of a peak. Although these explanations can not directly be applied to the present variations in the peak shape, observations are of interest in showing that the shape of the DTA curve is clearly affected by the state of the distribution of NH_4Cl.

Estimation of the Orientation Maximum of NH_4Cl on Halloysite (DTA)

The orientation maximum of NH_4Cl on halloysite was also estimated by DTA. The sum of the interlayer and external orientation was determined by assuming that the endothermic peak on the lower temperature

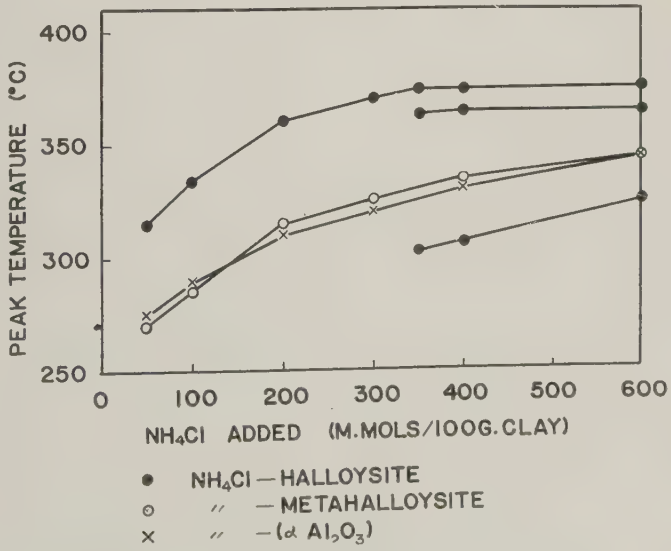

FIG. 5. Effect of orientation on the peak temperature of the thermal decomposition of NH_4Cl.

side (Fig. 4 & 5) appeared only after the sites for orientation were saturated by NH_4Cl. Although this assumption is rather arbitrary, because NH_4Cl oriented on the external surface also contributes to this peak at least potentially, the minimum rate of the NH_4Cl addition necessary to cause this, 330 ± 10 m.mols per 100 g. of air-dried clay, shows a good agreement with the orientation maximum 325 m.mols obtained on the basis of the *x*-ray data.

Interlayer orientation of NH_4Cl was determined as follows: as is already described, a peak appears on the lower temperature side when more than 330 m.mols of NH_4Cl is added per 100 g. of air-dried clay (Fig. 4 & 5). If it is allowed to allocate this peak to the NH_4Cl oriented on the external surface and to the free NH_4Cl, its peak temperature would give a measure of the amount of NH_4Cl not oriented between the silicate layers, because there is a relation between the NH_4Cl content of the samples and the peak temperature as shown in Fig. 5. Thus, the interlayer orientation maximum of NH_4Cl was estimated at 240 50 m.mols per 100 g. of air-dried clay, which is considerably higher than the value 185 m.mols estimated on the *x*-ray data. The reason for this difference will be discussed later in comparison with the third estimate for this value.

Wet and Dry Preparation of the NH_4Cl-Halloysite Complex

It was previously shown (6) that merely grinding hydrated halloysite with NH_4Cl crystals in an agate mortar for 10 to 15 minutes (dry preparation) produces the same 10.5 Å. of basal spacing. DTA curves of thus prepared samples (100 and 400 m.mols NH_4Cl per 100 g. of air-dried clay) are entirely identical to those of wet preparations shown in Fig. 4, indicating that both preparations are the same also in the quantitative aspect of the formation of the NH_4Cl-halloysite complex. It is of interest in dry preparation that NH_4Cl disperses very rapidly from visible crystals to the monomolecular state in the absence of free water molecules, although a stickiness develops on grinding, probably due to the replacement of the interlayer water. Since the similar reaction does not occur with metahalloysite and probably not with kaolinite, dry preparation can be utilized for differentiation of halloysite (hydrated or partially hydrated) from these 1:1 minerals on DTA curves on account of its rapidity and simplicity.

Replacement of the Interlayer Water

Effects of the NH_4Cl-treatment on the water content of halloysite and metahalloysite are shown in Fig. 6. Determination of the water content

was carried out on the samples equilibrated at a relative humidity of 65 per cent, that was selected on the basis of the fact that the water content of metahalloysite and halloysite showed nearly constant values in the range of R.H. 60 to 80 per cent, avoiding possible dehydration or condensation.

The water content of halloysite at first decreases rapidly and then gradually with the increase of the rate of NH_4Cl addition. The first reduction of the water content indicates that approximately two mole-

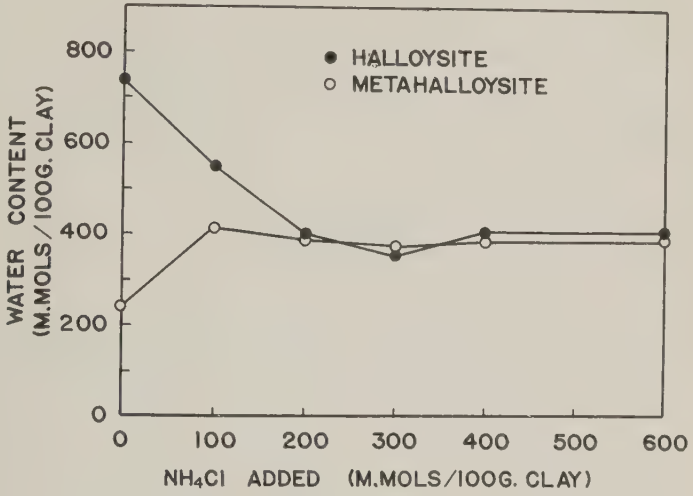

FIG. 6. Water content of NH_4Cl-treated halloysite and metahalloysite.

cules of the interlayer water are replaced by one molecule of NH_4Cl. *X*-ray analysis and DTA have shown that two molecules of NH_4Cl orient per unit cell of halloysite. Hence the 2/1 ratio implies that four molecules of water orient per unit cell of halloysite in accordance with Hendricks and Jefferson's "hexagonal net theory" (2). The following slower reduction suggests that NH_4Cl orients also on the external surface as well as on the interlayer surface with the increasing rate of NH_4Cl addition. Even on the interlayer surface, the replacement ratio may differ on its periphery from its central portion, but as a whole, it is very nearly one to one. For metahalloysite, the NH_4Cl-treatment results in increase in the water content apparently at the rate of 1 to 1 (Fig. 6), suggesting that NH_4Cl orients together with the extra water on the external surface.

Providing the ratios of 2/1 and 1/1 are assumed in the replacement and

adsorption of the water on the interlayer and external surfaces, a calculation affords an approximate estimate for the interlayer orientation maximum of NH_4Cl (x).

$$2x-(330-x)=340$$

Orientation maximum on halloysite (x-ray & DTA) — Total reduction of water content of halloysite (Fig. 6)

$x=220$ m.mols/100 g. of air-dry clay

This is comparable to the 240 m.mols estimated by DTA, but x-ray data have shown a little lower value (185 m.mols) on the assumption that the area of the external surface is the same for halloysite and metahalloysite. Therefore, the simple subtraction of the orientation value for metahalloysite from that for halloysite seems likely to induce an overestimation for the area of the external surface. When halloysite is heated at 300° C., a part of the interlayer surface may be exposed as a new external surface owing to the peeling off of the curved sheet of halloysite, and/or the interlayer spaces may not completely close to the penetration of NH_4Cl.*

The replacement of the interlayer water by NH_4Cl is indicative of the greater strength in bonding between NH_4Cl and halloysite than that between water and halloysite. Upon drying halloysite from the solutions, the molar ratio of NH_4Cl to water in the bulk solution is not likely to exceed that in the saturated solution of NH_4Cl, namely, 1/7.75 at 30° C. Although the interlayer NH_4Cl is leached out again by washing with water (6), if only a mass action effect is assumed, it seems difficult to account for the observed replacement of the interlayer water.

Conclusion

It is concluded that two molecules of NH_4Cl per unit cell, in the form of a monomolecular layer, orient on the SiO-sheet of the silicate layer, probably mainly owing to the geometrical fitting of NH_4^+ in the cavity of the oxygen hexagon in the SiO-sheet. The bonding forces between

* A recent study (**) has shown that grinding metahalloysite with NH_4Cl for 1 hour causes a shift of the 7.3 Å reflection to 10.3–10.4 Å, indicating penetration of NH_4Cl between its silicate layers. Sample preparation in this study involves manual grinding of NH_4Cl-treated halloysite and metahalloysite for 10–15 minutes to obtain powder samples fine enough for quantitative x-ray analysis. Reexamination of the x-ray pattern of the NH_4Cl-treated metahalloysite has revealed a slight shift of the 7.3 Å reflection towards 10 Å. Partial penetration of NH_4Cl into metahalloysite may largely account for the overestimation for the external surface area. The true orientation maximum on the external surface has been estimated at 40 m.mols per 100 g. of air-dry clay.

** "Use of salt complex for differentiation of halloysite from kaolinite," Read at the Second Annual Meeting of the Clay Mineral Group of Japan (Tokyo), December, 1958.

NH_4Cl and halloysite at the interlayer spaces are greater than those between the interlayer water and halloysite.

Oriented NH_4Cl no longer contributes to the x-ray diffraction as the normal salt, and shows some distinctive structural and thermochemical features depending on the orientation site. The preparation of the NH_4Cl-treated-clay samples, by either drying from an NH_4Cl solution or dry grinding with NH_4Cl crystals could be utilized for differentiation of halloysite (hydrated or partially dehydrated) from metahalloysite and kaolinite.

Acknowledgments

The author wishes to express his most sincere thanks to Dr. S. Aomine of Kyushu University for helpful encouragement in this work. He also wishes to thank Dr. W. Sakai and Dr. T. Seiyama of the Department of Technology at Kyushu University for permission to use the x-ray diffractometer. The research was supported in part by a grant from the Science Research Fund of the Japanese Ministry of Education.

References

1. Aomine, S. and Higashi, T. (1955), Clay Minerals of decomposed andesitic agglomeratic lava at Yoake. *Mineral. Jour.* (Japan), **1,** 278–289.
2. Hendricks, S. B. and Jefferson, M. E. (1938), Structures of kaolin and talc-pyrophyllite hydrates and their bearing on water sorption of the clays. *Am. Mineral.*, **23,** 865–875.
3. Kissinger, H. E. (1957), Reaction kinetics in differential thermal analysis. *Anal. Chem.*, **29,** 1702–1706.
4. Klug, H. P. and Alexander, L. E. (1954), *X-ray diffraction procedure for polycrystalline and amorphous materials.* John Wiley & Sons, Inc., New York.
5. Stone, R. L. (1953), Preliminary study of the effects of water vapor pressure on thermograms of kaolinitic soils. *Proc. Second Nat. Conf. on Clays and Clay Minerals*, 315–324.
6. Wada, K. (1959), Oriented penetration of ionic compounds between the silicate layers of halloysite. *Am. Mineral.*, **44,** 153–165.
7. Wada, K. (1959), Reaction of phosphate with allophane and halloysite. *Soil Science*, **87,** 325–330.

UMOHOITE FROM CAMERON, ARIZONA

PEGGY-KAY HAMILTON* AND PAUL F. KERR, *Columbia University, New York N. Y.*

ABSTRACT

Studies indicate that the hydrous uranium-molybdate, umohoite, is a more widely distributed mineral than has been previously known. The original crystalline material was found at Marysvale, Utah. Similar crystalline material has since been reported by Coleman and Appleman from the Gas Hills district, Wyoming. Recently, a new occurrence in a fine-grained form has been discovered at Cameron, Arizona. A similar fine aggregate has been recognized in recently collected material from Marysvale. The identification of fine-grained umohoite has also been confirmed from an undisclosed locality in the U.S.S.R.

The change in lattice dimensions under *x*-ray bombardment or variable conditions of humidity and temperature has constituted a problem in the *x*-ray diffraction study of this mineral. In order to overcome this difficulty, the adsorption of the large ethylene glycol molecule into the water positions has been utilized to stabilize the umohoite structure. This may be accomplished without destruction of the structure.

Three coexistent structural modifications are recognized in umohoite. These are designated Modes 1, 2 and 3. The modes range in intensity of development as shown by *x*-ray diffraction. In fine-grained umohoite (Cameron, fine Marysvale and U.S.S.R.) Modes 2 and 3 are better developed than Mode 1. In coarser Marysvale umohoite Mode 1 is more prominent than Modes 2 and 3. The coexistence in the same mineral of three systematic sequences of lattice variation (or modes), each exhibiting a range in crystallinity in response to physical conditions, is an unusual mineralogical feature.

INTRODUCTION

Umohoite was first discovered (Brophy and Kerr, 1953) in the Freedom No. 2 mine at Marysvale, Utah, where it occurs in distinct bluish black plate-like crystals. Subsequently, Coleman and Appleman (1957) reported a second occurrence of crystalline umohoite aggregates at the Lucky Mc mine in the Gas Hills, Wyoming.

During the investigation of uranium mineralization and associated alteration at Cameron, Arizona, radioactive blue-black sooty masses and carbonaceous trash replacements at the Alyce Tolino mine were obtained through the courtesy of Mr. Page Blakemore, Jr., geologist for the Cameron Uranium Company. After a few days' exposure to the atmosphere, a freshly broken surface of this material develops a bright blue water soluble molybdenum efflorescence which is mainly ilsemannite. Such areas have been found to contain umohoite, although the aggregate differs in megascopic appearance from previously described crystals.

The three U.S. localities, as well as an occurrence in the U.S.S.R., indicate that this unusual hydrous uranium-molybdate may be more widespread than was considered likely at the time of the original dis-

* Deceased. See note on page 1260.

covery. Knowledge of the existence of several other localities on the Colorado Plateau where secondary molybdenum is associated with uranium suggests the possibility that further study may disclose an even more widespread distribution of umohoite.

In the examination of the fine-grained molybdenum-uranium aggregate from Cameron, it was first found necessary to re-examine reference umohoite from Marysvale. A major difficulty recognized since the original investigation of umohoite by *x*-ray diffraction has been its tendency to produce shifting reflections as the mineral loses or gains water during *x*-ray bombardment. Kamhi (1959) in a restudy of individual Marysvale crystals carried on in this laboratory has shown that the lattice dimension normal to the flat flakes varies directly with ordinary variations in atmospheric humidity, and inversely with increasing temperature. In studying the Cameron material, it has been found necessary to re-examine this unusual behavior of the Marysvale umohoite. The study has also led to the investigation of umohoite shown in the U.S.S.R. exhibit at the first Geneva Conference on the Peaceful Uses of Atomic Energy (1955) and made available by Dr. A. P. Vinogradov of the Vernadsky Institute of Geochemistry and Analytical Chemistry, Moscow.

Technique

In the examination of umohoite, it has been found desirable to stabilize the structure both during *x*-ray bombardment and under varying conditions of temperature and humidity. The analogy between the layered structure of umohoite, as well as the range in states of hydration, with the well-known shifts in basal spacing observed for the clay mineral montmorillonite, suggested the use of ethylene glycol to establish lattice stability. Umohoite crystals were chopped in distilled water in the Waring Blendor, sedimented onto a glass slide and then placed in an ethylene glycol atmosphere for two days in a closed container at room temperature. The slide was then transferred directly to the Norelco *x*-ray diffractometer (Fig. 1A).

No fundamental change in umohoite appears to accompany the adsorption of ethylene glycol. No shift in reflections as shown in Table 1 and Figure 1B appeared, nor were new lines produced. The only difference noted in the unglycolated and glycolated spacings lies in the intensity of reflections. After *x*-ray bombardment a gradual return takes place to the unglycolated intensities (Fig. 1C) which would not be the condition if a change in structure had occurred. After glycolation of the umohoite, changes under *x*-ray bombardment and variations with temperature and humidity disappear. The presence of a large organic molecule in the water positions seems to support the surrounding layers

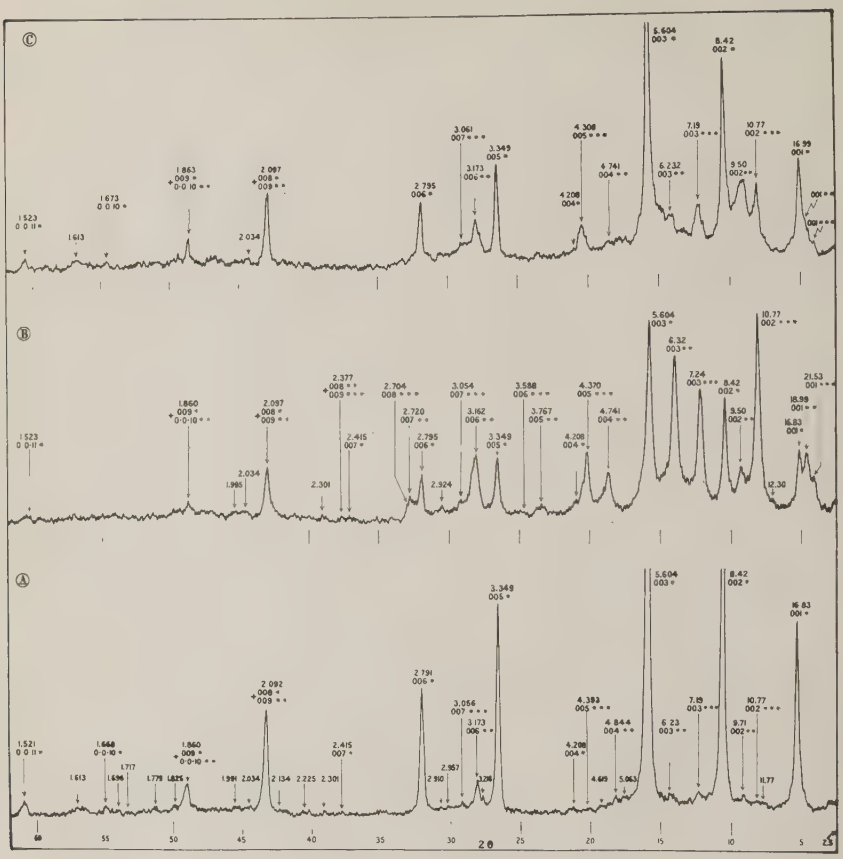

FIG. 1. *X*-ray diffractometer patterns of oriented, coarsely crystalline umohoite, Marysvale, Utah.

(A) Unglycolated material shows more intense Mode 1 reflections (=*) in contrast to Modes 2 and 3 (=** and =***). General *hkl* reflections are shown without asterisks.

(*B*) Glycolated material shows the stabilized structure. Modes 2 and 3 are increased in intensity while Mode 1 is decreased. Reflections 21.53 Å and 18.99 Å represent increased intensities which merely cause a slight asymmetry in pattern A.

(C) The same sample following *x*-ray bombardment. The pattern returns toward type A. Mode 1 shows stronger reflections than Modes 2 and 3. Asymmetry returns to peak 16.99 Å which corresponds to 16.83 Å of A.

and inhibit their shift or collapse with dehydration. It seems possible that the glycolated condition is in effect equivalent to a maximum state of hydration.

Study of the glycolated crystalline umohoite *x*-ray diffraction pattern (Fig. 1) shows that there are three distinct first order (001) reflections in

which values are respectively: (1) 16.83 Å, (2) 18.99 Å and (3) 21.53 Å. Each stands at the head of a successive sequence of about 12 higher order reflections all present in the same pattern. These groups are designated Modes 1, 2 and 3. Table 2 compares the calculated interplanar spacings with observed diffractometer values for each of the three modes. The intensities of each mode (Table 2) are determined independently and are based on the intensity of the strongest reflection for each mode.

It is noted that except for the weak 4.2, 2.4 and 1.668 Å spacings in unglycolated crystalline umohoite, the Mode 1 (Fig. 1) reflections before glycolation are stronger than those given by Modes 2 and 3. The adsorption of the organic molecule appears systematically to strengthen the intensity of Mode 2 and 3 reflections (Fig. 1), and to decrease that of

TABLE 1. *X*-RAY DIFFRACTION POWDER DATA FOR COARSELY CRYSTALLINE UMOHOITE, MARYSVALE, UTAH

Cu radiation, Ni filter $\lambda = 1.5418$ Å

(no glycol)		(glycolated)		(no glycol)		(glycolated)	
*d*Å	I	*d*Å	I	*d*Å	I	*d*Å	I
		21.53	15	2.957	2		
		18.99	29	2.910	2	2.924	5
16.83	68	16.83	31	2.791	45	2.795	22
11.77	2	12.30	5			2.720	13
10.77	2	10.77***	100			2.704	9
9.71	4	9.50	13	2.415	2	2.415	3
8.42	100	8.42	53			2.377	3
7.19	5	7.24	57	2.301	2	2.301	2
6.23	4	6.32**	66	2.225	2		
5.604*	100	5.604	83	2.134	3		
5.063	2			2.092	37	2.097	26
4.844	3	4.741	19	2.034	2	2.034	4
4.619	3			1.991	2	1.995	4
4.393	2	4.370	26	1.860	10	1.860	7
4.208	3	4.208	4	1.825	3		
		3.767	5	1.779	3		
		3.588	3	1.717	2		
3.349	74	3.349	31	1.696	2		
3.218	3			1.668	3		
3.173	10	3.162	29	1.613	3		
3.056	3	3.054	5	1.521	6	1.523	4

* Strong Mode 1.
** Strong Mode 2.
*** Strong Mode 3.

TABLE 2. *X*-RAY DIFFRACTION POWDER DATA FOR MODES RECOGNIZED IN GLYCOLATED COARSELY CRYSTALLINE UMOHOITE, MARYSVALE, UTAH

Cu radiation, Ni filter $\lambda = 1.5418$ Å

	Mode 3		Mode 2		Mode 1			Mode 3		Mode 2		Mode 1	
hkl	*d*Å obs. (calc.)	I	*d*Å obs. (calc.)	I	*d*Å obs. (calc.)	I	*hkl*	*d*Å obs. (calc.)	I	*d*Å obs. (calc.)	I	*d*Å obs. (calc.)	I
001	21.53 (21.57)	18					007	3.054 (3.08)	9				
			18.99 (18.92)	44						2.720 (2.70)	20		
					16.83 (16.80)	37						2.415 (2.40)	4
002	10.77 (10.79)	100					008	2.704 (2.70)	9				
			9.50 (9.46)	20						2.377 (2.377)	4		
					8.42 (8.40)	63						2.097 (2.10)	33
003	7.24 (7.19)	57					009	2.377 (2.40)	4				
			6.32 (6.31)	100						2.097 (2.10)	40		
					5.604 (5.60)	100						1.860 (1.37)	9
004	— (5.39)						0·0·10	— (2.16)					
			4.471 (4.73)	29						1.860 (1.89)	11		
					4.208 (4.20)	5						— (1.68)	
005	4.37 (4.31)	26					0·0·11	— (1.96)					
			3.767 (3.78)	9						— (1.72)			
					3.349 (3.36)	37						1.523 (1.53)	5
006	3.588 (3.60)	3					0·0·12	— (1.80)					
			3.162 (3.15)	42						— (1.58)			
					2.795 (2.80)	26						— (1.40)	

Mode 1. The latter, however, remains the strongest. After bombardment of glycolated Marysvale umohoite (Fig. 1) Mode 1 becomes more intense and Modes 2 and 3 decrease in intensity. Although the 18.9 Å and 21.5 Å glycolated spacings (Fig. 1) of Modes 2 and 3 (Table 1) appear to be new, a definite asymmetry (Fig. 1) toward the lower angles is present in both the unglycolated and glycolated bombarded 16.8 Å reflection. Since the (002) reflections at 10.7 and 9.5 Å are much more intense, it seems likely that before glycolation these weaker (001) reflections are only strong enough to produce asymmetry. Likewise, the 3.7 Å and 3.5 Å Mode 2 and 3 reflections are weak in the glycolated material and do not appear at all in the unglycolated specimen. The 1.860 Å line is believed to be principally a Mode 1 (009) reflection, although this is also the spacing for the Mode 2 (0·0·10) 1.90 Å reflection. After glycolation this 1.860 Å peak decreases in intensity; after bombardment it becomes stronger. This behavior is characteristic of Mode 1 reflections; so the peak is assigned to this mode. Likewise, the 2.092 Å reflection decreases in intensity with glycolation, and increases after bombardment; so it is believed to be mainly Mode 1 (008), although it overlaps the (009) Mode 2 spacing.

Fine-Grained Cameron Umohoite

Microscopic Observation

Thin-section study shows that the Cameron material is blue-black, opaque and contains no pleochroic blue-green umohoite crystals as reported either by Brophy and Kerr (1953) or Coleman and Appleman (1957). Scattered grains of angular quartz are associated with prominent bands of carbonate and pyrite. A few fragments of an unidentified secondary uranium mineral occur with the umohoite. Polished surfaces of this black fine-grained umohoite are isotropic. The apparent lack of double refraction is attributed to the extremely finely divided state. Associated with the umohoite are small cubes of cobalt-rich pyrite which enclose marcasite.

X-ray Diffraction

The identification of fine-grained Cameron umohoite depends largely on *x*-ray diffraction data. The material was purified by stirring in cool, distilled water in order to remove ilsemannite and any other water soluble impurities. After the water soluble fraction was decanted, more cool, distilled water was added to the residue, after which it was stirred briefly and allowed to settle for a few minutes. Umohoite (Sp. Gr. 4.55 4.93) settles from suspension after pyrite (Sp. Gr. 4.95–5.10) and before quartz (Sp. Gr. 2.653–2.660). However, no fine-grained umohoite fraction

was separated which was entirely free from quartz. Umohoite was next sedimented onto a glass slide so that a preferred orientation developed (Brophy and Kerr, 1953). The slide was mounted directly in a Norelco x-ray diffractometer.

X-ray diffraction investigation shows that the fine-grained Cameron umohoite develops a preferred orientation and responds to ethylene glycol as do the coarse Marysvale umohoite crystals. Unoriented samples of both forms of umohoite give weak, diffuse patterns which improve moderately after orientation. Thus the Cameron particles which are estimated to be a few microns in diameter develop a preferred orientation which is similar to that of the coarse Marysvale crystals which are tenths of a millimeter in diameter. The adsorption of ethylene glycol stabilizes the Cameron umohoite lattice in the same way that it does the Marysvale. Therefore the x-ray diffraction pattern shows a consistent increase of Mode 2 and 3 intensities (Fig. 2). After bombardment by x-rays, the

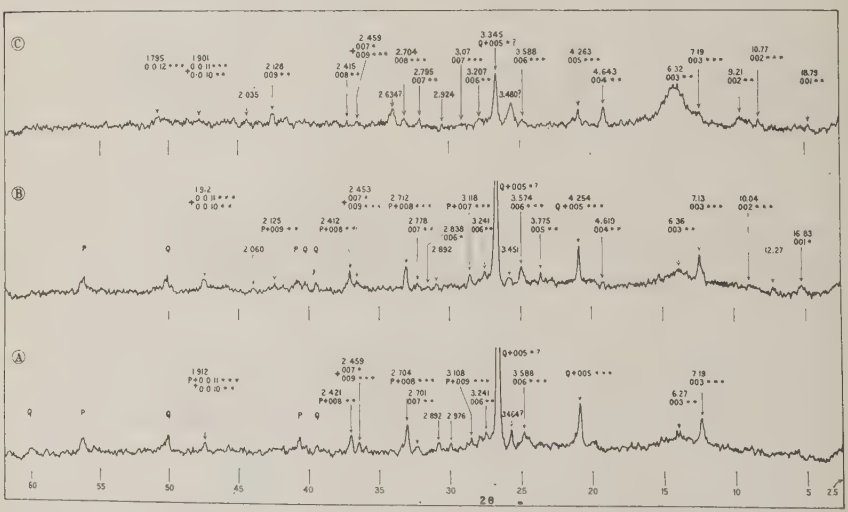

FIG. 2. X-ray diffractometer patterns of oriented fine-grained umohoite, Cameron, Arizona.

(A) Unglycolated material shows characteristic Mode 2 and Mode 3 reflections. However, these reflections are weaker than those of the coarsely crystalline umohoite (Fig. 1). Mode 1 reflections are weak or missing. Quartz (Q) and pyrite (P) mask several umohoite 00*l* reflections.

(B) Ethylene glycol adsorption strengthens coexistent Modes 2 and 3. The strong 7.13 Å reflection shows that in this specimen Mode 3 is more prominent than Mode 2.

(C) In this glycolated specimen the intensity of the 6.32 Å reflection shows that Mode 2 is stronger than Mode 3.

intensity of these modes decreases to resemble that of the unglycolated specimen which also is similar to the behavior of the coarse crystals. Although the Cameron diffraction patterns (Fig. 2) do not approach the definition and intensity of those of the Marysvale crystals (Fig. 1), they are similar.

The *x*-ray diffraction pattern of the Cameron umohoite (Table 3) is characterized by prominent Mode 2 and 3 reflections and weak or missing Mode 1 reflections. This differs from crystalline Marysvale umohoite which has strong Mode 1 reflections, and relatively weaker Mode 2 and 3 reflections. In one Cameron specimen (Fig. 2C) Mode 2 is stronger than coexistent Mode 3 (Table 3); whereas in another, Mode 3 is dominant (Fig. 2B). In the stronger Mode 2 pattern it is interesting to note that the 18.79 Å (001) Mode 2 reflection appears only after glycolation as in the diffraction pattern of the coarsely crystalline Marysvale umohoite. The intensities of the Cameron Mode 2 and 3 reflections also have the same relation to each other as those in the Marysvale crystals. However, an unexplained exception occurs in the Cameron strong Mode 3 pattern (Table 3, Fig. 2B) since the 7.1 Å (003) reflection is considerably stronger than the 10 Å (002) reflection, whereas in the Marysvale crystals (Table 1, Fig. 1) the 10 Å spacing is stronger.

In the Cameron material (Fig. 2B) in which Mode 3 is prominent, Mode 1 is fairly well developed. The following reflections from this mode appear: (001) 16.83, (006) 2.838 and (007) 2.453 Å. Quartz may mask the strong umohoite Mode 1 3.3 Å line and pyrite the umohoite Mode 1 2. 7Å reflection. However, the strongest Mode 1 reflection in the coarsely crystalline umohoite at 5.6 Å is missing in the Cameron specimens. At present there is no direct evidence for the degree to which Modes 1, 2 and 3 may be developed. However, further investigation may reveal the relationship of the oxidation state, hydration and uranium-molybdenum ratio to the intensities of modes in umohoite.

X-ray Spectrograph

X-ray spectrographic analyses confirm the presence of uranium and molybdenum. These elements are accompanied in decreasing order by: silica, sulfur, iron, cobalt, nickel, arsenic and thallium. The presence of thallium as an associated impurity is interesting, but the site of its occurrence is unknown. It is not localized to any extent in the accompanying pyrite. The 3.4 Å and 2.6 Å (Fig. 2) unidentified *x*-ray diffraction reflections in the Cameron specimens may be caused by a mineral which contains some of these accompanying elements. It is worthy of note that no evidence for the presence of molybdenite or molybdite was found during the investigation.

TABLE 3. X-RAY DIFFRACTION POWDER DATA FOR FINE-GRAINED GLYCOLATED UMOHOITE

hkl	Mode	Cameron, Arizona				Marysvale, Utah		U.S.S.R.	
		*d*Å	I	*d*Å	I	*d*Å	I	*d*Å	I
001	(3)							19.62	100
	(2)			18.79	20	18.99**	86	18.79	100
	(1)	16.83	50			16.67*	100	17.01	86
002	(3)	10.04	40	10.77	33	10.77	14	9.93	43
	(2)			9.21	20				
	(1)							8.34	57
003	(3)	7.13***	100	7.19	33	7.13***	43	7.36	43
	(2)	6.36	40	6.32**	100	6.02	71	6.34**	57
	(1)					5.604	29	5.607*	43
004	(3)								
	(2)	4.619	30	4.643	47	4.692	43		
	(1)								
005	(3)	4.254+Q	100	4.263+Q	40	4.263+Q	100	4.350***	57
	(2)	3.775	50			3.675	43	3.767	43
	(1)	3.342+Q	100	3.345+Q	100	3.349+Q	100	3.349+Q	100
006	(3)	3.574	60	3.588	20	3.588	14	3.631	57
	(2)	3.241	40	3.207	20	3.184	14	3.184	100
	(1)	2.838	20						
007	(3)	3.118+P	50	3.07	13	3.104	29	3.051	43
	(2)	2.778	30	2.795	27			2.769	43
	(1)	2.453	30	2.459	20				
008	(3)	2.712+P	80	2.704	20	2.712	14		
	(2)	2.412+P	80	2.415	13	2.453+Q	100	2.453+Q	100
	(1)								
009	(3)	2.453	30	2.459	20				
	(2)	2.125	40	2.128	27	2.123+Q	86	2.127+Q	100
	(1)								
0·0·10	(3)								
	(2)	1.912+P	40	1.901	13			1.862	29
	(1)								
0·0·11	(3)	1.912+P	40	1.901	13			1.862	29
	(2)								
	(1)								
0·0·12	(3)			1.795	20			1.795	43
	(2)								
	(1)								

P pyrite.
Q quartz.
* Strong Mode 1.
** Strong Mode 2.
*** Strong Mode 3.

Additional Fine-Grained Umohoite Localities

Marysvale, Utah

Recently, fine-grained blue-black umohoite masses have been found at Marysvale, Utah. The occurrence is significant as it establishes the presence of this form of umohoite at the type locality. The nature of its geologic relation to coarsely crystalline umohoite requires further study.

The intensity and definition of the *x*-ray diffraction pattern of this material are similar to that of the Cameron umohoite. An oriented, glycolated specimen (Fig. 3, Table 3) shows Mode 1, 2 and 3 reflections. Mode 2 is somewhat better developed than Mode 3. Since pyrite is not detected by *x*-ray diffraction in this fine-grained umohoite, the Mode 3 3.10 Å (007) and 2.7 Å (008) umohoite reflections are not obscured. This confirms the assignment of these spacings in the pyrite contaminated Cameron material (Table 3, Fig. 2) to umohoite masked by pyrite. It is interesting to note that as in the Cameron umohoite the Mode 1 16.67 Å (001) reflection is conspicuous, although several higher orders are missing.

X-ray spectrographic analyses show that uranium and molybdenum are accompanied by iron, thallium and arsenic as contamination. Although thallium and arsenic impurities are not reported by Brophy and Kerr (1953) in the coarsely crystalline Marysvale umohoite, they are associated with the fine-grained umohoite from Marysvale and

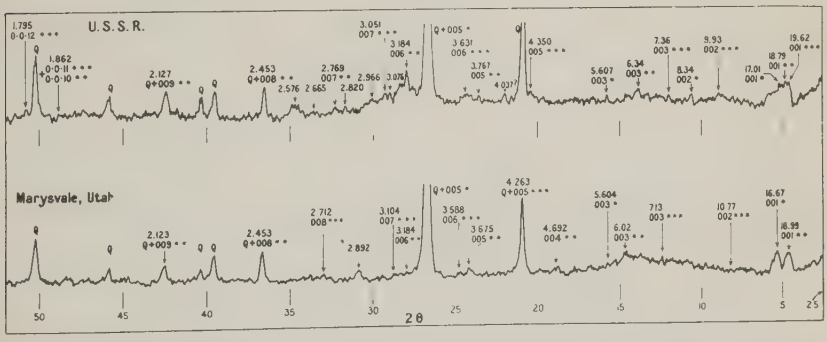

Fig. 3. *X*-ray diffractometer powder patterns of oriented and glycolated, fine-grained umohoite from Marysvale, Utah and the U.S.S.R.

Marysvale material shows the characteristic coexistent modes which are identified in the coarse crystals (Fig. 1). Mode 2 is somewhat better developed than Mode 3. Note that as in one Cameron specimen (Fig. 2B) the 16.67 Å reflection is conspicuous, although many Mode 1 higher orders are missing.

The U.S.S.R. specimen has prominent coexistent Mode 1, 2 and 3 reflections. Therefore this material more closely resembles the coarsely crystalline Marysvale umohoite (1B) than the fine-grained specimens from Cameron and Marysvale.

Cameron. The association of thallium and arsenic as impurities at both localities may have some genetic significance.

U.S.S.R.

A specimen of fine-grained umohoite from an unknown locality in the U.S.S.R. was sent to the Mineralogical Laboratory, Columbia University, by A. P. Vinogradov of the Vernadsky Institute of Geochemistry and Analytical Chemistry, Moscow. The specimen is very interesting since it comes from a distant locality and suggests that umohoite may be rather widespread. The fine-grained black umohoite matrix includes granules of quartz and unidentified vitreous dark brown material. A soft yellow mineral occurs as blebs which are scattered throughout the specimen and as a coating along one edge.

X-ray spectrographic analyses confirm the presence of uranium and molybdenum in this material. Thallium and arsenic were not detected in this fine-grained umohoite. Iron, vanadium and lead are the principal accompanying impurities.

The *x*-ray diffraction pattern (Fig. 3, Table 3) of the oriented, glycolated black matrix is similar to that of the fine-grained umohoite from Cameron and Marysvale. Vinogradov (written communication) suggested that this specimen contained more than one form of umohoite. An interesting feature of the diffraction pattern (Table 3, Fig. 3) is that it shows prominent Mode 1 reflections. Coexistent Modes 2 and 3 also are well developed so that this umohoite is the most similar of the three fine-grained umohoites to the coarsely crystalline umohoite from Marysvale. Its tendency to orient and respond to ethylene glycol also is similar. Thus after glycolation Mode 2 and 3 reflections are strengthened whereas Mode 1 reflections are weakened. This is particularly evident in the glycolated (001) reflections since Modes 2 and 3 are present, whereas before glycolation they appear only as a diffuse asymmetric reflection. In addition to quartz, reflections from an unidentified impurity are present; however, they do not interfere with the identification of umohoite.

Conclusions

Umohoite adsorbs ethylene glycol at room temperature and pressure. This stablizes the structure without a shift of interplanar spacings or the appearance of new reflections. Once stability is established, there are no lattice dimension changes with varying conditions of temperature and humidity. The presence of the large organic molecule in the water positions seems to support the surrounding layers and inhibit their shift or

collapse. It is possible that the glycolated condition is equivalent to a maximum hydration state.

The presence of three coexistent structural modifications, Modes 1, 2 and 3, in umohoite is established. *X*-ray diffraction study shows that each mode exhibits an orderly sequence of reflections, and all three groups appear in the same diffraction pattern. With the adsorption of ethylene glycol there is a systematic increase in the intensities of Modes 2 and 3, along with a decrease of Mode 1 intensities. This response to ethylene glycol is a characteristic property of umohoite which is useful in identification, and should provide assistance in future structural studies.

A fine-grained form of umohoite has been recognized. It gives a weak and somewhat diffuse *x*-ray diffraction pattern, but the same three modes are present as in the coarse crystals. Modes 2 and 3 tend to be somewhat more prominent than Mode 1 in the fine-grained form, whereas Mode 1 is stronger in the coarse crystals. The relative intensities of Modes 2 and 3 may vary, even among specimens from the same locality.

Coarse umohoite crystals from Marysvale, Utah (Brophy and Kerr, 1953) and the Gas Hills area, Wyoming (Coleman and Appleman, 1957) have been described. The occurrence at Cameron, Arizona, of fine-grained umohoite establishes a third locality in the United States for this hydrous uranium-molybdate. The identity of an interesting specimen of fine-grained umohoite from the U.S.S.R. is confirmed. Thus, umohoite is more widespread in occurrence than was known previously, and the fine-grained form may be considerably more abundant than is now known.

Acknowledgments

This investigation has been made possible through the cooperation of the U. S. Atomic Energy Commission, Division of Research and the Division of Raw Materials. The writers wish to express particular appreciation to Dr. Daniel R. Miller, Director of the Division of Research.

Umohoite specimens from Cameron, Arizona, were made available by Mr. Page P. Blakemore, Jr. of the Cameron Uranium Company. Dr. Gerald P. Brophy, Amherst College, has cooperated by supplying umohoite crystals from Marysvale, Utah. Dr. A. P. Vinogradov, Vernadsky Institute of Geochemistry, Moscow, U.S.S.R. has submitted a specimen from Russia. Among the mineralogy group at Columbia University, the authors wish to thank Dr. Otto C. Kopp and Messrs. William A. Bassett, Edgar M. Bollin and Samuel R. Kamhi for their helpful discussions and technical assistance. Mr. Arthur N. Rohl's observation of the polished surfaces is appreciated.

References

Brophy, G. P., and Kerr, P. F. (1953), Hydrous uranium molybdate in Marysvale ore: Annual Report from June 30, 1952 to April 1, 1953, U. S. Atomic Energy Commission, RME-3046, 45–51.

Coleman, R. G., and Appleman, D. E. (1957), Umohoite from the Lucky Mc mine, Wyoming: *Am. Mineral.*, **42**, 567–660.

Kamhi, S. R. (1959), An x-ray study of umohoite: *Am. Mineral.*, **44**, 920–925.

Kerr, P. F., Brophy, G. P., Dahl, H. M., Green, J., and Woolard, L. E. (1957), Marysvale, Utah, uranium area: Geol. Soc. Am. Special Paper 64, 66–69.

Manuscript received April 1, 1959.

Miss Peggy-Kay Hamilton, Research Associate in Mineralogy, Columbia University, passed away on September 19, following an operation. Miss Hamilton was a Fellow of the Mineralogical Society of America.

MANGANIAN ANDALUSITE FROM KIAWA MOUNTAIN, RIO ARRIBA COUNTY, NEW MEXICO*

E. Wm. Heinrich and A. F. Corey, *Department of Mineralogy, The University of Michigan, Ann Arbor, Michigan and 2619 Greenfield, Arcadia, California*

Abstract

Manganian, ferrian andalusite (viridine) occurs abundantly in kyanite-hematite quartzite of the Precambrian Kiawa Mountain formation at Kiawa Mountain, Rio Arriba County, New Mexico. Its extraordinary pleochroism (golden yellow to emerald green) results from the copresence of $Mn^{+3}(Mn_2O_3=4.5\%)$ and $Fe^{+3}(Fe_2O_3=3.0\%)$. The andalusite apparently formed essentially contemporaneously with the kyanite.

Introduction

In fall of 1952 the writers examined Precambrian rock exposures on the flanks of Kiawa Mountain about 8 airline miles northwest of Petaca, Rio Arriba County, New Mexico (Fig. 1), and discovered in the quartzite bands of a fine-grained bright green mineral which megascopically resembles epidote. Subsequently it was identified as the rare manganian variety of andalusite, usually referred to as viridine, which has been reported from only six other localities in the world.

The writers are indebted to R. W. Deane for separating a sample of the mineral. Professor R. M. Denning kindly checked the absorption spectrum of the mineral. Dr. M. Fleischer of the U. S. Geological Survey generously shared a specimen of viridine from Ultevis, Sweden, and also read the manuscript critically. Costs of thin and polished sections were paid for by the Department of Mineralogy, The University of Michigan. The study of the kyanite deposits of the Petaca district by Corey (1953) was supported by the New Mexico Bureau of Mines and Mineral Resources.

Mangan-andalusite was first found by De Gerr (1889) in the Vestanå district in south Sweden and was described subsequently by Bäckström (1896, 1897). Klemm (1911) found a similar mineral near Darmstadt in Hesse, Germany, and called it viridine. Wülfing (1917) decided viridine was an independent species and not a variety of andalusite. A mineral called gosseletite by Anten (1923) from Salm-Château, Belgium, was later identified as viridine by Corin (1933, 1934). Ödman (1947, 1950) found viridine relatively abundant in metasediments associated with manganese deposits in the Ultevis district, Jokkmokk, northern Sweden. Viridine that occurs at Timptonsk, Yakutia, A.S.S.R., has been

* Contribution from the Department of Mineralogy, The University of Michigan, No. 222.

FIG. 1. Index map of north-central New Mexico, showing location of Kiawa Mountain. One inch equals about 14 miles.

described by Serdyuchenko (1949) and by Shabynin (1950). An occurrence in Lume Valley in the Ruwenzori Massif, Belgian Congo, has been described briefly by Thonnart (1954).

GEOLOGY

The rock that contains the manganian andalusite is an aluminous quartzite, a variety of the rock originally called the Ortega quartzite, a Precambrian unit defined by Just (1937). Generally similar rocks extending south of Kiawa Mountain and underlying La Jarita Mesa were mapped by Just (1937) as the Petaca schist, a subordinate unit within the Ortega, consisting mainly of quartzite and muscovite-quartz schist. The area has been studied by Barker (1958), who was able to subdivide Just's units. The quartzite of Kiawa Mountain is called by Barker the upper quartzite member of the Kiawa Mountain formation, and is the youngest Precambrian metasedimentary unit in the area. Passing west-northwest through Kiawa Mountain is the axis of a major overturned syncline (Kiawa syncline). Foliation on the north side of the mountain strikes generally N. 65–80° W. with dips 70° SW. to vertical. Locally the quartzite banding is highly contorted. Small kyanite-bearing quartz veins are not uncommon on the east and northeast sides of the mountain.

Petrology

The aluminous quartzite is well banded, generally gray-green to buff rock of uniformly fine grain. Variations in composition are marked, even within hand specimens (Fig. 2). Generally quartz or kyanite-quartz bands predominate and are thickest. These may or may not contain green andalusite. Gray quartzose bands commonly contain andalusite abundant enough to be conspicuous megascopically, whereas buff quartzose bands usually are andalusite-free. The gray color results from the presence of kyanite and some hematite. Thus layers of relatively pure quartz or of quartz and muscovite usually do not contain andalusite, whereas hematite-kyanite quartz bands commonly do. A few layers consist of quartz, andalusite, minor hematite, but no kyanite. Locally the gray quartzite contains ellipsoidal augen of white, coarser grained quartz representing deformed pebbles. In some specimens relict cross-bedding may be deciphered (Fig. 2).

Microscopically the rock can be seen to consist of the following main constituents in their approximate order of abundance, although from band to band the percentages vary greatly: quartz, kyanite, green andalusite, muscovite, and specular hematite. Rutile is locally abundant; other accessories are zircon, apatite, hematite, and ilmenite.

Quartz grains are usually very uniform in size, especially within individual bands, averaging between 0.3 to 0.6 mm. in diameter, but in some hematite-rich bands the grains may be considerably smaller, down to 0.1 mm. in average diameter. The grains tend to be slightly elongate,

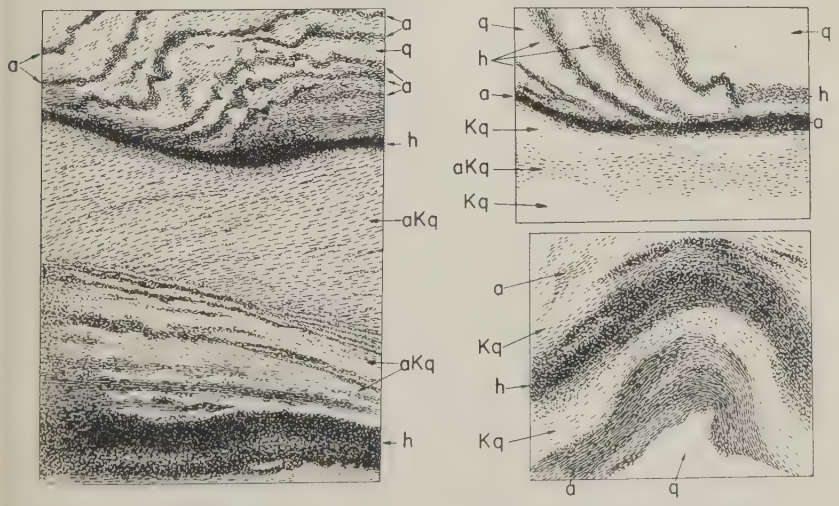

Fig. 2. Mineralogical banding in kyanite-andalusite quartzite, Kiawa Mountain, New Mexico (×0.6). q=quartz, h=hematite, a=andalusite, K=kyanite.

with patterns varying from nearly mosaic to somewhat interlocking. Kyanite is in blades with irregular terminations or in anhedra; inclusions of hematite are common. The blades are poorly oriented.

Andalusite usually forms anhedra or spongy clusters of anhedra peppered with minute inclusions of hematite, rutile and quartz; kyanite is rarely included. In one quartz-muscovite band andalusite appears as minute slender elongated inclusion-free prisms, enclosed in quartz grains, euhedral, and in parallel orientation.

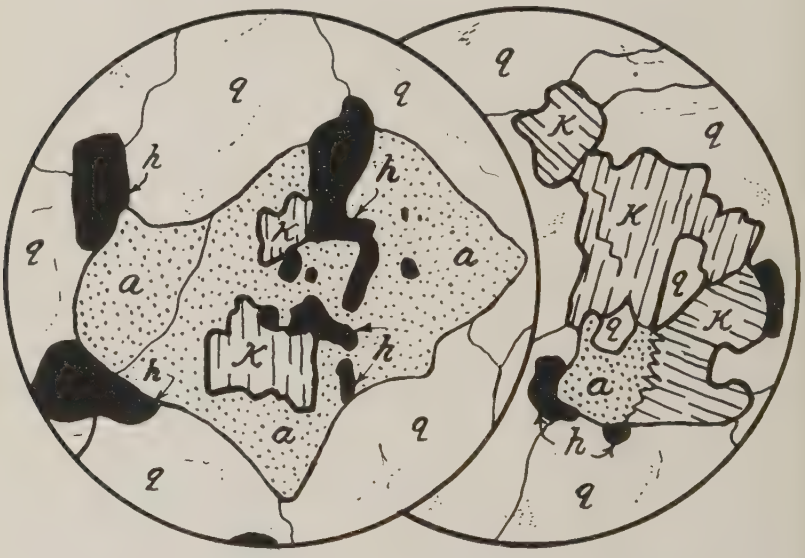

FIG. 3. Andalusite (a)-kyanite (k) intergrowths drawn for thin sections of quartzite, Kiawa Mountain, New Mexico (×80). q=quartz, h=hematite.

Muscovite plates and sheaves, usually along quartz grain contacts, are commonly in subparallel arrangement. Secondary finer-grained muscovite, partly stained by secondary hematite, may replace kyanite preferentially to andalusite.

In iron-rich bands hematite and rutile are closely intergrown. Some rutile is zoned, with red cores and golden yellow margins. Zircon is anhedral to euhedral, with some euhedra showing either concentric zoning (variation in birefringence) or crystallographically oriented opaque inclusions (as in chiastolite).

Generally andalusite and kyanite show no significant textural relationships with respect to each other, but in a very few grains clusters it appears that one may have replaced the other (Fig. 3), but the relations are far from clear. In rare examples subhedral kyanite laths lie decussate

across the fabric of an aggregate of andalusite anhedra. Textures indicate that the two species formed throughout essentially the same time period, but that some kyanite may have continued to form after all the andalusite had crystallized. This conclusion is substantiated by the presence of kyanite in veins cutting these rocks.

The kyanite veins of Kiawa Mountain transect the foliation of quartzite that generally may be poor in kyanite and may contain little or no andalusite. These veins, up to about a foot thick and a few feet long, are

Table 1. Optical Properties of Manganian Andalusite from Kiawa Mountains (A) Compared with those of Viridine from Ultevis, Sweden (B) (Data from Ödman, 1950), and with Those of Ordinary Andalusite (C)

		A	B	C
Pleochroism	α	emerald green	yellowish green	pink
	β	yellow green	emerald green	colorless, pale yellow
	γ	golden yellow	golden yellow	colorless, pale yellow
Indices of refraction			(Na)	
	α	1.649	1.658	1.629–1.640
	β	1.654	1.662	1.633–1.644
	γ	1.662	1.670	1.639–1.647
2V		65–70°	72°	80–85°
Sign		(+)	(+)	(−)
Dispersion		r<v, very strong	r<v	r<v

tabular, lensoid, or sinuous. They contain quartz, with kyanite locally very abundant (10–55%), and small amounts of hematite and secondary pale green muscovite. In kyanite-rich parts the kyanite forms buff to silvery gray blades generally no more than $\frac{3}{4}$ inch long (max. about 2 inches), usually tending to be oriented normal to the sharply defined vein walls or in semi-rosettes or subradial clusters.

Manganian Andalusite

The andalusite is an intensely and beautifully pleochroic mineral (Table 1). The colors are somewhat variable from grain to grain, and the intensity of the pleochroism varies even in single grains. This is similar to variations noted by Ödman (1950). It is also in conformity with color variations in ordinary andalusite in which single grains may be uniformly pinkish, or zoned pink-colorless, or contain irregularly distributed

patches of color. Other optical properties are listed in Table 1. The interference colors in some orientations are markedly anomalous.

The identification of the mineral as a variety of andalusite is confirmed on the basis of the *x*-ray powder pattern (Table 2).

The preparation of a pure sample for analysis proved exceedingly difficult owing to the very fine inclusions of hematite and to the closely associated kyanite. Separation of a heavy mineral fraction in bromoform

Table 2. *X*-Ray Powder Diffraction Data for Manganian Andalusite from Kiawa Mountain (A) and for Andalusite from White Mountain, California (B) (ASTM card II-446)

A		B		A		B	
d	*I*	*d*	*I*	*d*	*I*	*d*	*I*
5.52	9	5.58	7	1.75	3	1.74	2
4.56	10	4.52	10				
3.92	7	3.92	6			1.65	1n
3.52	7	3.49	5	1.59	4	1.59	3
		3.33	4	1.54	4	1.53	4
2.77	9	2.75	9	1.51	1		
2.47	7	2.47	6	1.49	7		
2.38	4	2.35	2	1.48	3	1.47	10
2.35	4					1.42	½n
2.27	8	2.26	9	1.39	6	1.38	5
2.17	8	2.17	10			1.34	1
1.97	2	1.97	1	1.29	3		
1.95	1			1.28	3	1.28	5n
1.89	2			1.24	5	1.24	5
1.85	2	1.83	2	1.21	1	1.21	2
1.80	3			1.19	1		
1.79	3	1.79	2	1.18	1	1.18	2

was followed by repeated fractionation by means of a Frantz isodynamic separator. Eventually a product was obtained which was estimated microscopically to contain about 6% of species other than andalusite, the chief contaminant being kyanite (about 5%), the rest (about 1%) chiefly hematite and quartz, with a trace of rutile.

This fraction was analyzed by *x*-ray fluorescence (A, Table 3). The magnetic fraction, consisting chiefly of hematite with some rutile, traces of zircon, and appreciable manganian andalusite in grains that are characterized by abundant hematite inclusions, also was analyzed in similar manner (B, Table 3).

All of the Mn probably may be assigned to andalusite, but a small amount of the Fe belongs to included hematite and a very little of the Ti

TABLE 3. ANALYSIS OF MANGANIAN ANDALUSITE CONCENTRATE (A) AND OF MAGNETIC CONCENTRATE (B), KIAWA MOUNTAIN, NEW MEXICO. BY *X*-RAY FLUORESCENCE

	A	*B*
Mn	3.9%	1.3%
Fe	2.7	60.0
Ti	0.8	1.8
Zn	0.02	—
Zr	0.2	0.09
Cu	0.04	
Ni	0.02	
Sr	0.03	
Nb	0.01	
Y	0.02	
Cr	abs.	
V	abs.	

to included rutile. A comparison of the composition of the Kiawa andalusite with those of other green andalusites is presented in Table 4.

DISCUSSION OF COLOR

Many andalusites show faint pleochroism of the type pink to green, and in relatively thick grains the color change may be marked.

The color of the Kiawa andalusite heated in air at 1100° C. for three hours showed no change in hue or intensity upon cooling. Probably both Fe^3 and Mn^3 contribute to the unusual pleochroism of the mineral. Macdonald and Merriam (1938) have described andalusite from Fresno County, California, which in hand specimen varies in color from pale pink to dark reddish violet. The pleochroisms and compositions of their two extreme varieties are:

	Lightest	*Darkest*
α	Nearly colorless	Deep pink
$\beta=\gamma$	Both colorless to very pale	Oil green
Fe_2O_3	0.51%	2.44
FeO	0.60	0.42

TABLE 4. Mn, Fe AND Ti CONTENT OF GREEN ANDALUSITES

	Kiawa Mtn.	Ultevis	Vestanå	Darmstadt
Mn_2O_3	5.6	3.63	6.91	4.77
Fe_2O_3	3.0*	3.4	—	4.16
TiO_2	1.2**	0.07	—	1.04

* Corrected for included hematite.

** Corrected for included rutile.

Both were shown to contain no Ti or Mn spectrographically. Thus it appears that, if Mn is absent, the intensity of the absorption for the α direction increases with increasing Fe^3. With large amounts of Mn present the α direction displays green tints. The absorption spectrum of viridine (Corin, 1934) shows two bands: one between 496–505 mμ at the border between blue and green, the other at 550 mμ at the border between green and yellow. The Kiawa viridine shows an absorption band at 555 ± 5 mμ, but the sensitivity of the apparatus was too low to detect the absorption band in the red. Absorption curves for manganic acetate solutions in phosphoric acid (Kolbe, 1935) show peaks from 520–500 mμ. Some other Mn^3 compounds also are green, *e.g.* $Mn_2(SO_4)_3$, $MnCl_3$, and $MnPO_4 \cdot H_2O$. According to Weyl (1951), Mn^{+3} in silicate glasses shows a strong absorption band with a maximum between 470 and 520 mμ.

The presence of Mn^{+3} in many other silicate species produces a pink coloration, e.g. in pink muscovite and lepidolite (Heinrich and Levinson, 1953) and in piedmontite, thulite, and kunzite (Claffy, 1953).

The viridine from Yakutia is reported by Serdyuchenko (1949) as containing 10.91% MnO, 6.60% Fe_2O_3, and 0.35 TiO_2, and by Shabynin (1948) as containing 7.66% Mn (or 9.89% MnO) and 9.60% Fe_2O_3. It is not known whether the two analyses were made on the same sample, but, if this was the case, the discrepancies are disturbing. If the two analyses represent viridine from different parts of the same deposit, then the differences are less significant. However, both investigators argue that the Mn is present as Mn^{+2}. Serdyuchenko (1949) claims that the color is related only to the Fe^{+3} content because spectrophotometric analysis shows only the absorption characteristics of Fe^{+3} silicates and, since the coloring power of Mn^{+3} generally and by far exceeds that of Fe^{+3} (according to Serdyuchenko), the Mn must be present as Mn^{+2}. These data are inconsistent. First, in silicates the coloring power of Fe^{+3} is usually considerably greater than that of Mn^{+3} (e.g. Heinrich and Levinson, 1953). Second, the andalusite structure is incapable of containing Mn^{+2} in any appreciable amounts; Mn^{+3} and Fe^{+3} may proxy for Al but Mn^{+2} is unlikely both because of differences in ionic size and because of difficulties in compensating for valence differences. Third, the analysis by Serdyuchenko (1949) also shows CaO+1.61% and $H_2O = 1.31\%$, further attesting to the inhomogeneity of the analyzed andalusite.

Isomorphism in Al_2SiO_5 Minerals

The three Al_2SiO_5 minerals, andalusite, kyanite, and sillimanite, can be cited as examples of species whose compositions are unusually constant, for silicates. There appears to be essentially no subsitution of Al or other elements for Si in the tetrahedral positions. In sillimanite only

very small amounts of Fe^3 have been reported. The kyanite structure appears to be capable of permitting slightly more varied substitutions, with Fe^3, Ti, and even Cr (Ozerov and Bykhover, 1936) reported. Jakob (1937, 1940, 1941) has reported that Na, K, and H_2O may participate as minor constituents in kyanite. Inasmuch as muscovite is commonly intergrown with kyanite or replaces it and since no mention is made of checks on the purity of his analyzed material, Jakob's claim cannot be regarded as verified. Furthermore, new analyses by Henriques (1957) show that Na_2O+K_2O does not exceed 0.06% in pure kyanite. Of the three, andalusite shows by far the greatest variation in properties—indices, 2V, sign, color, and specific gravity, and analyses show that at

Table 5. Comparison of the Paragenesis and Origin of Manganian Andalusite

Locality	Host Rock	Associated Minerals	Parent Material	Origin
Vestana district, south Sweden (Bäckström, 1896, 1897; Wülfing, 1917)	Quartzose mica schist	Quartz, muscovite. Acc. zircon, garnet	Manganiferous argillaceous sandstone	Low- to medium-grade regional metamorphism
Darmstadt, Hesse, Germany (Klemm, 1911; Wülfing, 1917)	Schistose quartz-rich hornfels	Quartz; psilomelane, piedmontite, muscovite, biotite; acc. apatite, rutile, garnet, hematite		Low-grade contact metamorphism
Salm-Château, Belgium (Anten, 1923; Corin, 1933, 1934)	Manganiferous phyllites	Quartz, hematite, spessartite, ottrelite		Low-grade regional metamorphism
Ultevis, Jokkmokk, Sweden (Ödman, 1947, 1950)	Quartzite, feldspathic quartzite (leptite)	Quartz, microcline, sodic plagioclase, hematite, muscovite, apatite, epidote, tourmaline, zircon, piedmontite, scheelite	Manganiferous argillaceous and feldspathic sandstones and mixed impure clastic and tuffaceous sediments	Low-grade regional metamorphism
	Pegmatitic veinlets cutting leptite	Quartz, microcline, orthopyroxene?, Mn-garnet		
Timptonsk, South Yakutia, A.S.S.R. (Serdyuchenko, 1949; Shabynin, 1950)	Quartzite	Quartz, biotite, feldspar, sillimanite, almandite, rutile, apatite, graphite, magnetite, hematite, chlorite		Medium- to high-grade(?) regional metamorphism associated with sillimanite-cordierite gneisses and magnetite schists
Lume Valley, Ruwenzori Massif, Belgian Congo (Thonnart, 1954)	Quartzite	Quartz, piedmontite, sericite		
Kiawa Mtn., N.M.	Aluminous quartzite	Quartz, kyanite, muscovite, hematite; rutile, zircon	Mn- and Fe-bearing kaolinitic sandstone	Medium-grade regional metamorphism

least as much as about 10% $Fe_2O_3+Mn_2O_3+TiO_2$ may be present. Andalusite has the lowest specific gravity of the three Al_2SiO_5 minerals, and it is expectable that its structure would be the one most able to tolerate the presence in modest amounts of ions other than Al, Si, and O.

Origin

The parageneses of the recorded occurrences of manganian andalusite are summarized in Table 5. The chief and striking difference between the paragenesis of the Kiawa Mountain andalusite and those of the other manganian andalusites is the copresence of abundant kyanite at Kiawa Mountain. Textural relations indicate that here these two minerals were formed essentially together. The rocks of the Petaca area were metaphosed under regional metamorphic conditions whose intensities reached those of the kyanite-staurolite subfacies of the amphibolite facies. From mineral assemblages in rocks elsewhere in the area the rocks achieved equilibrium. Normally under these conditions andalusite, if it were formed earlier at lower temperatures, would not persist. Usually where two or more modifications of Al_2SiO_5 occur together it can be seen that inversions have taken place (see, for example, Hietanen, 1956). Since the composition of the Kiawa andalusite is distinctly modified from that of ordinary andalusite, it is probable that its stability field has been extended over that suggested by Clark et al. (1957), probably toward higher temperatures and pressures, and may overlap the kyanite field. Possibly the formation of the manganian andalusite within the environment normal to kyanite was governed by the availability of trivalent manganese and structurally tolerable ferric iron, and when the supply of manganese was exhausted the kyanite modification remained as the sole stable aluminous phase. Where manganese was not present in the aluminous rocks and the iron remained largely unoxidized, staurolite instead of andalusite was developed along with kyanite. The staurolite rocks contain magnetite instead of hematite.

References

Anten, J. (1923). Le Salmien métamorphic du Sud du Massif Stavelot: *Mém. Acad. Roy. Belgique, Cl. Ser.* **II, 5,** fasc. 3.

Bäckström, H. (1896). Manganandalusit från Vestanå: *Geol. För. Förh.* **18,** 386–389.

——— (1897). Vestanåfältet. En petrogenetisk studie: *Sveriges. Geol. Unders.*, Ser. **C,** No. 168.

Barker, F. (1958). Precambrian and Tertiary geology of Las Tablas Quadrangle, New Mexico: *New Mex. Bur. Mines Min. Res. Bull.* **45.**

Claffy, E. W. (1953). Composition, tenebrescence and luminescence of spodumene minerals: *Am. Mineral.* **38,** 919–31.

Clark, S. P., Sr., E. C. Robertson, and F. Birch (1957). Experimental determination of kyanite-sillimanite equilibrium relations at high temperatures and pressures: *Am. Jour. Sci.* **255,** 628–640.

Corey, A. F. (1953). Kyanite deposits of the Petaca district, Rio Arriba County, New Mexico: *Univ. Michigan Ph.D. Thesis*, 141 pp.

Corin, F. (1933). Identité probable de la gosseletite et de la viridine (mangandalousite). Occurrence de la viridine à Salm-Château: *Ann. Soc. Géol. Belgique* **77,** B 152–157.

——— (1934). Spectre d'absorption de la viridine: *Bull. Soc. Belge Géol.* **44,** 313–315.

De Geer, G. (1889). Beskrivning till Kartbladet "Bäckaslog": *Sver. Geol. Unders. Ser. Aa* No. **103.**

Heinrich, E. Wm., and A. F. Corey (1952). Kyanite deposits near Petaca, New Mexico (abs.): *Am. Inst. Min. Eng. Program, Ind. Min. Divis. Ann. Meet. 1952*, p. 3.

———, and A. A. Levinson (1953). Studies in the mica group; mineralogy of the rose muscovites: *Am. Mineral.* **38,** 25–49.

Henriques, Åke (1957). The alkali content of kyanite. *Ark. Mineral. Geol.* **2(12),** 271–274.

Hietanen, A. (1956). Kyanite, andalusite, and sillimanite in the schist in Boehls Butte quadrangle, Idaho: *Am. Mineral.* **41,** 1–27.

Jakob, J. (1937). Ueber den Alkaligehalt der Disthene: *Schweiz. Min. Petro. Mitt.* **17,** 214–219.

——— (1940). Über den Chemismus des Andalusits: *Schweiz. Min. Petro. Mitt.* **20,** 8–10.

——— (1941). Chemische und strukturelle Untersuchungen am Disthen: *Schweiz. Min. Petro. Mitt.* **21,** 131–135.

Jahns, R. H. (1946). Mica deposits of the Petaca district, Rio Arriba County, New Mexico: *New Mex. Bur. Mines Mineral Res. Bull.* **25.**

Just, E. (1937). Geology and economic features of the pegmatites of Taos and Rio Arriba counties, New Mexico: *New Mex. Bur. Mines Mineral Res. Bull.* **13.**

Klemm, G. (1911). Über Viridin, eine Abart des Andalusits: *Not.-Bl. Ver. Erdkunde Darmstadt*, **32.**

Kolbe, E. (1935). Über die Färbung von Mineralien durch Mangan, Chrom und Eisen: *Neues Jahrb. Min. BeB.* **69(A),** 183–254.

Macdonald, G. A., and R. Merriam (1938). Andalusite in pegmatite from Fresno County, California: *Am. Mineral.* **23,** 588–594.

Northrop, S. A. (1942). Minerals of New Mexico: *Univ. New Mex. Bull., Geol. Ser.*, **6,** No. 10.

Ödman, O. H. (1947). Manganese mineralization in the Ultevis district, Jokkmokk, North Sweden. Part I: Geology: *Sveriges Geol. Unders.* **41,** No. 6.

——— (1950). Manganese mineralization in the Ultevis district, Jokkmokk, North Sweden. Part 2: Mineralogical Notes: *Sveriges Geol. Unders. Årsbok* **44,** No. 2.

Ozerov, K. N., and N. A. Bykhover (1936). Corundum and kyanite deposits of the Verkhne-Timpton district of the Yakutian A.S.S.R.: *Trans. Centr. Geol. Prosp. Inst. U.S.S.R.* **82,** 106 pp.

Serdyuchenko, D. P. (1949). O sostave i khimicheskoi constitutsii margantsovistykh andaluzitov: Vsesoyuz. Miner. Obshch., Zap. (*Mem. Soc. Russe Mineral.*) **78**(2), 133–135 (*Chem. Abs.* **43,** 6119, 1949).

Shabynin, L. I. (1948). Viridin iz Yakutii: Vsesoyuz. Miner. Obshch., Zap. (*Mem. Soc. Russe Mineral.*) **77**(3), 203–214 (*Chem. Abs.* **44,** 7721, 1950).

Thonnart, Pierre (1954). Découverte de manganandalousite dans le massif du Ruwenzori, au Congo Belge. *Compt. Rendu* **238,** 1140–1141.

Weyl, W. (1951). Coloured glasses: *Soc. Glass Tech. Publ., Sheffield, England.*

Wülfing, E. A. (1917). Der Viridine und seine Beziehung zum Andalusit: *Sitzb. Heidel. Akad. Wiss, Math.-naturw. Kl., Abt. A.*

Manuscript received March 31, 1959.

THE AMERICAN MINERALOGIST, VOL. 44, NOVEMBER–DECEMBER, 1959

USE OF THE SPINDLE STAGE FOR DETERMINATION OF PRINCIPAL INDICES OF REFRACTION OF CRYSTAL FRAGMENTS*

RAY E. WILCOX, *U. S. Geological Survey, Federal Center, Denver, Colorado*

ABSTRACT

A small crystal or crystal fragment mounted on the tip of a spindle in a suitable holder on the polarizing microscope stage may be oriented quickly and accurately for measurement of all its principal indices of refraction by the immersion method. Independent measurements or estimations of other properties, such as optic angle, optic sign, dispersion, pleochroism, and the relation of the indicatrix to cleavage or crystal faces may be made on the same fragment. Besides its usefulness in determininative mineralogy, this inexpensive device has much to recommend it as a teaching aid in optical crystallography, since, with its help, the student rapidly acquires facility and confidence in the application of interference figures and extinction angles to mineralogic and petrographic problems. The device used here is based on that of Rosenfeld (1950) but is of somewhat more rugged construction and provides for reading of angular rotations about the spindle axis. For mounting the fragment a mixture of ordinary carpenter's glue and molasses is recommended. Either orthoscopic or conoscopic illumination may be used to orient the fragment for measurement of its principal indices. The orthoscopic procedure can give results to the limit of accuracy of the immersion method employed, while the conoscopic procedure is usually faster and gives results sufficiently accurate for all but the most exacting work, besides providing additional optical information.

INTRODUCTION

The device described, for which the general name "spindle stage" is used here, is designed to rotate a crystal fragment in a matching liquid whose upper and lower plane surfaces remain perpendicular to the microscope axis. This, it should be noted, is different from the universal stage, which rotates not only the crystal, but also the plane surfaces of the liquid. Because of this and other mechanical features, the spindle stage has several advantages over the universal stage for study of individual crystal fragments by the immersion method: (1) The crystal may be viewed in *any* direction at right angles to the spindle, and *any* desired line in the crystal may be rotated into the plane of the microscope stage. Thus all three principal indices may be determined on the same fragment. (2) There are no corrections to be made to the angular rotations, and no appreciable disturbing effects due to high birefringence. (3) Either orthoscopic or wide-angle conoscopic illumination may be used as desired. (4) It is simple and inexpensive.

The conoscopic method suggested by Rosenfeld (1950) for direct determination of all principal indices of refraction of anisotropic crystal grains using a spindle is so effective and so instructive in itself that the

* Publication authorized by the Director, U. S. Geological Survey.

following extension, together with a brief review of other possible applications, is provided as a recommendation for its wider use in determinative and descriptive mineralogy as well as for teaching optical crystallography.

Briefly the procedure is as follows: The crystal fragment is attached with glue to the tip of a spindle (Fig. 1), which is turn is clamped over a glass window in a flat metal plate so that the grain lies in immersion liquid in a small cell formed by window, coverglass, and supporting

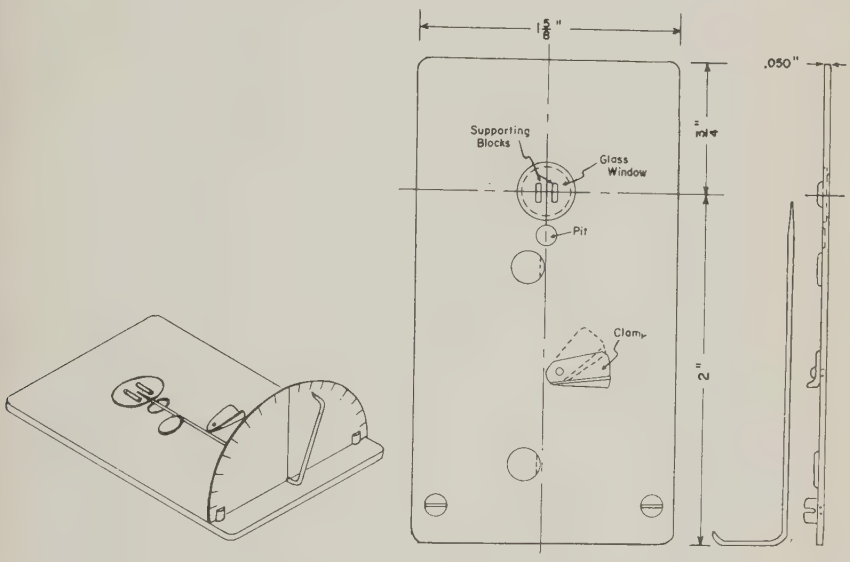

FIG. 1. Sketch of spindle stage, showing detachable plastic scale for reading angular rotations about the spindle axis. Cover glass is not shown.

blocks. To compare a principal index of refraction of the crystal with the immersion liquid it is only necessary to rotate the appropriate symmetry axis of the indicatrix into the plane of the microscope stage and the vibration plane of the lower nicol.

The method is suited for determining optical properties of homogeneous transparent anisotropic crystals or fragments of appropriate size, say between 0.03 and 0.3 mm. diameter for the form of the device illustrated here; no doubt somewhat larger or smaller grains could be handled by special design. In a uniaxial crystal both principal indices, and in a biaxial crystal all three principal indices, may be measured on the same grain. In case such complete data are not required for identification of an unknown or for locating a mineral accurately in its isomor-

phous series, the grain may simply be oriented for a desired principal index. In the common clinopyroxenes for instance it is sufficient to measure the beta index and the optic angle (which in many cases also may be measured on the same grain). In orthopyroxenes and olivine it is usually sufficient to measure α or γ. In micaceous minerals α, difficult to measure by ordinary methods, becomes tractable with this device, as do the principal indices of refraction of minerals with prominent oblique cleavages, such as the carbonates and amphiboles. Difficulties arise with minerals of strong selective absorption, such as the very dark micas and hornblendes, due to their abnormal interference figures, yet even some of these can be handled conoscopically by taking into account observable characteristics of the pleochroism (Schumann, 1948), or orthoscopically by working on thin wedge-shaped edges.

In case only a small amount of material is available, as sometimes happens in work with heavy mineral concentrates or products of microchemical tests, the complete set of optical properties may be measured on a single grain and, if desired, this grain retained attached to the spindle for future reference. Where repeated measurements are to be made on the same grain, the grain may be attached to and detached from the spindle at will. A simple modification of the spindle should permit relating x-ray and optical data of the same grain. The device is especially effective in the not uncommon situation in which the "unknown" is actually a mixture of two or more substances of similar optical properties, for identifications may be made from complete optical properties of each grain of a series.

The potential of the instrument under conoscopic observation is appreciated when one notes that the interference figure is a "directions-image," that is, each point in the field shows the behavior of light traversing the crystal between crossed nicols in a specific direction, and the position of the point is nearly the orthogonal projection of that direction. The cone of observation *in the crystal* using an objective of N. A. 0.85 is commonly 60° to 70° wide, depending on the refractive index of the crystal. By rotating the grain about the axis of the spindle, the number of directions that may be studied is greatly increased, and a wide choice of favorable orientations is made available for observation of crystallographic elements and for special optical tests. The directions-image cone of a 0.65 N. A. objective, although less broad than that of a 0.85 N. A. objective, is quite adequate for most work, and objectives of even smaller numerical aperture may furnish useable interference figures. Under orthoscopic illumination, on the other hand, the field is a projected image of the object itself, and as used here shows the behavior of light vibrating essentially perpendicular to the microscope axis. Hence, although a smaller number of directions is available in which the behavior of light in the crystal may be studied during rotation of the spindle, a more precise, if less direct, means of determining optical properties is furnished.

Construction of the Spindle Stage

Possibly the first of the many rotating devices of this type was that of von Ebner in 1874 (Johannsen, 1918, p. 301). Others have been described by Vedeneeva and Kolotushkin (1934), Rawlins and Hawksley (1934), Wood and Ayliffe (1935), Bernal and Carlisle (1947), Rosenfeld (1950), Hartshorne and Stuart (1950, p. 215), Tatarskiĭ (1951) and Hartshorne and Swift (1955). In addition Steinbach and Gibb (1957) provide for tilting the spindle axis as much as 30° from horizontal. Many more variants of this simple apparatus are possible for general use and for special problems. In working with several forms of the device I have been led to the one described below, essentially a modification of Rosenfeld's (1950) device, as a practical combination of ruggedness, ease of construction and effectiveness in problems of determinative mineralogy. The disadvantages of most previous devices inherent in the use of a drum or round ball for rotating the spindle have been avoided by bending the spindle into an L, the arm of which may be moved to rotate the crystal about the spindle axis. The resulting limit of 180° for angular rotation is no hindrance, for further rotation would merely reciprocate orientations already attained; rather it has the advantages of preventing inadvertent duplication of settings and of providing a pointer for reading values of angular rotation about the spindle axis. While such angular readings are not specifically required in the procedures suggested here for determination of indices of refraction, they do aid in returning quickly to previous settings. Angular readings are required for plotting relations of crystallographic and optical elements stereographically and for determination of optic angle by extinction characteristics.

As shown in Fig. 1, a stainless steel plate about 0.040 or 0.050 inch thick is bored to receive and seat a slightly thinner glass window so that the top surface of the glass, when cemented into its seat, is essentially flush with that of the plate. Two steel slugs are slightly undercut and soldered to the plate along one side of the center line of the spindle, and an undercut clamp is riveted to swing in against the other side of the spindle and hold it with the desired firmness. Two short lengths of the spindle stock are cemented to the glass window on either side of the center line of the spindle about a sixteenth of an inch apart to support the cover glass and form a cell of thickness equal to the diameter of the spindle.* A pit bored into the upper surface of the steel plate along the

* To accommodate the short working distance of the 0.85 N. A. objectives of American Optical and of Bausch and Lomb, material about 0.20 inch thick may be used to support the cover glass instead of the 1/32-inch material of the spindle stock. This of course decreases somewhat the maximum permissible size of crystal fragment and freedom of movement within the cell. "Cementyte A" of Schaar & Company serves to cement the supporting blocks to the window and to seal the glass window in its seat. A satisfactory expedient is the mixture of carpenter's glue and molasses described below for mounting the grain.

axis of the spindle just behind the window helps to break the capillary between spindle and plate and decreases creeping of immersion liquid along the shank of the needle. (A drop of water in the pit during operation further prevents the escape of immersion liquid.)

The spindle is made of a straight $2\frac{1}{2}$-inch length of piano wire 1/32 inch in diameter, tapered for about a quarter of an inch at the end but with a definite flat blunting of the extreme tip. The other end of the spindle is bent into a right angle just at the heel of the holder plate, as shown in Fig. 1, taking care not to bend the shank of the spindle, especially near the sharpened tip. It is convenient to have a half dozen or more of these spindles on hand. The small protractor scale is cut out of the 6-inch transparent plastic ruler no. W-5 of the C-thru Ruler Company of Hartford, Conn., and fits into the slots of two stainless steel machine screws in the heel of the base plate. (Care should be taken when using methylene iodide-sulfur immersion liquids of index greater than 1.7 as they soften this plastic after prolonged contact.)

Mounting the Grain

For many beginners the task of fastening the grain to the tip of the spindle is the most difficult part of the procedure, but dexterity and confidence are usually quickly acquired with practice. The choice of adhesive is of primary importance, for it must remain tacky until contact has been made with the grain, yet should set rapidly thereafter and be insoluble in the index liquids and whatever cleaning fluid is used. Dental cement is suggested by Rawlins and Hawksley (1934) and dental "sticky wax" by Wood and Ayliffe (1935). Vedeneeva (1937) suggested the use of water glass, Kolotushkin (1940) suggested "sindetikon" "koloditikon" or "plain office glue," and Rosenfeld (1950) suggested beeswax, subsequently coated with waterglass to prevent solution in the index oils; Tatarskiĭ (1951) reports success with freshly melted Rochelle salts, and also states that melted sugar moistened with water may be used.

I have found that several common mucilages (Lepage, Sanford, Ross) are satisfactory for mounts at room temperature. Most dependable, however, has been a mixture of about 4 parts of common water-soluble carpenter's glue (such as Lepage's "Liquid Glue") and one part of crude ("black-strap") molasses. This mixture has the desired tackiness and setting time, will hold a grain firmly and indefinitely in the immersion oils commonly used in mineralogical laboratories, and is affected by acetone only after prolonged contact. Liquids of the methylene iodide-sulfur series above 1.7 appear to decompose somewhat more rapidly than usual in contact with this adhesive, and it is therefore advisable to test the Becke effect immediately after their introduction into the cell, as of course it is

also advisable to do in any immersion mount of these liquids. For immersion liquids made up of water solutions (Bryant, 1932), this adhesive would be unsuitable, and an appropriate one may be sought among the many water-insoluble adhesives now available.

In detail the mounting procedure is as follows: A drop of the adhesive is placed on a flat surface and the tip of the spindle is just touched to it in order to bring up the minimal quantity that will hold the crystal fragment. (To ensure tackiness, Kolotushkin (1940) recommends touching the glue-tipped spindle to water before bringing it to the desired grain.) The spindle is brought down to touch the desired grain so that it will become attached as nearly as possible in line with the spindle axis. For platy or elongate grains a choice may be made for orientation of the grain in respect to the spindle axis, although this is not usually necessary because all appropriate positions for measuring the principal indices may be reached regardless of the relation of spindle axis to grain elongation or optic indicatrix. For substances of strong birefringence, dispersion, or pleochroism a smaller grain is generally easier to work with optically than a larger one. For mounting very small grains, or for picking a particular type of grain from a mixture, it is helpful to use a binocular microscope or hand lens. In some cases spreading the grains on a soft electrostatically charged surface, such as rubber or plastic, may facilitate securing the grain in a desired position on the spindle point. Limited adjustment of the position of the grain may be made by nudging the grain with another spindle under the binocular before the adhesive sets. The glue of course should not mantle the grain, and, in case the grain is to be removed for remounting, it is essential to rinse off the glue completely, as a film of glue will prevent index comparisons.

After allowing the glue to harden, the spindle is clamped in position and the protractor scale inserted. A small coverglass or fragment of coverglass is placed across the supporting blocks on the window and a drop or two of a chosen immersion liquid introduced into the open-ended cell so formed, where it is held by surface tension. The device may be fastened to the microscope with the stage clips or directly in the jaws of a mechanical stage. The grain may be centered in the usual manner, or if desired, under a high power objective with the Bertrand lens inserted and the tube raised.

Orientation and Index Determination

Conoscopic Procedure

As pointed out by Rosenfeld (1950), a symmetry axis of the indicatrix lies horizontal NS when an isogyre lies EW across the center of the cono-

scopic field,* and there are three such settings of spindle axis and microscope stage for a biaxial crystal, corresponding to the three principal indices of refraction. With a high power objective (say 0.65 or 0.85 N. A.), crossed nicols and conoscopic illumination, the crystal is rotated on the spindle and microscope stage until an isogyre has been maneuvered into a position symmetrically along the EW crosshair, that is, so that the EW crosshair divides the isogyre brush into two mirrow-image halves. Examples of such interference figures as seen with a 0.65 N. A. objective and Bertrand lens are sketched in Fig. 2. Upon reaching the position at which the isogyre lies symmetrically along the EW crosshair, the readings of spindle and stage scales may be noted for convenience in returning later to this setting. Then, under orthoscopic illumination with the analyzer removed, the relation between index of crystal and of liquid is noted. Restoring crossed nicols and conoscopic illumination, the same procedure is repeated to reach a second and third position at which an isogyre lies symmetrically along the EW crosshair, taking care not to duplicate a position on the microscope stage at 180° from one already found.

With this preliminary information, often also a knowledge of optic sign, approximate optic angle, dispersion, and pleochroism observed at strategic points in the orientation procedure, one is ready to determine specifically the indices of refraction. The initial liquid may be drawn off conveniently with a fragment of filter paper or blotting paper placed against the spindle at the edge of the cell, after which the cell is rinsed with acetone or with a drop or two of the appropriate new liquid (being careful to avoid contamination of the liquid in the bottle) and again drawing off with the absorbent paper. This may be repeated once or twice to completely flush out the old liquid. Then with the new liquid in the cell the indices of liquid and crystal are again compared and noted at the respective oriented positions. The procedure is then repeated with other chosen liquids until all principal indices have been determined.

Accuracy of orientation is aided by attention to the following details: For interference figures, the substage assembly should be centered, the Bertrand lens adjusted symmetrically to the crosshairs, and of course the nicols adjusted parallel to the crosshairs. It will be noted on many microscopes that the readability of an interference figure with a Bertrand lens is much improved by slightly raising the tube of the microscope with the fine-focus drum until the interference figure fills the whole field and becomes smooth. The same technique may be used in confirming the optic orientation of the very edge of the grain on which the Becke line

* Throughout the lower nicol is assumed to be NS, as in most microscopes of U. S. manufacture.

effect is to be observed. In a microscope without a useable Bertrand lens, the isogyre is seen with the pinhole ocular (thus without crosshairs) and may be brought by eye sufficiently close to a symmetrical EW position for much determinative work. If the grain migrates due to excentric mounting it must be recentered by slight shifting of the device on the microscope stage. If angular readings of the microscope stage are to be used in plotting, as in the optic angle method mentioned below, the alignment of the needle axis must be preserved during such shifts, and this may be guaranteed by placing the device in a mechanical stage. Comparison of index between liquid and crystal using the central illumination effect is best made with a low power objective, say a 10× or 20×, rather than the high power objective used for the interference figure.

The basis of the centered EW isogyre as a criterion of correct orienta-

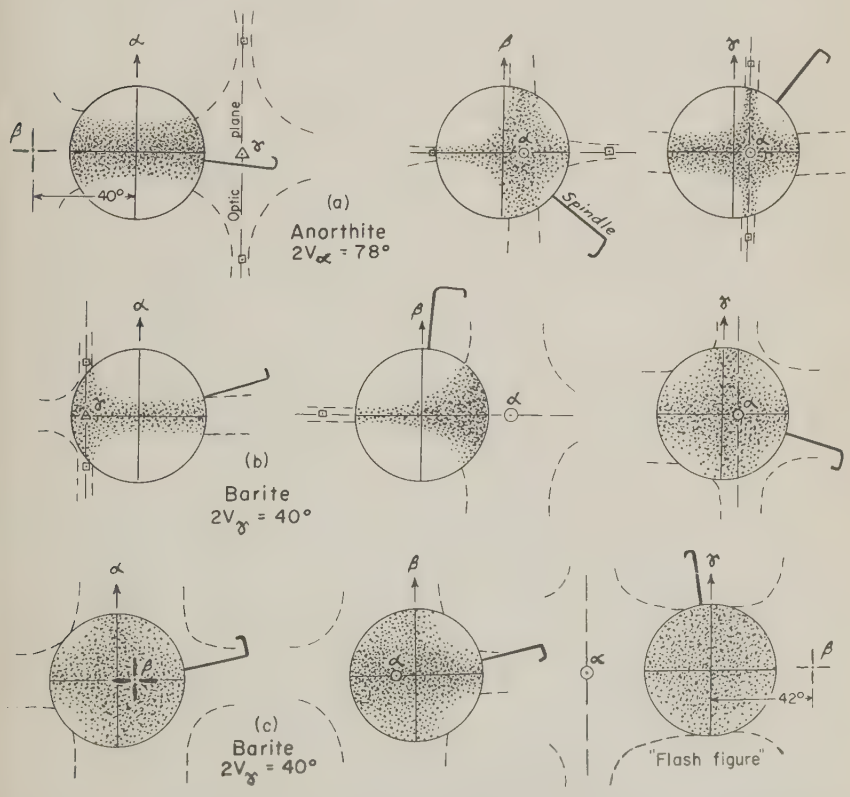

FIG. 2. Conoscopic fields of view (in circles), using .65 N. A. objective and Bertrand lens, with crystals in positions for measuring principal indices of refraction. (a) Anorthite, $2V_\alpha = 78°$. (b) and (c) Barite, $2V\gamma = 40°$.

tion may be demonstrated by skiodrome diagrams (Becke, 1905a; Johannsen, 1918, p. 424, 429 ff) or the alternative diagrams proposed by Kamb (1958). The centered EW isogyre indicates that an optical symmetry plane is vertical and EW and that therefore the normal to this plane, a principal axis of the indicatrix, is horizontal and NS. This is an extinction position under orthoscopic observation, and, with the analyzer removed, the light observed vibrates parallel to this symmetry axis and has the corresponding principal index of refraction. Generally at the other extinction position on the microscope stage, a wave is passed having a nonprincipal index of refraction, α' or γ'. It may be shown that centered interference figures represent special cases as follows: a centered optic axis figure furnishes β in all positions of the microscope stage; a truly centered bisectrix figure furnishes β at one extinction position and either α or γ at the other; a truly centered optic normal figure (flash figure) furnishes α and γ at respective extinction positions. In working with apparent obtuse bisectrix or optic normal figures, however, it should be kept in mind that the bisectrix or optic normal may actually diverge appreciably from the microscope axis, as implied by Becke (1905*a*) and as discussed below for crystals of small optic angle, and in this case only one of the extinction positions furnishes a principal index.

Uniaxial crystals could be oriented in the same manner as biaxial, but, except for checking that the crystal is indeed uniaxial, it is only necessary to orient to obtain the flash figure, for in that position the indices of both the ordinary and principal extraordinary waves may be measured at their respective extinction positions on the microscope stage. In this orientation also the optic sign may be determined by use of the accessory plates and Lommel's Rule, which states that the optic axis lies in the quadrants from which the brushes of the flash figure leave the field upon slight rotation of the microscope stage.

An often overlooked characteristic of biaxial crystals of small to moderate optic angle is that *when the acute bisectrix is horizontal*, regardless of the position of the optic plane otherwise, *the interference figure behaves much like the flash figure of a uniaxial crystal.* Thus one is unable to distinguish whether a particular figure at hand is that of an optic normal section, obtuse bisectrix section or *any intermediate section.* In orienting such crystals, two general situations may be considered here: (1) that in which the acute bisectrix is at a large angle to the spindle axis, and (2) that in which the acute bisectrix is at a small angle to the spindle axis. These situations are illustrated in Figs. 2*b* and 2*c*, respectively, for different mounts of barite of $2V_\gamma = 40°$.

(1) If the crystal fragment happens to be mounted so that the acute bisectrix is at a large angle to the spindle axis, as in Fig. 2*b*, the orienta-

tion may be carried out much in the usual manner. During rotation about the spindle axis the acute bisectrix or an optic axis may become visible in the conoscopic field and at once reveal the biaxial character. If both optic axes lie outside the conoscopic field the biaxial character may often be recognized by a difference in behavior of the isogyres near the respective oriented positions. Mounted thus, there are only two settings of the spindle arm, in addition to the setting for the "flash figure," in which an isogyre may be placed strictly symmetrically along the EW crosshair. With a similarly mounted uniaxial crystal, on the other hand-there are any number of such settings of the spindle arm before the setting for the flash figure is reached. This distinction becomes more difficult of course as the optic angle approaches zero. Having reached the spindle setting for the "flash figure," one may locate the acute bisectrix by analogy to Lommel's Rule for uniaxial crystals and place it in the NS position for measuring its index of refraction.

(2) If the acute bisectrix of the crystal with small optic angle lies at a small angle to the spindle axis, the "flash figure" is again obtained when the acute bisectrix is horizontal, and generally broad and diffuse isogyres are obtained when the other two symmetry axes are horizontal. A fragment of barite mounted with γ at 22° to the spindle axis serves as an example, and Fig. 2*c* represents the conoscopic fields observed for NS positions of α, β, and γ. Repeated trials with this mount under conoscopic illumination gave a range of spindle arm settings about 5° on either side of the settings for α and β that were indicated by stereographic plotting according to the "extinction curve" method of Joel and Garaycochea (1957). It is important to note here that, in spite of the $\pm 5°$ range of uncertainty of the settings for α and β, only small errors in their principal indices could result (see for instance the discussion in the later section on "precision"). Although the "flash figure" of the setting for gamma of this mount of barite behaved quite normally—that is, the dark field separated into two isogyres that swept rapidly out of the field from the quadrants into which the acute bisectrix had been moved by slight rotation of the stage—the stereographic plot indicated that in reality the optic normal was 42° from parallelism with the microscope axis. Thus, with the acute bisectrix NS, γ may be measured accurately, but at the other extinction position only a non-critical index is measured. If the situation justifies it, more exact settings of α and β than obtained above may perhaps be obtained by remounting the grain or another grain with the hope or design that the acute bisectrix will be at a large enough angle to the spindle axis to enable orientation in the manner outlined for case (1), as well as direct observation of the size of the optic angle. Or, if a sufficiently precise immersion index facility is available, such as single- or

double-variation, the principal indices of this barite or other crystals of low birefringence, mounted as in Fig. 2*c*, could be determined with greater accuracy using the simplified orthoscopic procedure described below.

Orthoscopic Procedure

Separate orthoscopic procedures for bringing the crystal into correct positions for measuring its principal indices of refraction have been outlined by Vedeneeva and Kolotushkin (1934; see also Vedeneeva, 1937; Kolotushkin, 1940) and by Joel (1950; see also Joel and Garaycochea, 1957). Both require stereographic constructions, and that of Vedeneeva and Kolotushkin is subject to error in the setting for β. A simplified orthoscopic procedure, which removes the tedium of graphical plotting and furthermore is accurate for all three principal indices, is as follows:

Rotate the microscope stage to make the spindle axis EW and rotate *about the spindle axis* to extinction. Then by incremental rotations about the spindle axis and subsequent slight corrections of extinction by rotation of the microscope stage and observation of the Becke effect (changing liquids as necessary), determine both the maximum index and minimum index encountered during the full 180° traverse about the spindle axis. One of these extreme values is β and the other is an extreme principal index, α or γ. Rotate now on the microscope stage to make the spindle axis NS and rotate about the spindle axis to extinction. Observing the refractive index, there are two possibilities: (1) If the index is lower in this new position than before, the extreme principal index determined before was γ, and α will be found as the minimum in a new series of incremental rotations about the spindle axis from this new extinction position. (The maximum index in this series will be a nonprincipal index, α', and need not be determined.) (2) If the index is higher in the second extinction position, the extreme principal index determined before was α, and γ may be determined as the maximum index of this new series of extinction positions. In this procedure it is not necessary to read the microscope stage or spindle arm settings except as reference positions for convenience in returning to them later. It is good practice of course to confirm the correctness of setting for each principal index by observing the interference figure in the oriented position, as described above for the conoscopic method.

The basis for this procedure rests on the Biot-Fresnel law and on the relations between indicatrix (fixed on the spindle axis), microscope stage axis, and plane of the polarizer. As the circular sections of the indicatrix are perpendicular to the optic axes, the Biot-Fresnel law may be stated in the manner used by Joel and Garaycochea (1957) quite simply as fol-

lows: *For a given position of the crystal the vibration directions of light bisect the traces of the circular sections of the indicatrix in the plane of the microscope stage.* As shown in Fig. 3, these vibration directions are 90° apart, and extinction results when, by suitable rotation of the microscope stage, they are made parallel to the directions of light vibration in the polarizer and analyzer. A small rotation of the crystal about the spindle axis to a new setting will result in a new pair of vibration directions, which again may be rotated on the stage into parallelism with the nicols to restore extinction.

These extinction positions, plotted stereographically, as in Fig. 4, trace out two curves whose corresponding points at a given setting of the spindle arm are 90° apart. Each curve is confined to its respective pair of dihedral angles formed by the circular sections. Duparc and Pearce (1907) plotted such extinction curves for representative crystallographic zone axes—analogous here to the spindle axis—and these showed that the curve of extinction positions passing through the zone (spindle) axis also passes through one of the bisectrices, α or γ. The curve of extinction positions passing through a point of the great circle of the zone (spindle) axis also passes through the other bisectrix and the optic normal, β. These curves were studied in detail by Joel and Garaycochea (1957), who named them the "polar" and "equatorial" curves, respectively. Referring to Figs. 3 and 4, it will be seen that by rotating on the microscope stage to make the spindle axis EW, then rotating about the spindle axis, one will reach the extinction position E in Fig. 4. This is on the equatorial series of extinction positions, and following this series by small rotations on the microscope and spindle axes, one must pass through the positions in which β and one of the bisectrices, here γ, become horizontal.

Recognition of the principal indices is made possible by the fact that they must be either the maximum or minimum values of indices encountered on their respective series of extinction positions. The extreme principal index α is of course the smallest value of index in the extinction series of lower indices, while γ is the largest value encountered in the extinction series of higher values. Again with reference to Figs. 3 and 4, and starting with the horizontal NS position of γ, the indices at successive extinction positions decrease but never reach β until the optic normal itself is horizontal NS at which position β may be measured. This is the minimum index on this extinction series, for with further rotation about the spindle axis the extinction position passes into the opposite dihedral angle and the index at successive extinction positions becomes progressively greater, until it again passes through the maximum, γ (assuming the spindle may be rotated that far). Had α been the extreme principal index in the equatorial series, similar reasoning could be applied to dem-

onstrate that β would be the maximum of index encountered upon 180° of rotation about the spindle axis.

A special situation, illustrated in Fig. 4*b*, occurs when the biaxial crystal fragment happens to be mounted with one of its optic axes nearly or exactly perpendicular to the spindle axis. As before, two sets of extinction positions at 90° from each other may be followed, but as the optic axis approaches parallelism with the microscope axis the definition of the two

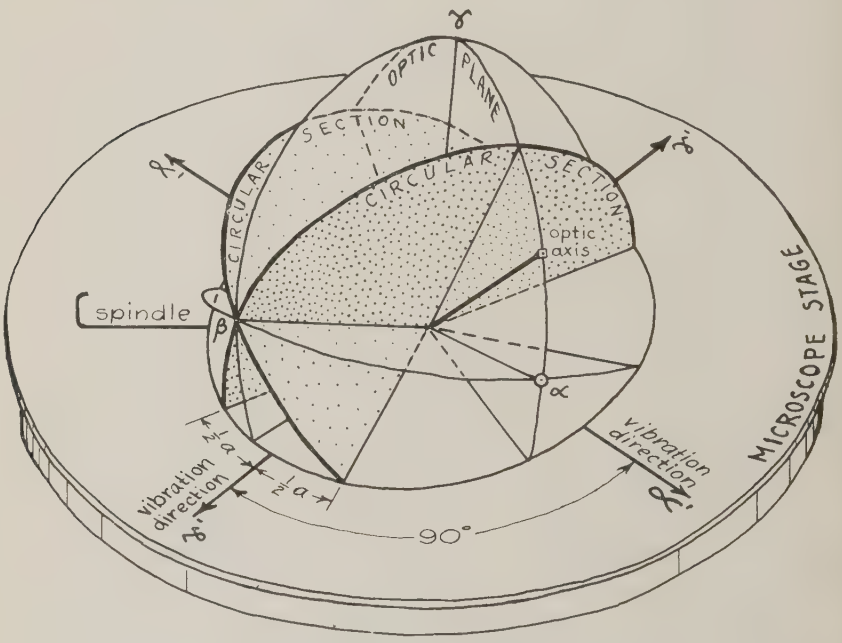

FIG. 3. Vibration directions in a biaxial crystal with the symmetry axes of the indicatrix inclined to the microscope stage and spindle axis.

extinction positions fades, and the crystal remains equally dark on complete rotation of the microscope stage. As the optic axis is advanced beyond parallelism with the axis of the microscope the extinction positions once more become definite, apparently a continuation of the same trends (although in reality, as seen in Fig. 4*b*, the curves bend sharply and follow their prescribed course close along the circular section). Fortunately no practical problem arises, for the one apparent series of extinction positions includes α as its minimum and γ as its maximum index, and β may be measured at that setting in which the distinction between extinction positions is lost, that is, when the optic axis coincides with

the microscope axis. Here also a nearly centered optic axis figure may be observed under conoscopic illumination, and if desired the true course of the extinction curves may be followed by the interference figure. With crystals having marked dispersion a disturbing behavior simlar to that just described may occur if an optic axis is merely in the neighborhood of perpendicularity to the spindle axis, and therefore only becomes roughly coincident with the microscope axis. It becomes ad-

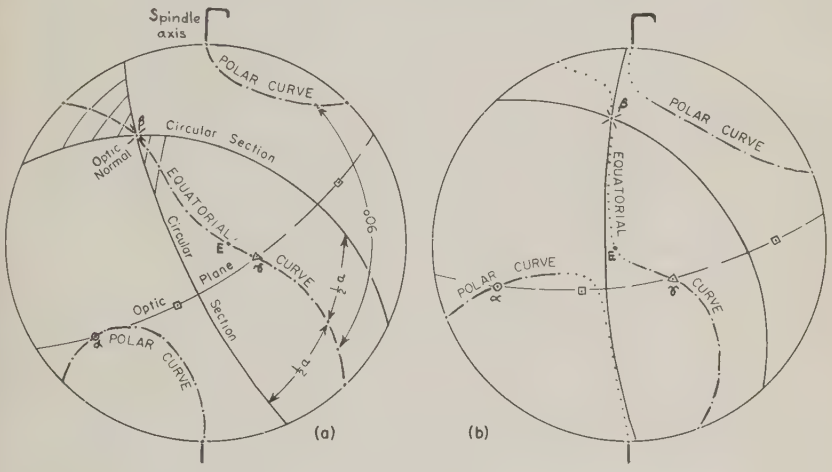

FIG. 4. Locus of extinction positions of anorthite, $2V_\alpha = 78°$, plotted stereographically in relation to the spindle axis. (*a*) Spindle axis at 23° from a circular section of the indicatrix. (*b*) Spindle axis at 2° from a circular section.

vantageous in this case to follow the two series of extinction positions with monochromatic illumination.

Other special situations arise when a symmetry axis of the indicatrix happens to coincide with the spindle axis, recognized orthoscopically by the fact that no adjustment is necessary on the microscope stage to restore extinction as the grain is rotated about the spindle axis. Again no particular problem is presented, for when either of the bisectrices coincides with the spindle axis, measurements of the maximum and minimum indices encountered in the equatorial series and the one index of the polar series as before furnish the three desired principal indices. When the optic normal coincides with the spindle axis, both optic axes may be seen to pass through the field during rotation about the spindle axis. In the case of optically uniaxial crystals, the values of indices encountered in the equatorial series of extinction positions do not vary. If the crystal is biaxial with low optic angle and low birefringence, the range of index

through the equatorial series of extinction positions might be so small as to go unnoticed in ordinary immersion procedures, and interference figures would be necessary to demonstrate its biaxial character.

Precision

Errors in index of refraction of an anisotropic crystal determined by the immersion method arise mainly from two sources, one the inherent limitations in the sensitivity of the Becke line or its allied effects, and the other the misorientation of the optical indicatrix. With sodium light, small intervals of spacing of index liquids, and close attention to temperature corrections, the error from the first source may probably be held to $\pm .001$. With double variation techniques under favorable conditions it may be held perhaps to $\pm .0002$ (Emmons, 1943) or with additional special techniques perhaps to $\pm .0001$ (Saylor, 1935, Micheelsen, 1957).

In the orthoscopic procedure outlined above it seems clear that the chances of errors in principal index due to misorientation are small, since in following it carefully one cannot avoid passing through each of the principal indices as maximum or minimum values of index in one or the other series of extinction positions. The errors of determination of indices therefore reduce mainly to those of the particular immersion method employed. (It is worth noting that this technique may also be used on the universal stage for confirming or refining the accuracy of the principal indices of refraction obtained at oriented settings.) The orthoscopic procedure of Joel and Garaycochea (1957) for finding the positions of α, β and γ likewise appears to be very precise, provided errors do not enter during the plotting and reading off of the proper settings. The orthoscopic procedure of Vedeneeva (1937) and Kolotushkin (1940) may be made to furnish precise values for α and β, but the setting for β and thence the value of the index β is subject to some uncertainty because it is derived from the orientations of α and γ determined at very flat minima and maxima of index.

In the conoscopic procedure the chances of error due to misorientation would appear greater than in the orthoscopic procedure described above, since it depends on the positioning of sometimes broad and diffuse isogyres. On the basis of tests described below, however, it is concluded that the actual error of index of refraction due to misorientation in most cases is smaller than that of all but the most precise immersion methods, so that it usually is not a matter of great concern. This may be illustrated by the case in which the optic plane of the crystal is perpendicular to the spindle axis. The index then varies with angular distance from α or γ according to the equation of the ellipse as written out in Fig. 5.

To enable general application, it is convenient to represent error in

index due to misorientation as a percentage of the birefringence, and on this basis the two curves of Fig. 5 are plotted against the angular divergences from the correct setting. It is seen that the percentage error is very slight for the first degree or so of misorientation and increases at an increasing rate for succeeding increments. Taking as an example a crystal of extreme birefringence, say .100, and placing the optic plane in the NS position with γ at 2° from its correct horizontal position, a very exact measurement of the index of refraction would give a result differing from true γ by 0.13 per cent of the birefringence of that NS section, or an index of refraction that is .00013 too low. With γ placed 4° off, the index measured would be .00054 too low. Similarly a divergence of 4° from the correct setting for α would lead to an index about .00044 too high. It should be noted that, since in this example the crystal has been mounted with the optic plane perpendicular to the spindle, these represent the maximum errors that might be encountered due to these amounts of angular misorientation of this crystal. The error in index for

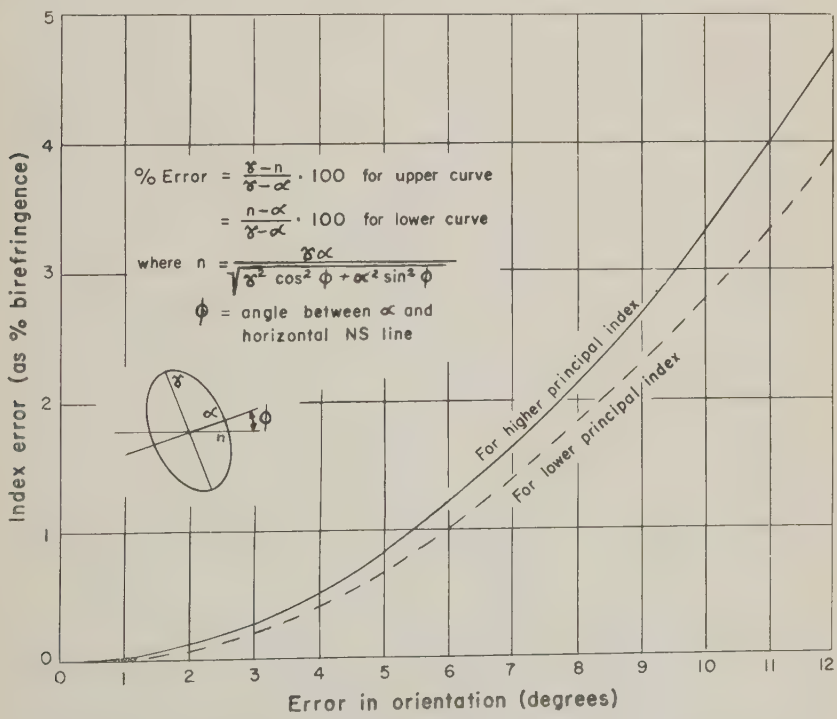

Fig. 5. Error in principal index of refraction due to misorientation in the optic plane, expressed in terms of percent of total birefringence.

the same amount of misorientation in any other cross section of this crystal would be less, usually much less, since the erroneous settings follow courses of smaller variation of index than that of the optic plane. Likewise for other crystals of smaller birefringence the analogous errors in index would be proportionately less.

The question of what amount of angular error may be expected in orienting a grain by the conoscopic method cannot be answered precisely, but it is instructive to compare such orientations with those obtained on the universal stage. For this a special miniature model of the spindle stage similar to that described at another place (Wilcox, 1959) was made as follows: A hole was bored in a thin 1×2-inch brass plate and a slot cut to accommodate a spindle made of a small sewing needle of diameter equal to the thickness of the plate, and a plate-size coverglass was cemented to the bottom of the plate. After mounting the crystal grain on the spindle it was placed in the slot with a few drops of immersion liquid, and a large coverglass was slid over the cavity, taking care not to trap bubbles. The device was then clipped to the microscope stage and the grain oriented conoscopically, as described earlier, to a position in which an isogyre lay symmetrically along the EW crosshair. Thereupon the spindle was secured with a small drop of glue at the end of the slot, and, after the glue had hardened, the plate-and-spindle assembly was transferred with due care to a 5-axis universal stage on another microscope. There the orientation of the grain was carried out independently by rotations about the axes of the universal stage without disturbing the spindle. A measure of discrepancy between the results of the two methods was given by the reading on the scale of the appropriate horizontal axis of the universal stage (here the Inner East-West axis). In all cases the reading of the vertical axes - the microscope stage for the device alone and the Inner Vertical axis for the universal stage—turned out to be within a degree of each other, about the precision with which the transfer could be made.

The results of such tests on six crystalline substances of moderate to large optic angle are summarized in Table 1. Of the eighteen determinations, the largest discrepancy was 4°, for α of a strongly colored hedenbergite of optic angle $(+)2V = 58°$. A discrepancy of 3° was found in the setting for γ of sucrose of optic angle $(-)2V = 47°$. For all remaining settings the divergence was 2° or less. No minerals of optic angle smaller than 40° were tested, since for these, accurate distinction between the obtuse bisectrix and optic normal becomes increasingly difficult with either the spindle stage or universal stage. Since it is not known what the true orientations should be in the cases tested, we cannot tell whether those of the universal stage are any closer than those of the spindle. The

striking feature, however, is that they do correspond so closely, and to me this suggests that both instruments are capable of about the same precision, and that it is fairly good.

If it be assumed for comparative purposes, however, that the universal

TABLE 1. ANGULAR DIFFERENCES BETWEEN ORIENTATIONS OF OPTICAL SYMMETRY AXES USING SPINDLE STAGE AND USING UNIVERSAL STAGE

Crystal, birefringence, and 2V	Symmetry axis horizontal NS	Appearance of isogyre on EW crosshair	Difference (universal stage reading on IEW axis)
Olivine	α	broad	1°S
.037	β	narrow, optic axis at west edge of field	0°
−84°	γ	broad, Bx_a east of center	2°S
Montecellite	α	Bx_o centered	2°S
.020	β		1°S
−73°	γ	broad	0°
Hedenbergite	α	broad	4°N
.025	β	broad, optic axis beyond west edge of field	2°S
+58°	γ	broad, Bx_o east of center	0°
Sucrose	α	"flash figure" east of center	1°S
.032	β	narrow, optic axis just west of center	1°N
−47°	γ	broad	3°N
Wollastonite	α	"flash figure"	1°S
.014	β	narrow, optic axis just beyond west edge of field	1°N
−41°	γ	moderately narrow isogyre	1°S
Barite	α	broad	1°S
.012	β	Bx_o east of center	0°
+40°	γ	"flash figure"	1°S

stage orientation was correct, the error of index may be estimated. Had the presumed 4° error of orientation of α of the hedenbergite been in the optic plane, the index α as determined on the spindle device would have been about .0001 too high. Since it was not in this plane, but in some non-planar figure of much less severe variation, the error would amount to something appreciably less than .0001. Similarly, the presumed 3° error in the setting for γ of the sucrose implies that the error of index would be something less than .0001. Those of the other tested crystals would be even less. Such amounts of error are dwarfed by the inherent

errors in routine work using the Becke effects and hence may be considered negligible. For crystals of higher birefringence, the generally narrower isogyres permit more precise orientation and hence should keep the error of index correspondingly low.

From this it appears that the precision of determination of a principal index at a setting established conoscopically on the spindle would not be much different than that on the universal stage, and, although the absolute angular accuracy of neither method has been determined, it is probably very good for practical purposes. Should extreme accuracy be required, the results may be refined to the limit of accuracy of the particular immersion method by use of the orthoscopic procedure. Nevertheless, one should not fail at the same time to take advantage of the very direct information concerning the other optical properties of the crystal available from interference figures.

Additional Applications

The spindle device can be used to determine other properties and may be of help in any problem requiring viewing the fragment in different positions. Both indicatrix and crystallographic elements, for instance, may be plotted stereographically in relation to the spindle axis and microscope axis using readings of the spindle scale and microscope stage taken at the horizontal NS position of each *linear* element. Thus a symmetry axis, α, β, or γ is horizontal NS when an isogyre is placed symmetrically along the EW crosshair, and the pole of a crystallographic plane (cleavage or crystal face) is horizontal NS when the plane is rotated into a vertical EW position.

The optic angle may be determined on the same grain as the indices of refraction if the indicatrix axes are oblique to the spindle axis. (Only exceptionally will the optic plane be perpendicular to the spindle axis, thus in position to measure the optic angle directly in the manner of Wood and Ayliffe, 1935). One first plots the extinction curves and positions of the indicatrix axes by the method of Joel and Garaycochea (1957), then chooses plausible optic angles and tests them by Fresnel constructions. This leads quickly to the correct optic angle, whose constructed extinction positions fall on the observed extinction curve. Although based on the same principal as the Berek-Dodge indirect method with the universal stage (Emmons, 1943, p. 58), this spindle stage procedure does not require the rotational corrections which make the Berek-Dodge method and that of Joel and Muir (1958*b*) difficult and sometimes fruitless for crystals of high birefringence. The method furthermore appears to have greatest sensitivity with optic angles near 90°, just the ones most difficult to measure directly on the universal stage. A more precisely con-

structed spindle scale than used here, together with refinements in establishing exact extinction positions, would seem necessary to achieve the full accuracy of this method. The spindle stage may of course also be used to obtain favorable orientations for determination of optic angle by the conoscopic methods described by Becke (1905*b*), Tertsch (1940), Johannsen (1918, p. 418, 467) and recently by Kamb (1958), and precisely determined principal indices furnish a calculated value of optic angle (Wright, 1951).

I have used the double-variation technique to a limited extent with a temperature-control cell of the Vigfusson (1940) type, modified to hold a spindle.* The results of this work were highly satisfactory and, together with considerations of accuracy discussed above, lead me to conclude that the double-variation technique is quite feasible for use with the spindle stage. Further, a miniature of the spindle device may be constructed very simply for use on the universal stage (Wilcox, 1959) and enables rotation of the grain into positions for direct measurements of all three principal indices of refraction as well as increasing the possible cone of observation of the grain for determination of other optical and crystallographic properties.

Dispersion of the principal indices may be found using the spindle stage by precise determinations of each principal index of refraction for different wavelengths. Dispersion of the optic axes and bisectrices may be estimated in the usual manner from the appearance of the interference figures in white light, or the dispersion can be explored quantitatively with variable monochromatic light by interference figures and by tracing the extinction positions at different wavelengths.

An inexpensive microrefractometer is provided by mounting a known crystal with its optic plane perpendicular to the spindle axis (Wood and Ayliffe, 1935). The index may be calculated from the equation of the ellipse, using the angle of rotation from α or γ to the position of match with the unknown liquid. Actually with proper calibration, it should not be necessary to make the optic plane perpendicular to the spindle axis, and a uniaxial would serve as well as a biaxial crystal.

As a teaching aid in optical crystallography the spindle stage with a few judiciously mounted crystals enables the student to familiarize himself with a wide range of interference figures, to see their interrelations, and thence to put to good use the variety of off-center figures he will encounter in working with thin sections and random immersion mounts. The optical behavior of a crystal under conoscopic illumination may be

* This cell was constructed by Lyman Nichols, Fort Collins, Colo., according to specifications.

compared directly to that under orthoscopic illumination, and the operation of the Biot-Fresnel law, which is so fundamental in applied crystal optics, may be convincingly demonstrated. The simplicity of the spindle device makes it within the reach of many teaching laboratories that could not afford more elaborate rotating devices, and within the capability of the student to construct himself if needed later in his career.

Acknowledgments

I am indebted to colleagues in the U. S. Geological Survey for helpful suggestions and discussions based on experience with various models of this device, to I. J. Mittin for translations of the Russian literature, to Elmer Wehrly for construction of spindle stages as illustrated in Fig. 1. and to B. F. Leonard. Constructive criticisms of an early draft of the manuscript were received from Prof. R. C. Emmons and Prof. R. M. Gates of the University of Wisconsin.

References

Becke, F., 1905*a*, Die Skiodromen. Tschermaks Min. Petr. Mitt., **24,** 1–34.

———, 1905*b*, Achsenwinkelmessung aus der Hyperbelkrümmung. *Tschermaks Min. Petr. Mitt.*, **24,** 35–45.

Bernal, J. D., and Carlisle, C. H., 1947, A simple stage goniometer for use in connexion with X-ray crystal analysis: *Jour. Sci. Instruments, London*, **24,** 107.

Bryant, W. M. D., 1932, Optical properties of some derivatives of lower aliphatic alcohols and aldehydes: *Am. Chem. Soc. , Jour.*, **64,** 3758–65.

Duparc, F., and Pearce, F., 1907, Ueber die Auslöschungswinkel der Flächen einer zone: *Zeit. f. Krist.*, **42,** 34–46.

Emmons, R. C., 1943, The universal stage: *Geol. Soc. America, Mem.* **8,** 1–205.

Hartshorne, N. H., and Stuart, A., 1950, Crystals and the polarizing microscope: 2d edition, Arnold, London, p. 1–473.

Hartshorne, N. H., and Swift, P. M., 1955, An improved single-axis rotation apparatus for the study of crystals under the polarizing microscope: *Royal Microscope Soc., Jour.*, **75,** 129.

Joel, N., 1950, A method to determine the indicatrix of small crystals: *Mineral. Mag.*, **29** (1950–52), 206–214.

Joel, N., and Garaycochea, Isabel, 1957, The "extinction curve" in the investigation of the optical indicatrix: *Acta Cryst.*, **10,** 399–405.

Joel, N., and Muir, I. D., 1958, New techniques for the universal stage. II. The determination of 2V when only one optic axis is accessible: *Mineral. Mag.*, **31,** 878–882.

Johannsen, Albert, 1918, Manual of petrographic methods: McGraw-Hill, New York, 1–649.

Kamb, W. B., 1958, Isogyres in interference figures: *Am. Mineral.*, **43,** 1029–1067.

Kolotushkin, A. G., 1940, Ismerenie͡ glavnykh pokazatelei prelomleniia͡ mikrokristallov metodom vrashchiuuschcheisia͡ igly [Measurement of the principal indices of refraction of microscopic crystals by the rotating needle method]: *Trudy Vses. Nauchno-Issled. Inst. Mineral. Syr'ia͡*, fasc. **165,** 56–66.

Micheelsen, Harry, 1957, An immersion method for exact determinations of refractive indices: *Meddel. Dansk Geol. Foren.*, **13,** 177–191.

Rawlins, F. I. G., and Hawksley, C. W., 1934, A cell for refractivity measurements on minute crystals: *Jour. Sci. Instruments, London*, **11,** 282–284.

Rosenfeld, J. L., 1950, Determination of all principal indices of refraction on difficultly oriented minerals by direct measurement: *Am. Mineral.* **35,** 902–905.

Saylor, C. P., 1935, Accuracy of microscopical methods for determining refractive index by immersion: *Nat. Bur. Standards, Jour. of Research,* **15,** 277–94.

Schumann, Hilmar, 1948, Über den Einfluss relativ starker selektiver Absorption auf konoskopischer Bilder: *Neues Jahrb. Min., Monatshefte,* Abt. A, für 1945–48, 100–6.

Steinbach, Betty J., and Gibb, T. R. P., Jr., 1957, Device for orienting small crystals under the microscope: *Analytical Chemistry,* **29,** 860.

Tatarskii, V. B., 1951, K praktike metoda vrashchaĭuschcheisi͡a igly [Application of the rotating needle method]: *Zapiski Vses. Mineral. Obshchestva,* ser. 2, pt. 80, p. 293–296.

Tertsch, Hermann, 1940, Becke's Achsenwinkel Bestimmung des Hyperbelkrümmung unter Verwendung des Schraubenmikrometer-Okulars: *Zentrbl, f. Min., Geol. u. Pal. Abt. A,* Jahrg. **1940,** 166–174.

Vedeneeva, N. E., 1937, Laboratornoe rukovodstvo po immersionnomu metodu. [Laboratory manual for the immersion method]: *Trudy Vses. Nauch.-Issled. Inst. Mineral. syr'i͡a, fasc.* no. **124,** 1–68.

Vedeneeva, N. E., and Kolotushkin, A., 1934, Determination of the main refractive indices of crystal grain by means of a rotating needle: *Trudy Inst. Prikladnoi Mineralogii, Moscow,* no. **61,** 19–20 (English summary p. 26–27).

Vigfusson, V. A., 1940, Equipment for the double variation method of refractive index determination; 1, An improved cell; 2, Variable temperature control apparatus: *Am. Mineral.* **25,** 763–766.

Wilcox, Ray E., 1959, Universal stage accessory for direct determination of the three principal indices of refraction: *Am. Mineral.,* **44,** 1064–1067.

Wood, R. G., and Ayliffe, S. H., 1935, An instrument for measuring the optical constants of small crystals: *Jour. Sci. Instruments, London,* **12,** 194–196.

Wright, F. E., 1951, Computation of the optic angle from the three principal refractive indices: *Am. Mineral.,* **36,** 543–556.

Manuscript received March 31, 1959.

NOTES AND NEWS

AN OCCURRENCE OF GENTHELVITE IN THE YOUNGER GRANITE PROVINCE OF NORTHERN NIGERIA*

O. VON KNORRING† AND P. DYSON‡

INTRODUCTION

Genthelvite, the zinc member of the helvite group is an extremely rare mineral and has so far been recorded only from three localities in El Paso County, Colorado.§ The original specimen was discovered by F. A. Genth in the 1890's and subsequently two additional crystals were reported by Glass and Adams (1953) and by Scott (1957). A notable amount of genthelvite has, however, recently been found by one of us (P.D.), during a field investigation of one of the economically important columbite-bearing members of the Younger Granite suite in Northern Nigeria, and the occurrence is of particular importance:

1. In view of the extreme rarity of the mineral;
2. As the first recorded occurrence of a beryllium mineral associated with the Nigerian Younger Granites, although beryl is not rare in the Basement Complex of the territory;
3. If present in commercial quantities it could represent a potential ore of beryllium since, unlike beryl, its physical properties are such that it would be amenable to recovery by conventional mineral dressing methods.

LOCATION AND FIELD RELATIONS

The genthelvite is associated with the later members of the granitic suite that make up the Jos-Bukuru complex in Northern Nigeria. Studies of this and other complexes have been made recently by MacLeod (1954) and by Jacobson, MacLeod and Black (1958) and no further general details will be given here. The exact location of the occurrence is 9°50′ N. and 8°55′ E.

The country rock consists of albitized granite which is intensely decomposed by deep weathering and has been exploited as a source of columbite (Williams and others, 1956).

The genthelvite has been found in different associations at two adjacent localities which are only a hundred feet or so apart. The first occur-

* Publication authorized by the Directors of A. O. Nigeria, Ltd.

† Research Institute of African Geology, University of Leeds.

‡ Formerly of A. O. Nigeria Ltd., P.O. Jos, N. Nigeria.

§ E. M. Eskova has recently described a manganese-rich genthelvite from alkaline pegmatites in Kola peninsula. (Doklady Acad. Sci. U.S.S.R., 1957, 116, 481–483).

rence is within a rather irregular vein of almost pure albite which intersects the later of two albite-biotite granites and runs close to and parallel with the contact. This vein contains irregular rounded masses or "knots" of genthelvite, usually about four inches in diameter, but locally as much as seven inches across. In a single instance the "knot" was embedded in the wallrock, but still in contact with the vein on one side. Occasionally the knots consist of pure genthelvite, but commonly the outer part, or the whole, is partially replaced by albite. A selvedge of mica, related to protolithionite-zinnwaldite from 0.5 to 2 cm. thick, with accessory thorite, invariably surrounds the nodules which, from their mode of occurrence, suggest that they have not crystallized in situ, but are xenoliths in the albitic magma in relatively early stages of digestion. They may, in fact, have been derived from a disrupted pegmatite, similar to that described below.

FIG. 1. X-ray powder photograph of genthelvite from Jos, Northern Nigeria. The three strongest lines are 3.33A, 2.174A and 1.918A. CuK radiation, Camera diameter 9 cm.

A hundred feet away from the albite vein in the pegmatitic contact zone between the two albite-biotite-granite phases is the second occurrence in coarse pegmatites containing green amazonite microcline. Most of the genthelvite is coated superficially and along cracks with an unusually bright red laterite. No crystal forms are visible in the masses which are generally not more than one or two inches across at most. They are far more irregular than those in the albite vein and appear to be interstitial in texture. The mica selvedge is generally, but not invariably, present and may be altered to a dull black material not further investigated. No genthelvite has been found in any of the other numerous albite veins or microcline pegmatites in the area.

Mineralogy and Chemistry

The genthelvite in the knots is intimately intergrown with albite. It is granular (sugary) in appearance and resembles massive garnet as found in skarns or tactites. The individual grains are irregular in shape and are generally 1–3 mm., across, but larger masses of the mineral are also quite common. The color is purplish-pink, rather like that of almandine garnet. It is brittle and translucent with resinous luster and has a hardness of about 6. In thin section the irregular grains of genthelvite are greyish

Table 1. Chemical Composition of Genthelvite from Jos, N. Nigeria Compared with Genthelvite from W. Cheyenne Cañon

	1	2
SiO_2	30.70	30.26
TiO_2	n.d.	—
Al_2O_3	0.18	0.51
BeO	12.39	12.70
FeO	11.73	6.81
MnO	1.72	1.22
ZnO	40.56	46.20
MgO	tr.	—
CaO	tr.	—
Na_2O	tr.	—
S	5.50	5.49
	102.78	103.19
Less O≡S	2.74	2.74
	100.04	100.45

1. Genthelvite from Jos, N. Nigeria. Analyst: O. von Knorring.
2. Genthelvite from W. Cheyenne Cañon. Analyst: F. A. Genth (Glass *et al.*, p. 180, 1944)

Atomic ratios to 13 (O+S), anal. 1, and excluding Al_2O_3 as albite impurities:

$$(Zn_{2.94}Fe_{0.96}Mn_{0.14})Be_{2.92}Si_{3.02}O_{11.99}S_{1.01}$$

or very nearly $Zn_3FeBe_3Si_3O_{12}S$.

Table 2. Chemical Composition of Protolithionite Associated with Genthelvite from Jos, N. Nigeria

Analyst: E. Padget

SiO_2	41.11	Li_2O	1.85
TiO_2	0.30	H_2O^+	1.12
Al_2O_3	16.59	H_2O^-	0.29
Fe_2O_3	2.00	F	5.49
FeO	22.61	Cl	tr.
MnO	0.67		102.24
MgO	0.13	Less O≡F	2.31
CaO	n.d.		99.93
Na_2O	0.16		
K_2O	9.92		

Atomic ratios to 24 (O, OH, F):

$$(K_{1.94}Li_{1.06})(Fe_{2.90}^{2+}Mn_{0.09}Mg_{0.03}Na_{0.05}Li_{0.08}Al_{1.30}Fe_{0.23}^{3+}Ti_{0.03})$$
$$(Si_{6.30}Al_{1.70})O_{20.19}OH_{1.15}F_{2.66}$$

in color, isotropic and intersected by numerous cracks. Some aggregates, however, show triangular outlines which are emphasized by the enclosing albite laths. Inclusions of columbite, zircon and cassiterite are common, and in addition thorite (orangite) has been identified. The following properties were determined on genthelvite: specific gravity (Berman balance) $3.62 \pm .01$; $n = 1.745 \pm .002$. *X*-ray diffraction data are given in Table 3.

The dark-gray mica which envelops the genthelvite knots also contains albite, and, at times, narrow bands of albite and some micro-perthite rimmed with mica intersect the knots and replace the genthelvite.

Table 3. *X*-Ray Diffraction Data for Genthelvite from Jos, N. Nigeria
Cu-Kα radiation, camera diameter, 9 cm.

d meas. Å	I estimated	d meas.	I estimated	d meas. Å	I estimated	d meas.	I estimated
4.07	m	1.778	w	1.258	s	.989	w
3.65	m	1.735	w	1.230	w	.973	w
3.33	vs	1.663	s	1.215	w	.961	w
2.875	m	1.596	m	1.200	w	.948	w
2.577	s	1.513	w	1.176	w	.936	w
2.351	m	1.489	s	1.152	w	.923	w
2.258	w	1.441	s	1.119	w	.911	w
2.174	vs	1.399	s	1.109	s	.900	w
2.036	m	1.359	s	1.072	w	.890	w
1.918	vs	1.322	s	1.035	m	.880	w
1.822	s	1.288	w	1.004	s	.860	vs

w = weak; m = medium; s = strong; vs = very strong. Calculated unit cell size $a_0 \simeq 8.12 \pm .01$ Å.

Under the microscope the mica appears to be uniaxial with distinct pleochroism: X = light yellow and Y = Z = pale green. Some grains contain inclusions of zircon surrounded by pleochroic haloes. The following physical properties were determined on the mica: Specific gravity $3.17 \pm .01$ (by suspension in Clerici solution) $\beta = \gamma = 1.612 \pm .002$. The chemical analysis of genthelvite is given in Table 1. In comparison with the analysis of the original genthelvite from W. Cheyenne Cañon, the present one is poorer in zinc, and richer in iron and to some extent in manganese. The analysis of the associated mica is given in Table 2. It is a lithium-iron mica, closely related to zinnwaldite and containing a large amount of the protolithionite component of the lepidolite series.

REFERENCES

Glass, J. J., Jahns, R. H., and Stevens, R. E. (1944). Helvite and danalite from New Mexico and the helvite group. *Am. Mineral.*, **29**, 163–191.

Glass, J. J., and Adams, J. W. (1953). Genthelvite crystal from El Paso County, Colorado. *Am. Mineral.*, **38**, 858–160.

Jacobson, R. R. E., MacLeod, W. N., and Black, R. (1958). Ring Complexes in the Younger Granite province of Northern Nigeria. *Geol. Soc.*, London, Memoir 1, 1–72.

MacLeod, W. N. (1954). The Geology of the Jos-Bukuru complex with particular reference to the distribution of columbite. *Rec. Geol. Survey Nigeria*, 17–34.

Scott, G. R. (1957). Genthelvite from Cookstove Mountain, El Paso County, Colorado. *Am. Mineral.*, **42**, 425–429.

Williams, F. A., Meehan, J. A., Paulo, K. L., John, T. U., and Rushton, H. G. (1956). Economic geology of the decomposed columbite-bearing granites, Jos. Plateau, Nigeria. *Econ. Geol.*, **51**, 303–332.

THE AMERICAN MINERALOGIST, VOL. 44, NOVEMBER–DECEMBER, 1959

AN OCCURRENCE OF PSEUDOMALACHITE AT SAFFORD, ARIZONA

C. Osborne Hutton, *Stanford University, California*

Occurrence

Occurrences of the basic copper phosphate—pseudomalachite—have been recorded in only a few instances from United States localities, and some of the better known of these include the following: the Wheatley Mines, Chester Co., and the Ecton and Perkiomen Mines, Montgomery Co., Pennsylvania, Carbarrus Co., N. Carolina (Palache *et al.* 1951, p. 800); Black Pine Tungsten Project, Maxville, Montana (Kauffman *et al.* 1950, p. 19); the Empire-Nevada Mine, Yerrington, Nevada (Berry, 1950, p. 367). Other localities at which this mineral may have been recognized include the Calavada Mine, Nevada where Goudey (1945, p. 640) has described dihydrite, and the Silver Bell Mine, Lincoln, Nevada where Kauffman *et al.* (1950, p. 15) have noted the occurrence of a mineral described by them as tagilite. Dihydrite and tagilite are included here since most of the minerals so named and studied by Berry (1950) have been shown by him to have the properties of pseudomalachite.

Examination of the minor accessory minerals in some metasomatized latites, andesites and similarly altered volcanic rocks from Safford, Graham Co., Arizona, has led to the recognition of a number of interesting minerals, one of which is pseudomalachite. In view of the comparative rarity of this mineral in the United States it seems desirable that the occurrence be placed on record.

The copper phosphate is associated with the following minor constituents: malachite, brochantite, antlerite, carbonate-apatite, chrysocolla, jarosite, lepidocrocite, and a variety of other oxides of iron, covellite, chalcopyrite, pyrite, and a deep blue cupriferous mineral that has not been satisfactorily diagnosed so far.

Physical Properties

Pseudomalachite is found in centrifuged concentrates as broken prismatic crystals, many of which are almost hair-like in size, and occasional fragments appear to be portions of radiating aggregates with wavy extinction. The mineral has a more decidedly green color than that of the associated brochantite with which it may be easily confused upon first inspection. The mineral is notably attracted and concentrated, but not exclusively so, by the Frantz Separator at approximately 0.6 amps (slope 15°, tilt 8°), and for material concentrated in this way the following optical properties and other physical data have been determined:

$\alpha = 1.791 \pm 0.002$.	X = pale green
$\beta = 1.856$	Z = green with a trace of a bluish tinge in some instances.
$\gamma = 1.867$	Z > X, marked.
$\gamma - \alpha = 0.076$	S. G. (22°C.) = 4.32 ± 0.02
2V = 48° (−)	Dispersion very faint with $\rho < v$.

These data agree quite closely with those reported by Barth and Berman (1930, p. 32, Table 3, No. 5) for ehlite from Ehl-on-Rhine and by Chukhrov (1950) for colloform ehlite (=pseudomalachite) from Altyntyube, Kazakhstan. Furthermore, the absence of arsenic, as shown by microchemical tests, supports the conclusion that the phosphate is an end-member of the pseudomalachite-cornwallite series.

In view of the dominant form displayed by crystal fragments of the mineral, some care was taken to prepare a specimen for *x*-ray diffraction so that the powder pattern yielded by the mineral would not exhibit any preferred orientation effects whatsoever. The pattern yielded by the Safford mineral is set out in Table 1, and it is compared there with the powder data recorded by Berry (1950, p. 377) for pseudomalachite from three localities in Germany. At angles greater than about 72° 2 θ the reflections become very faint and quite diffuse, but nevertheless sufficient density was developed to permit a check on film shrinkage.

The *d*-spacings and estimated intensities of the two powder patterns are very similar, with the following exceptions:

(1) The films yielded by pseudomalachite from Safford exhibit several faint reflections that are not listed by Berry (1950, p. 377), but it must be noted that that writer specifically states that he omitted on purpose, from his table, a few weak reflections that were observed by him on one film.

(2) The intensity of the reflection at $d = 3.02$ Å. (<1) in the film yielded by the Safford mineral is very much weaker than that for the corresponding line listed by Berry, *viz.* 3.04 (2).

(3) Berry lists a single line at 2.42 Å with an intensity of 6; in films of Safford pseudomalachite a distinct doublet may be observed at this point,

and this situation is also the case for the present writer's films of pseudomalachite from Rheinbreitbach, Germany (Specimen No. 22,188).

Prismatic fragments mounted for rotation about the length of the crystals yielded *b*-axis photographs, but the particles were found to con-

TABLE 1. *X*-RAY POWDER PATTERNS OF PSEUDOMALACHITE

Camera diameter: 114.59 mm. $Cuk_\alpha = 1.5418$ Å. Spacings corrected for film shrinkage. Cut-off = 18 Å approximately.

1		2		1		2	
d meas.	I	*d* meas.	I	*d* meas.	I	*d* meas.	I
8.51	<1	—	—	1.855	3	1.854	2
4.78	1	4.75	½	1.816	1	—	—
4.49	10	4.48	10	1.791	1	—	—
3.46	5	3.46	5	1.765	4	1.763	4
3.34	<1	—	—	1.730	5	1.728	5
3.256	<1	3.27	½	1.703	1	—	—
3.11	4	3.12	2	1.692	1	—	—
3.05	3	3.09	4	1.670	2	1.670	2
3.02	<1	3.04	2	1.624	2	1.624	1
2.98	4	2.97	4	1.595	3	1.597	2
2.92	3	2.93	3	1.575	1	—	—
2.867	1	2.85	1	1.560	4	1.559	4
2.832	1	—	—	1.527	3	1.527	2
2.724	3	2.72	3	1.505	2	1.498	2
2.700	1	—	—	1.492	1	1.491	2
2.561	2	2.56	1	1.464	2	1.462	1
2.468	3	—	—	1.433	3	1.431	3
2.443	6	2.42	6	1.417	2	1.419	3
2.418	6			1.395	3	1.392	4
2.386	7	2.39	8	1.384	1	—	—
2.324	5	2.32	5	1.366	1	1.365	1
2.234	4	2.23	5	1.347	2	1.350	2
2.196	1	2.19	1	1.332	3	1.335	3
2.129	1	2.12	1	1.320	1	1.319	2
2.094	2	2.09	3	1.310	2	1.310	3
2.018	1	2.01	1	1.212	1	1.212	1
1.993	1	—	—	1.197	1	1.196	1
1.961	1	1.963	2	1.075	1	1.076	½
1.945	<1	1.939	1	1.040	2	1.039	3
1.906	<1	—	—	—	—	1.014	3

1. Pseudomalachite, Safford, Graham County, Arizona. A number of faint, diffuse lines follow after the last spacing listed but they could not be measured with precision.
2. Pseudomalachite (Berry 1950, p. 377, Table 8). Average of measurements from three films yielded by the phosphate from German localities. Berry lists fifteen additional spacings after the line at 1.014 Å.

sist of bundles of fibers, rather than fragments of single crystals, with common *b*-axes and *a* and *c* in disorientation. Measurements of the rotation films gave an uncorrected value of 5.77 Å, but Weissenberg films for the same axis of rotation could not be interpreted.

Acknowledgments

The writer is much indebted to Mr. Annan Cook and to the Directors of the Kennecott Copper Corporation for permission to record the data set out herein.

References

Barth, T. and Berman, H. (1930), Neue optische Daten wenig bekannter Minerale. (Die Einbettungsmethode), *Chemie der Erde*, **5**, 22–42.

Berry, L. G. (1950), On pseudomalachite and cornetite, *Am. Mineral.*, **35**, 365–385.

Chukhrov, F. V. (1950), Ehlite (=pseudomalachite) from the steppe region of Kazakhstan, Doklady Acad. Sci. USSR., **72**, 573–575.

Goudey, H. (1945), Dihydrite from Mineral County, Nevada, *Am. Mineral.*, **30**, 640.

Kauffman, A. J., Mortimore, D. M., and Hess, H. D. (1950), A study of certain uncommon minerals found in the Pacific Northwest, *Bur. Mines, Rept. Invest.* **4721**, 1–22.

Palache, C., Berman, H., and Frondel, C. (1951), The System of Mineralogy, vol. 2, 7th ed., John Wiley and Sons, Inc., New York.

THE AMERICAN MINERALOGIST, VOL. 44, NOVEMBER-DECEMBER, 1959

ON THE STABILITY AND SYNTHESIS OF UVAROVITE, $Ca_3Cr_2Si_3O_{12}$*

F. P. Glasser, *Pennsylvania State University, University Park, Pa.*†

Although uvarovite is not one of the common garnets, even a relatively scarce mineral may be a valuable indicator of P-T conditions prevailing during the formation of assemblages containing that mineral. The stability limits of the indicator mineral must, of course, be known. Thus the experimental mineralogist has advanced his goal from the mere synthesis of naturally-occurring minerals to determining the P-T-X stability limits of the phase. To this end, experimenters have a wide variety of equipment permitting studies to be made at high temperature, high pressure, or at simultaneous high pressures and high temperatures. The synthesis of a mineral at some convenient pressure and temperature, however, does not necessarily provide any meaningful information. This is true in the case of several recent reports dealing with the synthesis of uvarovite.

* Contribution Number 58-127, Mineral Industries Experiment Station, College of Mineral Industries, Pennsylvania State University, University Park, Pennsylvania.

† Present address, Chemistry Dept., University of Aberdeen, Old Aberdeen, Scotland.

Synthesis of uvarovite was first reported by Hummel (1) who prepared it by heating an oxide mixture at several temperatures between 885° and 1490° C. Uvarovite was produced at temperatures up to 1400° C., but not at 1490° C. In a later investigation, Glasser and Osborn (2) confirmed this synthesis of uvarovite, and delineated its stability role in the system CaO-Cr_2O_3-SiO_2. The following facts were established:

1. The maximum stability temperature of uvarovite is $1370° \pm 10°$ C. It is readily synthesized from a variety of starting materials, including crystalline mixtures of $(CaO+SiO_2+Cr_2O_3)$ or $(CaSiO_3+Cr_2O_3)$, or a gel of appropriate composition. The reaction

$$CaSiO_3 + Cr_2O_3 \underset{1370° \pm 10}{\overset{1 \text{ atm.}}{\rightleftharpoons}} Ca_3Cr_2Si_3O_{12}$$

   is readily reversible with only a small hysteresis. The temperatures reported were measured with calibrated platinum vs. platinum rhodium thermoelements, using controlled temperature furnaces for the equilibration runs.
2. No appreciable solid solution exists between uvarovite and any other component in the CaO-Cr_2O_3-SiO_2 system.
3. No evidence was found to indicate that uvarovite would again break down at lower temperatures.

This work is in contradiction with that of Geller and Miller (3), who report the synthesis of uvarovite. They prepared uvarovite from oxide mixtures at 1400° C, and also at a lower temperature. This apparently duplicates the results of Hummel, although Geller and Miller state: "The direct synthesis of this garnet has been reported by Hummel, whose results we have corroborated only in part." The more detailed study by Glasser and Osborn is not mentioned.

Hall (1958) states: "Naturally occurring high pressure minerals other than diamond that have been synthesized in recent years include the garnets: pyrope, andradite, almandite, spessartite, grossularite, and uvarovite. These garnets are easily synthesized from the metallic oxides in the presence of water at pressures ranging from 20,000 to 35,000 atm. at temperatures near 1000° C." The implication that uvarovite, like diamond, is stable only at high pressures is unfounded. Uvarovite—and several other members of the garnet series mentioned above —are "pressure independent" minerals, inasmuch as they also have a thermodynamic stability range at 1 atm. pressure. Hall was apparently unaware of the work of Hummel.

It is hoped that this note will reduce the possibility of confusion arising from recent contradictory reports in the literature concerning the stability of uvarovite, $Ca_3Cr_2Si_3O_{12}$.

References

(1) Hummel, F. A. (1950), Synthesis of Uvarovite, *Am. Mineral.*, **35,** 324–325.
(2) Glasser, F. P., and Osborn, E. F. (1958), Phase Equilibrium Studies in the System CaO-Cr_2O_3-SiO_2, *Jour. Amer. Ceramic Soc.*, **41,** (9), 358–367.
(3) Geller, S., and Miller, C. E. (1959), The Synthesis of Uvarovite, *Am. Mineral.*, **44,** 445–446.
(4) Hall, H. T. (1958), Ultrahigh-Pressure Research, *Science*, **128,** (3322), 445–449.

THE AMERICAN MINERALOGIST, VOL. 44, NOVEMBER–DECEMBER, 1959

DETECTION OF ZONING IN ORTHORHOMBIC AND UNIAXIAL COLORLESS MINERALS

Th. G. Sahama, *Institute of Geology, University of Helsinki, Finland*

In minerals that are colorless or nearly so in thin section, zoning may be revealed by slight differences in refractive indices between the successive zones, by zonal arrangement of inclusions, etc. In monoclinic and triclinic crystals the zoning usually is easily seen between crossed nicols because the position of extinction varies from zone to zone. In orthorhombic and optically uniaxial crystals the detection of slight zoning is often more difficult, especially if the zone boundaries are not quite sharp but gradual. The symmetry of such crystals does not allow any variation in the position of extinction. The use of phase contrast optics with or without nicols will in some instances make the zoning more visible. A successful use of the phase contrast optics is, however, largely limited to cases where the refractive indices of the mineral do not deviate too much from that of the Canada balsam. The applicability of the phase contrast optics into the thin section mineralogy would be greatly facilitated if balsams of different refractive indices would be available. Then the thin section could be made with a balsam that gives the lowest relief with the mineral to be studied.

For studying the minerals contained in the lavas of the Nyiragongo area in the Belgian Congo, a method for detecting and visualizing zoning has been used since some time at this Institute. The method is not new in principle, but is not generally employed. The zoning in many of the main constituents, like in olivine, melilite and nepheline, is very common in the rocks of the area and is petrographically and mineralogically important. Because these minerals are orthorhombic, tetragonal or hexagonal, the zoning is visible between crossed nicols only if the variation of the birefringence is large enough to cause a detectable change in the interference color. This is the case for some of the melilites and, very

rarely, for some olivines. For the most rocks of the area, the differences in the interference colors between the successive zones in these minerals are too slight to be detected by simple observation between crossed nicols. In such cases the rotating (elliptical) mica compensator manufactured by E. Leitz, Wetzlar, was found useful.

The rotating (elliptical) mica compensator is mostly used in detecting and measuring very small retardations such as they are found in biological materials. As an accessory of the petrographic microscope in thin section mineralogy it is mostly neglected. The compensator is usually delivered with a mica plate having a retardation of 1/10 λ to 1/30 λ or, on the other hand, of 1/4 λ. Also thicker plates, up to 1 λ, may be used. The compensator is inserted in the usual slit under the analyzer and the mica plate may be rotated around the microscope axis. The angle of rotation can be accurately read. By turning the compensator plate and the analyzer of the microscope, the retardation may be measured according to the known methods of H. H. Senarmont or D. B. Brace. Provided that the retardation in the mineral does not exceed that of the compensator plate, the method is very accurate and sensitive and, therefore, is recommended especially for minerals with very low birefringence. Because, in contrast to the Berek compensator, the plate of the rotating (elliptical) mica compensator is turned around the microscope axis, it affects the interference color in the same amount throughout the entire crystal.

At this Institute, a 1/4 λ plate was used in the compensator. A plate thinner than that is not suitable for the purpose of studying zoning. In the elliptically polarized light caused by the compensator, the interference colors are very highly sensitive to the positions of the compensator and of the analyzer as well as to the position of the mineral itself. This high sensitivity makes it possible to detect and visualize the extremely slight differences in birefringence between the successive zones. The experience gained has shown that, once the correct positions for the mineral, for the compensator and for the analyzer have been found, a zoning often becomes visible even in crystals that, without the compensator, look completely homogeneous. If, without the compensator, a very slight indication of zoning is observed, the compensator will quite considerably strengthen it.

Because the compensator just causes a detectable difference in the colors between the successive zones, the effect is difficult to show in black-and-white photographs. In a thin section of a tinguaite from Toror Hills, Karamoja, Uganda, a nepheline phenocryst was selected that seemed suitable for photographic illustration of the effect. Fig. 1 reproduces the crystal between crossed nicols without the compensator. The zoning is extremely weakly seen in the section and hardly at all in the photograph.

Fig. 2 shows the same crystal with the same magnification and with the compensator, analyzer and crystal all turned in a most suitable position. The zoning is very strong in the section and well visible in the photograph. Measured with the Berek compensator, the maximum difference in retardation between successive zones was found to be ca. 13 mμ. Taking the thickness of the section as 0.04 mm., this difference in retardation would correspond to ca. 0.0003 in birefringence. It may be

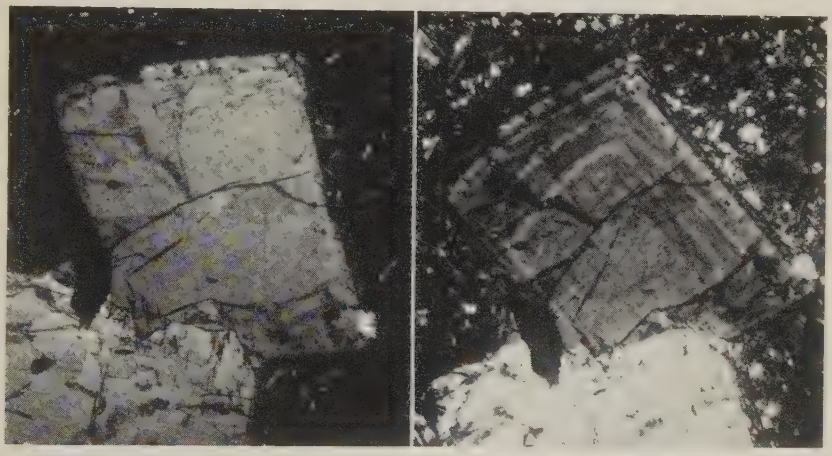

Fig. 1 (Left). Nepheline phenocryst in tinguaite, Toror Hills, Karamoja, Uganda. Nicols+. No compensator. Magnification ca. 25×. Zoning hardly visible in the photograph.
Fig. 2 (Right). The same crystal as in Fig. 1. Nicols slightly inclined. Rotating (elliptical) mica compensator in most suitable position to make the zoning visible.

added that the differences in retardation between successive zones in nepheline, melilite etc. in the Nyiragongo area lavas that are still detectable, are considerably smaller than in the Toror Hills nepheline crystal photographed.

In some instances it was found useful to place a gypsum plate (first order red) between the polarizer and the thin section so that it could be turned around the microscope axis. The simultaneous use of the two compensators, one below and the other above the section, was used especially on studying the zoning of higher birefringent minerals like olivine.

THE AMERICAN MINERALOGIST, VOL. 44, NOVEMBER-DECEMBER, 1959

LOW MAGNIFICATION THIN SECTION PHOTOGRAPHY*

J. MARTIN PULSFORD, *Geological Survey and Museum, London, England.*

Following the recent useful article by F. W. Atchley (1958) a few additional comments may be of use to persons taking photomicrographs at low magnification.

The "trial negative" or step test is by far the best method of determining the correct exposure, but a step test in a geometrical progression rather than an arithmetical progression is more likely to contain the correct exposure. The suggested steps of 3, 6, 9, 12, 15 seconds will give an exposure ratio of only 1:5 but if a progression of 2, 4, 8, 16, 32 seconds is used this will give an exposure ratio of 1:16. Such a step test is made by commencing exposure with the dark slide sheath fully withdrawn, giving an exposure of 2 seconds and then progressively closing the sheath at intervals of 2, 4, 8 and 16 seconds. The last step is thus exposed for $2+2+4+8+16=32$ seconds.

Since for the linear part of the characteristic curve of the emulsion, contrast is a function of development and not exposure, the exposure chosen should be that which produces the correct *density*.

Uneven field illumination is obtained when using a microscope at low magnification and attempting to cover a larger field than that for which the objective was designed. It may easily be compensated for by using a positive printing mask in which the denser parts correspond to the duller parts of the field, normally around the edges. The photomicrographic negative should have sufficient exposure to give satisfactory gradation in the less dense parts but not so much that the central portion is overexposed. This will not be possible if the illumination varies considerably between the center and margin of the field. In such a case the negative should be given the maximum exposure permissible without overexposing the central portion.

The mask is made by exposing a plate in the photomicrographic camera without a subject being present. This plate should be of the same type as that used for the photomicrographic negative and it should have identical processing to obtain the same degree of density variation. A print of this negative on process film is used as the mask, which should have a density of 0.1 or less at the centre and a density range the same as that of the negative from which it was printed. This density range may be controlled by development. If this mask is now placed in contact,

* Publication authorized by the Director, Geological Survey and Museum.

back-to-back with the photomicrographic negatives it will compensate for the density variations and make printing or enlarging a matter of comparative ease. It will not significantly affect definition.

REFERENCE

ATCHLEY, F. W. 1958. Low Magnification Thin Section Photography. *Am. Mineral.*, **43**, 997–1000.

THE AMERICAN MINERALOGIST, VOL. 44, NOVEMBER-DECEMBER, 1959

MAGNETIC SUSCEPTIBILITY OF NATURAL RUTILE, ANATASE, AND BROOKITE

TITUS PANKEY, *Howard University, Washington, D. C., and* FRANK SENFTLE, *U. S. Geological Survey, Washington, D. C.*

Precision measurements of the magnetic susceptibility of synthetic rutile and anatase have recently been made by Senftle and others (in press). On these specially purified forms of TiO_2, magnetic susceptibilities of $(0.067 \pm 0.0015) \times 10^{-6}$ and $(0.040 \pm 0.0003) \times 10^{-6}$ electromagnetic units per gram were obtained for rutile and anatase, respectively. Because of technical difficulties in preparation, it was not possible to prepare magnetically pure brookite; and, hence, no measurements were reported on this crystallographic form of TiO_2.

To compare the susceptibilities of natural crystals with the above data on synthetic crystals and to obtain approximate susceptibility data for brookite, the magnetic susceptibility of natural crystals of these minerals was measured at room temperature. The method of analysis has been described in detail by Senftle and others (1958). In each measurement corrections were made for ferromagnetic impurity by making a 1/H plot previously described. The results are shown in Table 1.

The per cent variation for rutile is significantly less than for anatase, whereas that for brookite is very large. This variation is a function of the purity of the crystals. It is relatively easy to prepare magnetically pure rutile, anatase is considerably more difficult, and as far as is known, no magnetically pure brookite has ever been made. M. D. Beals (National Lead Company, oral communication, 1958) finds that to a large extent the impurity in anatase consists of volatile compounds that are removed above 650° C. when rutile is formed. The higher purity would account for the smaller range in susceptibility of rutile. The higher temperatures, however, convert the impurities to compounds with somewhat higher

susceptibilities. This phenomenon has been noticed when heating otherwise stable minerals to temperatures above 600° C.

Some of the brookite specimens contained a fairly large amount of impurity. Specimen R-2108 showed no ferromagnetic impurity, but the paramagnetic impurities were significant. The inhomogeneous dispersion of the impurities in the crystal was evident in the color change from a light transparent brown to a dark opaque brown, as well as from the spread in the susceptibility observed for several fragments of the same

Table 1. Magnetic Susceptibilities of Natural TiO_2 Minerals

TiO_2 Mineral	U.S. National Museum no.	Location	χ (10^{-6} emu/gram)
Rutile	2063	Blumberg, near Adelaide, South Australia	1.07
	R-2076	Alexander County, North Carolina	0.98
	112990	Brooks Farm, North Carolina	0.95
	52-MT-5*	Beach Sand, Melbourne, Australia	0.91
	45-MT-47*	Beach Sand, Vero Beach, North Carolina	0.83
Anatase	R-2097	Diamantina, Brazil	0.19
	112990	Brooks Farm, North Carolina	0.24
	2103	Tasdatsch, Tavetsch, Switzerland	0.36
Brookite	97016	Magnet Cove, Arkansas	1.15
	1710	Somerville, Massachusetts	0.83
	81463	Ulster County, New York	0.26
	R-2108	Von der Soule viven, Tyrol, Switzerland	0.63–1.53

* U. S. Geological Survey sample numbers.

crystal. The other three specimens of brookite showed weak ferromagnetism, but the impurities were more uniformly distributed.

The specimen from Ulster County, New York (No. 81463) is of particular interest because of its relative purity. Semiquantitative spectrographic analyses showed only silicon and iron in the range of 0.01 to 0.1 per cent, and copper, magnesium, and manganese in the range of 0.0001 to 0.001 per cent. This purity compares with that of the synthetic rutile previously reported. The magnetic susceptibility of 0.26×10^{-6} emu/gram can therefore be considered as an upper limit of pure brookite. However, in view of the low susceptibilities of synthetic rutile and anatase, this value is probably considerably higher than the true value.

The authors wish to acknowledge the generosity of Dr. George Switzer,

U. S. National Museum, who provided most of the crystals. This study is part of a program being conducted by the U. S. Geological Survey on behalf of the Division of Research, U. S. Atomic Energy Commission.

References

Senftle, F. E., Pankey, Titus, and Grant, Frank A. The magnetic susceptibility of the rutile and anatase forms of titanium dioxide. *Phys. Rev.* (in press).

Senftle, F. E., Lee, M. D., Monkewicz, A. A., Mayo, J. W., and Pankey, Titus (1958) Quartz helix magnetic susceptibility balance using the Curie-Cheneveau principle. *Rev. Sci. Instr.* **29**, 429–32.

THE AMERICAN MINERALOGIST, VOL. 44, NOVEMBER-DECEMBER, 1959

NATIVE SELENIUM FROM GRANTS, NEW MEXICO*

Ming-Shan Sun, *Mew Mexico Bureau of Mines & Mineral Resources Socorro, New Mexico* and R. J. Weege, *Uranium Division, Calumet & Hecla, Inc., Grants, New Mexico*

Introduction

In the course of working on a calibration curve for the determination of selenium by an *x*-ray spectroscopic method, a sample containing native selenium was encountered. This sample (No. 760) was collected from the Marquez mine of the Uranium Division, Calumet and Hecla, Inc., in Section 23, T.13N., R.9W., McKinley County, New Mexico, about 20 miles north of Grants.

Occurrence

The native selenium occurs in a claystone gall in the Brushy Basin member of the Jurassic Morrison formation. The Brushy Basin member is generally subdivided into three parts (see Freeman and Hilpert, 1956). The upper part consists mainly of claystone and clayey sandstone. The middle part is largely poorly sorted fine to coarse sandstone with some claystone lenses and galls. The lower part is mostly claystone.

In the Poison Canyon area and in the vicinity of the Marquez mine, the sandstone of the middle part of the Brushy Basin member is usually called Poison Canyon sandstone by local persons. Poison Canyon is about 5 miles due West of the Marquez mine. "Poison Canyon sandstone" has not been accepted as an official stratigraphic name, although it has

* Published with the permission of the Director, New Mexico Bureau of Mines and Mineral Resources.

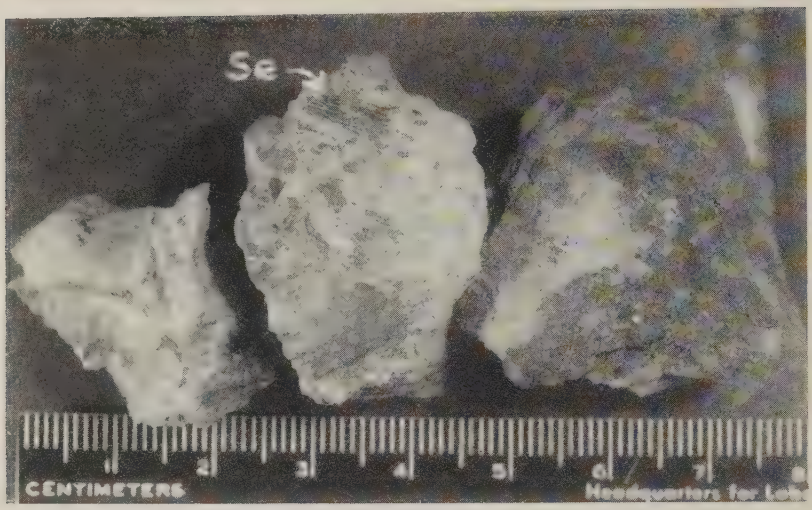

FIG. 1. Corrugated thin films of native selenium on slickensides of claystone gall in the so-called Poison Canyon sandstone, middle part of the Brushy Basin member of the Jurassic Morrison formation near Grants, New Mexico.

been used in many reports, such as those by Dodd (1956) and Hilpert and Freeman (1956).

The so-called Poison Canyon sandstone is the major uranium bearing sediment in the vicinity of Poison Canyon and the Marquez mine. The sandstone is predominantly medium to coarse grained. Minor seams of claystone and conglomerate occur between the sandstone beds. Claystone galls are found throughout the unit, but are generally found along bedding planes. Faults and fractures are not common at the Marquez

TABLE 1. *X*-RAY POWDER DIFFRACTION DATA OF NATIVE SELENIUM, NEAR GRANTS, NEW MEXICO

Radiation: CuKα = 1.54178 Å; Camera dia. = 114.59 mm.

d (Å)	I	*d* (Å)	I
3.79	7	1.43	2
3.00	10	1.38	<1
2.18	2	1.32	<1
2.07	5	1.18	1
1.99	3	1.12	1
1.77	4	1.08	<1
1.66	2	1.04	<1
1.51	2		

mine. There is, however, movement along some of the bedding planes and contacts. Slickensides are formed in these areas. One of the claystone (No. 760) was broken and thin films of native selenium were seen on the slickensides. Fig. 1 shows the selenium film on the slickensides. The selenium film is rather corrugated because it was deposited between the polished and striated surfaces of the slickensides. Numerous minute and fresh pyrite crystals appear in the claystone.

Identification

Some physical properties of the native selenium are as follows: Luster metallic, color grayish black; some with bluish tint. Because of this bluish tint, some thin films of the native selenium may be mistaken for molybdenite. Streak grayish black. Some of the thinnist fragments are brownish red in transmitted light. The x-ray powder diffraction data are listed in Table 1.

Acknowledgment

The permission of the Uranium Division, Calumet and Hecla, Inc., to publish this geological note is gratefully acknowledged.

References

Dodd, P. H. (1956) Examples of uranium deposits in the upper Jurassic formation of the Colorado plateau; *U. S. Geol. Survey Prof. Paper* **300,** 253–262.

Freeman, V. L., and Hilpert, L. S. (1956) Stratigraphy of the Morrison formation in part of northwestern New Mexico; *U. S. Geol. Survey Bull.* **1030-J.** 309–334.

Hilpert, L. S., and Freeman, V. L. (1956) Guides to uranium deposits in the Morrison formation, Gallup-Laguna area, *U. S. Geol. Survey Prof. Paper* **300,** 299–302.

THE AMERICAN MINERALOGIST, VOL. 44, NOVEMBER–DECEMBER, 1959

SIMPLE TECHNIQUE FOR THE CONSTRUCTION OF POLYHEDRAL STRUCTURE MODELS

Tibor Zoltai, *Crystallographic Laboratory, Massachusetts Institute of Technology, Cambridge, Massachusetts**

When complex crystal structures are studied the visualization of the structures requires good structure models. The standard ball models help this visualization, but they are often either too expensive to purchase or too time-consuming to construct. Most structures, however,

* Present address: Department of Geology and Mineralogy, University of Minnesota, Minneapolis, Minnesota.

can be illustrated by polyhedral models, where the polyhedra represent the coordination polyhedra of the cations. Such models not only illustrate the linkage of the polyhedra and the whole structure, in many cases better than a ball model, but also offer possibilities for simple and inexpensive model construction techniques.

The use of polyhedral models is not unknown among crystallographers. Most of the published models are made of cardboard paper and some are made of wooden blocks or plaster of paris. The first technique is simple and time-saving, but the models are primitive and temporary only. In studying tetrahedral structures the author sought a simple and fast technique for making over 40 structure models. An efficient and inexpensive technique was found which permits making well-constructed and sturdy models in a matter of a few hours.

(1) The tetrahedra of the model are made of acetate sheets. Acetate sheets of 15 mils thickness were found to be the most satisfactory for the construction of models on a scale of 1 inch to 2 Angströms. The acetate sheets are first dulled with steel-wool. This fogging renders the tetrahedra opaque and helps to hide the minor imperfections. Equilateral triangles are then cut out. This cutting can be achieved by a simple paper cutter, but if a large number of models is anticipated, it pays to have a die made for mechanical cutting. The acetate triangles are glued into tetrahedral form with acetone, which is a solvent of the acetate and dries very quickly. This process can be accelerated if a mold, such as shown in Fig. 1 is used for the assemblage of the tetrahedron.

(2) The tetrahedra are attached to each other by means of narrow acetate strips (1 mm. by 8 mm.). These are set at the approximate linkage angle and fastened to the corresponding corners of the tetrahedra with acetone. The two softened acetate surfaces stick immediately and the joint hardens in a matter of a few seconds. This approximate angle is later changed to the correct angle by softening the acetate strips with a drop of acetone. The model is assembled by following a good drawing of the structure, or by constructing the motif of tetrahedra of the structure and repeating it according to the symmetry of the space group.

(3) Before attaching the last few tetrahedra to the model, the model is placed in a $\frac{1}{8}$ inch brass wire frame. The frame might represent a unit cell or any multiple or fraction of the unit cell. The last tetrahedra are then added to the model to complete it. In some cases the brass wire has to be embedded in a tetrahedron. This can be done easily by cutting and partially opening the tetrahedron, and removing a circular area of acetate where the wire is to penetrate the face. The tetrahedron is then glued together again after it is placed on the frame. In order to fix the position of the model in the wire frame a few narrow strips of acetate can

be glued to peripherally-located tetrahedra and the frame. Transparent strips of acetate can be used for this purpose in order to prevent their interference in the appearance of the model. When the model is ready and all the linkage angles are set correctly, an extra acetate strip can be added to each connected corner to assure firm connections. The model with the frame can then be fixed to a base, if desired.

A model of high-quartz constructed by this technique is shown in Fig. 2. In this model the structure is extended beyond a unit cell in order

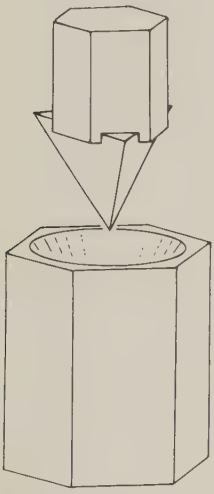

FIG. 1. Mold for assembling tetrahedra.

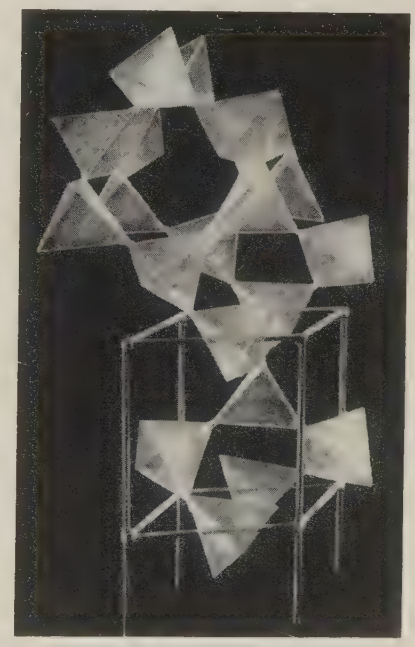

FIG. 2. Model of high-quartz.

to illustrate the 6- and 8-membered loops of tetrahedra. All the silica and silicate models can be constructed similarly and plastic balls can be added to illustrate the location of the non-tetrahedrally coordinated cations in silicates. Mica and clay models can be constructed by the combination of tetrahedral and octahedral sheets. If so desired the polyhedra of the different cations in a complex structure model can be painted in different colors.

The models constructed by this technique are fairly permanent. Unfortunately, the acetate becomes brittle after a few years and the model may fall apart if handled constantly. It is, therefore, advisable to keep the models in closed display cases as much as possible.

THE AMERICAN MINERALOGIST, VOL. 44, NOVEMBER–DECEMBER, 1959

WULFENITE AND CERUSSITE AT BETHEL, CONNECTICUT

RONALD JANUZZI, *Danbury, Connecticut*

Wulfenite and cerussite have recently been discovered in a complex pegmatite associated with the mineral bismutite at Bethel, Connecticut.

More than a score of orange, euhedral crystals of wulfenite of microscopic size were found in tiny vugs in albite associated with quartz, muscovite, and bismutite. These have a prismatic, dipyramidal habit.

Yellowish white crystals of cerussite were found with the wulfenite. In addition to free-growing crystals, the cerussite is also found as megascopic and microscopic crystalline masses and grains embedded in albite. It is more abundant than the wulfenite and many of the crystals can easily be seen without the aid of a hand lens. The predominating crystal habit is equant, dipyramidal, pseudo-hexagonal.

Bismutite occurs as a gray, compact, pulverulent material that is pseudomorphous after an unknown mineral. The original mineral was orthorhombic and lath-like in bent forms with deep vertical striations, suggesting a common habit of stibnite.

A similar occurrence of wulfenite associated with bismutite occurs at the Branchville Pegmatite in Connecticut. No reference to wulfenite or cerussite is made by Schairer (1931) or Sohon (1951).

REFERENCES

SCHAIRER, JOHN F. (1931) Minerals of Connecticut, *State Geological and Natural History Survey Bulletin* **51.**

SOHON, JULIAN A. (1951) Connecticut Minerals, *State Geological and Natural History Bulletin* **77.**

THE AMERICAN MINERALOGIST, VOL. 44, NOVEMBER–DECEMBER, 1959

DETERMINATION OF MIXED LAYERING IN GLAUCONITES BY INDEX OF REFRACTION

L. G. TOLER* AND JOHN HOWER, *Montana State University, Missoula, Montana*

Clay minerals with mixed-layered structures are quite common (Weaver, 1956). X-ray diffraction techniques for quantitatively determining structural types present and their relative percentages have been

* Present address: Department of Geology, University of Missouri, Columbia, Mo.

established by Brown and MacEwan (1951). Recently, Burst (1958a, 1958b) has shown that glauconites also occur as mixed-layered structures. The mixing is dominantly between expandable (montmorillonitic) layers and non-expandable 10 Å layers.

In glauconites a linear inverse relationship exists between the per cent of randomly interstratified expandable layers and the refractive index. The data presented here will enable those who do not have ready access to x-ray diffraction apparatus to obtain structural information on glauconites by a simple refractive index method.

Methods

Seventeen purified glauconite samples were used to determine the relationship between refractive index and per cent expandable layers. Eight of the samples were also analyzed for total iron calculated as Fe_2O_3. Samples were selected to exclude Burst's "mixed-mineral" variety of glauconite.

The per cent expandable layers was determined by the method described by Brown and MacEwan. The x-ray diffraction samples were prepared by disaggregating the glauconite pellets in distilled water in an ultrasonic cleaner and centrifuging the suspension through a porous porcelain plate following the technique described by Kinter and Diamond (1956). The position of the (001)/(001) of the mixed-layered structure was determined both on glycol solvated and potassium treated samples. The per cent expandable layers was then read from Brown and MacEwan's curves.

The refractive index was determined using sodium vapor light and oils 0.002 apart. The index was determined on mineral aggregates and is close to n_z. This index was approached from below. The first oil in which the Becke line was seen to have no component moving into the aggregate was assumed to have the Z index. Single crystal determinations were attempted but, because of small particle size, were obtained only on a few samples. The indices reported were reproducible to ± 0.002 on independent determinations by each writer.

The per cent iron, calculated as Fe_2O_3, was determined by x-ray spectrographic analysis. The results were obtained by using the Bashi Formation glauconite as a single standard on a one point working curve. The slope of the working curve was adjusted by calculation following the method outlined by Hower (1959). The iron determinations are thought to be good within ± 10 per cent of the amount present.

Results

The data on per cent expandable layers, refractive index, and iron

Table 1. Index, Per Cent Expandable and Total Iron, Calculated as Fe_2O_3 for Seventeen Glauconites

	Formation	Index	Per cent Expandable	Per cent Fe_2O_3
1	Sundance	1.584	29	8.9
2	Colorado Shale	1.584	28	9.4
3	Byram	1.590	36	
4	Moody's Branch	1.596	30	14.2
5	Carrizo	1.606	25	
6	Kinkaid	1.612	14	
7	Folkestone	1.614	13	14.8
8	"B" New Jersey	1.622	10	
9	Park Shale	1.622	8	
10	Gros Ventre (1)	1.626	13	
11	Gros Ventre (2)	1.626	10	
12	Bashi	1.626	10	22.7
13	Franconia	1.628	13	21.5
14	Boone Terre	1.630	6	
15	Birkmose	1.630	8	20.8
16	Reno	1.636	7	
17	Tonto	1.638	0	19.4

are presented in Table I. Figure 1 is a plot of per cent expandable layers against the Z refractive index of the seventeen glauconites. The slope of the regression line was calculated by the least squares method. The correlation coefficient calculated for the data presented in Fig. 1 is −0.94. This compares with correlation coefficients of −0.82 for the data relating per cent iron to per cent expandable layers and 0.91 for

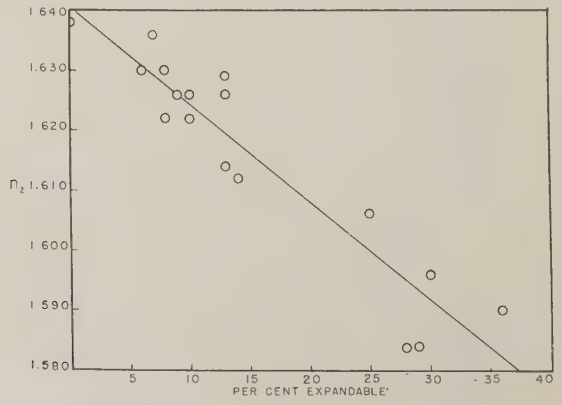

Fig. 1. Relation between index of refraction and per cent expandable layers in glauconites.

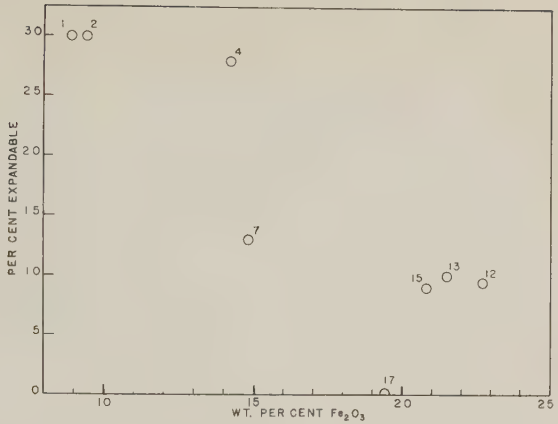

FIG. 2. Relation between per cent expandable layers and per cent Fe_2O_3 for eight glauconites. The numbers beside each point correspond to the glauconites listed in Table I.

the data relating per cent iron to the index of refraction. The curve of Fig. 1 can be used to estimate the per cent expandable layers by the simple aggregate refractive index technique described above.

The decrease in index with increasing percentage of expandable layers is caused in part by the presence of water molecules between the layers and in part because iron decreases with increasing amounts of expandable layers. Figure 2 is a plot of the available data of per cent expandable

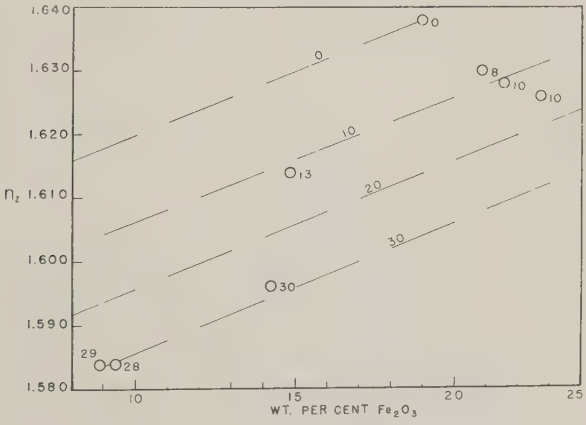

FIG. 3. Relation between index of refraction and per cent Fe_2O_3 in glauconites. The dashed lines are estimated curves for change in n_z with change in Fe_2O_3 for equal amounts of expandable layers. The numbers beside each point correspond to the amount of expandable layers for that sample.

layers against per cent Fe_2O_3. Figure 3 summarizes, on the basis of limited data, the effect of both per cent expandable layers and per cent Fe_2O_3 on the refractive index. Data taken from the literature on n_z versus per cent Fe_2O_3 (Hutton and Seelye, 1941, Hendricks and Ross, 1941) fall in with our points. The number beside each point is the per cent expandable layers for that sample; the dashed lines are estimated curves for increase in n_z with increasing iron for equal amounts of expandable layers. On the basis of Fig. 3 it can be tentatively concluded that the refractive index of glauconite decreases approximately 0.001/per cent expandable layers and increases approximately 0.002/per cent Fe_2O_3. These two factors enhance each other to give the relationship shown in Fig. 1. The writers believe that much of the scatter in the refractive index data of glauconite shown by Winchell (1951) is caused by variable amounts of mixed layering.

Acknowledgments

The writers gratefully acknowledge the support of this work by the National Science Foundation. J. F. Burst kindly supplied us with samples number 3, 4, 5, 6, 12, 14, 15, and 16.

References

Burst, J. F. (1958a), "Glauconite" Pellets: Their Mineral Nature and Applications to Stratigraphic Interpretations, *Am. Assoc. Petrol. Geol.*, **42,** 310–327.

Burst, J. F. (1958b), Mineral Heterogeneity in Glauconite Pellets, *Am. Mineral.*, **43,** pp. 481–497.

Brown, G. and MacEwan, D. M. C. (1951), X-ray Diffraction by Structures with Random Interstratification in Brindley, G. W. et al., X-ray Identification and Crystal Structure of Clay Minerals, Chapter XI, 266–284, *Mineralogical Society of Great Britain Monograph.*

Hendricks, S. B. and Ross, C. S. (1941), Chemical Composition and Genesis of Glauconite and Celadonite, *Am. Mineral.*, **26,** 683–708.

Hower, John (1959), Matrix Corrections in X-ray Spectrographic Trace Element Analysis, *Am. Mineral.*, **44,** 19–32.

Hutton, C. O. and Seelye, F. T. (1941), Composition and Properties of Some New Zealand Glauconites, *Am. Mineral.*, **26,** 595–604.

Kinter, E. B. and Diamond, Sidney (1956), A New Method for Preparation and Treatment of Soil Clays for X-ray Diffraction Analysis, *Soil Science*, **81,** 111–120.

Weaver, C. E. (1956), The Distribution and Identification of Mixed Layer Clays in Sedimentary Rocks, *Am. Mineral.*, **41,** 202–221.

Winchell, A. N. and Winchell, H. (1951), Elements of Optical Mineralogy, Part II, Descriptions of Minerals, John Wiley and Sons, Inc., New York.

International Mineralogical Association

The First Congress of the International Mineralogical Association was held at the Federal Institute of Technology in Zürich, Switzerland, on August 28 to September 4, 1959. Delegates attended from 19 of the 21 countries presently members of the Association. The Executive Committee of the IMA is composed of R. L. Parker (Zürich), President; F. E. Wickman (Stockholm), First Vice-President; D. P. Grigoriev (Leningrad), Second Vice-President; J. L. Amorós (Madrid), Secretary; D. J. Fisher (Chicago), Treasurer; T. Ito (Tokyo), E. Onorato (Rome), J. Orcel (Paris) as Councilors; and G. F. Claringbull (London), Advisory Member.

The work of the IMA centers about its Commissions. At the present time four Commissions have been formed: on Abstracts (E. Onorato, Chm., and N. F. Henry, Secy.); on Mineral Data (H. Strunz, Chm., and A. Pabst, Secy.); on New Minerals and Mineral Names (M. Fleischer, Chm., and C. Guillemin, Secy.) and on Museums (C. Frondel, Chm., and F. Leutwein, Secy.). The Commissions include representatives (in some instances also committees) from each of the countries that are members of the Association. The Commission on New Minerals and Mineral Names is primarily concerned with setting forth criteria for the definition and naming of new species and varieties and with the resolution of existing problems of nomenclature. The Mineral Data Commission presently is concerned with questions of the symbolization of the physical properties and the chemical and structural formulae of minerals. The Museum Commission has started the compilation of a World List of Mineral Collections, that will briefly characterize all permanent collections as to size and content; a following objective is to prepare finding-lists of type material and of analyzed and described material in these collections.

Following the business meetings of the Association, two Symposia of invited papers were held on the subjects of Twinning (participants: H. Curien, J. D. H. Donnay, M. J. Buerger, T. Ito, A. Neuhaus, F. Laves, I. Sunagawa, W. T. Holser) and on Alpine Fissure Minerals (participants: R. L. Parker, D. P. Grigoriev, G. Fagnani, K. Lietz). Two four-day field trips were taken by bus through the eastern and the western Alps after the close of the meeting.

Copies of the detailed proceedings of the Zurich meeting will be available from the Secretary, Prof. J. L. Amorós, Museo de Ciencias Naturales, Castellana 84, Madrid, Spain. The next meeting of the IMA will be held in Copenhagen in 1960 in conjunction with the XXI International Geological Congress. At that time round-table discussions will be held on proposals for the formation of Commissions on the nomenclature of petrology and on education in mineralogy and related sciences.

The Friedrich Becke Medal

The Friedrich Becke Medal of the Mineralogical Society of Austria was presented to Professor Clifford Frondel of Harvard University at the Zurich meeting of the International Mineralogical Association.

Mineralogical Abstracts

The councils of the Mineralogical Society of America and the Mineralogical Society (Great Britain and Ireland) are jointly sponsoring the publication of Mineralogical Abstracts as a separate publication, commencing with volume 14 for 1959.

The new journal has a two-column format with a page size of ($10\frac{3}{8}\times7\frac{7}{8}$) and will contain at the outset about twice the number of abstracts in the present issues. The journal will be published quarterly and the fourth number will include an index for the year.

Mineralogical Abstracts will be grouped under the following headings:

Age-determination
Apparatus and techniques
Bibliographies
Clay minerals
Crystal structure of minerals
Experimental mineralogy
Geochemistry
Gemstones
History and biography
Meteorites and tektites
Mineral data
New minerals
Notices of books
Ore deposits and economic mineralogy
Petrology
Physical properties of minerals
Topographical mineralogy
Various topics

The price of the new journal to subscribers other than personal members of the two sponsoring societies will be $9. U. S. per calendar year issue of 4 numbers. There will be a special price of $6. for educational institutions.*

It is proposed to make the journal available to personal members of the Mineralogical Society of America at $3. per calendar year. Members of the Mineralogical Society of Great Britain and Ireland, who already receive the abstracts as part of their privileges of membership, will continue to receive Mineralogical Abstracts for an increase in the annual membership fee of 10s.

* The price of the Mineralogical Magazine when separated from Mineralogical Abstracts will be reduced to £2 10s. 0d. per calendar year issue of 4 numbers.

American Geophysical Union
Section of Vulcanology, Geochemistry and Petrology
Washington 25, D. C.

The planning for the meeting of the International Union of Geodesy and Geophysics in Helsinki, Finland next summer has begun. The American Geophysical Union will will participate in the sessions of the I.U.G.G. as a member organization. Although the I.U.G.G. will meet from July 25 through August 6, we are planning to have our sessions during the first week (July 25–30) to allow time for those who plan to attend field excursions of the International Geologic Congress. (Copenhagen August 15–25).

In order to facilitate the presentation of a program to the I.U.G.G., a committee has been set up with the Section of Vulcanology, Geochemistry and Petrology to assemble such a program. This committee is composed of A. O. Nier, T. Aldrich, I. Friedman, S. Goldich, F. Schairer, and R. L. Smith.

NEW MINERAL NAMES

Novakite

Z. Johan and J. Hak. Novakit—(Cu, Ag)$_4$ As$_3$, ein neues Mineral. *Chem. der Erde*, **20,** 49–50 (1959).

A preliminary note. Analysis (mean of 2) gave Cu 41.39, As 43.30, Fe 5.13, Ag 1.96, Co 0.79, S 2.73, CaO 2.72, CO_2 2.13, sum 100.15%. After deducting calcite, S as chalcocite, and Fe as loellingite (these minerals were identified by microscopic and x-ray study) and recalculation to 100, this gives As 45.82, Cu 50.91, Ag 3.27%, corresponding to (Cu, Ag)$_{1.36}$ As or (Cu, Ag)$_4$ As$_3$ or (Cu, Ag)$_{11}$ As$_8$. When heated, the mineral decomposes below its melting point to Cu_2As and an unidentified phase. Etched by HNO_3 1:1, HCl 1:1, 20% $FeCl_3$ solution, not etched by 40% KOH or KCN.

The mineral is steel-gray on fresh fracture, tarnishes to dull colors and finally becomes nearly black. Alters easily to secondary minerals. In polished section the mineral appears white, somewhat yellowish compared to native As. Anisotropy medium strong, with dark bluish-gray to bright ocher-brown polarization colors. The reflecting power is slightly higher than that of native As. Hardness 3–3½. G approximately 6.7 (some chalcocite and loellingite present).

The strongest x-ray lines are 1.870 (10), 1.182 (10), 1.998 (9), 1.957 (9), 1.910 (7), 1.352 (6), 1.225 (6), 1.787 (5). From the powder pattern, novakite is tetragonal, with a_0 8.20$_6$ Å., c_0 11.88 Å., and is therefore pseudocubic. Cleavage none.

The mineral occurs in irregular grains in the carbonate gangue of the complex Cu-Co-Fe-As ores of Černý Dul (Schwarzenthal), Riesengebirge.

The name is for Jiří Novák, Professor of Mineralogy, Charles University, Prague.

Discussion. The constants given lead to a cell content of (Cu, Ag)$_{26.5}$ As$_{19.9}$.

Michael Fleischer

Cornubite

G. F. Claringbull, M. H. Hey, and R. J. Davis. Cornubite, a new mineral dimorphous with cornwallite. *Mineralog. Mag.*, **32,** 1–5 (1959).

X-ray data showed the existence of this new mineral at 5 localities in Cornwall, one in Devon, and one in Cumberland; associated minerals include cornwallite, obvenite, liroconite, and malachite. It is light-green, apple-green to dark-green, usually fibrous, but also massive, porcellanous. No optical data are given. Microchemical analysis on 6.6 mg. gave CuO 59.86, As_2O_3 35.07, H_2O (5.07) (by diff.), sum (100.00%), corresponding closely to $Cu_5(AsO_4)_2(OH)_4$. G. 4.64, calcd. from x-ray data 4.8. The mineral lost only 2.8% H_2O at 450°. A fiber photograph was indexed to give d_{100} 5.35 Å., d_{010} 4.72 Å., γ^* 88°; attempts to index completely indicate that the mineral is triclinic, with d_{100} and d_{010} double the above values. The strongest x-ray lines are 4.72 (10), 2.562 (10), 2.489 (10), 2.688 (9), 3.49 (8), 2.868 (7), 2.303 (7), 1.575 (7), 1.492 (7), 5.35 (6), 3.59 (6), 3.33 (6), 3.10 (6), 3.05 (6), 2.98 (6), 2.932 (67), 2.090 (6), 1.957 (6), 1.515 (6), 1.373 (6).

The name is from Cornubia, the Roman name for Cornwall.

M.F.

Delhayelite

Th. G. Sahama, and Kai Hytonen. Delhayelite, a new silicate from the Belgian Congo. *Mineralog. Mag.*, **32,** 6–9 (1959).

The new mineral occurs in platy crystals in kalsilite-melilite-nephelinite lava, Mt. Shaheru, Belgian Congo (see gotzenite, combeite, kirschsteinite, Am. Mineral. 43, 791–792

(1959)). It was purified with difficulty, the sp. gr. 2.60±0.03 being very close to those of kalsilite and nepheline. Treatment with warm dilute acetic acid dissolved kalsilite and attacked delhayelite only slightly. Analysis, after correction for 2% admixed nepheline, gave SiO_2 52.60, TiO_2 0.09, Al_2O_3 9.22, Fe_2O_3 (total iron) 2.72, MgO 1.03, MnO 0.07, CaO 7.99, Na_2O 3.20, K_2O 9.27, H_2O^- 3.35, H_2O+ 5.93, Cl 3.91, F 0.33, SO_3 1.31, sum 101.02 − (0 = F_2Cl_2) 1.01 = 100.01%. This corresponds to $(Na, K)_4Ca_5Al_6Si_{32}O_{80} \cdot 18\ H_2O \cdot 3(Na, K)_2(Cl_2, F_2, SO_4)$.

Rotation and Weissenberg photographs show the mineral to be orthorhombic, space group *P m n2* or *P m m n*; the unit cell has *a* 13.05±0.06, *b* 24.65±0.2, *c* 7.04±0.03 Å. Cleavage (010) distinct. Indexed *x*-ray powder data are given; the strongest lines are 3.078 (100), 12.30 (35), 6.158 (25), and 3.482 (10).

The mineral is colorless. In thin section shows a somewhat wavy extinction; interference colors very low, abnormally bluish-gray in sections perpendicular to the *b*-axis. Optically negative, 2V = 83±3° (by Berek compensator), birefringence 0.002–0.003, $\alpha \sim \beta \sim \gamma = 1.532 \pm 0.002$, $a = \alpha$, $b = \gamma$, $c = \beta$.

The unit cell dimensions are close to those for rhodesite, but the chemical composition and optical properties are different.

The name is for F. Delhaye, Belgian geologist, "a pioneer in the exploration of North Kivu."

M.F

Angelellite

Paul Ramdohr, F. Ahlfeld, and F. Berndt. Angelellit, ein natürliches triklines Eisen-Arsenat, $2\ Fe_2O_3 \cdot As_2O_5$. *Neues Jahrb. Mineral., Monatsh*, **1959**, No. 7, 145–151.

K. Weber. Eine kristallographische Untersuchung des Angelellits, $2Fe_2O_3 \cdot As_2O_5$. *Ibid.*, 152–158.

Analyses by Berndt (No. 1 fused with $KHSO_4$, others with HCl and KCl+$KClO_3$) gave:

	1	2	3
Fe_2O_3	55.8	43.8	59.3
As_2O_5	32.2	24.5	28.2
SiO_2	5.81	2.61	2.73
SnO_2	2.92	0.43	0.39
Al_2O_3	2.82	2.15	1.26
Insol.		25.62	8.16
	99.55	99.11	100.04
Fe_2O_3/As_2O_5 (calcd. by M.F.)	2.49	2.57	3.03

Later *x*-ray fluorescence study by Weber showed that about 3% Sb is present and that the ratio $Fe_2O_3 : As_2O_5$ was close to 2; his *x*-ray study showed the presence of cassiterite and also hematite, the latter as a thin overgrowth. The formula is therefore $Fe_4(As, Sb)_2O_{11}$. Difficulty fusible before the blowpipe to a magnetic bead. Slowly dissolved by HCl.

Weissenberg photographs show the mineral to be triclinic, space group C_1^1, or C^1., a_0 5.03, b_0 6.49, c_0 7.11 (all ±0.01) Å, α 114.4°, β 116.4°, γ 81.9° (all ±1°), Z = 1. Oriented intergrowths with hematite have *a* of angelellite parallel to the hexagonal *a*-axis of hematite (a_0 5.03 Å). Partially indexed *x*-ray powder data (29 lines) are given; the strongest are

3.152 (10) (10$\bar{2}$), 2.997 (7) (101), 2.856 (5), 2.489 (5), 2.072 (5), 2.960 (4), 2.955 (4). The crystals show the faces *c* (001), *a* (100), and *d* (02$\bar{1}$) well developed, also *f* (101) *g* (03$\bar{2}$), *h* (03$\bar{1}$), *i* ($\bar{1}$11), and *k* (101). Usually tabular with (001) and (001) dominant. An angle table is given. Cleavage (001), fracture conchoidal. Brittle.

The mineral is blackish-brown, streak reddish-brown, luster adamantine to semimetallic. H. 5½, G. 4.95, 4.86_7 (pycnometer), 4.86_2 (calcd. from *x*-ray data). Optically biaxial, positive, 2 V medium large, *ns* (by immersion in Se-S melts in Na light) α 2.13, β about 2.2, γ 2.40. Strongly pleochroic from deep blood-red to reddish-brown in thin section, to light yellow in powders. Absorption Z>X. Polishes well; in reflected light strongly anisotropic, reflecting power high, near that of sphalerite.

The mineral occurs as globular and crystalline incrustations on andesite from the Cerro Pululus tin mine, northwestern Argentina. It is believed to be of exhalative origin; probably deposited from fumarolic vapors.

The name is for V. Angelelli, Argentine mineralogist.

Discussion. Presumably to be classed with the anhydrous phosphates (Dana class 38), but differs from all known types.

M.F.

Unnamed (Mineral S)

H. Strunz. Tsumeb, seine Erze und Sekundär-mineralien, insbesondere der neu aufgeschlossenen zweiten Oxydationszone. *Fortschr. Mineral.*, **37**, 87–90 (1959).

Preliminary note. The mineral occurs as pyrite-like, highly reflecting crystals. Tetragonal with a_0 6.70, c_0 9.53Å., tetragonal cleavage distinct. The *x*-ray powder diagram resembles that of linneite and may indicate a deformed spinel structure. The strongest lines are 1.54 (10), 2.87 (8), 2.96 (7), 1.68 (6), 2.38 (5). Spectrographic analysis shows Ge and Ni with a little Cu and Fe; perhaps $(Ni, Cu)_2 GeS_4$. Hardness 3½–4, reflection in oil near 50%.

M.F.

Unnamed (Mineral R)

H. Strunz, *Fortschr. Mineral.*, **37**, 87–90 (1959).

Apparently a copper-zinc arsenate. Color light rose. Apparently triclinic, two pinacoidal cleavages, a_0 7.69, b_0 ?, c_0 6.59, *ns* α 1.583, β 1.62, γ 1.633. Soluble in HCl.

M. F.

Zinclavendulan

H. Strunz, *Fortschr. Mineral.*, **37**, 87–90 (1959).

Blue orthorhombic crystals, a_0 9.87, b_0 38.7, c_0 9.99 Å (compare *Am. Mineral.*, **42**, 123–124 (1957)) of $(Ca, Na)_2 (Cu, Zn)_5 Cl (AsO_4)_4 \cdot 4\text{–}5 H_2O$.

M. F.

Zincrosasite

H. Strunz. *Fortsch. Mineral.*, **37**, 87–90 (1959).

$(Zn, Cu)_2 (OH)_2 CO_3$ with atomic ratio Zn:Cu=58.6:51.9, whereas Cu is predominant in rosasite.

M. F.

p-Veatchite

Otto Braitsch. Über *p*-Veatchit, eine neue Veatchit-Varietät aus dem Zechsteinsalz. *Beitr. Mineral. u. Petrog.*, **6**, 352–356 (1959).

Material from the Königshall-Hindenburg Mine, Reyershausen, Germany, agrees in x-ray powder pattern and physical properties, but not in space group or unit cell constants with veatchite from California, and is named p-veatchite. It has space group $P2_1/m$ or $P2_1$, a_0 6.72, b_0 20.81, c_0 6.64$_7$ Å., β 119°4′, Z=4, whereas that from California (Clark et al., 1958) has space group A 2/a or Aa, a_0 20.81, b_0 11.75, c_0 6.63$_7$ A, β 92°2′, Z=8.

Discussion. Needs confirmation.

M. F.

Pandaite

E. Jager, E. Niggli, and A. H. Van der Veen. A hydrated barium-strontium pyrochlore in a biotite rock from Panda Hill, Tanganyika, *Mineralog. Mag.*, **32**, 10–25 (1959).

The mineral was found in a highly weathered biotite-rich rock occurring in a roof pendant of the Mbeya (also called the Panda Hill) carbonatite, near Mbeya, Tanganyika. The rock contains major biotite, kaolinized orthoclase, and limonite, minor fluorite, quartz, apatite, zircon, chlorite, plagioclase, rutile, and heamatite.

Analysis of a sample dried at 110° gave Na_2O 0.28, K_2O 0.25, CaO 1.35, BaO 12.5, SrO 6.4, PbO 0.01, rare earths 2, ThO_2 0.6, FeO (total iron) 0.45, MgO 0.07, MnO 0.01, CuO 0.01, TiO_2 3.9, Nb_2O_5 67, Ta_2O_5 0.22, ZrO_2 0.28, SnO_2 0.32, SiO_2 0.89, Al_2O_3 0.12, SO_3 trace, CO_2 0.1, F trace, P_2O_5 0.4, sum 10 1.16%. Another sample containing 67% Nb_2O_5 contained U 0.31, Th 0.72%. Spectrographic analysis showed the presence in the rare earths of Ce, Y, and La in the ratio 40:2:1. Infra-red spectrophotometry by J. H. L. Zwiers gave no indication of hydroxyl groups. This is corrected, deducting zircon 0.42, phlogopite 0.27, orthoclase 0.42, apatite 0.92, cassiterite 0.32, quartz 0.33, rutile 0.15%, giving the formula $(Ba_{0.30}Sr_{0.22}Ca_{0.05}Ce_{0.04}Na_{0.03}Fe_{0.02}K_{0.01}Th_{0.01})$ $(Nb_{1.83}Ta_{0.004}Ti_{0.17})O_{5.61}(H_2O)_{0.80}$, or $A_{0.68}B_2O_{5.61}(H_2O)_{0.80}$. D.T.A. study showed a large endothermic peak at 540°, and larger exothermic peaks at 800° and 820°. A dehydration curve showed complete loss of water below 350°.

The mineral is yellowish-gray to light olive-gray. It occurs in small enhedral crystals (largest 800) showing an octahedron with small cube faces. Hardness 550 (Vickers hardness no.) = $4\frac{1}{2}-5$. Fracture conchoidal, a very poor {111} cleavage was seen in polished section. G. 4.00 (dried at 110°), calculated from x-ray data 4.01. Radioactive. Isotropic with n mostly 2.08–2.09, but some crystals have 2.07–2.08, some 2.09–2.10. Reflectivity 13.2%.

Rotation and Weissenberg photographs show no indication of deviations from the pyrochlore structure. From powder data, $a = 10.562 \pm 0.006$ Å. The strongest lines are (av. of 2 samples) 3.045 (100), 6.10 (80), 1.865 (70), 1.591 (70).

The name is for the locality, Panda Hill, and is suggested for minerals of the pyrochlore group with Ba predominant in the A position. The material here described is a strontian pandaite.

M. F.

Avicennite

Kh. N. Karpova, E. A. Kon'kova, E. D. Larkin, and V. F. Savel'ev. Avicennite, a new mineral. *Doklady Akad. Nauk. Uzbekistan S.S.R.* **1958,** No. 2, 23–26 (in Russian).

The mineral occurs in crystals less than 1 mm. in size, somewhat resembling perovskite. Color grayish-black, luster metallic, streak grayish-black; very brittle, fracture uneven, cleavage indistinct. It dissolves with difficulty in acids. Microchemical analysis on 4.3 mg. gave Tl_2O_3 88.86, Fe_2O_3 4.46%, FeO none. Spectrographic analysis showed also Sb, Pb little; Sn, Ti, Mn, Ca, V, Al—very little; Si, Mg, Cu—trace. The formula is given as $7\ Tl_2O_3 \cdot Fe_2O_3$.

X-ray study of V. F. S. showed the mineral to be cubic with a_0 9.12 Å. The x-ray powder

pattern (indexed) gave 49 lines, of which the 9 strongest are stated to agree well with the lines for synthetic Tl_2O_3.

The mineral occurs near the village of Dzhuzumli, Mt. Zirabulaksk region, Bukhara, in a hematite—calcite vein cutting banded marmorized and silicified limestones near their contact with granite-gneisses of the Ketmenchinsk intrusive. The veins contain coarsely crystalline limestone, densely impregnated with iron oxides, iron-rich clays, and hematite.

The name is for Abu Ali ibn Sina (Avicenna) (980–1037 A.D.), Arab physician and scientist, who lived in Bukhara.

Discussion. The x-ray powder data agree well with those of the A.S.T.M. file for Tl_2O_3, but the indexing is entirely different, leading to a_0 10.543 Å. The mineral should be classed with bixbyite, Dana's System Group 445, 7th Ed., Vol. I, p. 550.

M. F.

Nasledovite

M. R. Enikeev. A new mineral, nasledovite, from the Altyn-Topkansk ore field. *Doklady Akad. Nauk Uzbek. S.S.R.* **1958,** No. 5, 13–16 (in Russian).

Analysis by T. F. Mukhova gave PbO 23.51, MnO 14.97, MnO_2 2.04, MgO 3.55, ZnO 0.73, Al_2O_3 19.72, Fe_2O_3 1.34, SO_3 4.60, CO_2 18.40, H_2O^- 0.60, H_2O^+ 9.80, SiO_2 1.58, sum 100.84%. After deduction of SiO_2 and MnO_2 as impurities, this corresponds to Pb 0.3 (Mn, Mg) 0.2 $Al_2O_3 \cdot 0.5\ SO_2 \cdot 4\ CO_2 \cdot 5\ H_2O$. Spectrographic analysis showed also 0.0n% Co, Cu, and Ti.

The mineral occurs as oölites 2–3 mm. in size, consisting of snow-white radiating fibers with silky luster, covered by a fine film of dark-brown to reddish material. Hardness 2, G. 3.069. The fibers show wavy extinction; γ 1.591, $c:\gamma = 2–23°$. The D.T.A. curve, by E. E. Rabaeva, shows a small endothermal effect at 120°, a large one at 605°, and a small exothermic effect at 770°.

The x-ray powder diagram, by L. A. Sokolova, shows 21 lines; the strongest are 3.261 (10), 2.028 (6), 2.019 (6), 1.462 (6), and 2.853 (5).

The mineral occurs as a fissure filling in altered granodiorite porphyries that enclose polymetallic ores at Sardob, eastern part of Altyn-Topkansk ore field, Kuraminsk Mountains. The oölites occur in sooty pyrolusite and ocherous iron oxide with crystals of cerussite.

The name is for Professor B. N. Nasledov, "tireless investigator of the mineral resources of Kara-Mazar."

Discussion. Perhaps to be grouped with the basic lead aluminum carbonate dundasite, *Dana's System*, 7th Ed., Vol. II, p. 279.

M. F.

Satpaevite, Al'vanite

E. A. Ankinovich. The new vanadium minerals satpaevite and al'vanite. *Zapiski Vses. Mineralog. Obshch.*, **88,** No. 2, 157–164 (1959) (in Russian).

These two new aluminum vanadates were found in several mines of the Kurumsak and Balasauskandyk ore fields, in the oxidation zone of the vanadiferous clay-anthraxolite horizon of northwestern Kara-Tau.

Satpaevite

Analysis by T. L. Valeshina gave CaO 1.70, MgO 1.20, Al_2O_3 32.00, 30.80, Fe_2O_3 0.25, SiO_2 (given as SiO_4) 1.40, V_2O_4 7.40, 7.30, V_2O_5 27.70, 27.66, H_2O 4.10, H_2O^+ 22.80, sum 98.55. This corresponds closely to $6Al_2O_3 \cdot V_2O_4 \cdot 3V_2O_5 \cdot 30H_2O$. Spectrographic analysis

gave also Zn 0.5, Cu 0.2, Ni 0.1, Cr 0.03, Ba 0.01. The mineral dissolves readily in cold dilute acids; in concentrated HCl it gives the characteristic reddish-brown solution of vanadates. When heated in a closed tube, it darkens to brownish-gray and gives off acid water. The D.T.A. curve gives sharp endothermal breaks at 90–210° and 290 and 350°, and a weak one at 600–620°C.

Satpaevite is canary-to saffron-yellow, occurring in floury aggregates of fine grains, but occasionally foliated and showing a perfect pinacoidal cleavage. Luster pearly on the cleavage, dull for fine-grained. G. 2.4. Hardness of dense aggregates $1\frac{1}{2}$. Under the microscope, greenish-yellow to pale olive, partly isotropic, partly birefringent crystals of 0.05–0.1 mm., with *ns* α' 1.676, γ' 1.690, biaxial, positive, 2V near 70°. Weakly pleochroic, Z deeper than X. Extinction parallel, orthorhombic (?). An electron microscope photograph by G. S. Gritsaenko shows platy form with rounded or hexagonal outline.

X-ray powder data by P. T. Tazhibaeva, E. M. Baigulov, G. I. Luk'Yantsev, and A. G. Kovalev are given for two samples. The strongest lines are 1.918, 1.926 (10); 2.330, 2.336 (9); 1.471, 1.469 (8); 3.905, 3.905 (7); 5.86, 5.87 (6). The pattern differs distinctly from that of steigerite, the only previously known aluminum vanadate, and from al'vanite.

Satpaevite occurs at depths of not more than 0.5–1.5 meters in a decomposed tremolite-carbonaceous shale, as veinlets and crusts. Associated minerals are gypsum, steigerite, hewettite, and delvauxite, all of which it cuts.

The name is for the Kazakhstan geologist Kanysh Imantaevich Satpaev.

Discussion. H. T. Evans, Jr., points out that one would expect a mineral containing both V^{+4} and V^{+5} to be bluish-black.

Al'vanite

Analysis by T. L. Valeshima gave CaO 0.5, MgO 0.5, ZnO 0.5, NiO 2.7 (given as Ni, but the mol. ratio corresponds to NiO. MF), Al_2O_3 39.6, 39.4, Fe_2O_3 trace, V_2O_3 not detected, V_2O_4 3.7, 3.8, V_2O_5 24.1, 24.3, SiO_2 1.8, H_2O^- 0.4, 0.6, H_2O^+ 25.6, 25.2, sum 99.4. This corresponds to $3Al_2O_3 \cdot V_2O_5 \cdot 11H_2O$ or $Al_6(VO_4)_2(OH)_{12} \cdot 5H_2O$. Soluble in HCl and HNO_3 only when heated. When heated in the closed tube, it gives off much acid water and turns brown.

The mineral is light bluish-green to bluish-black, streak white. Luster vitreous, pearly on the cleavage. Hardness 3–$3\frac{1}{2}$, G. (suspension) 2.41. Biaxial, neg., 2V 80–85°, *ns* α 1.658, γ 1.714. Dispersion strong, r<v. Both positive and negative elongation were observed.

The mineral occurs in mica-like platelets of hexagonal form. Measurements by V. Yu. Duletkulov showed the faces *c* (001), *b* (010), *a* (100), and *d* (101), and showed the mineral to be monoclinic with β 115°. The axial ratio was not determined. Cleavage (010) perfect. Under the microscope, polysynthetic twinning was observed with twinning plane parallel to the cleavage plane. X:cleavage = 14°.

X-ray powder data by P. T. Tazhibaeva and E. M. Baigulov are given; the strongest lines are 4.477 (10), 1.484 (9), 1.982 (8), 1.911 (6), 4.80 (5), and 1.686 (5).

The name is for the composition.

M. F.

Kivuite

L. Van Wambeke. Contribution a l'etude de la mineralisation radioactive de la pegmatite de Kobokobo et description d'une nouvelle espèce minérale radioactive de la série phosphuranylite—renardite: la kivuite. *Bull. soc. belge geol., paleontol., et hydrol.*, **67**, 383–403 (1958) (publ. 1959).

The mineral occurs in the Kobokobo pegmatite, Kivu, as yellow earthly masses associated with uraninite, cyrtolite, colombotantalite, and apatite. Analysis by Poncin of material kept in a desiccator for 24 hours gave CaO 0.60, PbO 1.84, ThO_2 8.32, UO_3 62.90,

P_2O_5 6.04, H_2O^- 6.24, H_2O^+ (at 450° C.) 8.09, sum 94.03%. The remainder is stated to have consisted of at least 4% cyrtolite plus some columbotantalite. *X*-ray fluorescence analysis also showed 0.1–0.2% BaO, 0.1–0.2% As_2O_5, traces of Be. The formula is approximately $(Th, Ca, Pb)H_2(UO_2)_4(PO_4)_2(OH)_8 \cdot 7H_2O$ and the mineral is therefore the thorium analogue of phosphuranylite (Ca) and renardite (Pb). The mineral is decomposed by HNO_3, nearly all the uranium, but only a little thorium and lead going into solution. The Th in the residue is not attacked by HF. The mineral does not fluoresce. Indexed *x*-ray powder data on the analyzed mineral and on an unanalyzed Pb-rich variety are very close to those of phosphuranylite. The strongest lines are 10.27 *vs*, 7.96 *s-vs*, 3.08 s, 2.87 s, 5.88, 4.43, 3.94, 3.86. The unit cell is calculated to be a_0 15.88, b_0 17.24, c_0 13.76 Å.

Both the analyzed mineral and the Pb-rich variety are Optically uniaxial to biaxial, negative, 2 V 0–5°, pleochroism X colorless, Y and Z greenish-yellow, r>v. For analyzed kivuite, α 1.618±0.002, β 1.654–1.655, γ 1.655±0.003; the Pb-rich variety had α 1.675 ±0.003, $\beta=\gamma=1.705\pm0.005$.

The name is for the Kivu region.

Discussion. The analysis is unsatisfactory, because one cannot tell how the impurities were deducted. Needs confirmation and tests for homogeneity, in view of the behavior with nitric acid.

M. F.

Idaite

Gerhard Frenzel. Ein neues Mineral: Idait, natürliches Cu_5FeS_6 Neues Jahrb. Mineral., Abhandl., **93,** p. 87–114 (1959).

This is the full account; a preliminary paper was abstracted in *Am. Mineral.*, **43,** 1219 (1958). *X*-ray powder data are given.

M. F.

Igdloite

Marianne Danø and Henning Sørensen. An examination of some rare minerals from the nepheline syenites of South West Greenland. *Meddelelser om Grønland* **162,** No. 5, 1–35 (1959).

The mineral occurs in lujavrite rock at Igdlunguaq, Greenland, in white masses and small bands associated with neptunite, analcime, altered eudialyte, and rarely with sphalerite. It is isotropic, but centers of grains are often anisotropic; *n* very high. Spectrographic analysis shows it to be rich in Ti, Nb, Na, Ca, Al, and to have traces of Sr and Ba. Rare earths were not looked for. The *x*-ray pattern (not given) is of the perovskite type, but $a=3.89$ Å, a little larger than for perovskite. The pattern is very similar to that of $NaNbO_3$. Further work is in progress. The name is for the locality.

Discussion. A premature name.

M. F.

Hsiang-hua-shih

Wen-Hui Huang, Shao-Hua Tu, K'ung-Hai Wang, Chun-Lin Chao, and Cheng-Chih Yu. Hsiang-hua-shih, a new beryllium mineral. *Ti-chih-yueh-k'an*, **7,** 35 (1958) (in Chinese). (From an abstract kindly prepared by E. C. T. Chao.)

Analysis gave BeO 15.78, SiO_2 25.66, CaO 34.6, Li_2O 5.85, F 7.81%, stated to yield the formula $Ca_3\ Be_3\ Li_2\ Si_3\ O_{12}\ F_2$. The mineral occurs in white trisoctahedral or dodecahedral crystals and granular masses, G 2.9–3.0, H. 6½, luster vitreous, transparent to translucent, *n* 1.6132. *X*-ray powder data (not given) show it to be cubic, space group $I4_13$, a_0 12.879 ±0.004 Å, Z=8.

The mineral occurs in phlogopite veins in the light-colored band of green and white banded metamorphosed Devonian limestone in Hunan Province. The limestone was intruded by granite. In the green band was found taaffeite (Be Mg Al_4O_8) (see *Am. Mineral.* **37,** 360 (1952)).

The Chinese name means fragrant flower.

Discussion. Very interesting, if true, but an inadequate description. Nothing is said of the missing part of the analysis (more than 10%). One wonders whether B and Al were tested for. The analysis as given gives the ratio $3CaO \cdot 3BeO \cdot Li_2O \cdot 2SiO_2 \cdot 2F$ (not $3SiO_2$).

M. F.

Hydroantigorite

J. Erdelyi, V. Koblencz, and N. S. Varga. Neuere strukturelle Regeln der Hydroglimmer. Hydroantigorit, ein neues Serpentinmineral und metakolloidaler Brucit vom Csodi-Berg bei Dunabogdany (Ungarn): *Acta geol. acad. sci. Hung.*, **6,** 65–93 (1959).

Pale rose material, occurring at the contact of andesite with brucite, had G. 2.42. Analysis gave SiO_2 42.25, Al_2O_3 0.29, Fe_2O_3 0.25, FeO 0.31, MnO 0.05, MgO 39.71, CaO 0.54, K_2O trace, Na_2O 0.02, P_2O_5 trace, CO_2 0.46, H_2O^- 3.21, H_2O^+ 13.02, sum 100.31%. After deducting calcite, H_2O^- and 0.43% SiO_2 as quartz (not seen in the sample), the analysis is calculated to the formula:

$$(Mg_{2.854}\ Fe^{+2}{}_{0.012}\ Mn_{0.002}\ Al_{0.016}\ Fe^{+3}{}_{0.009})_{2.893}\ Si_2O_{4.811}\ (OH)_{4.189}$$

The "excess" OH over the usual formula is balanced by the deficit in octahedral position; D. T. A. and *x*-ray powder data are given. The latter show that the mineral is identical with "ortho-antigorite" of Brindley and v. Knorring (*Am. Mineral.* **39,** 794–804 (1954)). It is monoclinic, a_0 9.23, b_0 9.17, c_0 14.48 Å, β 91°27′.

Discussion. The formula above is presumably calculated on the assumption that all water determined as H_2O^+ is present as hydroxyl. That this is incorrect is so well known that discussion seems unnecessary. But if it were true, does a 5% excess of (OH) justify a new name? I think not.

M. F.

Hydroamesite

J. Erdelyi, V. Koblencz, and N. S. Varga. Hydroamesit, ein neues Mineral aus den Hohlraumen des Basaltes von dem Halap-Berge am Plattenseegebiet (Komitat Veszprem): *Acta geol. acad. sci. Hung.*, **6,** 95–106 (1959).

Cavities in basalt were filled with white, porcelain-like masses, G. 2.35. Optical study showed the material to be faintly anisotropic (birefringence 0.001), but to contain fibers of chrysotile. Analysis gave SiO_2 32.32. TiO_2 trace, Al_2O_3 11.50, Fe_2O_3 0.56, FeO 0.15, MgO 32.61, MnO 0.13, CaO 2.01, K_2O 0.03, Na_2O 0.02, P_2O_5 0.06, H_2O^- 3.13, H_2O^+ 15.98, CO_2 1.84, sum 100.34%. After deducting calcite and H_2O^- the formula is calculated to be:

$$MG_{0.224}\ (Mg_{2.105}\ Al_{0.203}\ Fe^{+3}{}_{0.020})(Al_{0.448}\ Si_{1.552})\ O_{3.880}\ (OH)_{5.120}$$

Alternative calculations require $Al(OH)_3$ or $Mg(OH)_2$ to be assumed; the D.T.A. curve shows no breaks corresponding to their presence. *X*-ray powder indicate the mineral to be monoclinic, a_0 5.27, b_0 9.20, c_0 14.60 Å, β 90°59′.

Discussion. See preceeding remarks under Hydroantigorite. It seems likely that this gel-like material would contain appreciable amounts of non-essential water. A static dehydration curve would be interesting.

M. F.

Hydroparagonite

In *Am. Mineral.*, **43,** 1222 (1958), I criticized the re-naming of brammallite as hydroparagonite. J. Erdelyi has now replied in *Acta. geol. acad. sci. Hung.*, **6,** 273–274 (1959) that Bannister described brammallite as a sodium-illite, which it is not, and therefore it was proper to re-name it. But Bannister's description of the mineral was correct; even if his classification of it was incorrect, which I do not concede, this is not a valid reason for changing the name.

M. F.

NEW DATA

Kesterite (=Zn analogue of stannite)

V. V. Ivanov and Yu. A. Pyatenko. On the so-called kesterite. *Zapiski Vses. Mineral. Obshch.*, **88,** No. 2, 165–168 (1959) (in Russian) (see *Am. Mineral.* **43,** 1222–1223) (1958).

Re-examination of type material from the Kester deposit, Yakutsk A.S.S.R. showed it to be the zinc analogue of stannite. A new analysis by L. E. Novorossov on optically homogeneous material gave Cu 26.69, Ag 0.49, Zn 10.32, Fe 2.62, Sn 31.80, S 27.58, In 0.021, insol. 0.36, sum 99.88 per cent, corresponding to $Cu_{1.98}$ $(Zn, Fe)_{0.95}$ $Sn_{1.25}$ S_4. *X*-ray study showed it to be tetragonal with a 5.43, c 10.86 Å. An indexed *x*-ray powder pattern is given. It is suggested that this may be a partly disordered phase, intermediate between normal tetragonal stannite and cubic isostannite, and that the formula should perhaps be written $(Cu, Sn)_3$ $(Zn, Fe)S_4$. Color greenish-black, streak black, H 4.4, G 4.54–4.59.

Discussion. The authors consider the name superfluous for a zinc-bearing stannite, but if stannite is Cu_2FeSnS_4 this is the zinc analogue and would normally be given a special name. The name kesterite is objectionable because of confusion with custerite.

M. F.

DISCREDITED MINERALS

Erikite (=Monazite)

Marianne Danø and Henning Sørensen. An examination of some rare minerals from the nepheline syenites of South West Greenland. *Meddelelser om Grønland* **162,** 5, 1–35 (1959).

X-ray powder data are given for the type material from Nunarssuatsiaq, Greenland, described by Bøggild (Medd. Grønland 26, 93–139 (1904)); they are identical with those for monazite. The goniometric data by Bøggild are discussed; they fit fairly well those for eudialyte, and erikite is therefore probably a pseudomorph of monazite after eudialyte. Erikite from the Kola Peninsula (see Gerasimovskii, *Mineralog. Abs.*, **8,** 222 (1942)) has optical properties very different from those of monazite and is apparently not identical with the Greenland material.

M. F.

Igalikite
(=mixture of Analcime+Muscovite 1 M)

Marianne Danø and Henning Sørensen. An examination of some rare minerals from the nepheline syenites of South West Greenland. *Meddelelser om Grønland*, **162,** No. 5, 1–35 (1959).

Re-examination of the type material described by Bøggild (see *Am. Mineral.* **20,** 138 (1935)) by the *x*-ray powder method (data given) showed it to be an alteration product of nepheline, consisting of analcime and a muscovite-like mineral, nearest to muscovite 1 M. The lithium content is 50 ppm.

M. F.

INDEX TO VOLUME 44

Leading articles are in **bold face** type; notes, abstracts and reviews are in ordinary type. Only minerals for which definite data are given are indexed.

Articles to appear in early issues of The American Mineralogist

Crystal structure of perrierite. Glauco Gottardi

Effect of ion substitution on unit cell dimensions of pyroxenes. G. M. Brown

Blue asbestos from Northern Rhodesia. A. R. Drysdale and A. R. Newton

Chemical analysis of rocks with the petrographic microscope. G. M. Friedman

X-ray diffraction study of orientation in the Chattanooga shale. T. F. Bates and E. N. Silverman

Weeksite, a new uranium silicate. W. F. Outerbridge, M. H. Staatz, R. Meyrowitz, and A. M. Pommer

Paulingite, a new zeolite. W. B. Kamb and W. C. Oke

Doverite, a possible new yttrium fluocarbonate. W. L. Smith, J. Stone, D. R. Ross and H. Levine

Autunite from Mt. Spokane, Washington. G. W. Leo

Metamorphism of Lower Paleozoic rocks in Vermont. E-an Zen

Studies of the manganese oxides III. M. Fleischer

Reedmergnerite, $NaBSi_3O_8$, the boron analogue of albite. C. Milton, E. C. T. Chao and J. M. Axelrod

Crystal chemistry of dahllite. D. McConnell

RECENT ACQUISITIONS IN BULK MINERALS AND ROCKS

These are just a few of the many new items that we have acquired in recent months in order to better serve the growing demand for the best in bulk minerals and rocks for teaching, laboratory instruction or research work.

	Price per lb.
Analcime. Calif. Small xls in rock	$1.50
Ancylite. Montana. Crystalline	4.20
Atacamite. Australia. Crystalline	4.20
Cancrinite. Ontario. Crystalline pink	1.50
Cancrinite. Maine. Yellow in syenite	3.00
Cassiterite. Wash. Massive in andalusite	1.20
Corundum. Transvaal. Massive, nearly pure	1.00
Cryolite. Greenland. Pure white masses	1.80
Dumortierite. Nevada. Lilac colored masses	.60
Gadolinite. Norway. Black massive in feldspar	8.50
Garnet. (Andradite). Ariz. Greenish crystallized	2.50
Helvite. N.M. Yellow-brown in rock	3.50
Hemimorphite. Penna. Brown xline	3.50
Idocrase. (Vesuvianite). Me. Brown xline	1.50
Illite. N.Y. Shale containing 85% illite	1.00
Petalite. Rhodesia. White cleavable	1.00
Pyroxene. (Hedenbergite). Mont. Green xline	1.20
Rutile. Norway or Mexico. Nearly pure, red brown	7.00
Basalt. Lintz, Germany. Dense, black, some olivine aggregates	.70
Chert breccia. Okla. Gray chert in dark matrix	.70
Graywacke. Ontario. Dark colored	.70

REFERENCE CLAY MINERALS

An excellent suite of reference samples of important clays which can serve for purposes of comparison in the general field of clay mineralogy. Included in the suite are: halloysite, kaolinite, dickite, montmorillonite, metabentonite, illite and pyrophyllite.

See pp. 52-53, Ward's Geology Catalog No. 583

All prices are list at Rochester, N.Y.

WARD'S *NATURAL SCIENCE ESTABLISHMENT, INC.*
P.O. BOX 1712 ROCHESTER 3, N.Y.

GEORGE BANTA COMPANY, INC., MENASHA, WISCONSIN, U.S.A.